17.4.64
THE UNIVERSITY OF ADELAIDE

PRODUCTION OF HIGH PURITY IRON ALLOYS

BY

VACUUM INDUCTION MELTING

S. ARDMONGON, B.Sc. (Durham)

THE BONYTHON METALLURGICAL LABORATORIES,
SOUTH AUSTRALIAN INSTITUTE OF TECHNOLOGY

A Thesis

Submitted for the Degree of Master of Applied Science

in the Faculty of Engineering

of the University of Adelaide.

September, 1963

ACKNOWLEDGEMENT

I wish to express my sincere thanks to Dr. W. T. Denholm, my supervisor, for his help, guidance and encouragement throughout this work and to Mr. W. G. Forte, Head of the Electrical Engineering Department, South Australian Institute of Technology, for his help and advice on induction heating.

My gratitude and appreciation goes to the Workshop Staff, Bonython Laboratories, South Australian Institute of Technology, and in particular to Mr. F. Burden, for their help in manufacturing and installing the equipment.

I am much indebted to the Colombo Plan and the Government of Australia for granting me the Colombo Plan Scholarship to carry on this work.

STATEMENT

This is to certify that this thesis emobides the results of the author's work.

To the best of the author's knowledge and belief, the thesis contains no material previously submitted for a degree in any other University by the author or any other person except where due reference is made in the text of the thesis.

S. Ardmongon

September, 1963.

TABLE OF CONTENTS

		Page
	Summary	vii
	Introduction	1
Chapter		
I	INDUCTION HEATING	5
	Basic Principle of Induction Heating	5
	Motor-Generator	43
	Mass and Size of Charge	50
	Heat Loss from Charge	52
	Power Required to Melt Charge	56
	Clearance between Work-Coil and Charge	57
	Work-coil	60
	Melting Mild Steel Charge	86
	Auto-transformer	87
	Laminated Core of Work-Coil	103
II	VACUUM SYSTEM	109
	Basic Principle of Vacuum Technique	109
	General Description of Vacuum System	123
	Vacuum Tank	123
	Vacuum Pumps	144
	Evacuation of Vacuum Tank	151
	Vacuum Gauges	155
	Leak Testing	158

Chapter		Page
III	REFRACTORY	161
	Introduction	161
	Zircon lining	163
	Alumina Crucible	168
IV	REFINING	184
	Basic Principle of Refining Process	184
	Study of Oxidation of Impurities by Melting Iron in Air	191
	Study of Refining by Melting Iron under Controlled Atmosphere	204
	Preparation of Charge, Crucible and Mould	222
	Preliminary Melting Mild Steel in Air	229
	Preliminary Refining Armco Iron in Vacuum	232
	Refining of Armco Iron	237
	Chemical Analysis	243
V	DISCUSSION	245
	Induction Heating	245

Chapter		Page
V	Vacuum System	256
	Refractory	257
	Refining	260
	RECOMMENDATION	267
	REFERENCES	269

SUMMARY

The work which has been done in connection with the production of high purity iron alloys by vacuum induction melting may be summarized as follows:

Equipment

(1) A work-coil, 4 inches I.D. and 7 inches long was made. For the practical reason that the conductor was required to carry more than 1000 amperes, and needed water cooling, 17 turns of $\frac{3}{8}$ inch square copper bar was used with a $\frac{1}{4}$ inch copper cooling tube soldered to its outer surface. The impedance of this loaded coil at 500 c/s is low, i.e. 0.22 ohm with a parallel capacitor of 7230 micro-farads for unity power factor correction. It was necessary to use an impedance matching device, i.e. an auto-transformer, to raise the effective impedance of the heating circuit to about 3.22 ohms so that full power could be drawn from the power source (and also less capacitors would be required for unity power factor correction).

(2) An auto-transformer of 60 kVA was constructed. The primary of the transformer was connected to the parallel capacitors and power source; the secondary to the work-coil. By increasing the ratio of primary to secondary the effective impedance of the heating circuit is increased and less parallel capacitors are required

for unity power factor correction. The effective impedance could be increased up to about 3.22 ohms for the utilization of the full power source. The losses of the transformer at 10 kW input (i.e. approximately 60 kVA) is about 2.03 kW which is rather high, probably due to the thin copper tube 0.048 inch wall thickness which was used for the primary winding for ease of manufacture. This loss can probably be reduced by using a thicker tube. The overall efficiency of the transformer at full load is about 80% and changes very little from small load to full load, but when the losses are considered in relation to the 60 kVA circulating load, the efficiency is better than 95%. To eliminate the problem of using a flexible lead to carry high current of more than 1000 amperes from the secondary to the co-axial lead, the transformer was suspended directly on one end of the co-axial lead tube.

(3) A short piece of laminated iron was inserted at the bottom of the work-coil to increase the efficiency of induction heating and to reduce the capacity used for unity power factor correction of the heating circuit. The core surface was cooled by a water cooling pancake coil, coiled non-inductively so that the e.m.f. induced in it by the work-coil is at minimum resulting in negligible I^2R loss in the cooling coil.

(4) A stainless steel vacuum tank 30 inches diameter and 30 inches long was manufactured. With this dimension

the stray power loss on the tank shell from the work-coil situated about the middle of the tank is small and all necessary melting equipment can be accommodated. The cold leakage rate of this tank was about 2 μ Hg. per minute which is normal in practice.

(5) An electrical co-axial lead was constructed to carry both heavy current and cooling water from outside the vacuum tank to the work-coil inside and return. It also serves to support the work-coil and crucible on one of its ends (inside the vacuum tank) and the auto-transformer on its outside end. These rotate through an angle of about 135° while pouring. A heavy stainless steel tube with a flanged seal to the vacuum tank was used as a bearing housing to support the co-axial lead tube which carried the heavy weights. Two neoprene U-packings were used for vacuum seals between this housing and the rotating co-axial tube.

(6) Tamped sintered alumina crucibles were made in the laboratory and used in melting and refining the Armco iron throughout this work. The tamping mixture consisted of fused alumina of various grain sizes and alumina slip which was used as a binder for the green crucible instead of organic or inorganic binders to avoid contamination from the binders. The crucible mould was made of core, base and three segment liners. Sintering of the alumina crucible

was carried out in a graphite susceptor heated by 6 kW R.F. power source under nitrogen atmosphere. Using ample alumina powder to insulate around the graphite susceptor, the latter temperature could be raised to 1800°C within $2\frac{1}{2}$ hours. The sintered alumina crucibles have good thermal shock resistance after firing due to the wide range of particle sizes. The maximum number of heats attempted in any one crucible was three. The crucibles contain a large number of small pores, probably due to insufficient slip particles in the tamping mixture and to too low firing temperature. There was little contamination from alumina crucible judging from the aluminium present in the refined ingots.

(7) Armco iron sheet $3/64$ inch thickness (i.e. 18 gauge) was used as starting material. Although at first sight it appeared impossible to melt this material with 500 c/s power, it was found to melt readily when cut into $2\frac{3}{4}$ inch diameter discs, stacked up to $3\frac{3}{4}$ inches high and oxy-acetelene welded at the side. This simple procedure has overcome the problem of finding a high purity starting material in the form of a solid block from abroad, since thin Armco iron sheet is the only suitable starting material available in suitable quantity in Australia.

Refining

(1) The Armco iron was refined by first melting and

oxidising in air to remove some of its impurities, e.g. manganese, silicon and chromium, in the form of oxides. The oxidised ingot was then remelted under vacuum of 1 μ Hg for a further removal of carbon content as well as evaporation of other impurities which have high vapour pressure at the melting temperature of iron, e.g. copper and manganese. Hydrogen at 10 cm. Hg. was then admitted into the vacuum tank to decrease oxygen content in the melt. This was repeated three times. Finally hydrogen in the melt was decreased by keeping the melt under 5 cm. Hg. of hydrogen for 15 minutes before pouring.

(2) Five ingots were prepared by oxidation and pouring in air. Three of these were remelted and refined in vacuum, but only one was successfully poured into the temporary water-cooled copper mould under vacuum. With the remaining two, the water leaked out from the mould during pouring so gas analysis for oxygen, hydrogen and nitrogen was not done.

(3) The average values of chemical and spectrographic analysis of refined iron compared to that of Armco iron are shown in Table S.1.

The oxidised irons were analysed for carbon only. The vacuum treated irons were analysed for carbon and other impurities.

Table S.1. Average Values of Chemical and Spectrographic Analysis of Armco and Refined Iron

Iron	C* %	Cu+ %	Mn+ %	Si+ %	Cr+ %	Al+ %
Armco	0.02	0.04	0.07	<0.001	0.02	0.01
Oxidised	0.009	..	..	..	..	..
Vacuum treated	0.009	0.01	<0.005	<0.003	0.005	0.0005

* Chemical analysis (± 0.002%)

\+ Spectrographic analysis

Carbon content in Armco iron was decreased to 0.009% (± 0.002%) after oxidation in air, but remained practically constant after refining in vacuum at 1 μ Hg. for 15 minutes. This indicates that a prolonged treatment in vacuum is needed to reduce the low carbon content further.

In theory copper content cannot be removed in significant amounts from liquid iron by oxidation, but the result shows that part of it can be removed by evaporation under vacuum. Manganese content was decreased to a low value by oxidation in air and evaporation under vacuum. Silicon content does not change much after refining; probably there was silicon contamination from the loosened pieces of zircon filling at the top of the alumina crucible. Chromium content was decreased to 0.005 per cent by oxidation. Aluminium content was decreased to a low value (0.0005%) indicating the success of oxidation and showing how little contamination results from the alumina crucible.

BRIEF SUMMARY

Equipment for vacuum induction melting, except the motor-generator set and vacuum pumps, was designed, manufactured and tested. The major items were the work-coil, 60 kVA auto-transformer, stainless steel vacuum tank, electrical co-axial lead and tamped sintered alumina crucibles.

Five to ten pound iron ingots, low in carbon, manganese, chromium and aluminium content, were produced from Armco iron sheet, 3/64 inch thickness, by induction melting stacks of discs using the 500 c/s power source, oxidising in air, and refining in vacuum.

LIBRARY OF THE UNIVERSITY OF ADELAIDE

INTRODUCTION

In the past, high purity iron has been required for use in the electrical industry, and for the investigation of physical and mechanical properties of iron and iron-base alloys made from pure starting materials.

The methods of production of high purity iron may be divided into electrochemical, chemical and metallurgical.

The electrochemical method employs electrolysis of aqueous solutions of iron salts. The electrolytic iron produced usually contains small amounts of impurities due to co-deposition and trapping of impurities at the cathode.

The chemical method involves production of iron salts by precipitation and recrystallization followed by conversion of the iron salt to iron oxide, which is deoxidised to sponge iron by hydrogen. This method can produce very high purity iron but it is a long process, and only small amounts can be made at a time.

The metallurgical method may employ solid or liquid processes. Rengstorff and Goodwin[1] prepared high purity iron by treating flakes of electrolytic iron, in solid, by wet and dry hydrogen. Hopkins et al[2] produced 25 lb. batches of high purity iron by melting and oxidising Swedish iron in air, then remelting the oxidised iron and refining in vacuum and in hydrogen.

Another method is zone refining. The charge is usually a long solid rod, a portion of which is melted by a short induction coil and the molten zone moved slowly from one end to the other. The solute impurities are then concentrated at one end, leaving purer iron at the other.

The aim of the present work was to attempt to produce high purity iron alloys from Armco iron sheet with the power source available (namely a 10 kW, 500 cycle per second, single phase motor-generator). The method of production chosen for investigation was induction melting and refining in air and in vacuum. It is similar to that of B.E. Hopkins et al[2] which was a modification of the method of Adcock.[3] This method has certain advantages, namely:

(a) The melt is isolated from the atmosphere, thus contamination from gases in the atmosphere is prevented and the system can be treated thermodynamically.

(b) The pressure of the system can be controlled.

(c) The melt is strongly stirred by induced currents. This homogenizes the melt as well as increases the reaction rate of chemical reaction within the melt, e.g. by bringing reactants to the reaction site.

(d) Time can be prolonged for the refining reaction to go to completion.

This method is a flexible one, and the equipment constructed may be used to produce high quality alloys in future work.

The problems to be dealt with at the beginning of the work were:

(a) The power output and frequency of the power source are rather low, i.e. 10 kW continuous, 500 c/s, for melting Armco iron sheet of about 5-10 lbs. and supplying power loss from the molten iron during refining and I^2R loss in the electrical heating circuit.

(b) With this low frequency the impedance of any practical design of heating-coil will be low, so to utilize the full power from the source an impedance matching device (i.e. a transformer) is required.

(c) The major items of equipment required in vacuum induction melting and refining in the present work (other than the motor-generator set and vacuum pumps) were:

(1) Heating coil or work coil

(2) 60 kVA auto-transformer

(3) Vacuum tank

(4) Co-axial lead to carry heavy current in and out of the vacuum tank

(5) Alumina crucible.

These needed to be designed, manufactured and tested before the melting and refining could begin.

Thus the programme of the work was divided into:

(a) Design, manufacture and testing of the equipment. This took the major part of the time in this project.

(b) Induction melting of a stack of Armco iron sheet by 10 kW, 500 c/s power source, and refining by oxidising in air and treatment in vacuum.

The production of high purity iron alloys by vacuum induction melting involved four fields of study, namely: induction heating, vacuum technique, refractories and physical chemistry of refining impurities from liquid iron. This thesis is accordingly divided into five chapters.

Chapters I and II begin with basic principles of induction heating and vacuum technique followed by the design, construction and testing of equipment.

Chapter III deals with the manufacture of zircon linings and alumina crucibles.

Chapter IV begins with the basic principles of the refining process, then deals with the theoretical basis of refining to remove impurities from liquid iron, followed by refining procedure and results.

Chapter V presents a discussion of the design, problems encountered and results of the refining operation.

Then recommendation is made for a future work.

CHAPTER I

INDUCTION HEATING

1.1 Basic Principle of Induction Heating

An induction heating installation is basically a transformer of which the heating coil is the primary and the work piece (charge or conductor) is the single turn secondary. The power is transferred from the coil to heat the work piece by means of an alternating (or varying) magnetic flux.

1.1.1 Heat Development in Conductor

The heat development in a magnetic conductor under the imposition of an alternating magnetic flux depends on two factors:

(a) hysteresis effect

(b) eddy current effect.

Hysteresis Heating - The hysteresis heating is the heat dissipated in a magnetic conductor when it has undergone a complete cycle of magnetization. It is associated with the energy required to align magnetic elements (domains, electron spins) in the direction of the magnetizing force.[4]

The hysteresis power per cycle of magnetization may be calculated from the area surrounded by the hysteresis loop.

Steinmetz has given the formula for the hysteresis power as follows:

$$P_h = \eta \cdot B^{1.6} \text{ ergs per cycle} \quad \ldots \quad (1.1)$$

per cc. of magnetic conductor

η = constant depends on material

B = maximum flux density, maxwells $cm.^{-2}$

When the frequency is increased the hysteresis power is nearly constant in the range of low and medium frequency of magnetization and decreases to a negligible value at high frequency.[5] This occurs because at high frequency the magnetic flux tends to confine itself to the surface of the conductor, therefore the mass which is subjected to the hysteresis effect is small. The hysteresis power is also decreased with increasing temperature and becomes practically zero when the conductor becomes non-magnetic at its Curie point and above.

Thus the hysteresis effect is not an important factor in the present work which aims at melting iron.

Eddy Current Heating - The eddy current heating is the heat developed in the conductor due to the eddy current flow in it.

Under the alternating flux the e.m.f. is induced in the conductor.

Faraday's law

$$e = -\frac{d\phi}{dt} \cdot 10^{-8} \text{ volts} \quad \ldots \quad (1.2)$$

$\frac{d\phi}{dt}$ = rate of change of flux in maxwells per second.

The induced e.m.f. causes eddy current to flow in the conductor and the heat developed is

$$H = 0.24\ I^2R \text{ calories/sec.} \quad \ldots \quad (1.3)$$

I = eddy current, amperes.

R = resistance of conductor, ohms.

Nearly all of the heat developed in non-magnetic material or magnetic material at temperature above its Curie point is due to eddy current heating. Other than heating up the conductor, the eddy current induces a magnetic flux in a direction which tends to reduce the magnitude as well as changing the direction of the flux which is imposed on it. This is an important factor in induction heating, because it effects the magnetic flux, eddy current and power distribution in the conductor.

1.1.2 Magnetic Flux and Eddy Current Distribution in Conductor[6,7,8]

The alternating magnetic flux produced by the work-coil causes the eddy current to flow in the conductor. The flow of eddy current produces an opposing flux. They

are interrelated and effect each other and will be dealt with together.

For a long work-coil carrying alternating current, the magnetic field inside the coil may be considered parallel to its axis. If a solid cylindrical conductor is put inside the coil, the eddy current distribution in the conductor will be the same at any cross section area along its length.

Consider a ring of unit length whose radius is r cm. and thickness dr, Fig. 1.1(b).

Let H = magnetic force at radius r, oersted.

The total flux ϕ_r at radius r is

$$\phi_r = \mu \int_0^r 2\pi x \, H \, dx \qquad \ldots\ldots (1.4)$$

μ = permeability of the conductor assumed to be constant.

The e.m.f. induced in the ring dr is the rate of change of flux within radius r.

$$dE = -\frac{d\phi_r}{dt}$$

$$dE = -2\pi\mu \int_0^r x \frac{\partial H}{\partial t} \, dx \qquad \ldots\ldots (1.5)$$

If the flux varies sinusoidally

$$\frac{\partial H}{\partial t} = j\omega H$$

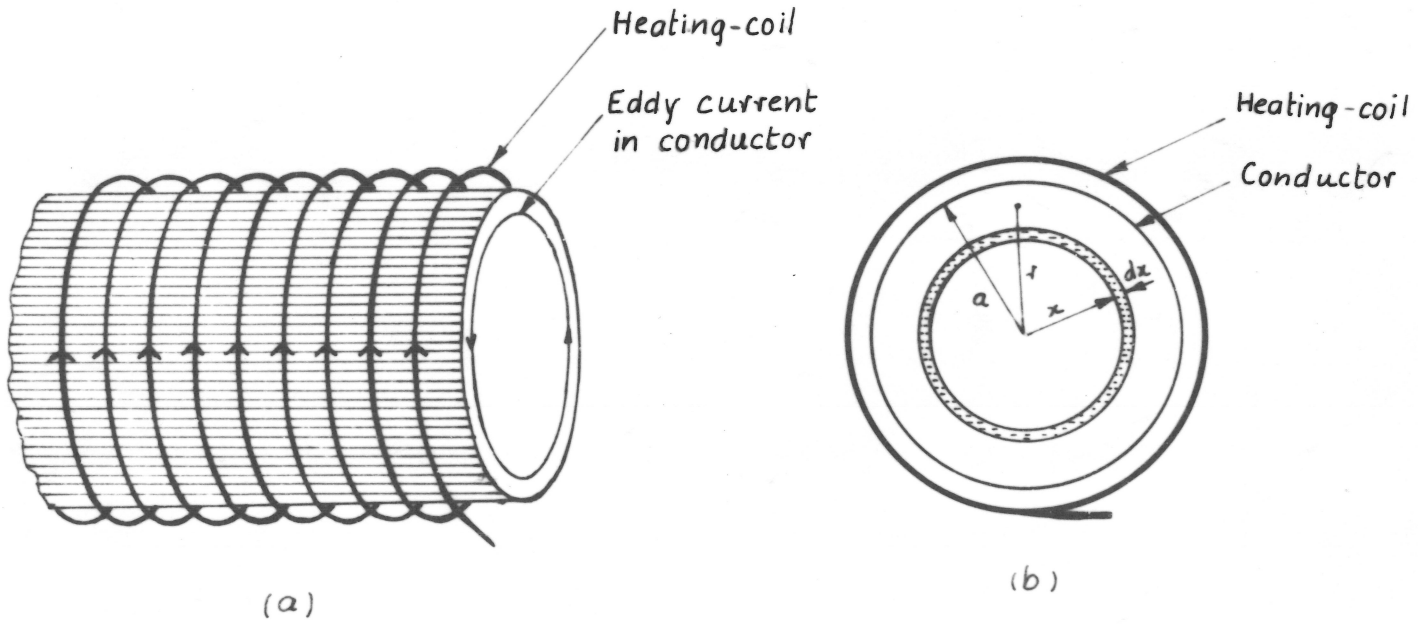


Fig. 1.1 Heating Coil and Conductor

$$j = \sqrt{-1}$$

$$\omega = 2\pi f$$

f = frequency, cycle sec^{-1}

$$\therefore \quad dE = -2\pi\mu j\omega \int_o^r x.H.dx \qquad \ldots . \quad (1.6)$$

Let $\sigma\, dr$ be the current flow in ring dr of unit length where σ is the current density at dr.

$$\therefore \quad \sigma\, dr = \frac{dE}{R}$$

$$R = \frac{2\pi r\rho}{dr}$$

ρ = resistivity of conductor, e.m.u.

$$\therefore \quad \sigma = \frac{1}{2\pi r\rho} \cdot dE$$

$$\sigma = -\frac{\mu j\omega}{r\rho} \int_o^r x.H.dx \qquad \ldots . \quad (1.7)$$

The eddy current $\sigma\, dr$ in the ring dr of unit length, produces an opposing magnetic force $-dH$.

$$-dH = 4\pi\sigma\, dr$$

$$\sigma = -\frac{1}{4\pi} \cdot \frac{dH}{dr} \qquad \ldots . \quad (1.8)$$

Equating (1.7) and (1.8)

$$-\frac{1}{4\pi}\frac{dH}{dr} = -\frac{\mu j\omega}{r\rho} \int_o^r x.H.dx$$

$$r\frac{dH}{dr} = \frac{4\pi\mu\omega j}{\rho} \int_o^r x.H.dx \qquad \ldots . \quad (1.9)$$

Differentiating equation (1.9) with respect to r and inserting the limits gives

$$r \frac{d^2H}{dr^2} + \frac{dH}{dr} = \frac{4\pi\mu\omega j}{\rho} H.r$$

or $$\frac{d^2H}{dr^2} + \frac{1}{r}\frac{dH}{dr} - j\, m^2 H = 0 \quad \ldots\ldots (1.10)$$

where $$m^2 = \frac{4\pi\mu\omega}{\rho} = \frac{8\pi^2\mu f}{\rho} \quad \ldots (1.11)$$

The standard solution for equation (1.10) is

$$H = A\, I_o(mr\sqrt{j}) + B\, K_o(mr\sqrt{j}) \quad \ldots\ldots (1.12)$$

A and B = constant

$I_o(mr\sqrt{j})$ = modified of Bessel function of the first kind of zero order

$K_o(mr\sqrt{j})$ = modified of Bessel function of the second kind of zero order

In the solid cylinder conductor when r = 0, H in equation (1.12) is not infinite, but when r = 0, $K_o(mr\sqrt{j})$ is infinite, hence B in equation (1.12) must be zero. Therefore equation (1.12) may be written

$$H = A\, I_o(mr\sqrt{j}) \quad \ldots\ldots (1.13)$$

If the real and imaginary terms of $I_o(mr\sqrt{j})$ are grouped separately, it may be written as

$$I_o(mr\sqrt{j}) = \text{ber } mr + j \text{ bei } mr$$

$$\therefore \quad H = A(\text{ber } mr + j \text{ bei } mr) \quad \ldots\ldots \quad (1.14)$$

At the surface of the conductor r = a and H = Ho (root mean square value)

$$\therefore \quad H_o = A(\text{ber } ma + j \text{ bei } ma) \quad \ldots\ldots \quad (1.15)$$

Dividing equation (1.14) by equation (1.15)

$$\frac{H}{H_o} = \frac{\text{ber } mr + j \text{ bei } mr}{\text{ber } ma + j \text{ bei } ma} \quad \ldots\ldots \quad (1.16)$$

If the induction frequency is high or the diameter of the conductor is large equation (1.16) may be simplified by writing

$$\text{ber } mr = \frac{e^{mr/\sqrt{2}}}{\sqrt{2\pi mr}} \cos\left(\frac{mr}{\sqrt{2}} - \frac{\pi}{8}\right)$$

$$\text{bei } mr = \frac{e^{mr/\sqrt{2}}}{\sqrt{2\pi mr}} \sin\left(\frac{mr}{\sqrt{2}} - \frac{\pi}{8}\right)$$

then

$$\frac{H}{H_o} = \frac{\sqrt{2\pi mr}\; e^{mr/\sqrt{2}}}{\sqrt{2\pi ma}\; e^{ma/\sqrt{2}}} \left[\frac{\cos\left(\frac{mr}{\sqrt{2}} - \frac{\pi}{8}\right) + j \sin\left(\frac{mr}{\sqrt{2}} - \frac{\pi}{8}\right)}{\cos\left(\frac{ma}{\sqrt{2}} - \frac{\pi}{8}\right) + j \sin\left(\frac{ma}{\sqrt{2}} - \frac{\pi}{8}\right)}\right]$$

$$\ldots\ldots \quad (1.17)$$

When r and a are very large or at high frequency induction the expression within the square bracket of equation (1.17) tends to one and

$$\frac{\sqrt{2\pi mr}}{\sqrt{2\pi ma}} \longrightarrow 1$$

$$\therefore \quad \frac{H}{H_o} = e^{\sqrt{\frac{m}{2}}(r-a)}$$

$$= e^{\frac{-m}{\sqrt{2}}(a-r)}$$

Let $a - r = x$

x = distance from conductor surface, cms.

$$\therefore \quad H = H_o\, e^{\frac{-m}{\sqrt{2}} \cdot x},$$

$$\text{or } H = H_o\, e^{\frac{-x}{\delta}}, \text{ oersted} \qquad \ldots\ldots \quad (1.18)$$

Where $\delta = \frac{\sqrt{2}}{m}$

From equation (1.11)

$$m^2 = \frac{8\pi^2 \mu f}{\rho}$$

$$\therefore \quad \delta = \frac{1}{2\pi}\sqrt{\frac{\rho}{\mu f}} \text{ cms.} \qquad \ldots\ldots \quad (1.19)$$

Since $B = \mu H$

B = flux density, maxwell/cm^2 $\qquad \ldots\ldots \quad (1.20)$

It may be written

$$B = B_o \cdot e^{\frac{-x}{\delta}}$$

B_o = flux density at surface of conductor.

Similarly the eddy current density distribution may be derived from equation (1.8) which is

$$\sigma = \frac{1}{4\pi} \cdot \frac{dH}{dr}$$

From this the result will be

$$\sigma = -\frac{Am}{4\pi} (\text{ber}'mr + j\,\text{bei}'\,mr) \quad \ldots . \quad (1.21)$$

where

$$\text{ber}'mr = \frac{e^{mr/\sqrt{2}}}{\sqrt{2\pi\, mr}} \cos\left(\frac{mr}{\sqrt{2}} + \frac{\pi}{8}\right)$$

$$\text{bei}'mr = \frac{e^{mr/\sqrt{2}}}{\sqrt{2\pi\, mr}} \sin\left(\frac{mr}{\sqrt{2}} + \frac{\pi}{8}\right)$$

and $$\sigma_o = -\frac{Am}{4\pi} (\text{ber}'ma + j\,\text{bei}'ma) \quad \ldots . \quad (1.22)$$

σ_o = current density at surface of conductor

$$\therefore \frac{\sigma}{\sigma_o} = \frac{\text{ber}'mr + j\,\text{bei}'mr}{\text{ber}'ma + j\,\text{bei}'ma}$$

and $$\sigma = \sigma_o . e^{-\frac{x}{\delta}} \text{ ampere cm}^{-2}, \text{ e.m.u.} \quad \ldots . \quad (1.23)$$

x = distance from surface of conductor

$$\delta = \frac{1}{2\pi}\sqrt{\frac{\rho}{\mu f}} \text{ cms.}$$

A typical curve of the eddy current or magnetic flux distribution is shown in Fig. 1.2.

Considering eddy current density distribution, the area under curve AC is the total current flow per unit length from surface to centre of the conductor. This is equal to

$$\int_o^\alpha \sigma_o . e^{-\frac{x}{\delta}} . dx = \sigma_o . \delta = i \quad \ldots . \quad (1.24)$$

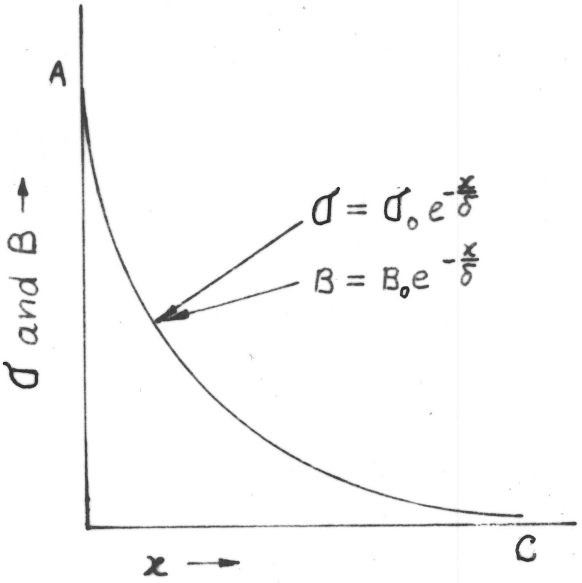


Fig. 1.2 A typical magnetic flux and eddy current density distribution in solid cylinder conductor

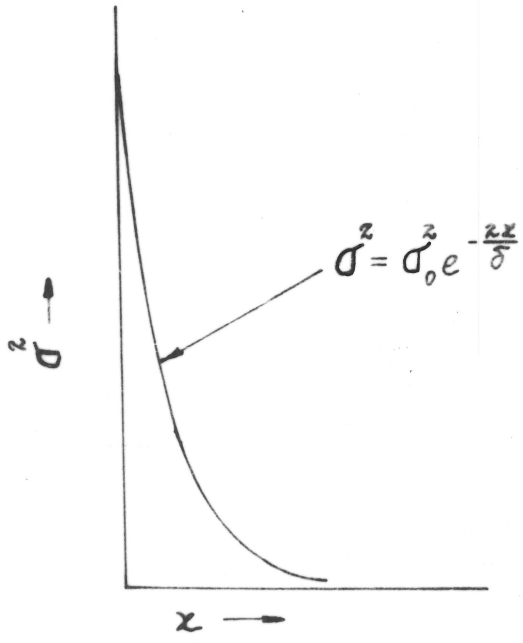


Fig. 1.3 Power distribution in solid cylinder conductor

Equation (1.24) shows that if the current density σ_o penetrates uniformly into the depth δ the total current in this region will be equal to the total current existing in a unit length of the conductor which is i.

δ is called equivalent depth of current penetration.

1.1.3 Power Distribution in Conductor

The power developed in any ring (Fig. 1.1(b)) of unit cross section area (along its length) is

$$dW = \sigma^2 . R \text{ ergs sec}^{-1} \quad \ldots . \quad (1.25)$$

$$R_r = 2\pi r \rho \text{ e.m.u.}$$

or $R_r = 2\pi(a - x)\rho$

x = distance from surface, cm.

a = radius of conductor, cm.

$\therefore \quad dW = \sigma^2 \, 2\pi(a-x)\rho$

or $dW = \sigma_o^2 \, e^{\frac{-2x}{\delta}} \, 2\pi(a-x)\rho \text{ ergs sec}^{-1}$

$\ldots . \quad (1.26)$

In practice σ^2 is much greater than R and at high frequency x is small, therefore it may be considered that the power developed in the ring of conductor is proportional to σ^2 or $\sigma_o^2 \cdot e^{\frac{-2x}{\delta}}$. The power distribution may be represented in Fig. 1.3. It shows that the power distribution decreases from surface to centre of conductor at a higher ratio more than the eddy current distribution.

From equation (1.26) it may be derived that, at high frequency the power dissipated in the region of depth of current penetration is about 94% of the total power dissipated in the conductor.

1.1.4 Power Development in Conductor[6,7]

The power development in conductor is the important aspect in induction heating. It may be derived as follows.

From equation (1.21)

$$\sigma = -\frac{Am}{4\pi}(\text{ber}'mr + j\,\text{bei}'mr)$$

From Fig. 1.1(b) the amount of current flow in the ring of radius r, width dr and of unit length is $\sigma dr \times 1$. The resistance of this ring is $\rho \frac{2\pi r}{dr}$, hence the power developed in the ring is $\sigma^2 \rho 2\pi r\, dr$. So the total power developed per unit length of conductor is

$$P_1 = \int_0^a \frac{|A|^2 m^2}{16\pi^2}(\text{ber}'^2 mr + \text{bei}'^2 mr)\rho\, 2\pi r\, dr \quad \ldots\ (1.27)$$

$$= \frac{|A|^2 ma}{8\pi}(\text{ber}\ ma\ \text{ber}'\ ma + \text{bei}\ ma\ \text{bei}'\ ma)$$

$|A|$ = absolute value of A

From equation (1.15)

$$|A|^2 = \frac{H_o^2}{\text{ber}^2 ma + \text{bei}^2 ma}$$

$$\therefore \quad P_1 = \frac{H_o^2 \rho ma}{8\pi} \frac{(\underline{ber\ ma\ ber'ma + bei\ ma\ bei'ma})}{ber^2 ma + bei^2 ma} \qquad \ldots\ldots (1.28)$$

This is for a unit length of charge, for a unit volume

$$P_1 = \frac{H_o^2 \rho m}{8\pi^2 a} \frac{(\underline{ber\ ma\ ber'ma + bei\ ma\ bei'ma})}{ber^2 ma + bei^2 ma}$$

$$\text{ergs sec}^{-1}\ \text{cm}^{-3} \qquad \ldots\ldots (1.29)$$

For a long coil

$$H_o = \frac{4\pi n I}{l} \text{ r.m.s.}$$

n = total number of turns of coil

I = root means square of current, e.m.u.

l = length of coil, cm.

$$\therefore \quad P_1 = \frac{4\pi n^2 \mu\omega}{l^2} .I^2_{\text{r.m.s.}} W(ma) \qquad \ldots\ldots (1.30)$$

where $W(ma) = \frac{2}{ma} \frac{(\underline{ber\ ma\ ber'ma + bei\ ma\ bei'ma})}{ber^2 ma + bei^2 ma}$

and $m^2 = \frac{4\pi\mu\omega}{\rho}$

If V is the volume of conductor in cm^3, the power developed in it is

$$P = \frac{4\pi n^2 \mu\omega}{l^2} I^2_{\text{r.m.s.}} V\ W(ma) \qquad \ldots\ldots (1.31)$$

$$\text{ergs sec}^{-1}$$

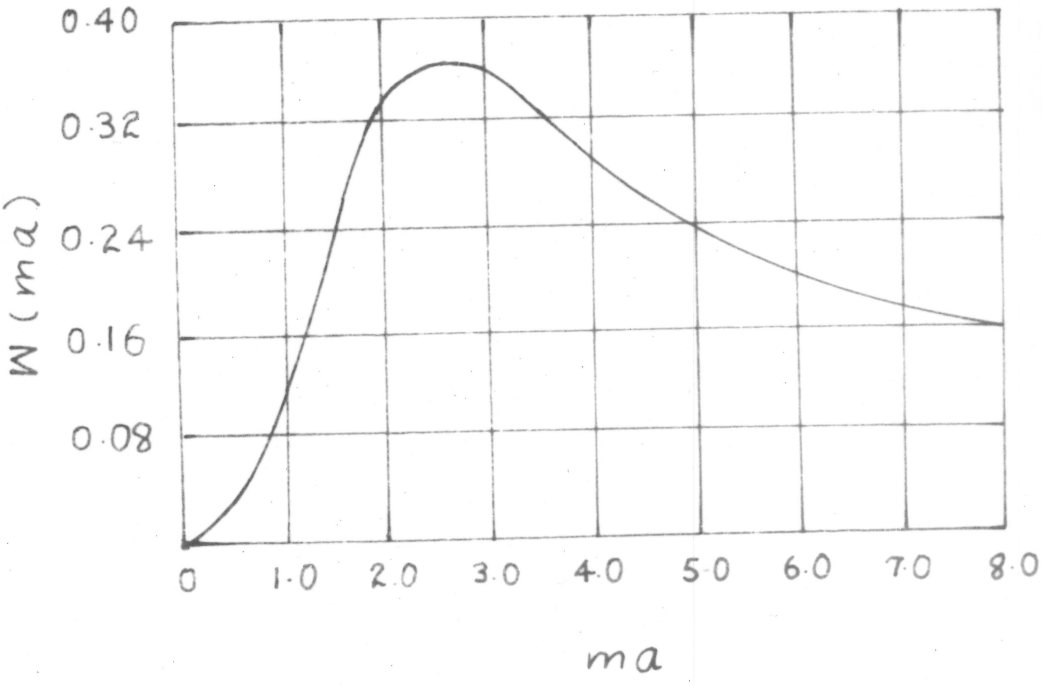


Fig. 1.4 Power function for a solid cylindrical conductor.[7]

The graph of power function W(ma) is shown in Fig. 1.4. The maximum power occurs when

$$ma \doteq 2.5 \qquad \ldots . \quad (1.32)$$

or $W(ma) = 0.36$

1.1.5 Magnetic coupling between Work-Coil and Conductor[9]

The power development in conductor is transferred from the work-coil by magnetic coupling between them. The magnitude of this coupling may be conveniently represented by coupled resistance and coupled reactance. They are the equivalent resistance and reactance of the conductor referred to the work-coil circuit. The diagram of work-coil and conductor is shown in Fig. 1.5.

L_1 = inductance of the work-coil circuit which is magnetically linked with L_2.

L_2 = inductance of charge linked with L_1.

M = mutual inductance of L_1 and L_2.

Z_A = impedance of work-coil circuit other than L_1.

Z_B = impedance of conductor other than L_2.

V_1 = voltage of supply line

E_2 = induced e.m.f. in conductor.

The total impedance of work-coil circuit is

$$Z_1 = Z_A + j\omega L_1 \qquad \ldots . \quad (1.33)$$

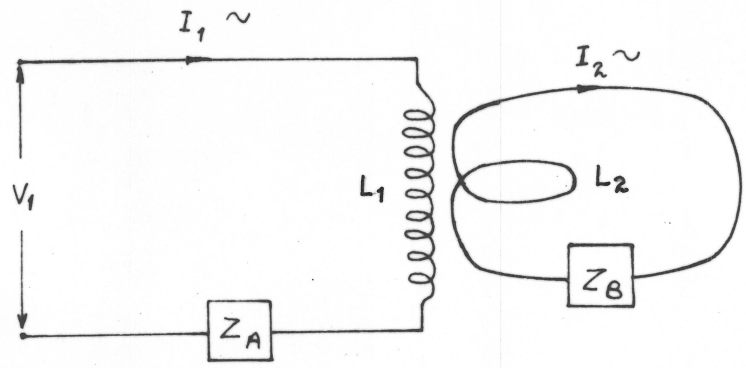


Fig. 1.5 Circuit diagram of loaded work-coil.

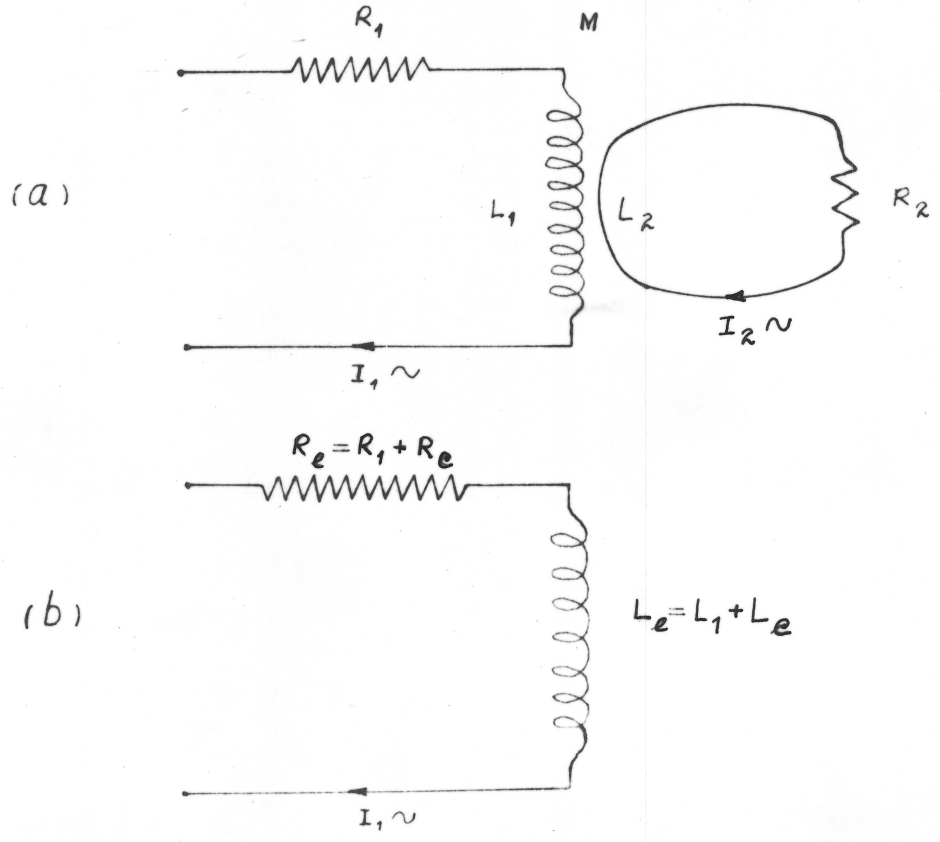


Fig. 1.6 Equivalent circuit diagrams of loaded work-coil

and of conductor

$$Z_2 = Z_B + j\omega L_2 \qquad \ldots . \qquad (1.34)$$

The total supply voltage

$$V_1 = I_1 Z_1 + j\omega M I_2 \qquad \ldots . \qquad (1.35)$$

$$I_2 = -\frac{E_2}{Z_2} = -\frac{j\omega M I_1}{Z_2} \qquad \ldots . \qquad (1.36)$$

$$\therefore \quad V_1 = I_1 \left(Z_1 + \frac{\omega^2 . M^2}{Z_2}\right) \qquad \ldots . \qquad (1.37)$$

The effective impedance

$$Z_{eff} = \frac{V_1}{I_1} \qquad \ldots . \qquad (1.38)$$

$$\therefore \quad Z_{eff} = Z_1 + \frac{\omega^2 M^2}{Z_2} \qquad \ldots . \qquad (1.39)$$

Equation (1.39) shows that the presence of charge caused the change of impedance of the unloaded work-coil by the quantity $\frac{\omega^2 M^2}{Z_2}$ which is called the coupled impedance which may be separated into two parts

$$\frac{\omega^2 M^2}{Z_2} = \frac{\omega^2 M^2}{R_2 + j X_2}$$

$$= \frac{\omega^2 M^2 (R_2 - j X_2)}{|Z_2|^2}$$

$|Z_2|$ = absolute value

$\frac{\omega^2 M^2 R_2}{|Z_2|^2}$ is called coupled resistance $\ldots .$ (1.40)

$\frac{-j\omega^2M^2X_2}{|Z_2|^2}$ is called coupled reactance . . . . (1.41)

These show that $R_{coupled}$ and $X_{coupled}$ will be large at high frequency (ω) and/give good magnetic coupling (M) between work-coil and conductor. With the negative sign $X_{coupled}$ acts as a series capacitive reactance in the work-coil circuit.

The presence of $R_{coupled}$ and $X_{coupled}$ in the loaded work-coil may be seen clearly from the simplifying diagram, Fig. 1.6(a) with its equivalent diagram, Fig. 1.6(b).

If R_1, X_1, L_1 = resistance, reactance and inductance of unloaded work-coil respectively

R_c, X_c, L_c = coupled resistance, reactance and inductance of conductor referred to work-coil circuit

R_e, X_e, L_e = effective resistance, reactance and inductance of loaded work-coil.

$\therefore \quad R_e = R_1 + R_c$ . . . . (1.42)

$X_e = X_1 + X_c$ . . . . (1.43)

and $L_e = L_1 + L_c$ . . . . (1.44)

Burges and Davis derived formulae for the coupled resistance of a long coil and a long cylindrical conductor and give:[10]

$$R_{coupled} = 2\pi\sqrt{2\pi}\, r_o\, l_o n^2 \sqrt{\omega \rho_o \mu_o}\; F_1\left(\frac{r_o}{\beta}\right) 10^{-9} \text{ ohms} \quad \ldots . \quad (1.45)$$

r_o = outer radius of cylindrical conductor, cms.

l_o = axial length of conductor, cms.

n = turns/cm. axial length of conductor

ρ_o = resistivity of conductor, e.m.u.

μ_o = permeability of conductor

β = equivalent of flux penetration[9]

$$\beta = \frac{1}{2\pi}\sqrt{\frac{\rho}{2\mu f}} \text{ cms.} \quad \ldots . \quad (1.46)$$

$F_1(\frac{r_o}{\beta})$ is a function of $\frac{r_o}{\beta}$ which is shown in curve I, Fig. 1.7.

The corresponding coupled reactance for a non-magnetic conductor is

$$X_{coupled} = -\, 4\pi^2\, r_o^2\, l_o n^2\, \omega\, F_2\left(\frac{r_o}{\beta}\right) 10^{-9} \text{ ohms} \quad \ldots . \quad (1.47)$$

$F_2(\frac{r_o}{\beta})$ is a function of $(\frac{r_o}{\beta})$ which is shown in curve II, Fig. 1.7.

Curve I of Fig. 1.7 shows that the coupled resistance rises rapidly with increasing value of $\frac{r_o}{\beta}$ up to $\frac{r_o}{\beta} \doteq 3$. Beyond this point the increase is not great indicating that for a good magnetic coupling the radius of the charge should not be less than three times the depth of magnetix flux penetration.

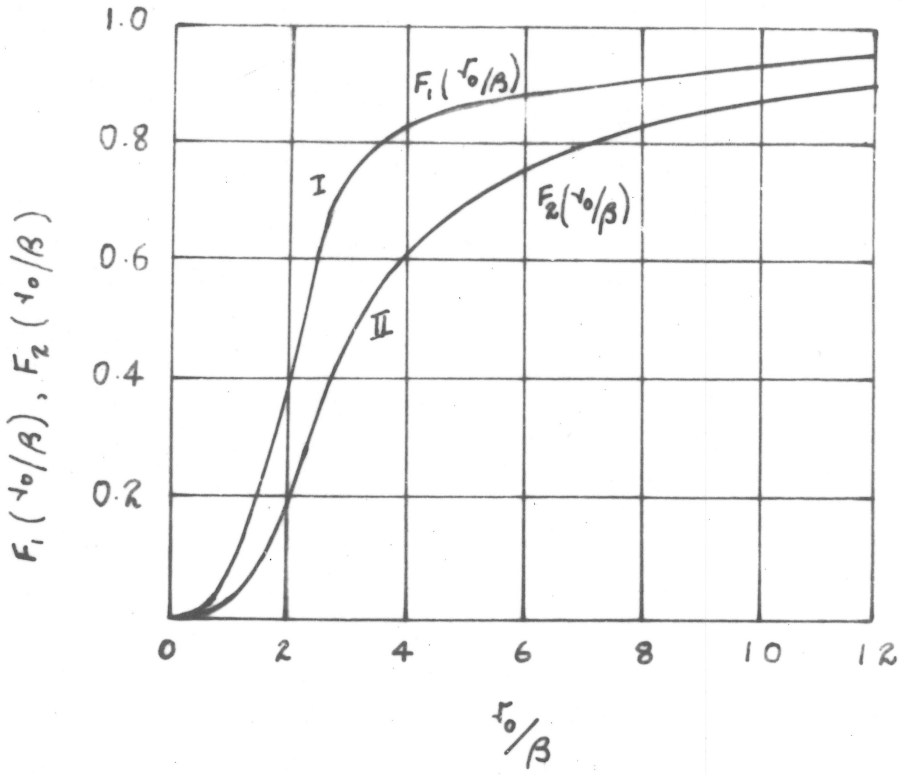


Fig. 1.7 Coupled resistance and reactance function for long coil and long charge.[10]

In melting practice, the work-coil is not long. The charge (conductor) is usually shorter than the work-coil and a space must be given between them for crucible, therefore the magnetic flux linkage between the work-coil and the conductor is not uniform along the axial length and is less than that which Burges and Davis derived in the equations for R_e and X_e. Thus corrections are needed for R_e and X_e for short work-coil and short charge.

1.1.6 Correction for R_e and X_e [9]

(a) Correction for a short work-coil and for clearance between the work-coil and conductor.

R_e in equation (1.45) is to be multiplied by $\frac{H^2}{H_o^2}$

H^2 = average square of magnetic field strength over surface of charge

H_o = field strength within a long coil

Fig. 1.8 is an example of the ratio of $\frac{H}{H_o}$, the area under the curve divided by its base length is the average of ratio $\frac{H}{H_o}$.

(b) Correction for shortness of charge (diameter of charge is large and kept constant, its length changes)

(1) R_e in equation (1.45) is to be multiplied

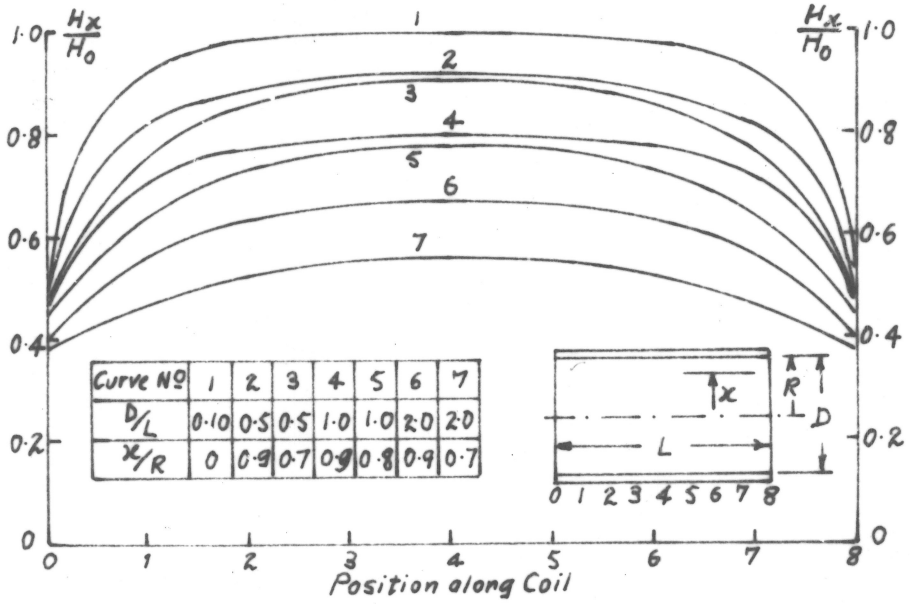


Fig. 1.8 Magnetic Field Strength in Short Coil.[9]

by $\frac{1}{K}$. K is Nagaoka's constant for the conductor ratio $\frac{d_o}{l_o}$ in Fig. 1.9.

(2) X_e in equation (1.47) is to be multiplied by K in Fig. 1.9.

1.1.7 Efficiency of Power Transference of Work-Coil[9]

The efficiency of power transference may be expressed in terms of the power input to the work-coil and the power developed in the conductor.

The power input to the work-coil is

$$P_1 = I_1^2 (R_1 + R_c) \quad \ldots\ldots (1.48)$$

I_1 = coil current

R_1 = coil resistance

R_c = coupled resistance

The power developed in the conductor is

$$P_2 = I_1^2 R_c \quad \ldots\ldots (1.49)$$

The efficiency is

$$\eta = \frac{R_c}{R_1 + R_c} \quad \ldots\ldots (1.50)$$

The approximate value of the work-coil resistance (R_1) may be calculated from the resistance corresponding to the depth of current penetration. This value is higher than the actual resistance of the work-coil but at high frequency the difference is small.

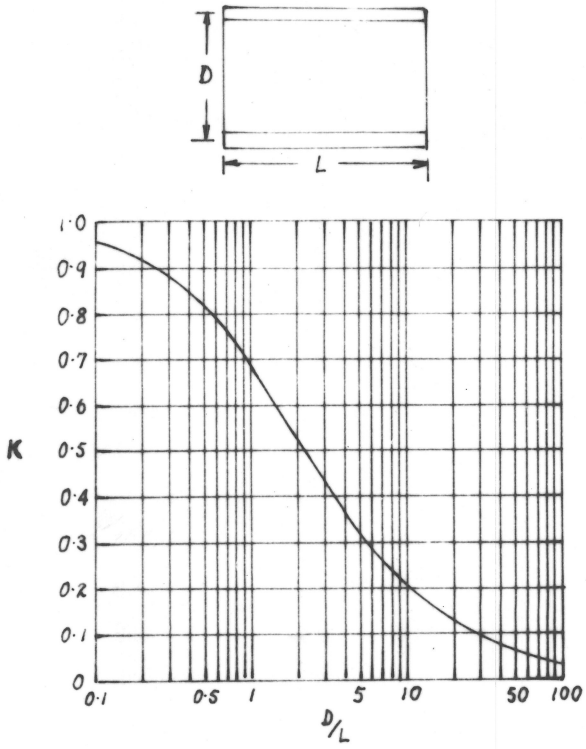


Fig. 1.9 Nagaoka and Lorenz constant[9]

Let r_1 = inside radius of work-coil, cms.

n = number of turns per cm.

w = width of coil, cms.

$= \frac{1}{n}$ for close wound coil

l_1 = axial length of coil, cms.

ρ_1 = resistivity of coil, e.m.u.

μ_1 = permeability of coil

δ = depth of current penetration, cms.

$$\delta = \frac{1}{2\pi}\sqrt{\frac{\rho}{\mu f}}$$

$$R_1 = \frac{\rho . 2\pi r_1 n . l_1}{w \times \delta} \text{ e.m.u.}$$

$$\text{or } R_1 = 4\pi^2 r_1 l_1 n^2 \sqrt{\rho_1 \mu_1 f}. 10^{-9} \text{ ohms} \qquad \ldots . (1.51)$$

From equation (1.45) and $F_1 (\frac{r_o}{\beta}) \doteqdot 1$

$$R_c = 4\pi^2 r_o l_o n^2 \sqrt{\rho_o \mu_o f}. 10^{-9}$$

$$\therefore \quad \eta = \frac{r_o l_o \sqrt{\rho_o \mu_o}}{r_o l_o \sqrt{\rho_o \mu_o} + r_1 l_1 \sqrt{\rho_1 \mu_1}} \qquad \ldots . (1.52)$$

If the work-coil is made of copper $\mu_1 = 1$, and for a non-magnetic conductor $\mu_o = 1$, e.g. iron at temperature above its Curie point, then

$$\eta = \frac{r_o l_o \sqrt{\rho_o}}{r_o l_o \sqrt{\rho_o} + r_1 l_1 \sqrt{\rho_1}} \qquad \ldots . (1.53)$$

Dividing through by $r_o l_o \sqrt{\rho_o}$

$$\therefore \quad \eta = \frac{1}{1 + \frac{r_1 l_1 \sqrt{\rho_1}}{r_o l_o \sqrt{\rho_o}}} \qquad \ldots\ldots \quad (1.54)$$

Equation (1.54) shows that the efficiency of power transference will be high when

(a) the conductor is long and its radius is close to the work-coil radius,

(b) the resistivity of the conductor is high.

1.1.8 Resistivity and Permeability of Charge

Resistivity and permeability appear in many considerations of induction heating, e.g. magnetic flux, eddy current and power distribution in conductor. During heating of a magnetic conductor its resistivity and permeability change with temperature. They may be considered as follows.

Resistivity - At room temperature the resistivity of a high purity metal is low. The irregularities in the metal such as foreign atoms in crystal, dislocations, grain boundary causes high resistivity. When the temperature rises the thermal vibration throws the atoms out of their alignment which causes a higher resistivity for most metals. Fig. 1.10 shows the change of resistivity with temperature for electrolytic iron and 1% carbon steel.

At the melting point the resistivity of metal would

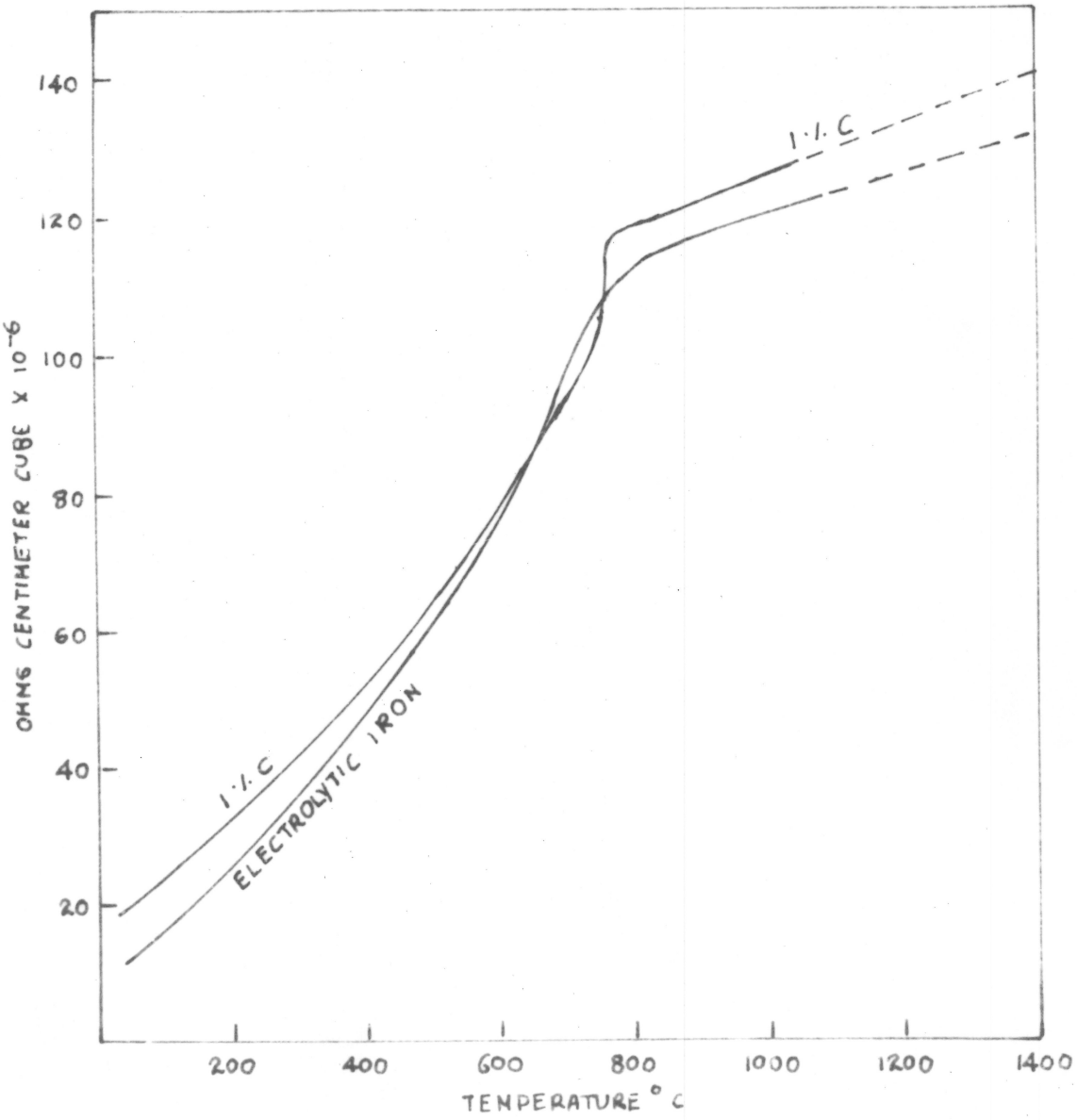


Fig. 1.10 Resistivity temperature curve of electrolytic iron and steel.[5]

rise sharply due to the irregularity of atomic arrangement in liquid state.

Permeability - In the early stages of heating an iron charge the temperature has little effect on its permeability, but when the temperature rises to near its Curie point the permeability starts to decrease and falls to unity at the Curie point. The effect of temperature on permeability of carbon steel is shown in Fig 1.11. The other factor which has great effect on the permeability is magnetic force. The relative permeability of an electrolytic iron melted in vacuum is shown in Fig. 1.12. At the flux density of 9,000 maxwell per sq. cm. the permeability reaches its maximum value of 18,800.

1.1.9 Parallel-resonance Circuit[12]

A series or parallel capacitor may be used to correct the power factor of an inductive circuit to unity. In the present work if the series capacitor is used, at resonance, the impedance of the circuit is equal approximately to the resistance of the work-coil which is usually low in the order of a few milliohms, therefore higher current could not be drawn from the power source. Furthermore, in induction heating the inductance of the work-coil changes with the temperature of the conductor and in a certain case with load, e.g. when a laminated iron core is used to surround the coil. It is therefore necessary to use a bank of parallel capacitors for unity power factor

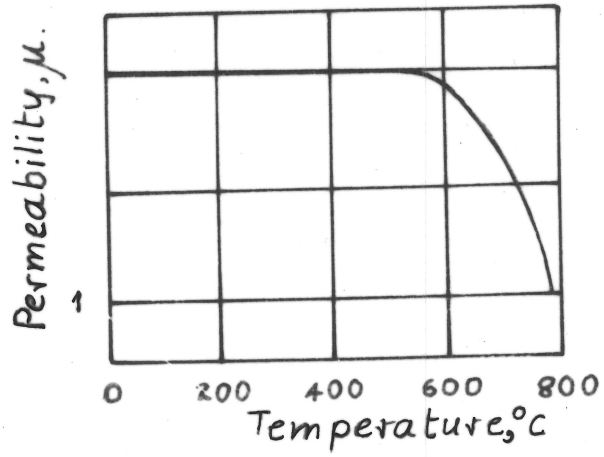


Fig. 1.11 Effect of heat on the permeability of carbon steel.[5]

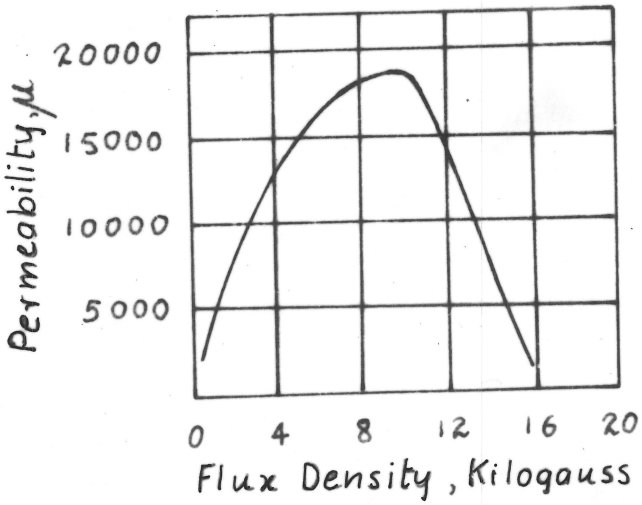


Fig. 1.12 Permeability of electrolytic vacuum melted iron.[11]

correction in inductance melting.

In general the parallel circuit may be represented as in Fig. 1.13(a) with its vector diagram in Fig. 1.13(b).

Let Z_L, R_L, X_L = impedance, resistance and reactance of inductive branch.

Z_C, R_C, X_C = impedance, resistance and reactance of capacitive branch.

Using the admittance method the circuit elements may be tabulated as in Table 1.1.

Table 1.1 Circuit Elements of Parallel Circuit

	Capacitive Branch	Inductive Branch
Resistance	R_C	R_L
Reactance	X_C	X_L
Impedance	$\sqrt{R_C^2 + X_C^2}$	$\sqrt{R_L^2 + X_L^2}$
Conductance	$\frac{R_C}{R_C^2 + X_C^2}$	$\frac{R_L}{R_L^2 + X_L^2}$
Susceptance	$\frac{X_C}{R_C^2 + X_C^2}$	$-\frac{X_L}{R_L^2 + X_L^2}$

At resonance the total susceptance is zero and the supply current (I_s) is in phase with the supply voltage (V_s).

$$\therefore \quad \frac{X_L}{R_L^2 + X_L^2} = \frac{X_C}{R_C^2 + X_C^2} \qquad \ldots\ldots (1.55)$$

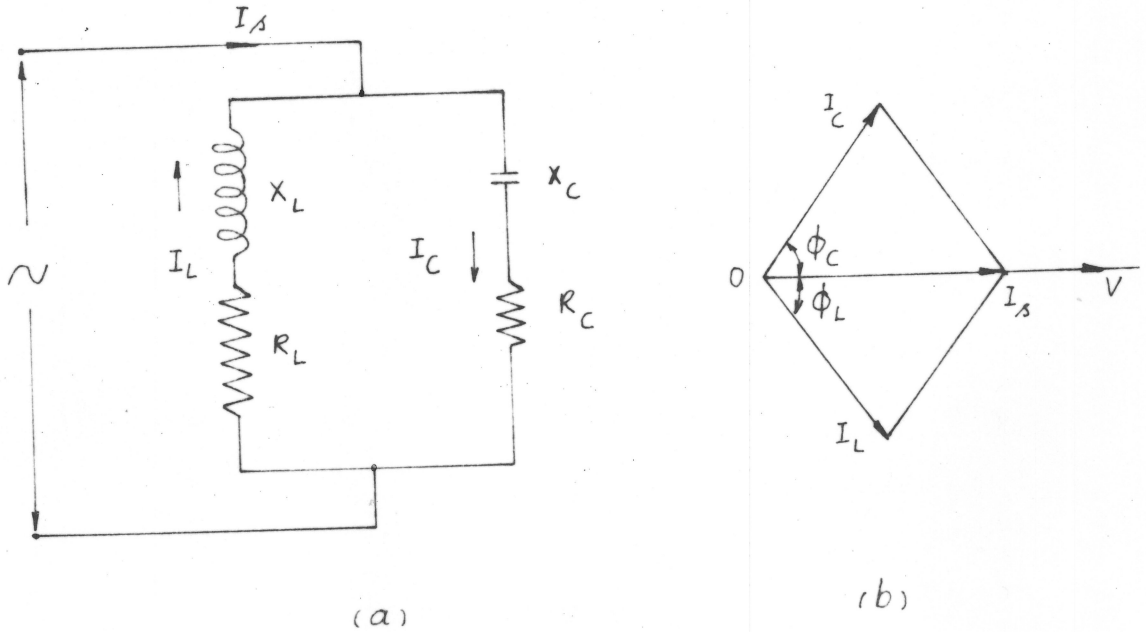


Fig. 1.13 Circuit diagram of parallel inductive and capacitive load.

$$\text{or} \quad \frac{R_L^2}{X_L} + X_L = \frac{R_C^2}{X_C} + X_C \qquad \ldots . \qquad (1.56)$$

In actual work $\frac{R_L^2}{X_L}$ and $\frac{R_C^2}{X_C}$ are less than one. Therefore it may be assumed that

$$X_L = X_C$$

Using the complex quantity method and assuming that X_L and X_C are much greater than R_L and R_C, the total parallel impedance may be written as

$$Z_p = \frac{(\omega_o L)^2}{Z_s} \qquad \ldots . \qquad (1.57)$$

Z_s is the series resonance of the closed circuit of R_L, X_L, R_C and X_C. ω_o is equal to $2\pi f_o$ (f_o is the series resonance frequency of the closed circuit). L is inductance of the coil.

$$Z_s = R_L + R_C$$

$$\doteqdot R_L \ (R_C \text{ is small})$$

$$\therefore \quad Z_p = \frac{(\omega_o L)^2}{R_L} \qquad \ldots . \qquad (1.58)$$

$$I_s = \frac{V_s}{Z_p}$$

$$= \frac{R_L}{\omega_o L} \cdot \frac{V_s}{\omega_o L}$$

$$= \frac{R_L}{\omega_o L} \cdot I_L$$

$$\text{or } I_L = \frac{\omega_o L}{R_L} \cdot I_s \qquad \ldots \quad (1.59)$$

$$\text{and} \qquad I_C = \frac{\omega_o L}{R_L} \cdot I_s \qquad \ldots \quad (1.60)$$

$\frac{\omega_o L}{R_L} = Q$ which is called the magnification factor which shows that the current flow in the branch circuit would be Q times the current flow in the supply line.

1.1.10 Principle of Auto-transformer[13]

The auto-transformer was used in the present work and its basic principle may be described as follows.

Assuming the transformation ratio is 3:1, Fig. 1.14 shows currents and voltages of primary and secondary.

Neglecting losses and magnetizing current, both are small,

Power in the primary ab is 40 x 30 = 1200 watts.

This power is transferred to the secondary cb which is 20 x 60 = 1200 watts.

But the total power delivered to load is 20 x 90 = 1800 watts.

Hence the power 1800-1200 = 600 watts is being conducted from primary to secondary.

From Fig. 1.14 it is clear that if it was a two winding transformer the amount of copper required for primary

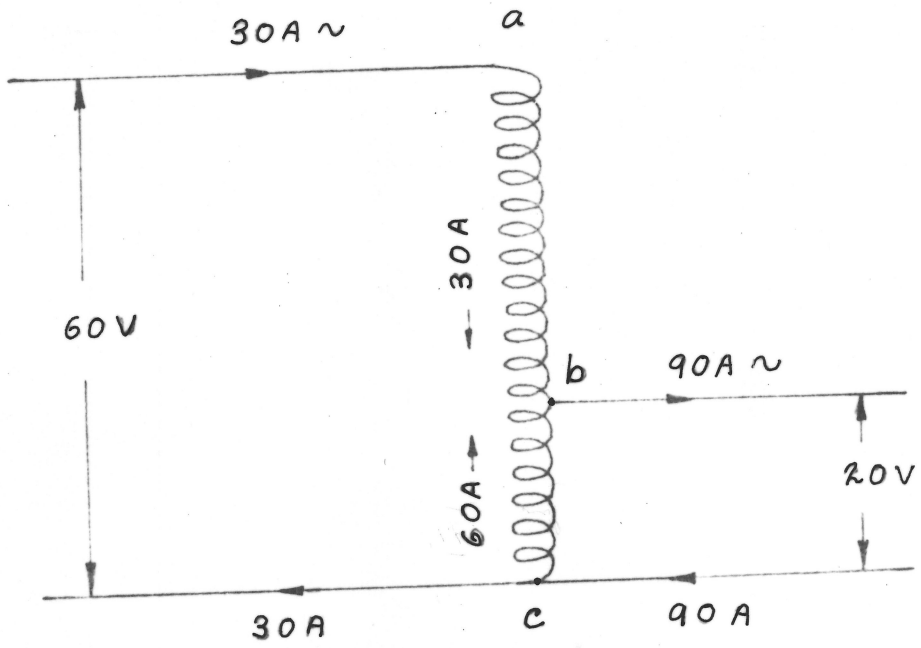


Fig. 1.14 Currents in auto-transformer

would be from a to c to carry 30 ampere current and for secondary from c to b to carry 90 ampere current. Therefore by using the auto-transformer the amount of copper winding is reduced. The advantage is more when the transformation ratio is near to unity. One of the disadvantages of auto-transformer is the secondary is connected to the high potential side. But this has no objection in the present work of induction melting.

1.1.11 Number of Turns of Transformer

The number of turns of primary of auto-transformer may be calculated from the maximum flux density of the transformer core, rated voltage and frequency of the power source. The relationship of these factors may be described as follows (Fig. 1.15(a) and (b)).

Let N_1 = No. of turns of primary

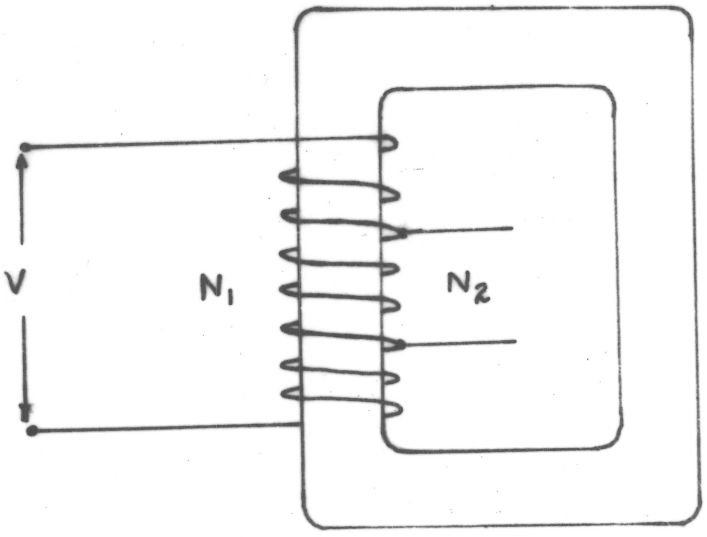
Let N_2 = No. of turns of secondary

The presence of N_2 will have very little effect on the maximum flux produced in the iron core. It will be omitted and treated as an open circuit.

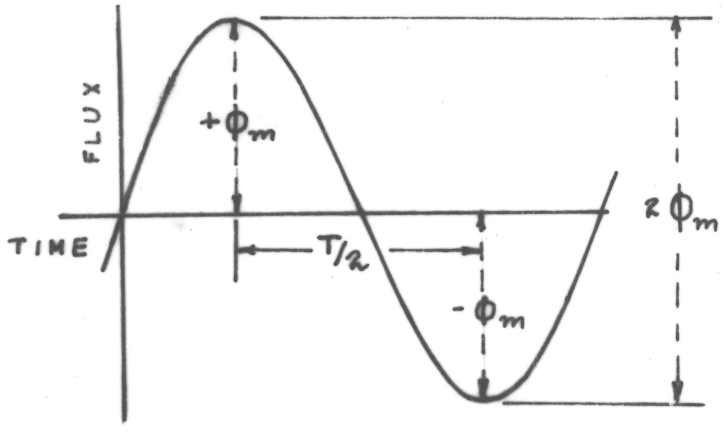
V_1 = applied voltage at primary

ϕ = flux produced in the iron core due to the ampere turn $N_1 I_1$

According to Lenz's law the alternating flux will tend to induce e.m.f. in each turn of the primary coil in the opposite direction to the applied voltage V_1. The sum



(a)



(b)

Fig. 1.15 Auto-transformer and sinusoidal variation of flux with time.

of the induced e.m.f. in each turn will equal the applied voltage.

The induced e.m.f. in the primary coil may be calculated assuming that the flux ϕ is sinusoidal, Fig. 1.15 (b).

Let f = frequency of alternating flux c/s

T = time in seconds for 1 cycle

$= \frac{1}{f}$, second

ϕ_m = maximum flux, maxwell

The average induced e.m.f. in each turn is the rate of change of flux link with the turn.

$$e_{av} = -2\phi_m \cdot 2f \cdot 10^{-8} \text{ volts} \quad \ldots\ldots (1.61)$$

For N_1 turns

$$e_{av} = -4\phi_m N_1 f \cdot 10^{-8} \text{ volts} \quad \ldots\ldots (1.62)$$

The average e.m.f. of a sinusoidal curve is $\frac{1}{1.11}$ of the root mean square e.m.f.

$$\therefore \quad E_{r.m.s.} = -4.44\phi_m N_1 f \cdot 10^{-8} \text{ volts} \quad \ldots\ldots (1.63)$$

$$N_1 = \frac{E_{r.m.s.}}{4.44\phi_m f 10^{-8}} \text{ turns} \quad \ldots\ldots (1.64)$$

1.1.12 Stirring of Liquid Iron

The stirring of liquid iron in induction melting is an inherent advantage in homogenizing the melt and increasing the chemical reaction rate in the refining process of the melt, the mechanism of which may be

described as follows.

For a single phase power source the instantaneous currents in work-coil and in the melt may be shown in Fig. 1.16(a). The induced e.m.f. is highest at about the middle of the charge because it corresponds to the position in which the magnetic flux produced by the work-coil is at maximum. The eddy current in each horizontal layer of liquid iron flows in the same direction and attracts each other. The attractive force is the highest at the middle layer, so the liquid on the top will flow down and at the bottom will flow up. There is a repulsive force between work-coil and liquid metal because their currents flow in opposite directions and cause the liquid iron to go inwards at about the middle. With these repulsive and attractive forces acting on the melt the stirring motion is as shown in Fig. 1.16(a).

It may be mentioned that the stirring of the melt by a multiphase power source will give a better effect than the single phase shown in Fig. 1.16(b). Some induction melting units, therefore, employ single phase power for melting and multiphase for stirring.

1.2 Motor-Generator[14]

Originally the motor-generators were bought from the surplus stores of the Royal Australian Navy. They

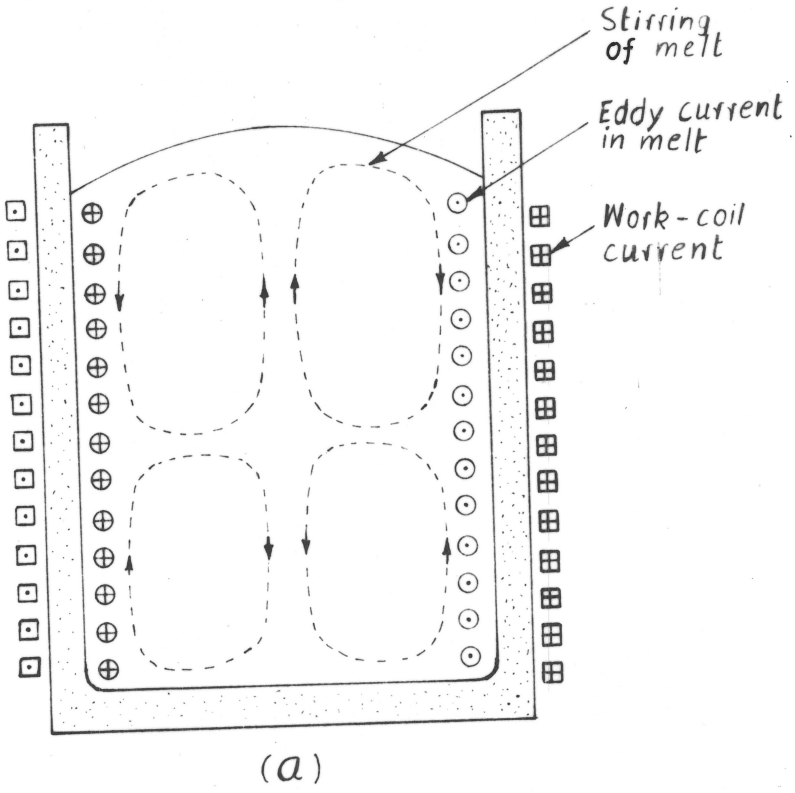


Fig. 1.16 Stirring of melt in induction melting.

originally consisted of 110V D.C. motors driving 5 kW, 500 c/s, single phase inductor-type alternators. The motors were modified to synchronous converters which can produce direct current from the original brushes or drive the alternators to produce A.C. at 500 c/s. The following modifications were necessary:

(a) Three slip rings were fitted on each shaft near the motor commutator. One lead was connected from each ring to commutator segment 120° apart.

(b) A slot was cut on each field pole to accommodate the single turn damper which was made of 1 x $\frac{1}{4}$ inch copper bar. Its purpose was to produce more starting torque when running the motor up to synchronous speed as well as to stabilize the operation of the motor from hunting at synchronous speed.

(c) Relay 1 was put in the armature circuit of the D.C. generator, No. 1. It is a synchronising relay (polarized by a diode and filter system) which connects the field system of both motors to the D.C. output of the No. 1. armature, Fig. 1.17, when the speed of the motor is very close to synchronous speed (3000 r.p.m.). This is to ensure both synchronism and D.C. polarity.

(d) An eight micro-farad capacitor was connected across the contactor No. 3, as shown in Fig. 1.17, to

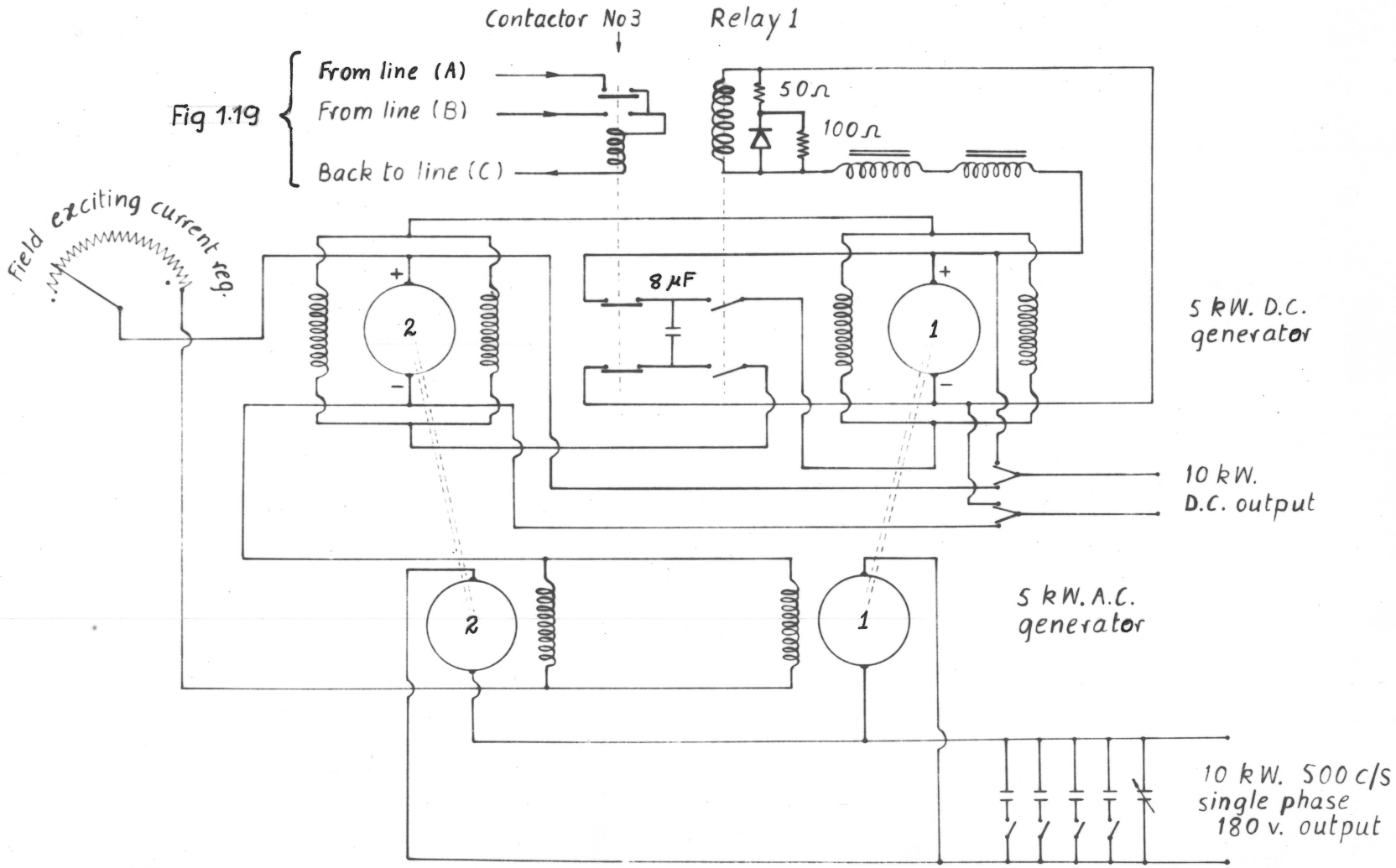


Fig. 1.17 Parallel circuit diagram of D.C. and A.C. generators with relay and capacitor.[14]

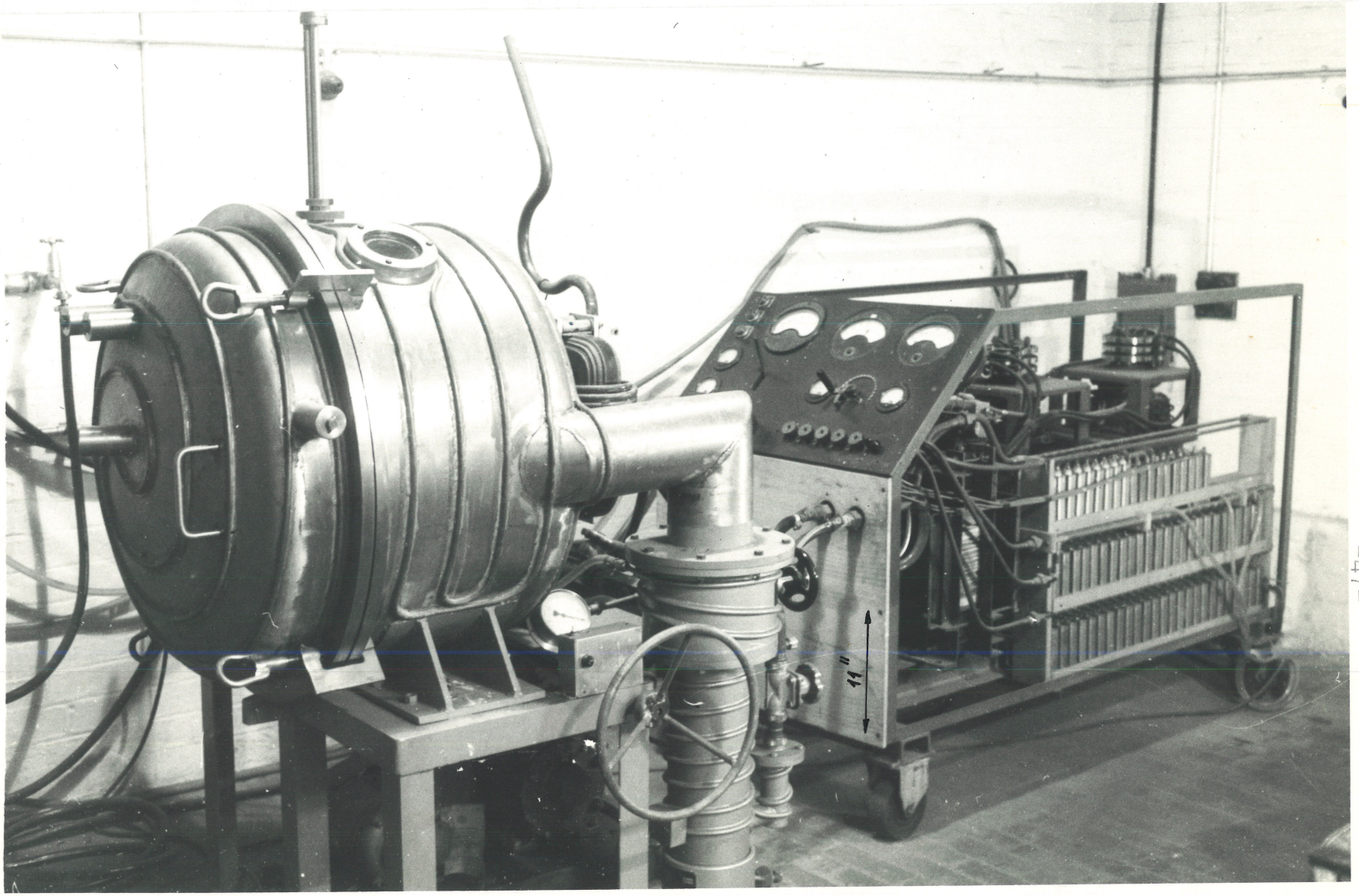


Fig. 1.18 Vacuum tank and motor-generator set

prevent the contact from excessive arcing due to high inductive voltage developed when the stop button is pressed to open the circuit and stop the motors.

In the present work two of the motor-generator sets are used, connected in parallel to provide the output of 10 kW, 180 V, 500 c/s, single phase.

A photograph of the motor-generators together with the vacuum tank is shown in Fig. 1.18. The circuit diagram of the parallel D.C. and A.C. generator with relay 1 is shown in Fig. 1.17.

1.2.1 Starting of Synchronous Motors[15]

The power supply is a three phase system. The voltage of each phase is 400 volts which is too high to apply directly into the armature winding of the motor. It is reduced to 31.5 volts by a step down three-phase transformer.

For starting the primary windings the transformer is connected into "star" (when the starter button is pressed), as shown in Fig. 1.19. This is to reduce the amount of current flowing into the motor while it is at rest. After the motor comes up to its synchronous speed, the "run" button is pressed to disconnect the "star" and at the same time the primary windings are reconnected into "delta" to supply full power to the motor.

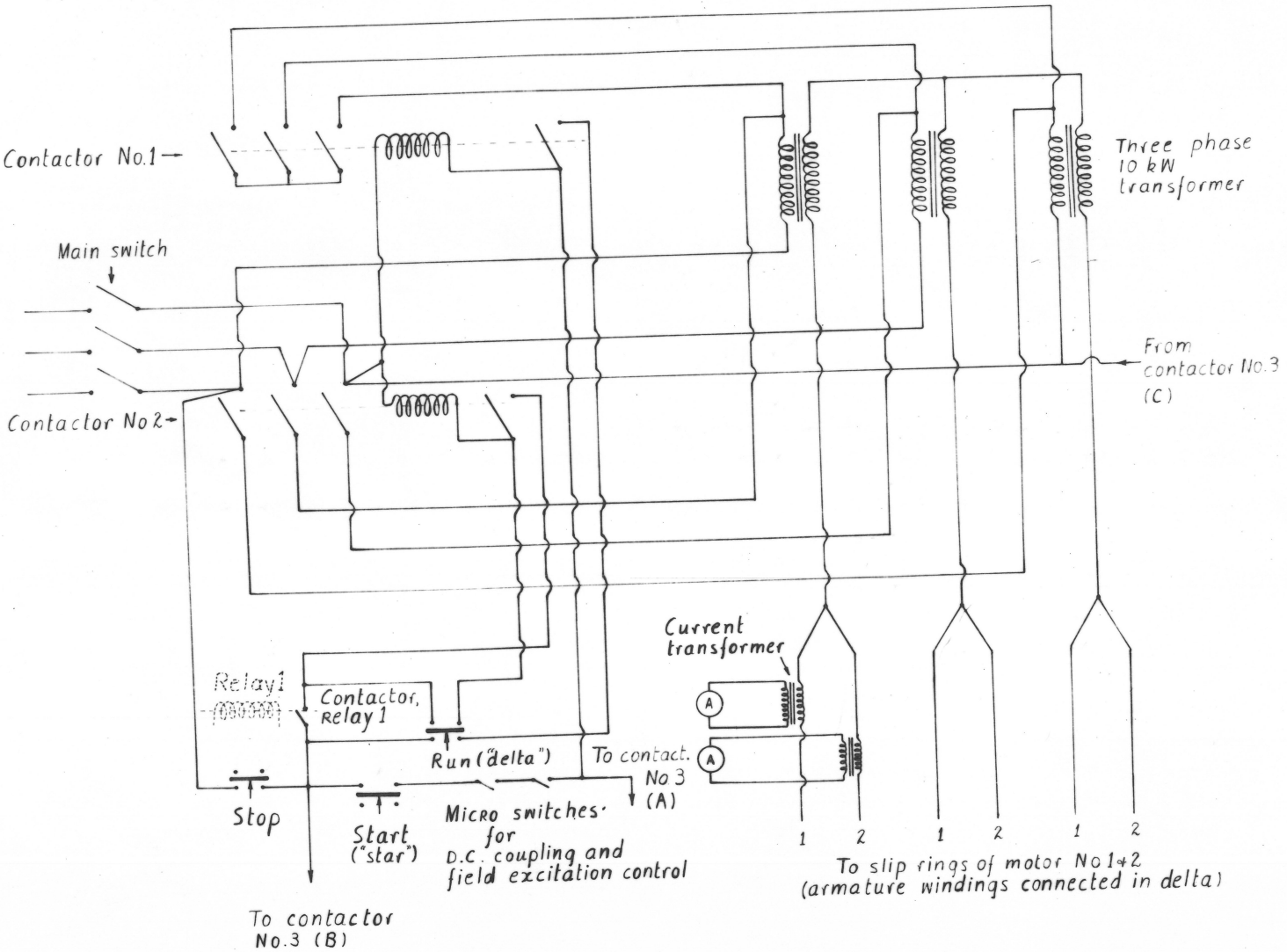


Fig. 1.19 Circuit diagram for starting of synchronous motor.

1.3 Mass and Size of Charge

With the limited power source of 10 kW and medium frequency of 500 c/s, it is not possible to melt a charge consisting of small pieces of iron because the heating efficiency would be very low. The charge should be a solid cylindrical iron. The rather low power source required some careful consideration of the mass and size of charge and heat loss from charge, so that melting and refining of Armco iron would be possible.

(a) Radius of the charge should be larger than the depth of current penetration for an efficient heating.

(b) Having a suitable mass which could be melted by 10 Kw, 500 c/s, within an hour

(c) Heat loss from the hot charge should not be too high and make melting difficult.

1.3.1 Radius of charge

The depth of current penetration in a non-magnetic charge under the imposing flux of 500 c/s is, equation (1.19),

$$\delta = \frac{1}{2\pi}\sqrt{\frac{\rho}{\mu f}} \text{ cms}$$

$\rho = 119.6 \times 10^{-6}$ ohms cm. for iron at 1000°C

$\mu = 1$ for iron above its Curie point

$f = 500$ c/s

$$\therefore \delta = \frac{1}{2\pi}\sqrt{\frac{119.6 \times 10^{-6} \times 10^{9}}{1 \times 500}}$$

$$= 2.46 \text{ cms.}$$

The radius of the charge should be more than 2.46 cms. From McLachlan's power equation (equation 1.32), the maximum power dissipated in the charge when

$$ma \div 2.5$$

a = radius of charge, cms.

$$m = 2\sqrt{2}\pi\sqrt{\frac{\mu f}{\rho}}$$

$$a = \frac{2.5}{2\sqrt{2}\pi}\sqrt{\frac{\rho}{\mu.f}}$$

$$= \frac{2.5}{2\sqrt{2}\pi}\sqrt{\frac{119.6 \times 10^{-6} \times 10^{9}}{1 \times 500}}$$

$$= 4.35 \text{ cms.}$$

$$= 1.7 \text{ in.}$$

Therefore the diameter of charge should be 3.4 inches.

1.3.2 Mass of Charge

The amount of power required to melt a piece of iron, if there is no heat loss, may be easily calculated. But the heat loss from the hot charge to the colder surrounding is high. In fact, the power (heat) loss from the small charge is more than the power required to melt it when isolated.

The heat loss depends largely on the surface area of the charge and the thickness of the refractory container. Therefore it is common to estimate the mass and length of the charge and lining thickness first, then do some calculation if it is workable.

A piece of stainless steel 10 lb. weight, 3.5 inches (8.9 cms.) diameter and 3.5 inches long was chosen as a first test piece. The stainless steel represents the non-magnetic property of iron above its Curie point.

From the specific heat and latent heat of fusion of iron, the heat required to melt one gramme of iron to temperature 1550°C is about 300 calories, 10 lbs. of iron will require 1365 kilo-calories. This is equal to power input of 1.59 kW-hour.

1.4 Heat Loss from Charge

The heat loss from hot charge may be considered from heat loss through lining, heat loss in heating up the lining and radiation loss.

1.4.1 Heat Loss through Lining

If we assumed the clearance between work-coil and charge is $\frac{1}{2}$ inch (1.27 cm.), this is about the thickness of the lining to be used, the amount of heat loss from hot charge by conduction through lining may be calculated.

$$H = \frac{K.A.T.}{d} \text{ kW} \qquad \ldots (1.65)$$

K = thermal conductivity in kW per sq. cm. of lining surface, cm. of thickness, per °C temperature difference across lining

= 1.5×10^{-5} kW for alumina lining at 1315°C[16]

A = wetted area of lining sq. cms.

T = temperature difference across lining, ^{o}C

d = thickness of lining, cms.

The surface area of side and bottom of the hot charge is

$$A = \pi d_o l_o + \frac{\pi d_o^2}{4}$$

d_o = diameter of charge

l_o = length of the charge

$$\therefore \quad A = \pi \times 8.9 \times 8.9 + \frac{\pi (8.9)^2}{4}$$

$$= 310 \text{ sq. cms.}$$

$$\therefore \quad H = \frac{1.5 \times 10^{-5} \times 310 \times 1525}{1.27}$$

$$= 5.56 \text{ kW}$$

The heat loss through the lining is alarmingly high compared to the power available. It could be cut down by reducing the surface area of the charge or increasing the lining thickness.

By trial and error calculation the suitable mass is 6.63 lbs. weight, $2\frac{3}{4}$ inches (6.7 cms.) diameter and $3\frac{3}{4}$ inches (9.52 cms.) long.

From previous calculation the best radius length was 1.7 inches. It was reduced to $1\frac{3}{8}$ inches to compromise for the heat loss through lining.

The surface area of the side and bottom of the new charge is 236 sq. cm. The heat loss through the alumina lining, $\frac{1}{2}$ inch thick, is 4.23 kW.

The heat content of 6.63 lbs. iron at 1550°C is 1.06 kW-hour.

1.4.2 Heat Loss in Heating up Lining

Volume of the alumina which surrounded the hot charge is 3 inches inside diameter (allowed $\frac{1}{8}$ inch clearance between charge and refractory container), 4 inches outside diameter, $3\frac{3}{4}$ inches long and $\frac{1}{2}$ inch thick is 24.1 cu. in. This is equal to the weight 1.42 lbs. or 0.645 kg.

The amount of heat required to raise temperature of the lining to 1550°C is

$$H = s(T_1 - T_2)m \text{ kilo-calories} \quad \ldots \quad (1.66)$$

s = specific heat of alumina

= 0.28 kilo-calory per kg, per °C

T_1, T_2 = initial and final temperature of alumina

m = weight of alumina, kg.

$\therefore \quad H = 0.28\ (1550-25)\ 0.645$

= 276 kilo-calories

This is equal to 0.321 kW-hour.

If the lining is made $1\frac{1}{2}$ inches higher than the surface of the melt, the extra volume would be 8.25 cu. in. It will consume another power of 0.11 kW-hour.

1.4.3 Radiation loss.

From Stefan-Boltzmann's law the radiation loss is

$$H = \sigma(T_1^4 - T_2^4) \text{ watts. cm}^{-2} \quad \ldots \quad (1.67)$$

σ = Stefan's constant

= 5.74×10^{-12} watt cm^{-2} deg^{-4} K for the black body radiation

T_1 = temperature of the black body, $^\circ$ absolute

T_2 = temperature of the surrounding, $^\circ$absolute

if $T_1 = (1550 + 273)^\circ K$

$T_2 = (25 + 273)^\circ K$

$H = 63.14$ watts. cm^{-2}

In vacuum melting there would be very little iron oxide on the surface of the molten iron. The emissivity of clear liquid iron at 1550°C is about 0.37 of that of the black body.[17] The surface area of the charge is 35.2 sq. cm. Therefore the radiation from the charge is

$$H = 63.14 \times 0.37 \times 35.2$$

$$= 822 \text{ watts.}$$

The radiation loss is quite high. But in practice the crucible lid is kept closed most of the time. It is opened occasionally to observe the condition of the melt and the crucible. The radiation loss is then cut to a minimum.

The radiation loss under the closed lid depends on the temperature of the melt and the temperature of inside the crucible above the melt including the lid. It also depends on the rate of heat being conducted through the refractory. A thick lid would reduce the rate of radiation loss. In the present work it may be assumed that the radiation loss is not more than 0.2 kW with the lid closed.

1.5 Power Required to Melt Charge

From the above considerations the power required to melt the 6.63 lbs. charge would be

Heat content of the molten iron = 1.06 kW - hour

Heat loss in heating up the lining = 0.431 kW - hour.

Heat loss through lining = 4.23 kW

Radiation loss = 0.2 kW

Power required = 5.9 kW

This means that if the power 5.9 kW is put into the iron charge of 6.63 lbs. it would melt the charge in about an hour. During this period the heat will be lost through the lining at the rate of 4.23 kW, radiation loss 0.2 kW, heating up the alumina lining of 32.35 cu.in. to 1550^{o}C in an hour.

The power required, 5.9 kW comes from the work-coil.

Usually the transference efficiency of the work-coil is about 0.7-0.8. Therefore the power input to the work-coil is in the order of 8.4 kW.

If all the other losses in the electrical system, e.g. loss in the work-coil, loss in transformer, are included, the power required would be near to 10 kW.

Therefore melting of the iron charge of 6.63 lbs. within an hour by a power source 10 kW, 500 c/s is possible.

1.6 Clearance between Work-Coil and Charge

The clearance between the work-coil and the charge effect the efficiency of melting in two ways:

(a) If the clearance is small the magnetic coupling between the work-coil and the charge is good, the efficiency of power transference will be high.

(b) When the clearance is small the heat loss through lining is high, resulting in low induction melting efficiency.

The heat loss through lining at different clearance or lining thickness may be calculated from equation (1.65). To investigate the magnetic coupling an experiment was carried out to measure the coupled resistance of the charge at various clearances.

An experimental work-coil, made of $^{3}/_{32}$ x $\frac{3}{8}$ inch insulated copper strip, consisting of 43 turns on edge, $3\frac{3}{4}$ inches diameter and 6 inches long was salvaged from an old control device. Four pieces of non-magnetic stainless steel were used, 2, $2\frac{1}{2}$, 3 and $3\frac{1}{2}$ inches in diameter, each $3\frac{1}{2}$ inches long.

The coupled resistance of various charges were measured by a Universal Impedance Bridge Type 314C, Serial No. 1894 made by Dawe Instrument Ltd., London. The results are shown in Table 1.2.

Table 1.2. Coupled Resistance and Heat Loss Through Lining

Coupled Resistance				
Clearance, in.	0.25	0.375	0.625	0.875
R_c, ohm	0.066	0.045	0.026	0.015
Heat Loss through Lining				
Clearance, in.	0.25	0.375	0.625	0.875
Loss, kW	14.9	8.62	4.32	2.32

The graphs of clearance against coupled resistance and heat loss through lining are plotted in Fig. 1.20.

The results show that good magnetic coupling is obtained at the expense of high heat loss through lining. The latter is more important than the former for the

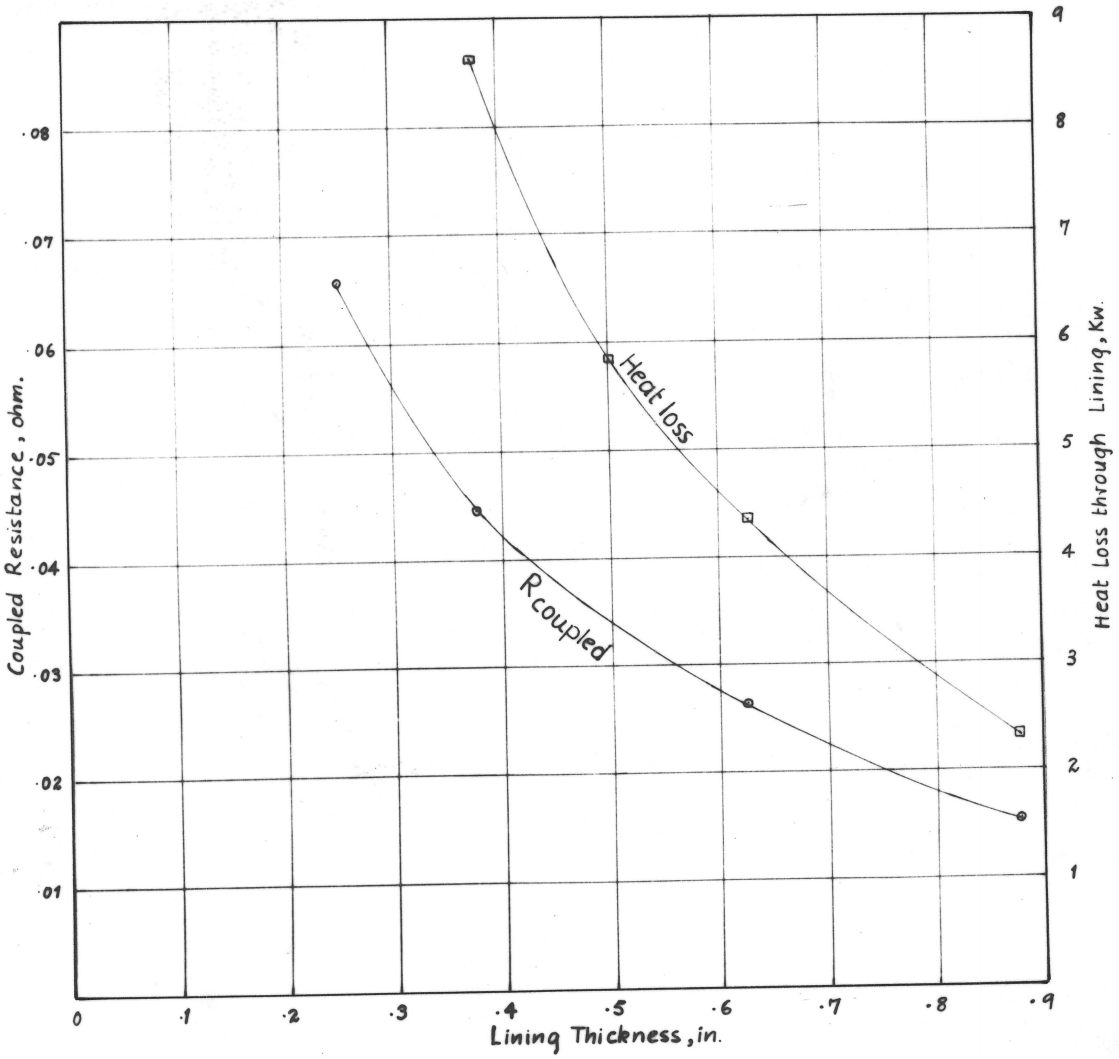


Fig. 1.20 Coupled resistance and heat loss through lining.

small power. If the heat loss is too high, e.g. 9 kW, the charge could not be melted at all. Therefore the clearance between the work-coil and the charge was chosen to be $\frac{1}{2}$ inch.

1.7 Work- Coil

1.7.1 Preliminary Testing

The work-coil used in melting iron at conventional frequencies usually consists of a small number of turns, but its resistance, inductance and impedance at 500 c/s would be very low. It is expected that at the rated voltage, if the work-coil is connected directly to the power source, the current in the supply line would be too high. The purpose of the preliminary testing was to find the resistance, reactance and impedance of the test work-coil and to attempt to increase its effective values.

The test work-coil was the same as that used for the coupled resistance testing. The resistance of this coil was low, and was difficult to measure accurately in the presence of its reactance with the Dawe Impedance bridge. To overcome this a measuring circuit was arranged,[15] Fig. 1.21(a), to cancel the reactive part of the work-coil so that the resistive part only was measured. A is a standard resistance which is slightly higher than

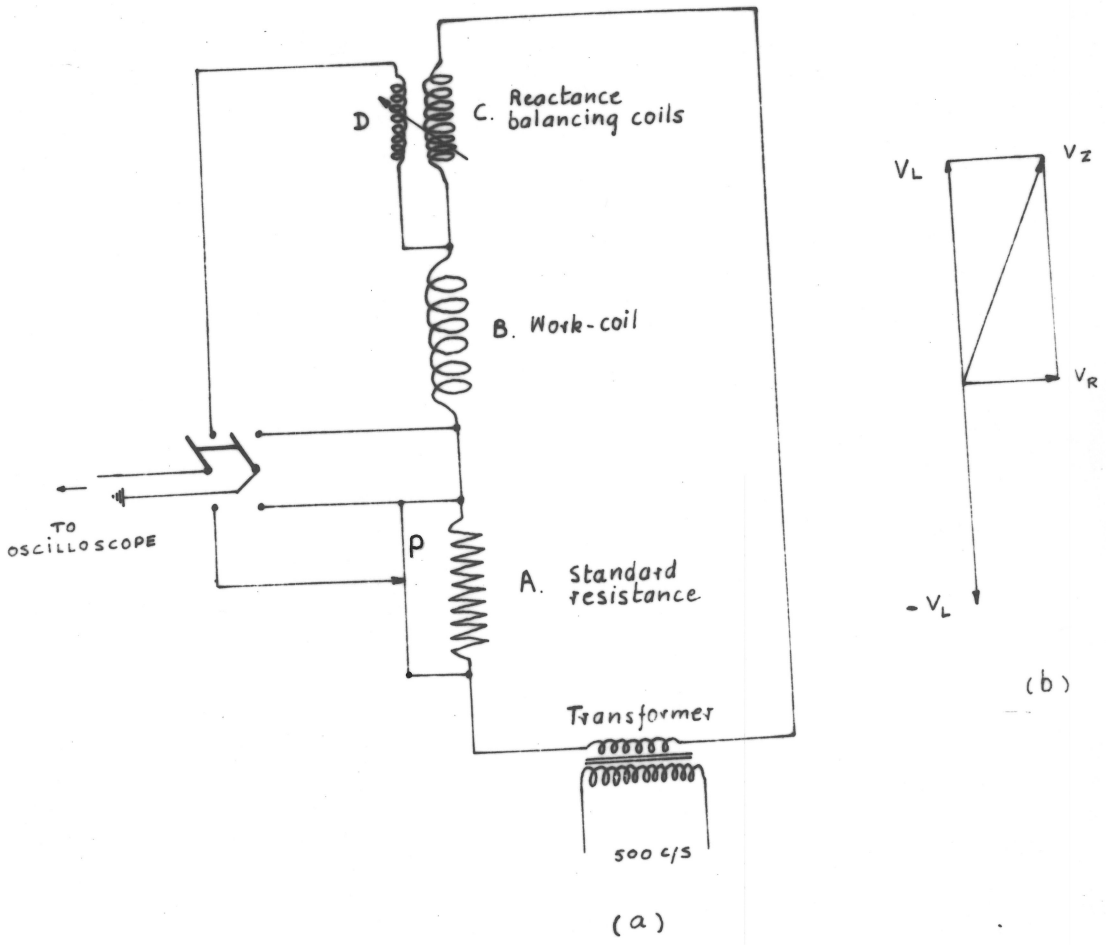


Fig. 1.21 Circuit diagram for impedance and resistance measurements.

the impedance of the coil for an accurate measurement. P is a potentiometer, with 100 divisions, connected to A, therefore one-hundredth of the resistance of A could be measured. B is the test work-coil and C is another coil with a few turns of heavy conductor connected in series with the work-coil. D is a compensating coil, coupled to the coil C. V_1 and V_2 are voltage drops across the work-coil and standard resistance respectively. V_1 is measured by comparison to V_2; they are connected to one beam of the oscilloscope through a double throw switch. The measurement was as follows.

(a) Impedance. Coil D was put away from coil C. The impedance drop of the work-coil was V_1, measured by comparing with the voltage drop across the standard resistance on the one beam of the oscilloscope through the double-throw switch. The impedance can be read directly from the potentiometer.

(b) Resistance. The voltage drop across the work-coil consists of two parts, resistive and inductive, Fig. 1.21(b). To measure the resistive drop only the inductive drop must be cancelled out. This may be done by sliding coil D inside coil C until the reversed induced e.m.f. ($-V_L$) in coil D by coil C cancels out the inductive part of the work-coil voltage. This is shown on the oscilloscope screen when the voltage across the

work-coil reaches its minimum value which is the resistive voltage drop only. The value of this voltage drop was compared to the voltage drop in the standard resistance by the potentiometer, and the pure resistance of the work-coil was thus obtained.

For resistance measurement it was found necessary that the number of turns of coil D must be large enough so that its induced e.m.f. at the centre of coil C must be greater than $-V_L$, Fig. 1.21(b), otherwise the induced e.m.f. would not be enough to cancel V_L.

A double beam method may be used to measure impedance, resistance and inductance of the work-coil, i.e. V_1 is connected to one beam and V_2 to the other. It has an advantage that the phase balance by coil D can be seen clearly on the screen of the oscilloscope, but there may be an error if the calibrations of the two traces are different, so the single beam method is preferable.

The results are shown in Table 1.3.

The impedance of coil with charge is 0.328 ohm. If the parallel capacitor of 987 μF is used for the unity power factor correction the total impedance of the parallel circuit is 1.68 ohm. At the rated voltage of 180 volts the current would be 107 amperes. This is too high because the rated current is only 56 amperes.

Table 1.3. Resistance, Impedance and Reactance of Test-Coil (at 500 c/s)

	Coil only	Coil with charge
Resistance, ohm	0.017	0.062
Impedance, ohm	0.368	0.328
+Reactance, ohm	0.368	0.322
+Inductance, μH		100.2
+Parallel capacitance for unity power factor, μF		987

charge = 3 inches diameter, $3\frac{1}{2}$ inches long non-magnetic steel.

\+ = calculated values

The required parallel impedance for the rated current at the rated voltage is

$$\frac{180}{56} = 3.21 \text{ ohms}$$

or at 25% overload,

$$\frac{180}{70} = 2.56 \text{ ohms.}$$

The result in Table 1.3 is for the test-coil which has 43 turns. In a practical work-coil the number of turns will need to be less than this because the conductors in the coil must be water-cooled, and so fewer turns of a larger conductor must be used. Assuming about 15-20 turns, its impedance will be much lower than that of the test-coil. It is clear that with the low impedance the full power source could not be utilized and the

parallel capacitor required for the unity power factor correction will be too high (and therefore too expensive).

In order to use the full power source it is necessary to increase the effective impedance of the work-coil circuit. It may be done by,

(a) placing a laminated silicon steel core around the work-coil to increase the magnetic flux produced by it,

(b) putting an auto-transformer between the work-coil and the power source. The effective impedance and inductance of the work-coil will be increased by the square of the ratio of primary to secondary turns, but the transformer must be rated for the full kVA of the load in work-coil (which has a low power factor).

A laminated silicon steel core was tried first. It had 2.97 sq. in. cross sectional area, 4 x 8 inch window size. It was found that with the core surrounding the loaded work-coil the capacitors available (760 microfarads) were not enough to correct the power factor of the work-coil to unity, so that the use of a transformer was necessary.

For testing a simple auto-transformer was made. The transformer core was made of grain oriented silicon steel sheet .004 inch thick. 6.95 sq.in. cross sectional area, 5 x 8 inches window size.

The number of primary turns calculated by equation (1.64) is 18 turns. But for testing, 15 turns were used to get more effect when the transformation ratio was changed. The primary and secondary were made of $\frac{1}{2}$ inch O.D. copper tube, 0.048 inch wall thickness. The tapping was arranged at the secondary for the transformation ratio of $\frac{15}{6}$, $\frac{15}{5}$ and $\frac{15}{4}$.

The test was carried out by connecting the high side of the transformer to the measuring circuit similar to Fig. 1.21(a) and the low side to the work-coil.

The impedance and resistance measured at the primary included those of the primary and the equivalent values of the secondary and work-coil referred to the primary.

By varying the ratio of the primary to secondary the equivalent impedance of secondary and work-coil may be increased or decreased until the right impedance is obtained, that is the full power could be drawn from the supply source to the primary. The result is shown in Table 1.4.

Table 1.4 shows that the impedance measured at the primary may be increased by increasing the ratio of primary to secondary.

A further test was carried out to measure the

Table 1.4. Impedance and Resistance of Loaded Test-Coil at Primary of Transformer

Ratio of P:S	Test-coil with Charge	
	Resistance ohm	Impedance ohm
15:6	0.405	1.79
15:5	0.560	2.46
15:4	0.925	3.54

number of ampere-turns of the test-coil required at full load, and unity power factor correction. This was done with the ratio of primary to secondary at 15:5 and the test-coil was surrounded by the core of 2.97 square inches cross section area used earlier. It was found that at 12.5 kW the number of ampere-turns required was 15,000.

1.7.2 Design

The physical size of the charge to be melted, allows an estimate to be made of the inside diameter and length of the work-coil. The number of turns and the conductor cross-section can then be determined.

The basic requirements for the work-coil are:

(a) There are enough ampere-turns to melt the charge.

(b) There is a good magnetic coupling between work-coil and charge.

(c) Heat loss in work-coil is at a minimum.

1.7.3 Ampere-turns

The number of ampere-turns was measured by the preliminary experiment, but it may be calculated as follows.

From previous consideration (section 1.5) the power input required in the work-coil is about 8.4 kW. Assuming a perfect magnetic coupling the power developed in the charge is also 8.4 kW. On this assumption equation (1.31) may be used to calculate the number of ampere-turns of the work-coil. The work-coil length is 7 inches.

$$P = \frac{4\pi N^2 \mu \omega I^2 . W(ma).V}{l^2} \quad \text{ergs sec}^{-1}$$

P = power developed in charge,

$= 8.4 \times 10^3 \times 10^7$ ergs sec^{-1}

V = volume of charge

$= 395$ cm^3

l = length of work-coil

$= 7 \times 2.54$ cms

$\mu = 1.$

W(ma) = .322 from Fig. 1.4 when m = .575, a = 1.35 x 2.54 and ma = 2.

$$\therefore N^2I^2 = \frac{8.4 \times 10^3 \times 10^7 \times (7 \times 2.54)^2}{4\pi \times 1 \times 2\pi 500 \times 0.322 \times 395}$$

$$= 5.27 \times 10^6$$

NI = 2270 ampere-turns, e.m.u.

= 22700 ampere-turns.

Assuming 70 per cent power transference efficiency, 22700 ampere-turns input to the work-coil will develop 5.9 kW in the charge. This is about the power required to melt 6.63 lbs. charge in an hour described in section 1.5.

The number of ampere-turns obtained from the preliminary experiment was 15000 ampere-turns. The big difference from the calculated value is due to the fact that in the experiment the work-coil was surrounded by the iron core so the number of ampere-turns was less.

1.7.4 Diameter and Length of Work-Coil

The magnetic coupling depends on the clearance between charge and work-coil and the diameter and length of both. The diameter of the work-coil is fixed by the diameter of the charge which is $2\frac{3}{4}$ inches and the clearance between them which is $\frac{1}{2}$ inch from the previous consideration. If a spacing of $\frac{1}{8}$ inch is allowed between the charge and the crucible the diameter of the work-coil is 4 inches.

In induction heating the length of the work-coil should be more than 20 times the spacing between the coil and the charge to minimize the end effect.[18] But this is

not practical for induction melting of small diameter charges, since it will complicate the making and repairing of crucible and pouring of the melt.

The proper length of the work-coil for a short charge may be found by measuring the coupled resistance of the charge at various lengths of the work-coil keeping the number of turns constant. This would require a few work-coils with different widths of copper strip. It was not attempted because long copper strip was needed and the coil made could not be used for further tests.

The length of the work-coil may be also judged from the distribution of magnetic flux inside it. The relative magnetic field intensity inside the coil was measured by a search-coil connected to an oscilloscope. The test coil was the same as that used for testing the coupled resistance. The result is shown in Table 1.5 and Fig. 1.22.

The relative magnetic field strength inside the coil may be calculated from,[19]

$$H_p = 2\pi I n (\cos\theta_1 - \cos\theta_2) \text{ oersted} \quad \ldots \quad (1.68)$$

H_p = magnetic field strength at p along the axis of coil.

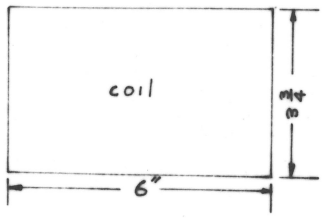
I = current in coil, abs.

n = number of turns per cm.

θ_1, θ_2 = are shown in Fig. 1.23.

Table 1.5 Relative magnetic field strength in coil

Distance from end, in	0	½	1	1½	2	2½	3	3½	4	4½	5	5½	6
Relative field strength	0.9	1.07	1.22	1.4	1.5	1.57	1.6	1.57	1.5	1.4	1.2	1.05	0.9



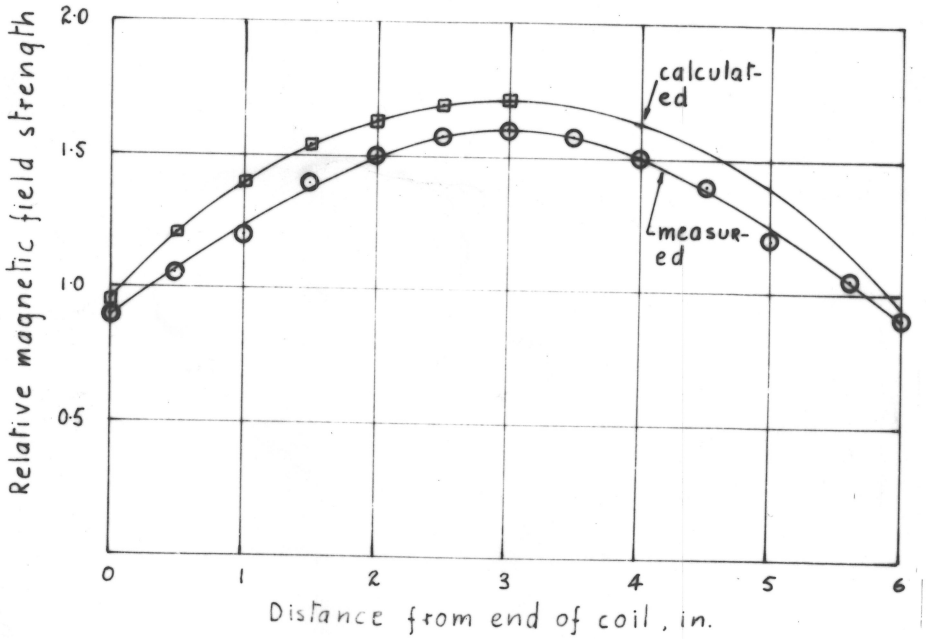


Fig. 1.22 Relative magnetic field strength in coil

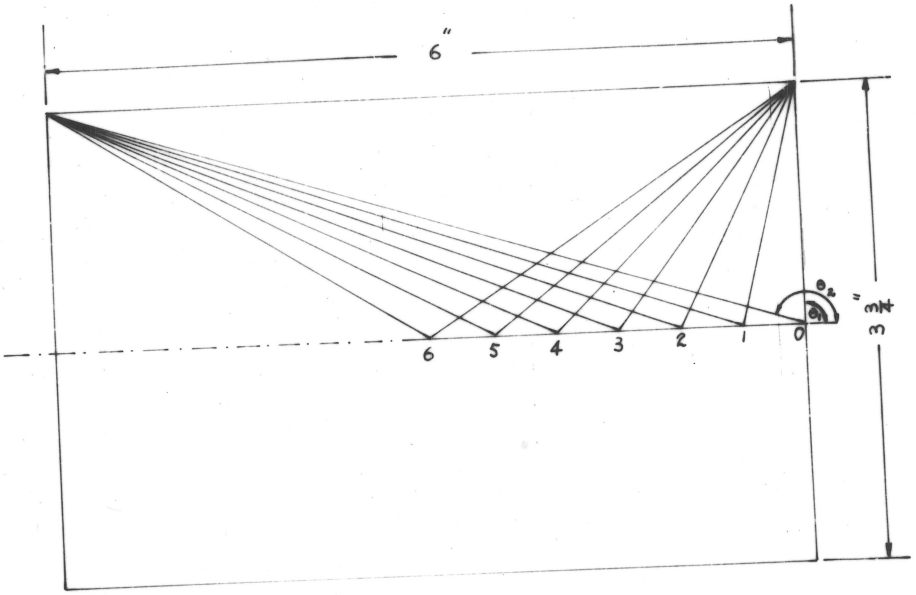


Fig. 1.23 Angles for relative magnetic field strength calculation.

Table 1.6 Calculated relative magnetic field strength in short coil

no.	θ_1	$\cos\theta_1$	θ_2	$\cos\theta_2$	$\cos\theta_1 - \cos\theta_2$
0	90	0	163	−0.956	0.956
1	75	0.259	161.5	−0.948	1.207
2	62	0.469	160	−0.939	1.408
3	51.5	0.622	158	−0.927	1.549
4	43.5	0.725	155.5	−0.910	1.635
5	37	0.798	152.5	−0.887	1.685
6	32	0.848	148.5	−0.853	1.701

The calculated relative field strength is shown in Table 1.6 and Fig. 1.22.

The calculated and measured results are in agreement and show that the magnetic field strength decreases rapidly from the centre towards its ends which are about 56% of that at the centre.

The magnetic lines of force was also traced by spreading iron powder on a white paper and inserting it inside the coil, Fig. 1.24. It shows that the magnetic lines of force comes out of the coil, to complete its magnetic circuit, not only at the ends but also at the side.

From above considerations the work-coil should have the same length or be shorter than the charge (which was chosen to be $3\frac{3}{4}$ inches long) for an efficient induction heating. But this is not practical for the induction melting. Therefore the work-coil length was chosen to be 7 inches allowing the spaces for a crucible and a laminated core which will be described later.

1.7.5 Number of Turns and Thickness of Copper Tube

For a given number of ampere-turns and a given diameter and length of work-coil and charge the number of turns of the work-coil is independent of the efficiency

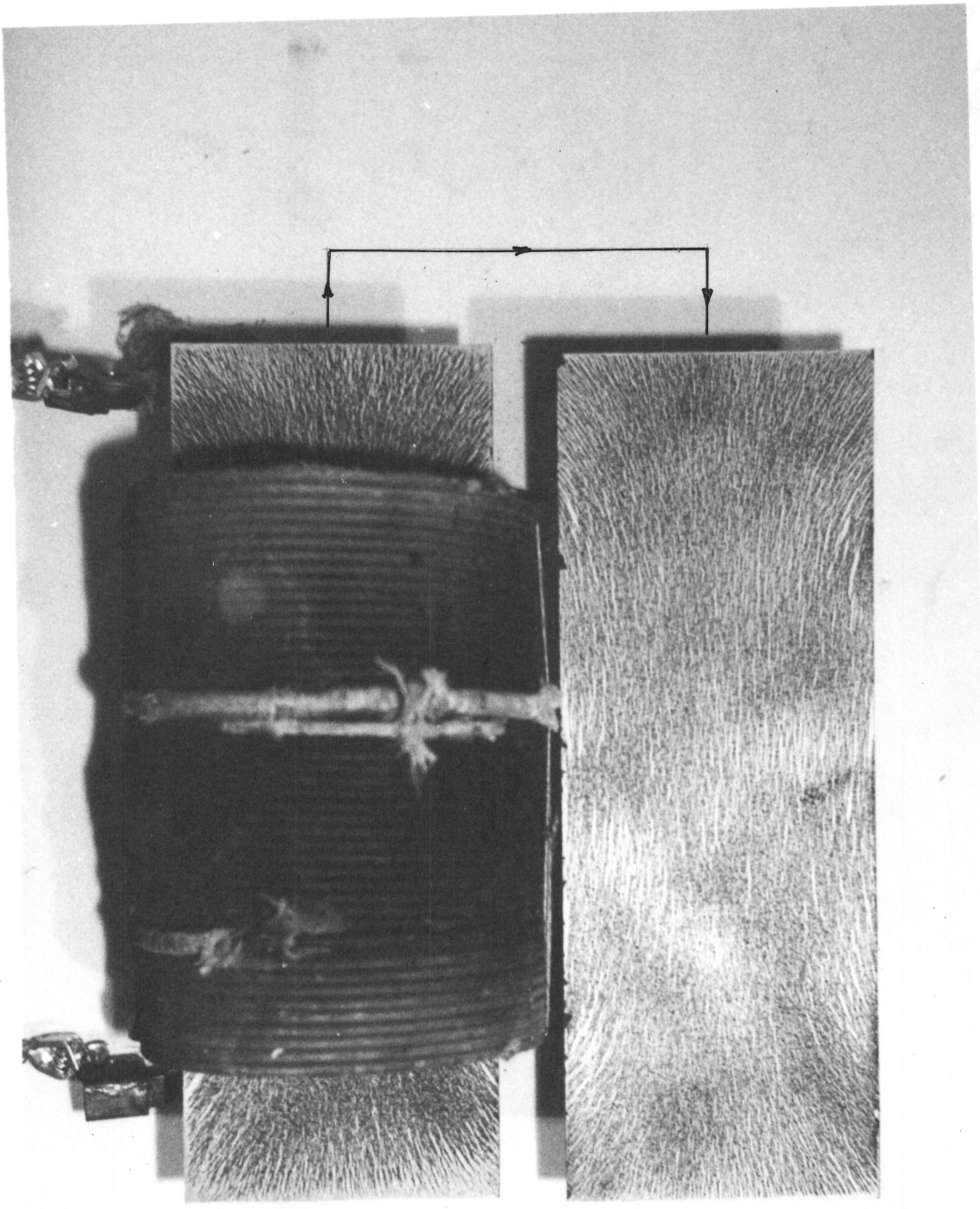


Fig. 1.24 Tracing of magnetic lines of force in short coil by iron powder.

of induction heating and the power loss in the coil. It only effects the work-coil inductance. They may be considered as follows.

From equation (1.50) for a long coil and long charge

$$\eta = \frac{R_c}{R_1 + R_c}$$

$$\text{or} \quad \eta = \frac{r_o l_o \sqrt{\rho_o \mu_o}}{r_o l_o \sqrt{\rho_o \mu_o} + r_1 l_1 \sqrt{\rho_1 \mu_1}}$$

The number of turns does not appear in the efficiency equation.

For a short coil and short charge, R_c is multiplied by a correction factor which is constant, therefore the above consideration is still valid.

The power loss in the work-coil operated at given ampere-turns and with a definite diameter and length is as follows:

Let NI = K

N = total number of turns of work-coil

I = current in work-coil

l = work-coil length

r = work-coil radius

ρ = work-coil resistivity

w = width of one coil

δ = depth of current penetration, it is constant at a constant frequency

$$N = \frac{1}{w}$$

$$\therefore \quad I = K.\frac{w}{1}$$

The resistance of work-coil is

$$R = \rho . \frac{L}{a}$$

$$L = 2\pi r N$$

$$= 2\pi r \frac{1}{w}$$

$$a = \delta . w$$

$$\therefore \quad R = \frac{\rho . 2\pi r 1}{\delta w^2}$$

Power loss in the work-coil is

$$P = I^2R$$

$$= \frac{K^2 \rho 2\pi r}{1 \delta}$$

$$= \text{constant}$$

This shows that for a given number of ampere-turns the two factors (ampere and turn) may be chosen, as long as their product remains constant, without effecting the I^2R loss of the work-coil.

The inductance of the work-coil may be expressed as follows:

$$L = \frac{N \Phi}{I.10^8} \text{ henries} \qquad \ldots . \qquad (1.69)$$

N = no. of turns of work-coil

I = current in coil, amperes

ϕ = magnetic flux produced by the coil, maxwells

$$\phi = \frac{0.4\pi N I}{\mathcal{R}} \qquad \ldots . \qquad (1.70)$$

$\mathcal{R}$ = reluctance of magnetic path

$$\mathcal{R} = \frac{l}{\mu A} \qquad \ldots . \qquad (1.71)$$

l = length of magnetic path, cm.

A = cross sectional area of magnetic path, cm^2

μ = relative permeability of magnetic path

$$\therefore \quad \phi = \frac{\mu\, 0.4\pi N I A}{l}$$

$$\therefore \quad L = \frac{\mu\, 0.4\pi N^2 A}{1.10^8} \text{ henries} \qquad \ldots . \qquad (1.72)$$

The current does not appear in equation (1.72). This indicates that for a given number of ampere-turns, at a constant frequency and permeability, the coil which has more turns has higher inductance than that with less turns.

In the present work it was necessary to use an auto-transformer to increase the effective impedance of the heating circuit, then the number of turns is not important in connection with the inductance and impedance.

The factor which limits the number of turns of the work-coil is the size of its cooling coil. In practice the amount of current flow in the work-coil is of the order of 1000 amperes or more. The I^2R loss of the work-coil is high and it will be too hot without cooling water. The cooling coil must have enough passage to allow the

water from the main supply to cool the work-coil down to a temperature of about 60°C. Also it should be free from blockage due to water sediments for a reasonable length of time of service. A copper tube $\frac{1}{4}$ inch O.D., $^{5}/_{32}$ inch I.D. was chosen for cooling. It was soft soldered on a $\frac{3}{8}$ x $\frac{3}{8}$ inch copper bar and they were wound to form the work-coil.

The thickness of copper bar for making the work-coil may be calculated from the depth of current penetration.

From equation (1.19)

$$\delta = \frac{1}{2\pi}\sqrt{\frac{\rho}{\mu f}} \text{ cms}$$

$\rho = 2 \times 10^{-6}$ ohms cm^3 for copper at 60°C

$= 2 \times 10^{3}$ e.m.u.

$\mu = 1$

$f = 500$ c/s

$$\therefore \quad \delta = \frac{1}{2\pi}\sqrt{\frac{2 \times 10^{3}}{1 \times 500}}$$

$= 0.318$ cms.

Stansel[5] showed that for a hollow copper tube the optimum radial thickness of the copper tube should be,

$r = 1.58\,\delta$

r = radial thickness of copper tube

$$\therefore \quad r = 1.58 \times 0.318$$

$= .502$ cms.

With the $\frac{1}{4}$ inch copper tube attached on $\frac{3}{8}$ x $\frac{3}{8}$ inch (.952 x

.952 cm) copper bar the heat loss in the work-coil should be at a minimum.

The coil length considered in section 1.7.4 was 7 inches, hence the number of turns of the work-coil was 17 turns.

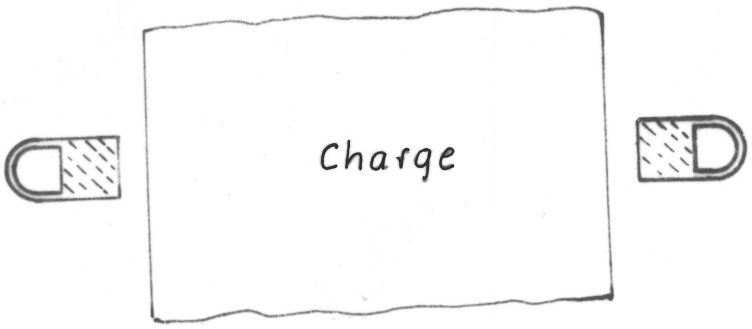
1.7.6 Cross-sectional Area

A few words may be said about the cross-sectional area of the work-coil tube. The induced eddy current in the charge will flow in the opposite direction to the alternating current flow in the work-coil. This causes the eddy current to concentrate at the surface of the charge and the alternating current to concentrate at the inner circumference of the work-coil. Thus the cross-sectional shape of the work-coil tube should be of one of the types shown in Fig. 1.25.

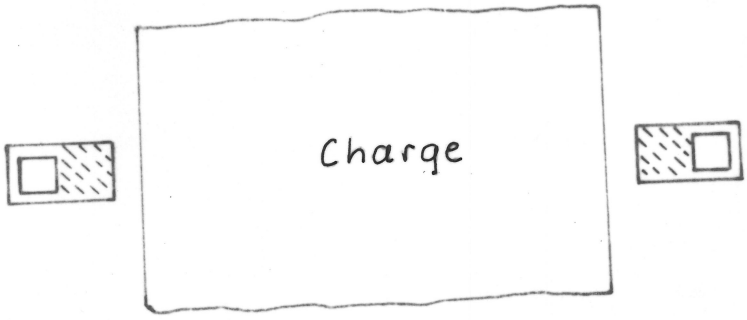
The copper tube having cross-sectional shape as in Fig. 1.25(a) and (b) was not available. Fig. 1.25(c) could be made at the workshop.

1.7.7 Construction

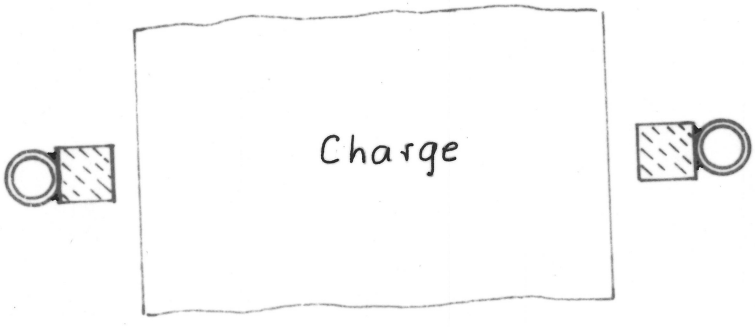
The $\frac{1}{4}$ inch copper tubing was soft soldered on a $\frac{3}{8}$ x $\frac{3}{8}$ inch copper bar. The copper bar was coiled on a steel pipe former on a lathe into the work-coil consisting of 17 turns of 4 inches inside diameter and 7 inches long. The soft soldering made the construction simple, but



(a)



(b)



(c)

Fig. 1.25 Cross-sectional area of work-coils

annealing after coiling to reduce the resistance of the work-coil to a minimum was not possible.

A glass tape was wound on the work-coil to insulate between turns, and the outside of the work-coil was covered with epoxy resin to increase its strength. This prevented movement along its length due to the magnetic force between adjacent coils when the current flows in them. The epoxy resin which spread inside the work-coil was cleaned off, otherwise it would burn during melting the charge and cause contamination to the molten charge. The section of three coils of the work-coil is shown in Fig. 1.26.

The bottom end of the work-coil was bolted to one end of a $\frac{3}{8}$ x $2\frac{1}{2}$ x 8 inch copper bar. The other end of the bar was connected to the outer tube of the co-axial lead. The top end of the work-coil was silver-brazed to a connection which clamped on the inner tube of the co-axial lead.

1.7.8 Testing

The work-coil was tested for

(a) Resistance, impedance and reactance

(b) Power factor

(c) Efficiency

(d) Melting Charge

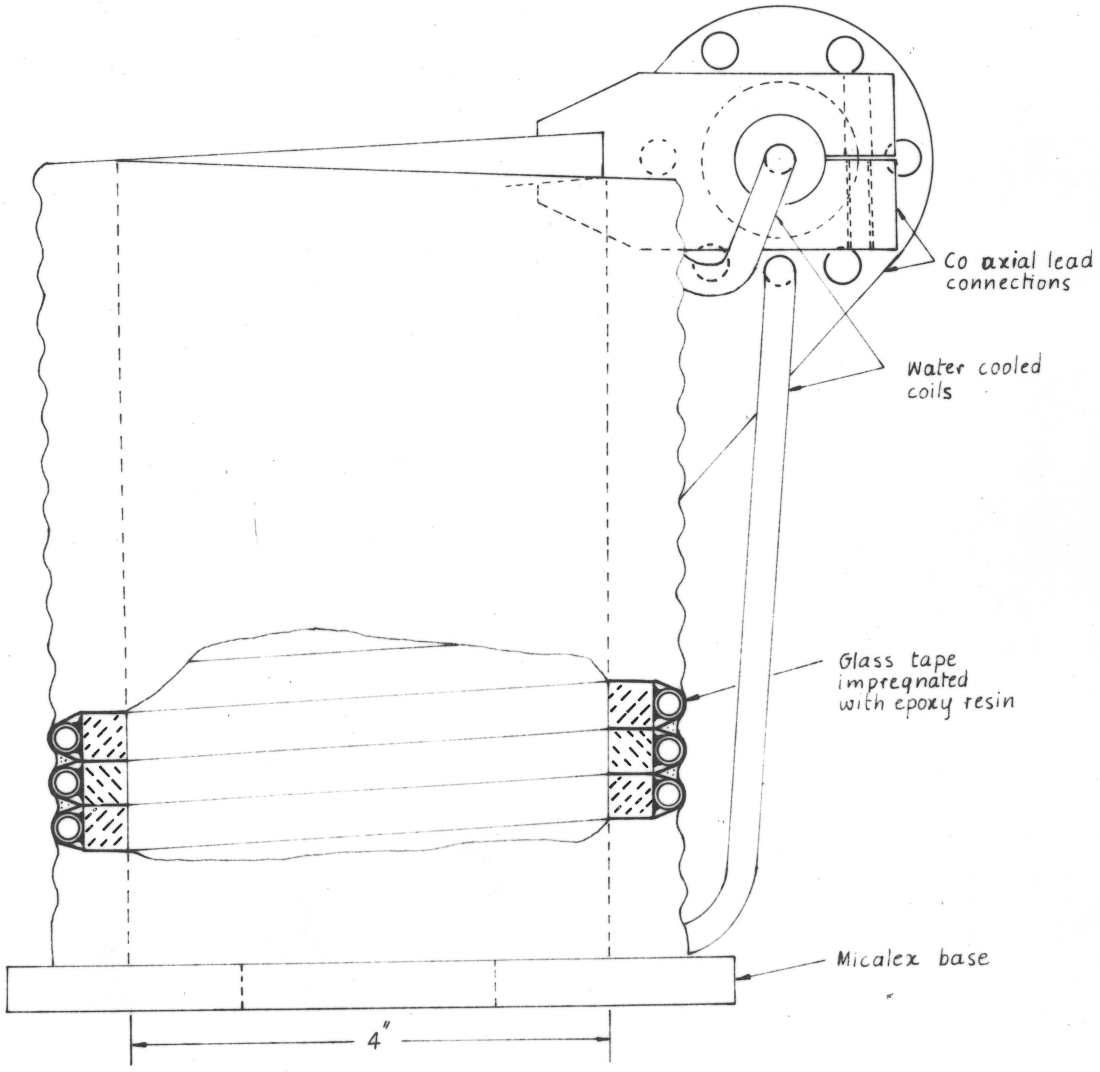


Fig. 1.26 Work-coil.

1.7.9 Resistance, Impedance and Reactance

The resistance and impedance of the work-coil was measured by the circuit set up in Fig. 1.20(a) with the oscilloscope. The result is shown in Table 1.7.

Table 1.7. Resistance, Impedance and Reactance of Work-coil (at 500 c/s)

	Work-Coil only	Work-coil and charge
Resistance, ohm	.0032	.0086
Impedance, ohm	.0515	.045
+Reactance, ohm		.044
+Inductance, μH		14.0
+Parallel capacitance for unity power factor, μF		7230

charge = 3 inches diameter, $3\frac{1}{2}$ inches long, non-magnetic steel.

\+ = calculated values

The impedance of the work-coil with charge is 0.045 ohm, its inductance is 14 μH, and required capacitors of 7230 μF for unity power factor correction. The parallel impedance of this circuit will be 0.221 ohm which is very low. It was necessary to use an auto-transformer to increase the effective impedance so that the full power source could be drawn from the power supply and also decrease the amount of capacitor for the unity power factor correction.

The effective impedance and resistance measured at the primary of the transformer at various transformation ratios is shown in Table 1.8.

Table 1.8 Effective Impedance, Resistance and Reactance of Work-coil at Primary (at 500 c/s)

Work-coil with charge	Ratio of P:S		
	15:6	15:5	15:4
Resistance, ohm	0.081	0.120	0.196
Impedance, ohm	0.314	0.452	0.691
+Reactance, ohm	0.303	0.435	0.663
+Parallel capacitance for unity power factor, μF	1050	732	480
+Parallel impedance, ohm	1.41	1.58	2.27

+ = calculated values

With the ratio of primary to secondary 15:4 the parallel impedance of the circuit is 2.27 ohm. This is a workable impedance.

The effect of using the core surrounding the work-coil was also tested, and shown in Table 1.9.

The presence of the core increases the magnetic flux produced by the work-coil, thus the effective reactance and coupled resistance were increased, but the use of the core introduces the problem of its weight, cost and fitting which will be described later.

Table 1.9 Effective Impedance, Resistance and Reactance of Work-coil Circuit at Primary with Core Surrounding Work-coil (at 500c/s)

Work-coil with charge and core	Ratio of P:S		
	15:6	15:5	15:4
Resistance, ohm	0.110	0.165	0.260
Impedance, ohm	0.445	0.635	0.985
+Reactance, ohm	0.431	0.615	0.950
+Parallel capacitor for unity power factor	737	518	335
+Parallel impedance, ohm	1.69	2.28	3.65

charge = 3 inches diameter, $3\frac{1}{2}$ inches long, non-magnetic steel.

core = grain oriented silicon steel, 2.97 sq. in. cross section area, 4 x 8 inch window size.

\+ = calculated values

1.7.10 Power factor

The power factor of the work-coil with 3 inches diameter, $3\frac{1}{2}$ inches long, non-magnetic steel, is from Table 1.7,

$$\cos\theta = \frac{0.0086}{0.045}$$

$$= 0.191$$

1.7.11 Efficiency of Work-coil

From Table 1.7, the resistance of the work-coil is 0.0032 ohm (R_1) and the resistance of the work-coil with

non-magnetic charge is 0.0086 ohm ($R_1 + R_c$), therefore the work-coil efficiency is

$$\eta = \frac{R_c}{R_1 + R_c} \times 100$$

$$= \frac{0.0054}{0.0086} \times 100$$

$$= 62.8\%$$

1.8 Melting Mild Steel Charge

A melting of a mild steel charge in the new work-coil was carried out to ascertain that the overall system was workable.

The charge was a solid mild steel cylinder $2\frac{3}{4}$ inches diameter, $3\frac{3}{4}$ inches long. The lining of the work-coil was made of zircon sand, zircon flour and magnesium silicate bonding. A short piece of iron core, 2 inches long, 2.97 sq.in. cross sectional area was inserted at the bottom of the work-coil with a water cooled copper coil on its surface. The auto-transformer was the same as that used in the preliminary testing. The transformation ratio was 3:1. The capacitor used for a unity power factor correction above the Curie point of the mild steel was 720 microfarads (without the short piece of iron core the capacitor required was 760 microfarads).

After warming up period for five minutes with 5 kW the power was increased to 10 kW for 25 minutes. Then the power was raised to 12.5 kW and the charge melted in 10 minutes. The total melting time was 40 minutes.

1.9 Auto-Transformer

From the previous experiment in section 1.7.9, the transformation ratio required was about 3:1. At this moderate transformation ratio an auto-transformer has an advantage over a two winding transformer. It requires smaller amounts of copper winding.

1.9.1 Design

1.9.2 Number of Turns

The number of turns may be calculated from equation (1.64)

$$N_1 = \frac{E_{r.m.s.}}{4.44 \phi_m . f . 10^{-8}}$$

The transformer core was grain oriented silicon steel, 44.8 sq.cm. cross-section area and its maximum flux density was 10,000 maxwell per sq.cm.

$\therefore \phi_m$ = 10,000 x 44.8 maxwell

f = 500 c/s

E = 180 volts (rated voltage)

$$\therefore N_1 = \frac{180 \times 10^8}{4.44 \times 10,000 \times 44.8 \times 500}$$

= 18 turns

The induced e.m.f. per turn is $\frac{180}{18} = 10$ volts.

The number of turns was calculated for the condition that the iron core was operated at its maximum flux density. Under a certain operating voltage, e.g. 180 volts, if the tapping at the primary of the auto-transformer is arranged so that the number of turns is 15, this will cause an excessive loss in the core due to the flux produced in the core exceeding the maximum flux density, e.g.

When $E = 180$ volts

$f = 500$ c/s

$B_m = 10{,}000$ maxwell cm^{-2}

$N_1 = 18$

If $N = 15$ turns the flux density in the core would be

$$B = 10{,}000 \times \frac{18}{15}$$

$$= 12{,}000 \text{ maxwell } cm^{-2}$$

and the number of volts per turn is

$$\frac{180}{15} = 12 \text{ volts}$$

To produce the flux density of 12,000 maxwell per sq.cm. excessive magnetizing current is required and the core loss above its maximum flux density is high.

From the above consideration the number of volts per turn should be 10.

1.9.3 Construction

To minimize the I^2R loss the thickness of copper tube used for construction of the transformer winding should be 0.502 cms. (section 1.7.5), but for the ease of manufacturing the ordinary $\frac{1}{2}$ inch O.D. copper tube was chosen for primary winding.

The secondary was made of $\frac{1}{4}$ x 1 inch copper bar. It was coiled to six turns on a steel tube whose diameter was slightly larger than that of the core. A $\frac{1}{4}$ inch copper tube was soft-soldered on the secondary coil for water cooling. A glass tape was wound on it for insulation. The primary was made of $\frac{1}{2}$ inch diameter copper tube, 0.048 inch wall thickness, and coiled to 12 turns. The length of the primary coil is about the same as that of the secondary. One end of each coil was joined together by silver solder. This made the number of turns of the primary 18 and the secondary six. Tapping was arranged at the primary for the transformation ratios of $\frac{18}{6}$, $\frac{17}{6}$ and $\frac{15}{6}$. Two ends of the secondary were connected to the outer and inner tube of the co-axial lead.

The laminated transformer core has a cross-sectional area of 44.8 sq.cm. The thickness of the silicon steel

sheet is 0.004 inch. The thinnest available sheet was selected to reduce the core eddy current loss. The core consists of two parts. They are clamped together by a silicon steel strip and a tightening bolt and nut. Its window dimension if $7\frac{3}{4}$ x $4\frac{1}{4}$ inches and weight 67 lbs.

The primary, the secondary, and the transformer core when assembled together are hung on one end of the co-axial lead outside the vacuum tank. This design was to permit the auto-transformer to rotate with the crucible while pouring. The advantage of this setting was to avoid the use of a heavy flexible lead between the auto-tranformer and the co-axial lead which would be necessary if the auto-transformer were fixed. The copper loss through these leads was also eliminated.

To hold the auto-transformer firmly on the end of the co-axial lead, two aluminium plates $\frac{3}{8}$ x $3\frac{1}{2}$ x $16\frac{1}{2}$ inches were clamped on the auto-transformer core by four $\frac{5}{8}$ inch bolts and two one inch bolts.

It was found necessary to insulate these bolts from the two alumina plates, otherwise they would form a close loop around the transformer core and become hot due to eddy current heating.

The two top one inch bolts were machined off-centre at their ends. A $\frac{3}{8}$ inch hole was drilled through each

bolt. The two off-centre bolts were turned to press the top part of the transformer core on the bottom part while tightening up their nuts. In this way the two parts of the core were clamped together tightly, the vibration of the transformer core under the alternating flux of 500 c/s was reduced considerably.

A photograph of the transformer with two calmped aluminium plates hung on one end of the co-axial lead tubes, together with electrical and water connection and pouring handle is shown in Fig. 1.27.

1.9.4 Testing

The testing was done in a conventional way to determine:-

(a) Core loss

(b) Copper loss

(c) Leakage reactance

(d) Efficiency

1.9.5 Core Loss

The transformer core is subjected to the alternating flux produced by the primary winding. There will be hysteresis loss and eddy current loss in the core. They are called core loss.

From equation (1.1) the hysteresis loss is

$$P_h = \eta B_m^{1.6} \quad \text{ergs per cycle per cc. of core}$$

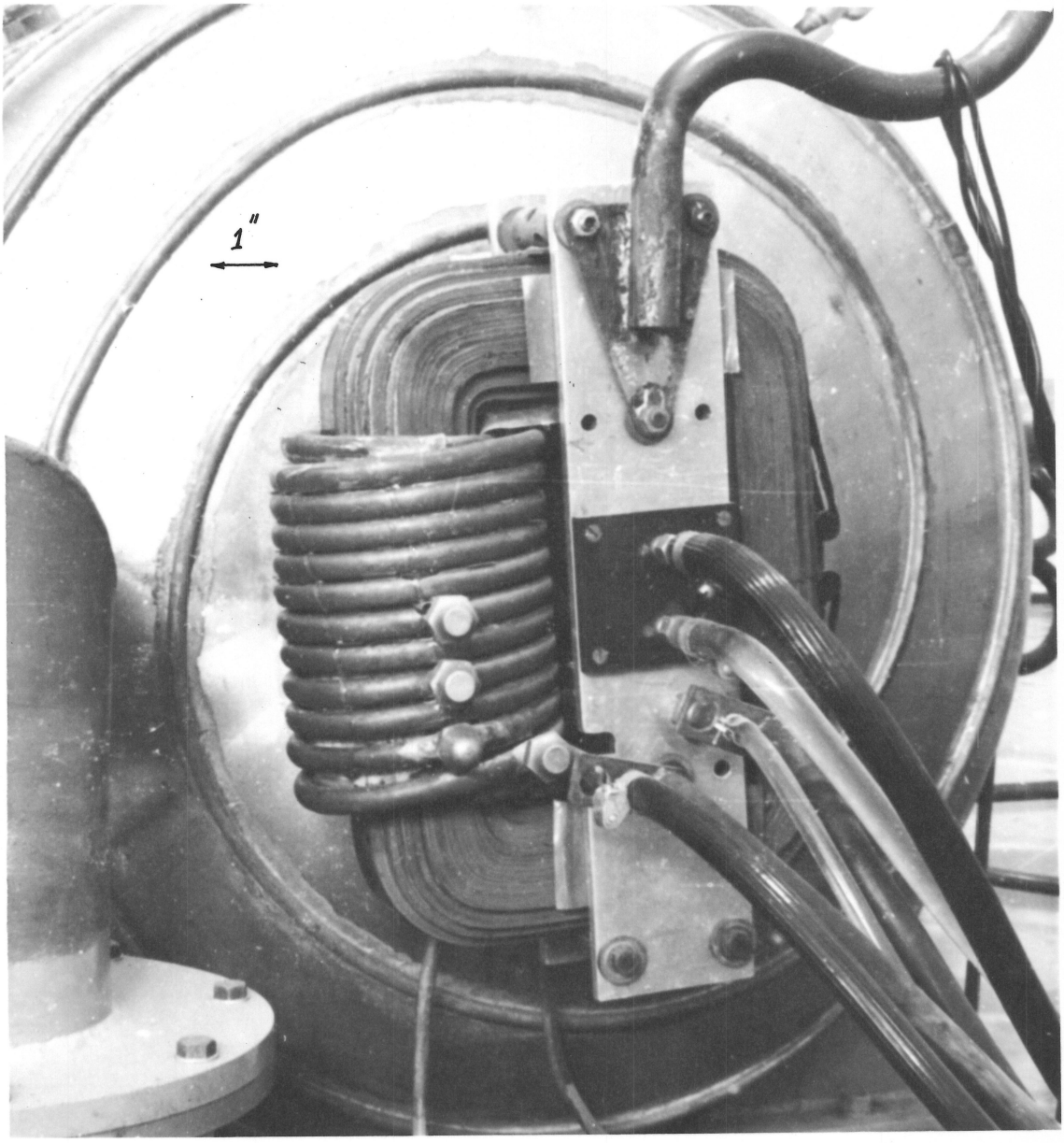


Fig. 1.27 Auto-transformer, with clamp, electrical and water connections and pouring handle.

η = a constant depending of the material

For very pure iron η is low, and the hysteresis loss of the pure iron would be low, but it is difficult to produce iron of sufficiently high purity at low cost. There are always small quantities of impurities present in the commercial transformer steel such as nitrogen. This will cause age-hardening of iron and increase the hysteresis loss. Silicon has been added to iron to prevent this ageing. When the silicon steel is cold rolled and properly annealed it will contain a large number of grains aligned in the direction of rolling. This will further reduce the hysteresis loss.

The eddy current loss may be considered from the following equation

$$P_e = \frac{(\pi t B_m)^2}{6\rho} \cdot 10^{-16} \text{ watts per cc. of core}$$

t = thickness of core sheet, cm.

f = frequency, c/s

ρ = resistivity of core material, ohm-cm.

The eddy current loss is reduced when t is small and ρ is high. The resistivity of silicon steel is higher than that of pure iron. So the silicon steel sheet was used for the transformer core. The thickness of the sheet was 0.004 inch.

The test for core loss is an open circuit test.

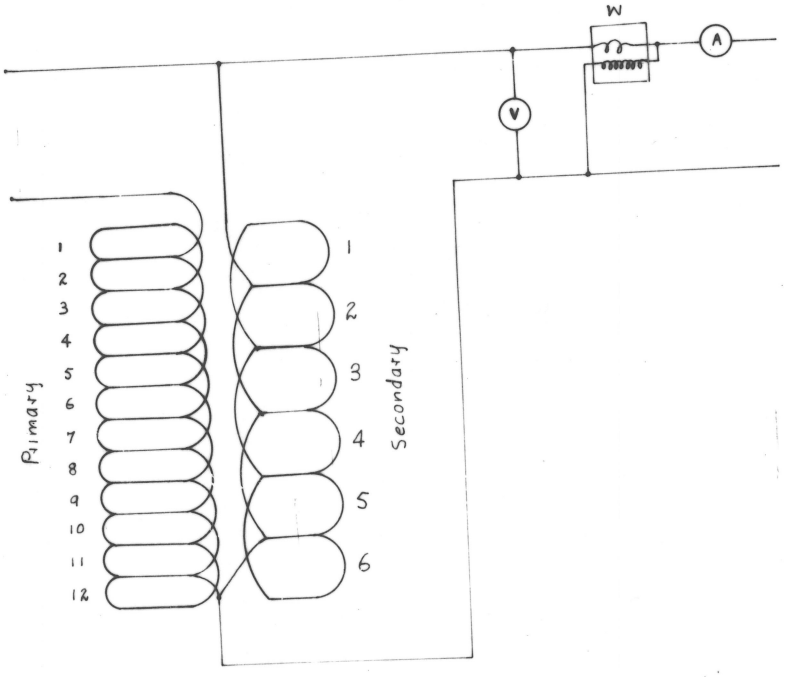


Fig. 1.28 Diagram of open circuit test for core loss.

In Fig. 1.28 the primary is open circuited and the power source was supplied to the secondary which is six turns. The power read from the wattmeter (after correcting the error due to meters) was the iron core loss and the secondary I^2R loss. As the exciting current was small and the resistance of the secondary winding was low, the I^2R loss may be neglected.

A series of readings for the various applied voltages was taken to evaluate the core loss as well as plot the magnetization curve. The results are in Table 1.10.

Table 1.10 Open Circuit Test, Primary Opened Circuit, Secondary Six Turns

Applied Voltage, Volts	No. of Volts per turn, V/6	Current, amp.	Core loss, watts
1.76	0.29	0.84	5
5.3	0.88	2.08	12
10.5	1.75	3.3	25
21.5	3.58	5.7	70
31.0	5.17	7.6	129
45.0	7.50	9.0	195
54.0	9.00	10.4	285
63.5	10.58	12.0	420
71.5	11.91	14.1	600
78.0	13.00	16.5	740
83.0	13.83	19.0	900
86.5	14.41	21.6	1000
88.5	14.75	23.0	1080

The magnetizing current against applied voltage and the core loss against number of volts per turn were plotted in Figs. 1.29 and 1.30 respectively.

The magnetization curve shows that when the applied voltage exceeds 63.5 volts or 10.6 volts per turn, the magnetizing current increases rapidly. This indicates that the permissible maximum flux density of the core should be 10.6 volts per turn. The core loss curve also shows that when the applied voltage exceeds 10.6 volts per turn the core loss is quite high.

1.9.6 Copper Loss

The copper loss is the I^2R loss of the primary and secondary winding. The test for copper loss was a short circuit method. Its purpose was to find the equivalent resistance of the primary and secondary winding. The connecting diagram is shown in Fig. 1.31. The secondary was short circuited. The voltage was applied to the primary. The result is shown in Table 1.11.

Table 1.11 Short Circuit Test

Volt	Ampere	Watt
1.29	64	48

The equivalent resistance at the primary is

$$I^2R_{01} = 48$$

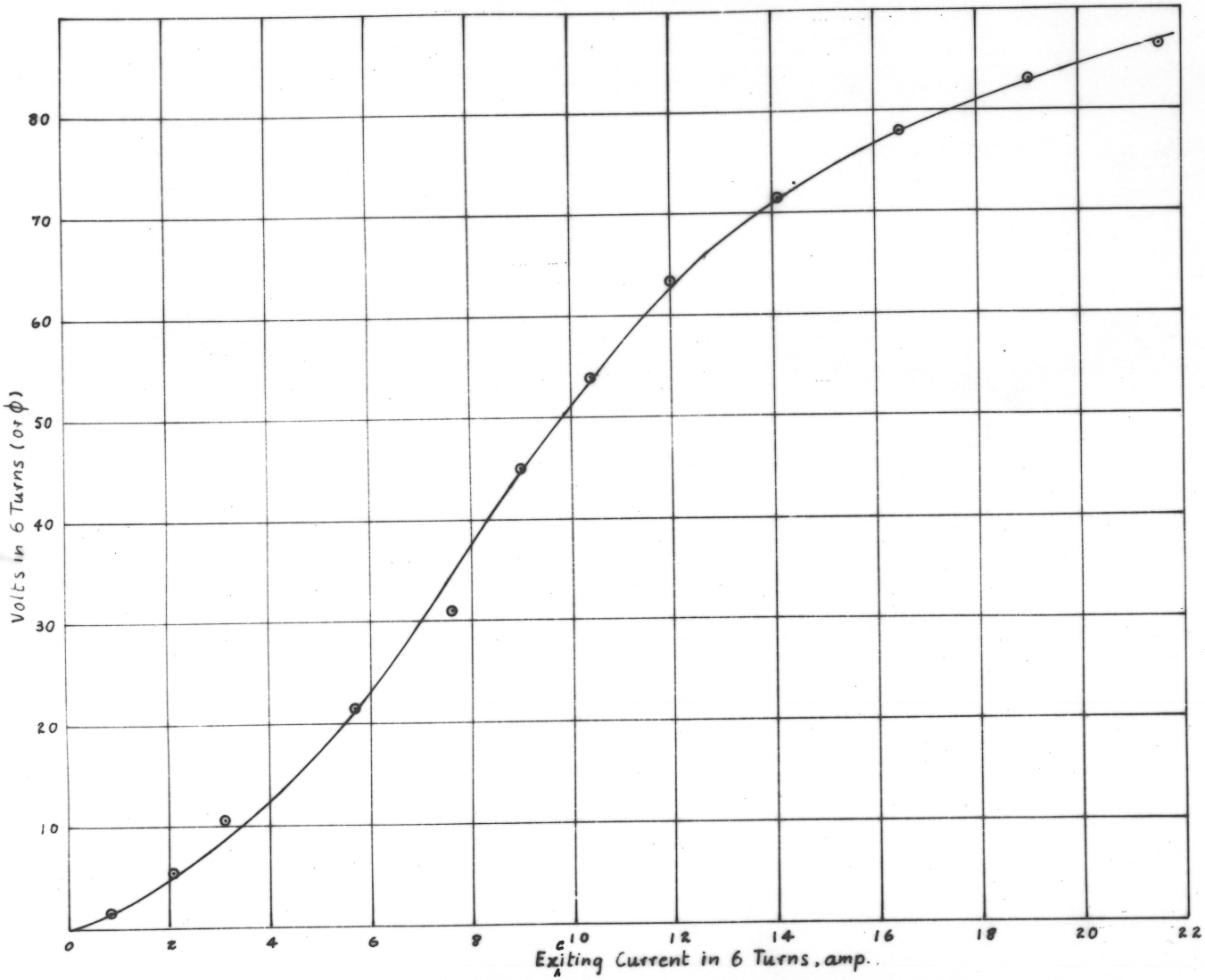


Fig. 1.29 Magnetization curve of transformer core.

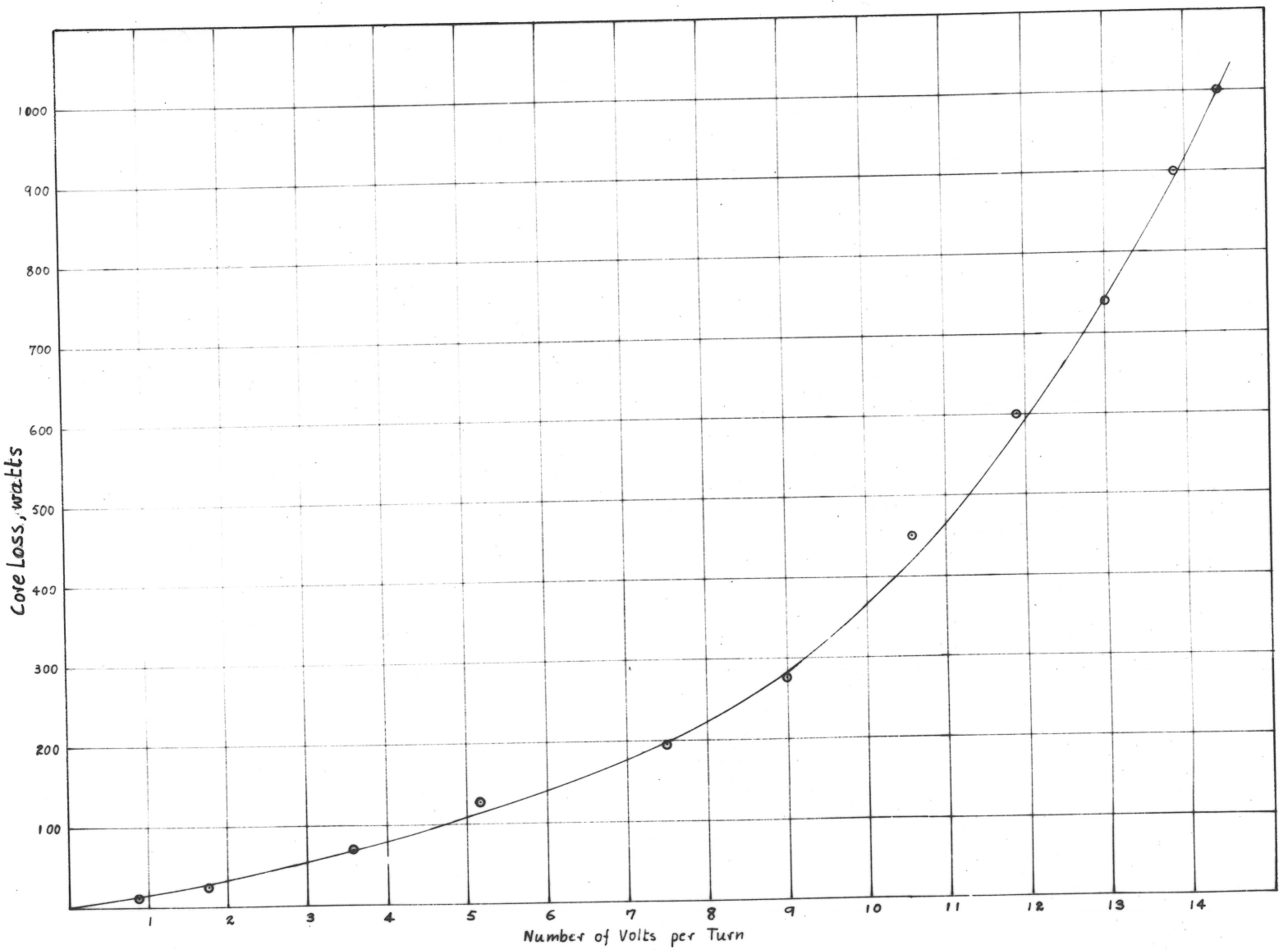


Fig. 1.30 Core loss.

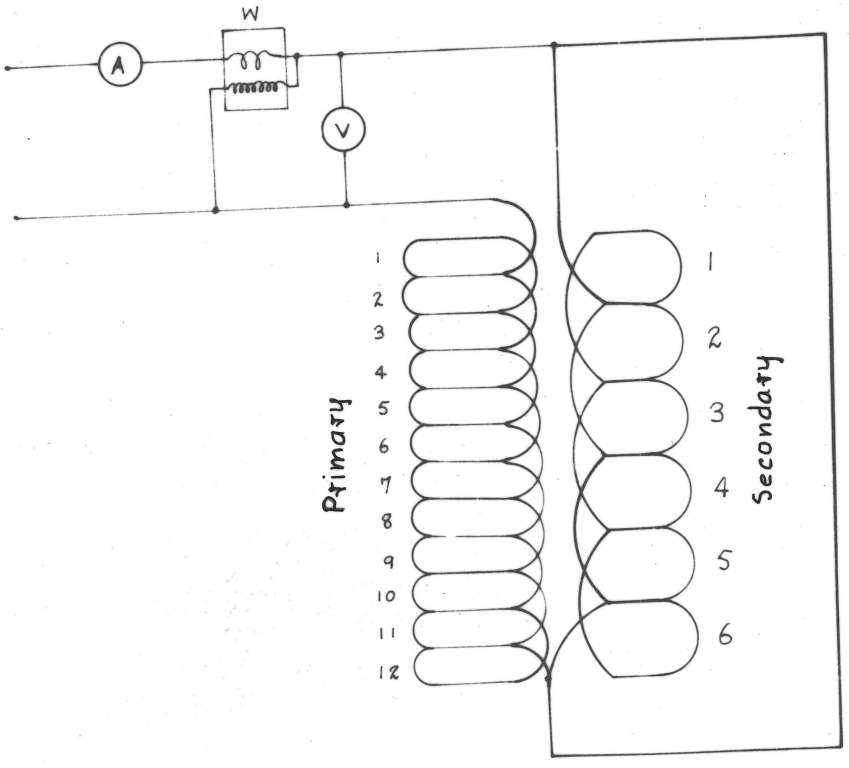


Fig.1.31 Diagram of short-circuit test for copper loss

$$R_{01} = \frac{48}{64 \times 64}$$

$$= 11.7 \times 10^{-3} \text{ ohm}$$

The copper loss for any amount of current flow in the primary winding may be calculated from $I^2 \times 11.7 \times 10^{-3}$ watts.

1.9.7 Leakage Reactance

From the short circuit test the equivalent impedance of the transformer at primary at no load may be calculated from Table 1.11.

$$Z_{01} = \frac{1.29}{64}$$

$$= 20.2 \times 10^{-3} \text{ ohm}$$

The equivalent impedance at no load consists of equivalent reactance or equivalent leakage reactance and equivalent resistance of the transformer measured at primary.

$$Z_{01} = \sqrt{X_{01}^2 + R_{01}^2}$$

$$R_{01} = 11.7 \times 10^{-3} \text{ ohm}$$

$$\therefore X_{01} = 16.4 \times 10^{-3} \text{ ohm}$$

X_{01} = equivalent leakage reactance measured at primary when the ratio of primary: secondary is 3:1

1.9.8 Efficiency

The efficiency of the transformer is

LIBRARY OF THE UNIVERSITY OF ADELAIDE

$$\eta = \frac{\text{input - losses}}{\text{input}}$$

The losses of transformer consist of core loss and copper loss. The core loss varies with the applied voltage, which can be found from Fig. 1.30. The copper loss varies with the current flow into the primary. This current is different from that of the supply current. In the parallel circuit of capacitor and transformer the current flows in the primary is greater than the current in the supply line. From equation (1.59)

$I_L = Q\, I_s$

I_s = current in supply line

I_L = current in primary

$Q = \frac{\omega L}{R}$

L = inductance at primary

R = resistance at primary

L and R change with the temperature and permeability of the charge and with the permeability of the iron core of the work-coil. Therefore these values when the charge is cold and low current flows in the work-coil are different from those when the charge is hot and high current flows.

The actual current flow in the primary was measured by heating the iron charge above its Curie point, then varying the load.

There is some loss in the leads which carry high

current from the supply line to the connections of primary. This loss was reduced to minimum by using the heavy lead which can carry 600 amperes. The lead's resistance is 2.08×10^{-3} ohms. To eliminate the error in the lead loss the potential poles of the watt meter were connected directly to the primary.

Table 1.12. Efficiency of Auto-Transformer

Input kW	I_s amp.	V_s volt	Current to primary amp.	Copper loss, watt.	Core loss, watt	Efficiency	
						$\eta_{\%1}$	$\eta_{\%2}$
1.7	24	68	155	281	40	81	97
2.17	26	80	190	422	70	77	96
4.37	28	103	245	702	110	81.5	96.6
6.88	52	130	320	1200	180	80	96.6
8.22	55	145	365	1417	230	80	96.7
10.43	60	160	390	1780	280	80	96.7
11.4	64	168	410	1970	310	80	96.6
12.86	66	178	430	2210	360	80	96.6

I_s = current in supply line

V_s = voltage in supply line

η_1 = efficiency based on kW input

η_2 = efficiency based on kVA of transformer

The copper loss and efficiency at various loads were calculated as shown in Table 1.12. The efficiency varies

very little from no load to full load. It is about 80% at all loads when kW input to the tank-circuit is considered and about 96.6% at all loads for kVA input at the transformer.

There is high power loss, $I_L^2.R_{01}$, in the primary and secondary winding. This is due to the resistance of the 12 turns of primary winding being high, because it was made of the ordinary copper tubing, $\frac{1}{2}$ inch O.D., 0.048 inch wall thickness. This resistance may be reduced by using the thicker copper tubing or the heavy lead which can carry 600 amperes, but time did not permit improvements to the transformer.

1.10 Laminated Core of Work-Coil

By putting a laminated grain oriented silicon steel core in the magnetic path of the work-coil, the magnetic flux produced by it is increased. This may be represented by

$$\phi = \frac{\mu 4\pi N I A}{l} \text{ maxwell} \quad \ldots . \quad (1.73)$$

μ = average relative permeability of the mediums of the magnetic path.

N I A l = no. of turns, current, cross-sectional area and length of work-coil respectively, c.g.s.

The magnetic flux (ϕ) produced by the coil is

proportional to the permeability (μ) if other factors are kept constant. The maximum permeability of the grain oriented silicon steel (4% Si) is about 6000 times that of air. So the induced magnetic flux will increase considerably when the work-coil is surrounded by the laminated core. This effects the induction heating in two ways.

(a) The power developed in the charge is increased. From equation (1.31),

$$P = \frac{\mu\, 4\pi n^2 \omega I^2}{l^2} V W(ma)_{r.m.s.} \text{ ergs sec}^{-1}$$

μ = permeability of charge.

If the space above and below the charge inside the work-coil is occupied by the high permeability iron core, the power (P) will be increased.

(b) The inductance of the work-coil is increased, from equation (1.69)

$$L = \frac{N\phi}{I.10^8} \text{ henries}$$

$$\text{or } L = \frac{\mu\ 0.4\pi N^2.A}{l.10^8} \text{ henries}$$

The inductance (L) increases with permeability (μ).

The best position to place the laminated core around the work-coil is to trap the number of lines of flux produced by the work-coil as much as possible. Fig. 1.32 shows magnetic line of force of a short work-coil. There

are two ways to place the laminated core.

(a) Placing the core around the work-coil as shown in Fig. 1.33(a). One end of the work-coil has to be cleared for pouring the molten metal out of the crucible inside the work-coil. This setting has been widely used, but required a large mass of the core. It also introduces problems of fittings and high cost of the core. It was not suitable for the present work.

(b) Placing the core as in Fig. 1.33(b). From the previous consideration about length of the work-coil (section 1.7.4) and Fig. 1.32, some of the magnetic lines of force go out at the side near both ends of the coil. Therefore if the core ends extended inside the coil it would give better results.

To pour the molten metal out, the work-coil must be rotated and the core cut at a certain angle as shown by the dotted lines aa and bb in Fig. 1.33(b). The portion bb and cc has to be lifted up before pouring.

Although most of the design of work-coil and auto-transformer was carried out on the results of tests with a core such as that shown in Fig. 1.33(b) it was subsequently found in tests with mild steel that with a short piece of the laminated core inserted in the bottom of the work-coil, the mild steel charge could be melted in the crucible.

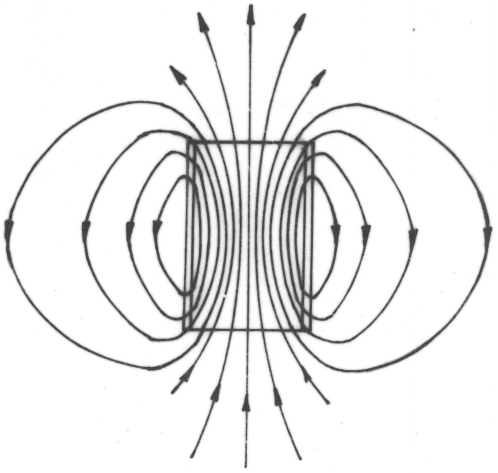


Fig. 1.32 Magnetic flux of short coil [20]

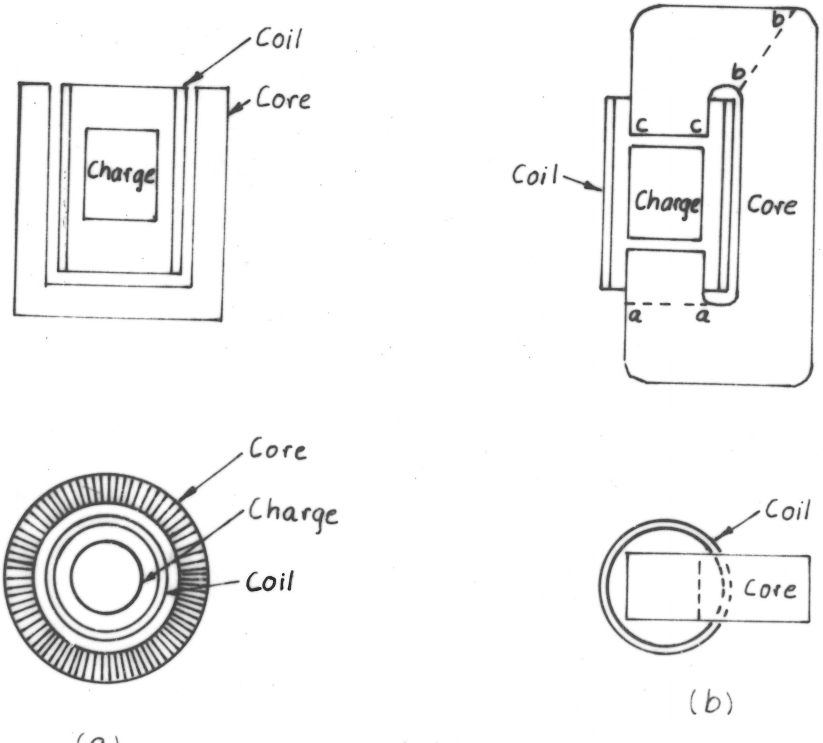


Fig. 1.33 Laminated core surrounding work-coil

So to reduce the problem of core fitting, cost, etc. only the short piece of iron core, 2 inches long, 2.97 sq.in. cross-sectional area was put at the bottom of the work-coil. It projected $1\frac{3}{4}$ inches inside the coil.

The surface of the core touched the bottom of the crucible lining which was at high temperature during melting, so it was necessary to cool the core surface. Otherwise the insulation between the laminated sheets of the core would be damaged. The water cooled coil was wound in such a way that the difference of the induced e.m.f. between its both ends was nearly zero as shown in Fig. 1.34.

At the instant when the work-coil current flows anti-clockwise the induced current in the cooling coil will flow out of the coil centre and the potential difference between a and b should be nearly zero. The power loss in the cooling coil is therefore eliminated.

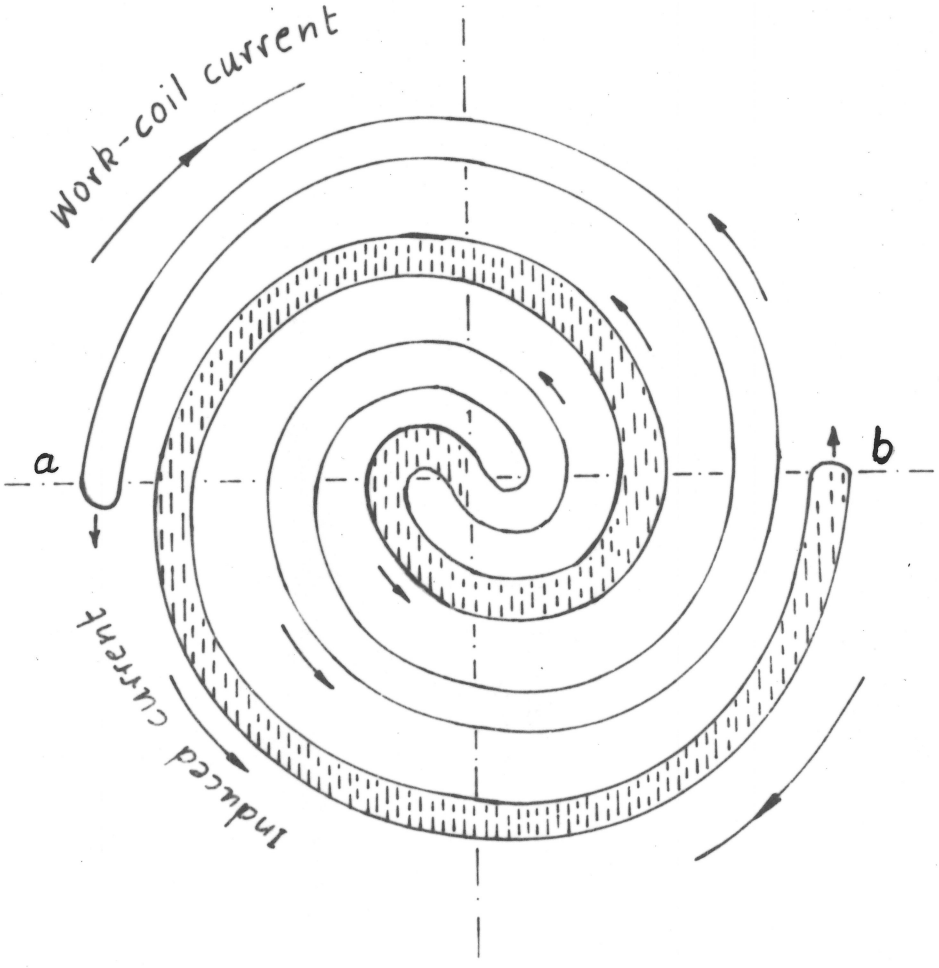


Fig. 1.34 Cooling coil of laminated core.

CHAPTER II

VACUUM SYSTEM

2.1 Basic Principle of Vacuum Technique[21,22]

Any vacuum system is concerned with a gas flow out of a vacuum enclosure through apertures, pipes, and vacuum pumps which eject the gas into the atmosphere. Vacuum gauges are attached to the system to indicate vacuum and assist in leak-detection.

2.1.1 Impedance, Conductance and Pumping Speed

In a system having a continuous gas flow and at a uniform temperature, the mass of gas flow passing through any cross-sectional area per unit time in the system is equal.

From the gas law, $n = \frac{1}{RT} \cdot PV$

where P = pressure of gas

V = volume of gas

R = gas constant

T = absolute temperature

n = number of moles of gas

At a uniform temperature

$$n \propto PV$$

Then the amount of gas flow in the system may be measured in terms of P and V.

If A = amount of gas flow in micron Hg-litre per second

V = volume of gas flow through any plane in the system in litres per second at pressure P

P = pressure in microns Hg in the plane in which the amount of gas flow is measured

$$A = PV \qquad \ldots\ldots\ldots \quad (2.1)$$

The impedance (or resistance) of any segment of the system is defined as the pressure drop at the segment per unit of gas flow.

$$I = \frac{P_1 - P_2}{A} \qquad \ldots\ldots\ldots \quad (2.2)$$

P_1, P_2 = pressure of gas at ends of the segment.

The conductance of the segment is

$$C = {}^1/_I$$

$$= \frac{A}{P_1 - P_2} \qquad \ldots\ldots\ldots \quad (2.3)$$

When there is more than one impedance in the system, the total impedance or conductance may be found as follows.

For series and parallel impedances:

$$I_{series} = I_1 + I_2 + I_3 + \ldots I_n$$

$$= \Sigma I_n \qquad \ldots\ldots\ldots \quad (2.4)$$

$$I_{parallel} = \frac{1}{I_1} + \frac{1}{I_2} + \frac{1}{I_3} + \ldots \frac{1}{I_n}$$

$$= \Sigma \frac{1}{I_n} \qquad \ldots\ldots\ldots \quad (2.5)$$

For series and parallel conductances:

$$\frac{1}{C_{series}} = I_{series}$$

$$= I_1 + I_2 + I_3 + \ldots I_n$$

$$= \frac{1}{C_1} + \frac{1}{C_2} + \frac{1}{C_3} + \ldots \frac{1}{C_n}$$

$$= \Sigma \frac{1}{C_n} \qquad \ldots\ldots\ldots \quad (2.6)$$

$$C_{parallel} = {}^{1}/I_{parallel}$$

$$= \frac{1}{I_1} + \frac{1}{I_2} + \frac{1}{I_3} + \cdots \frac{1}{I_n}$$

$$= C_1 + C_2 + C_3 + \cdots C_n$$

$$= \sum C_n \qquad \ldots\ldots\ldots \quad (2.7)$$

The speed of a pump at pressure P is defined as the volume of gas removed from the system per unit time, measured at pressure P.

If P = pressure at the inlet of the pump in micron Hg

V = volume of gas removed by the pump in litres per second

S_p = speed of the pump

$S_p = V$

From equation (2.1)

$$S_p = \frac{A}{P} \qquad \ldots\ldots\ldots \quad (2.8)$$

The flow quantity A may be measured anywhere in the system as the mass of gas flow is the same, but P is usually measured at the inlet to the pump.

2.1.2 Effective Pumping Speed

If a vacuum enclosure is connected to a pump by a

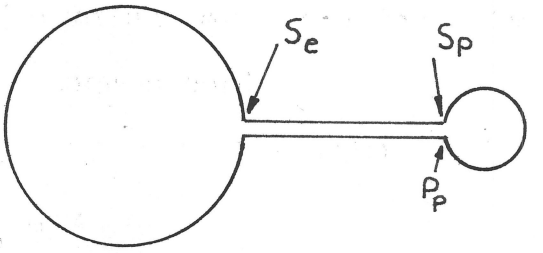
pipe the speed of gas flow out of the enclosure measured at the entrance to the pipe is called the effective pumping speed. This speed is less than the speed of the pump due to the resistance of the pipe to gas flow.

Consider an enclosure containing gas at pressure P connected by a pipe, impedance I, to a pump.

Let S_e = effective speed of the pump at the inlet to the impedance.

S_p = pumping speed of the pump at its inlet.

P_p = pressure at the inlet of the pump.



From equation (2.1)

$$A = P\,S_e = P_p\,S_p$$

$$\frac{1}{S_e} = \frac{P}{A}\,,\quad \frac{1}{S_p} = \frac{P_p}{A}$$

$$I = \frac{P - P_p}{A}$$

$$= \frac{P}{A} - \frac{P_p}{A}$$

$$= \frac{1}{S_e} - \frac{1}{S_p}$$

$$\therefore \frac{1}{S_e} = I + \frac{1}{S_p} \qquad \ldots\ldots \quad (2.9)$$

I is the impedance of the connection between the enclosure and the pump. It may contain a single, series or parallel impedance.

2.1.3 Real Speed of Pump

There is always some leak associated with a pumping system; this may arise from the oil pump or imperfection in vacuum joints. The latter source of leakage is many times larger than the former, and places a limit to the working pressure of the pump. When the pumping speed is equal to the leakage rate the pump cannot reduce the pressure of the system any further.

From equation (2.8)

$$S = \frac{A}{P}$$

Let A_o = fixed leakage rate

S_p = speed of a pump

The nett amount of gas removed by the pump at pressure P, at the inlet of the pump, is

$$A = S_p P - A_o$$

When the pressure is reduced to the limiting pressure, P_o, the speed of the pump is equal to the leakage rate, assuming a constant speed of the pump.

$$A = 0$$

$$A_o = S_p P_o$$

thus at pressure P,

$$S_r P = S_p P - S_p P_o$$

$$= S_p P \left(1 - \frac{P_o}{P}\right)$$

$$S_r = S_p \left(1 - \frac{P_o}{P}\right) \qquad \ldots\ldots \quad (2.10)$$

S_r = real speed of pump.

2.1.4 Turbulent, Viscous and Molecular Flow

In practice the evacuating speed at the outlet of the vacuum tank is always associated with the impedance or conductance of the pipe which connects the vacuum tank to the pump. The conductance of the pipe depends on the type of gas flow through it.

In general there are three types of gas flow through a pipe, namely turbulent, viscous and molecular. These flows may be considered in terms of pressure and velocity of the gas.

For turbulent flow the pressure and velocity of gas are high and the lines of flow turn and twist. By experiment the quantity of gas flow is proportional to the square root of pressure gradient,

$$A \propto \sqrt{dP}$$

dP = pressure gradient

In viscous glow the pressure and velocity of gas are usually less than those for molecular flow. The lines of flow are laminar. The viscosity or internal friction has an important effect on the nature and quantity of gas flow, and the quantity of gas flow is approximately proportional to the pressure gradient,

$$A \propto dP$$

The mean free path of gas in viscous flow is small compared to the size of the pipe. Most of the molecules will collide with each other; only the molecules near the surface will collide with it, so the size and shape of the pipe will effect the flow more than the nature of the pipe surface.

In molecular flow the pressure of the gas is low. The mean free path of the gas is nearly equal to or larger than the diameter of the pipe. The gas molecules migrate along the pipe independently, and they collide with the pipe

surface more than with each other. The direction of the moving molecule after collision at the solid surface is at random and depends largely on probability.

In vacuum practice the operating pressure is usually low and the pipe diameter is commonly large, so that the flow of gas is therefore viscous or molecular. Turbulent flow need not be considered.

From Knudsen's work the transition between viscous and molecular flow may be written as follows.[23]

Let P_a = average pressure of the pipe in microns

d = diameter of pipe in cms.

When $P_a.d > 500$ the flow is viscous . . . . . (2.11)

$P_a.d < 5$ the flow is molecular . . . . . (2.12)

2.1.5 Conductance of Viscous and Molecular Flow through Long Circular Pipe

From the work of Knudsen the general equation for the conductance of viscous and molecular flow may be written as follows.[21]

$$C = \left(\frac{\pi}{128} \cdot \frac{d^4.P_a}{\sigma 1}\right) + \left(\frac{1}{6} \cdot \frac{2\pi kT}{m} \cdot \frac{d^3}{1}\right)\left(\frac{1 + \sqrt{\frac{m}{kT}}\,\frac{d.P_a}{\sigma}}{1 + 1.24\sqrt{\frac{m}{kT}}\,.\frac{dP_a}{\sigma}}\right)$$

. . . . . (2.13)

d = diameter of the pipe, cms.

P_a = average pressure in the pipe, microns.

l = length of the pipe, cms.

= viscosity of the gas

k = Boltzmann constant

T = absolute temperature

m = mass of the molecule, gram.

In viscous flow the pressure is comparatively high and becomes the dominating factor. The conductance may be written as

$$C_v = \frac{\pi}{128} \cdot \frac{d^4 P_a}{\sigma l} \quad \ldots . \quad (2.14)$$

C_v = conductance of circular pipe under viscous flow.

For air at 20°C

$$C_v = 12.1 \cdot \frac{d^3}{l} \cdot F \text{ litres/sec.}$$

F is a function of $d.P_a$.

For a large value of $d.P_a$ which is the case for viscous flow,[21]

$$F = 0.0152\ d.P_a$$

$$C_v = 0.182 \frac{d^4}{l} P_a \text{ litres/sec.} \quad \ldots . \quad (2.15)$$

In the molecular flow the pressure is very small, any term which is multiplied by P_a could be neglected and the molecular conductance of a circular pipe will become

$$C_m = \frac{1}{6}\sqrt{\frac{2\pi kT}{m}} \cdot \frac{d^3}{l} \text{ cgs} \quad \ldots\ldots \quad (2.16)$$

C_m = conductance of circular pipe under molecular flow

For air at 20°C

$k = 1.381 \times 10^{-16}$ cm/sec.

$t = 293$ K

$m = 47.6 \times 10^{-24}$ g.

$$C_m = 12.1 \times 10^3 \frac{d^3}{l} \text{ cc/sec.}$$

or $$C_m = 12.1 \frac{d^3}{l} \text{ litres/sec.} \quad \ldots\ldots \quad (2.17)$$

Equation (2.17) is independent of the gas pressure. For high conductance in the molecular flow the pipe should have large diameter and short length.

2.1.6 Evacuating Speed of the Vacuum Enclosure

The evacuating speed of gas in the vacuum enclosure may be obtained by considering the effect of pipe conductance together with the speed and base pressure of the pump.

Let S_1 = pumping speed of the enclosure at the inlet to the impedance I

S_2 = effective pumping speed of the pump at pressure P_2

P_1 = pressure of the enclosure

P_2 = pressure at the inlet to the pump

S_p = pumping speed of the pump neglecting leakage

P_o = limiting pressure of the pump.

From equation (2.10)

$$S_2 = S_p \left(1 - \frac{P_o}{P_2}\right)$$

From equation (2.9)

$$\frac{1}{S_1} = I + \frac{1}{S_2}$$

$$\text{or } S_2 = \frac{S_1}{1 - S_1 I}$$

$$\frac{S_1}{1-S_1 I} = S_p \left(1 - \frac{P_o}{P_2}\right)$$

Since

$$P_1 S_1 = A = \frac{P_1 - P_2}{I}$$

$$P_2 = P_1 (1 - S_1 I)$$

$$\frac{S_1}{1 - S_1 I} = S_p \, 1 - \frac{P_o}{P_1 (1 - S_1 I)}$$

$$S_1 = S_p (1 - S_1 I - \frac{P_o}{P_1})$$

$$S_1 = \frac{S_p}{1 + S_p I} (1 - \frac{P_o}{P_1})$$

$$= \frac{1}{\frac{1}{S_p} + I} (1 - \frac{P_o}{P_1}) \qquad .... \qquad (2.18)$$

2.1.7 Evacuating Time of Vacuum Tank

For simplicity, the speed of the pump at the outlet of the vacuum tank (or enclosure) as in equation (2.9) is used.

Let V = volume of tank

P = pressure of gas

S_t = pumping speed at the outlet of the tank.

The amount of gas flowing out is:

$$A = S_t . P \text{ micron-litres per second.}$$

The amount of gas decreased in the tank per unit time is

$$A = - \frac{d (PV)}{dt} \text{ micron-litres per second}$$

The quantity of gas removed from the vacuum tank by a vacuum pump is equal to the quantity of gas decreased in the tank.

$$\therefore \quad S_t P = - V \frac{dP}{dt}$$

$$- \frac{S_t}{V} dt = \frac{1}{P} dP$$

Integrating both sides and inserting limits

$$t = 2.303 \frac{V}{S_t} \log \frac{P_1}{P} \text{ sec.} \quad \ldots \quad (2.19)$$

P_1 = initial pressure in the tank

P = pressure at time t.

From equation (2.19) it may be proved that

$$t_{\frac{1}{2^n}} = n \, t_{\frac{1}{2}} \quad \ldots \quad (2.20)$$

$t_{\frac{1}{2}}$ = time when pressure is reduced to half of initial pressure.

$t_{\frac{1}{2^n}}$ = time when pressure is reduced to $\frac{1}{2^n}$ of initial pressure.

2.2 General Description of Vacuum System

The vacuum tank is made from stainless steel plate 3/16 inch thick; it is 30 inches in diameter and 30 inches long, with volume about 11 cu. ft. or 310 litres. The enclosure is connected to an oil diffusion pump via an exhaust pipe, 6 inches in diameter with one 90° bend and total length 10½ inches. The oil diffusion pump has a volumetric speed of 600-650 litres per second without baffle valve or 300-350 litres per second with the baffle valve at pressure 10^{-3}-10^{-6} mm. Hg. The outlet of the oil diffusion pump is connected by a 1¼ inch copper tube to a mechanical pump which has pumping speed of 450 litres per minute at one atmosphere pressure. A pirani gauge and a bourdon gauge are employed to measure the pressure of the system. The diagram of the vacuum system is shown in Fig. 2.1.

2.3 Vacuum Tank

2.3.1 Design

Three main requirements had to be met in making the vacuum tank, namely:

(a) Suitable size and material to minimize the heat loss due to stray magnetic field outside the work-coil.

(b) Sufficient space to accommodate work-coil and crucible, mould and other equipment required for making high purity iron alloys.

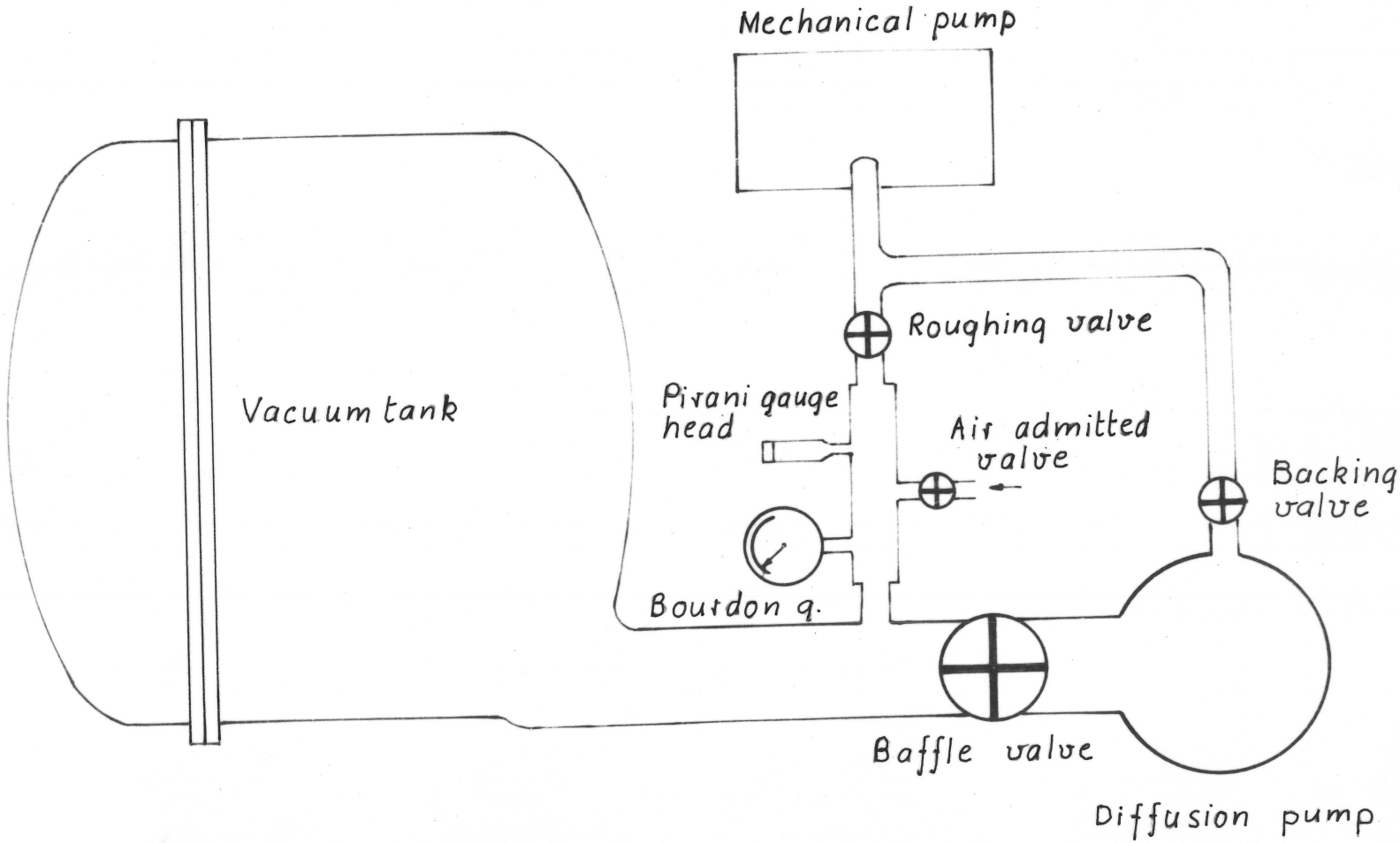


Fig. 2.1 Diagram of Vacuum System.

(c) Sufficient strength to withstand the atmospheric pressure acting from outside with the enclosure under vacuum.

2.3.2 Stray Magnetic Field

The relative strength and direction of stray magnetic field outside the work-coil were measured by placing a small search coil in the magnetic field. The search coil was connected to the y-axis of an oscilloscope. The height of the curve on the oscilloscope screen represented the relative field strength.

The measurements were taken along lines at 45° intervals as in Fig. 2.2.

Table 2.1 Relative Magnetic Field Strength of Work-Coil

Distance from centre of the work-coil - in inches	Relative Magnetic Field Strength			
	1	2	3	4
5.0	17.5	7.5	2.9	7.0
7.5	4.0	2.2	1.15	2.25
10.0	1.5	0.9	0.54	0.95
12.5	0.7	0.5	0.3	0.42
15.0	0.44	0.28	0.2	0.28
17.0	0.28			

The measurements were made on the right side of the work-coil only, since the magnetic field strength on the

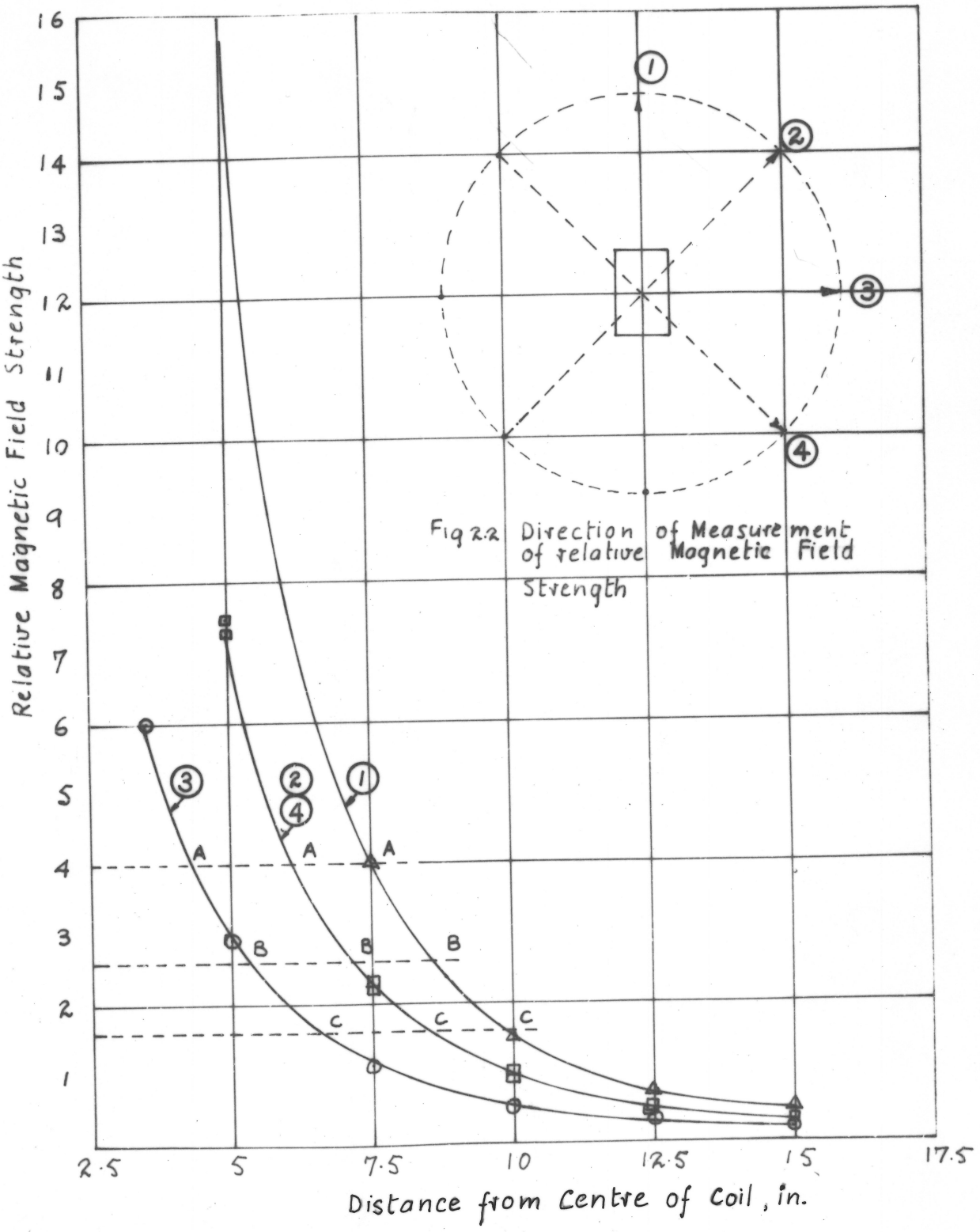


Fig 2.2 Direction of Measurement of relative Magnetic Field Strength

Fig. 2.3 Relative magnetic field strength around work-coil.

left would be the same. The results are shown in Table 2.1. The curves of relative magnetic field strength against the distance from the work-coil are plotted in Fig. 2.3. This figure shows that at the distance about 15 inches from the centre of the work-coil the magnetic field strength is small.

The relative magnetic field strength at the centre of the work-coil was measured. It was 35.6 times the magnetic field strength at 15 inches from the centre of the coil in the direction (1) and 56 times in the direction (2).

It is of interest to see the equivalent magnetic field strength around the work-coil. This could be obtained by drawing lines parallel to the distance axis in Fig. 2.3. The equivalent magnetic field strength was plotted in Fig. 2.4.

The lines of equivalent magnetic field strength in Fig. 2.4 form ellipses with major axis passing through the longitudinal axis of the work-coil. This indicates that the vacuum tank should preferably have an elliptical shape with its major axis vertical, but this is not a practical shape.

The vacuum tank was chosen to be a cylindrical shape with a large curvature on both ends. A radius of about 15 inches was chosen so that the heat loss in the shell due

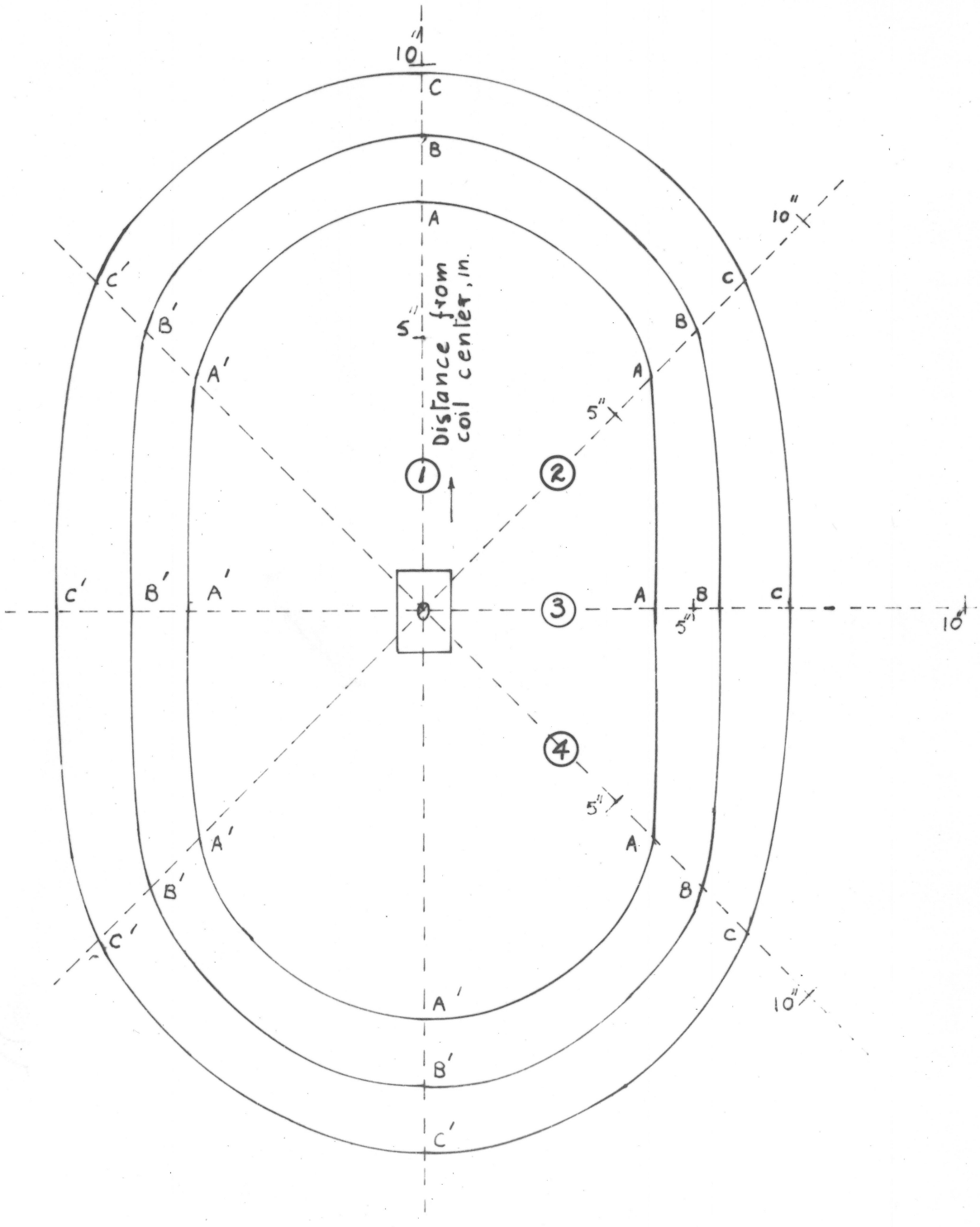


Fig. 2.4 Equivalent magnetic field strength around work-coil.

to the stray magnetic field would be small. With these dimensions all necessary melting equipment can be accommodated.

The tank was made of a non-magnetic stainless steel sheet, to minimize heat loss from the stray magnetic field and also to ensure good corrosion resistance, and reduce the amount of gases absorbed when opened to the atmosphere.

2.3.3 Thickness of Vacuum Tank Shell

The thickness of the stainless steel plate used in making the vacuum tank of 15 inches diameter and 15 inches long may be calculated from the Australian Boiler Code, Part 1, page 14.

Shell subjected to External Pressure

G-205. Thickness and Working Pressure Rule (for mild steel).

If W.P. = maximum external pressure in pound per square inch.

t = thickness of sheet in 32nds of an inch.

D_o = maximum outside diameter of steel in inches.

L = length of shell between point of rigid support or reinforcement in inches.

C = constant

= 1,450 where the longitudinal joint is welded.

C_1 = constant

= 50 where the longitudinal joint is welded.

The thickness of vacuum tank shell may be obtained from formula (a) or (b).

(a) $W.P. = \frac{C(t-1)^2}{(L+24)D_o}$

(b) $W.P. = \frac{C_1}{D_o}\ 10(t-1) - L$

} The greater thickness given by either of these formulae shall be used.

$L = 30$ inches, $D_o = 30$ inches

$W.P. = 14.7$ lbs./sq.in.

From (a)

$$14.7 = \frac{1450\ (t-1)^2}{(30+24)\ 30}$$

$$(t-1)^2 = \frac{14.7 \times 54 \times 30}{1450}$$

$$= 16.45$$

$$t-1 = 4.05$$

$$t = 5.05$$

$\therefore$ thickness of shell $= \frac{5.05}{32}$ inches

From (b)

$$14.7 = \frac{50}{30}\ 10(t-1) - 30$$

$$t-1 = \frac{14.7 \times 0.6 + 30}{10}$$

$$t-1 = 3.882$$

$$t = 4.882$$

$\therefore$ thickness of shell $= \frac{4.9}{32}$ inches

The thickness of shell was chosen to be $3/16$ inch for safety precautions and imperfection in manufacturing. This is the thickness of mild steel shell and it can be used for the stainless steel shell.

2.3.4 Construction

2.3.5 Body and Lid of Vacuum Tank

The vacuum tank was fabricated by J. Unsworth Ltd. of South Australia. The method of manufacture was as follows:

The tank consists of a lid and a body. They were made of five parts, A, B, C, M and N, joined together by welding as shown in Fig. 2.5. It was found necessary to do this to avoid distortion on machined parts after welding. There were three big flanges which had to be machined before welding to the shell, namely:

(1) Body flange, 30 inches inside diameter, 1 inch thick and 2 inches wide. The flange was first welded to part A (which was about 3 inches long) for machining. A dovetail groove was cut on this flange to accommodate a neoprene "O" ring of $\frac{1}{2}$ inch diameter. The cutting of the dovetail groove on 30 inch diameter flange was difficult but it serves two purposes, holding the "O" ring rubber in the groove in the vertical position and having ample space for the "O" ring to expand under load and give good vacuum seal.

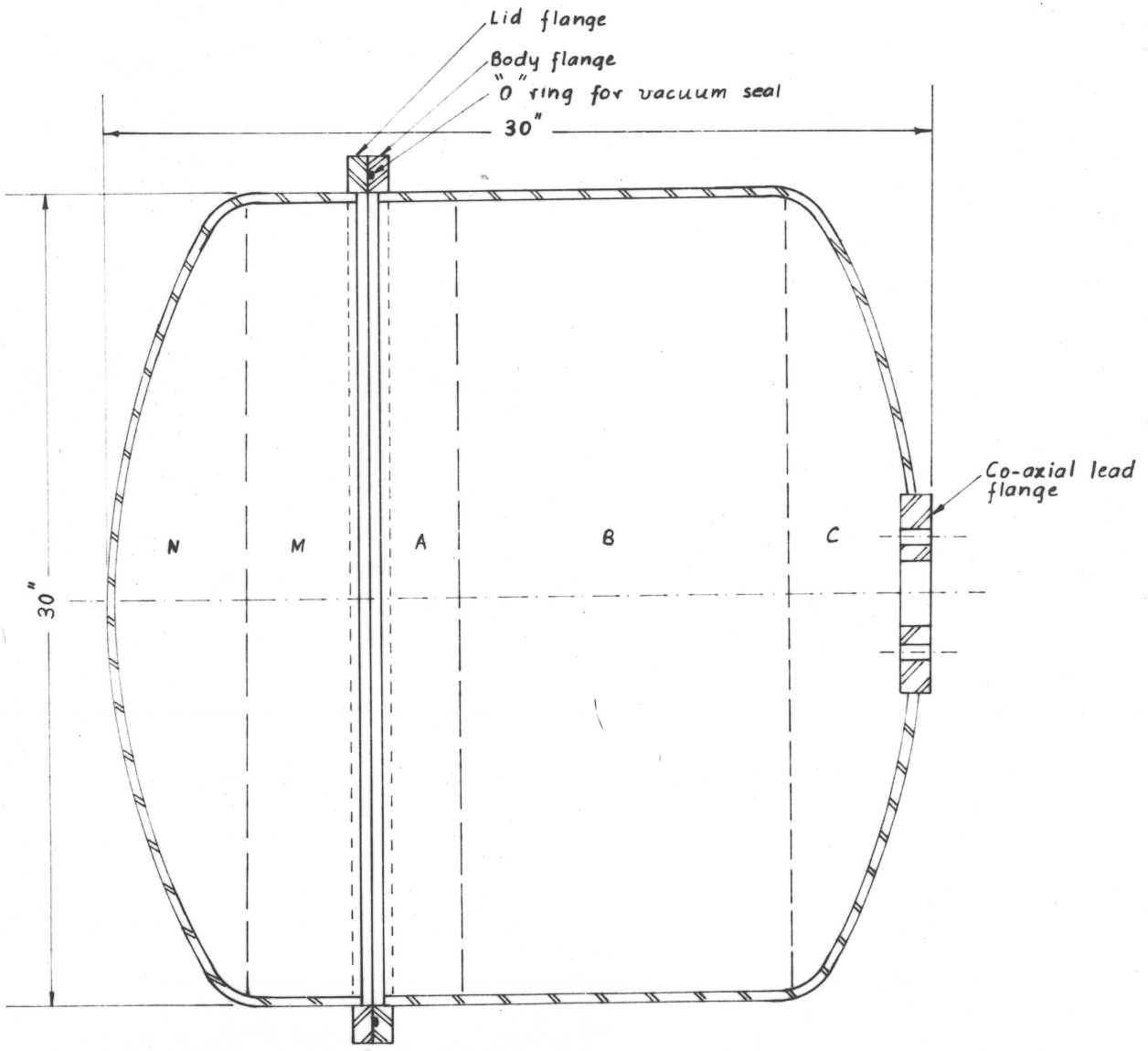


Fig. 2.5 Vacuum Tank.

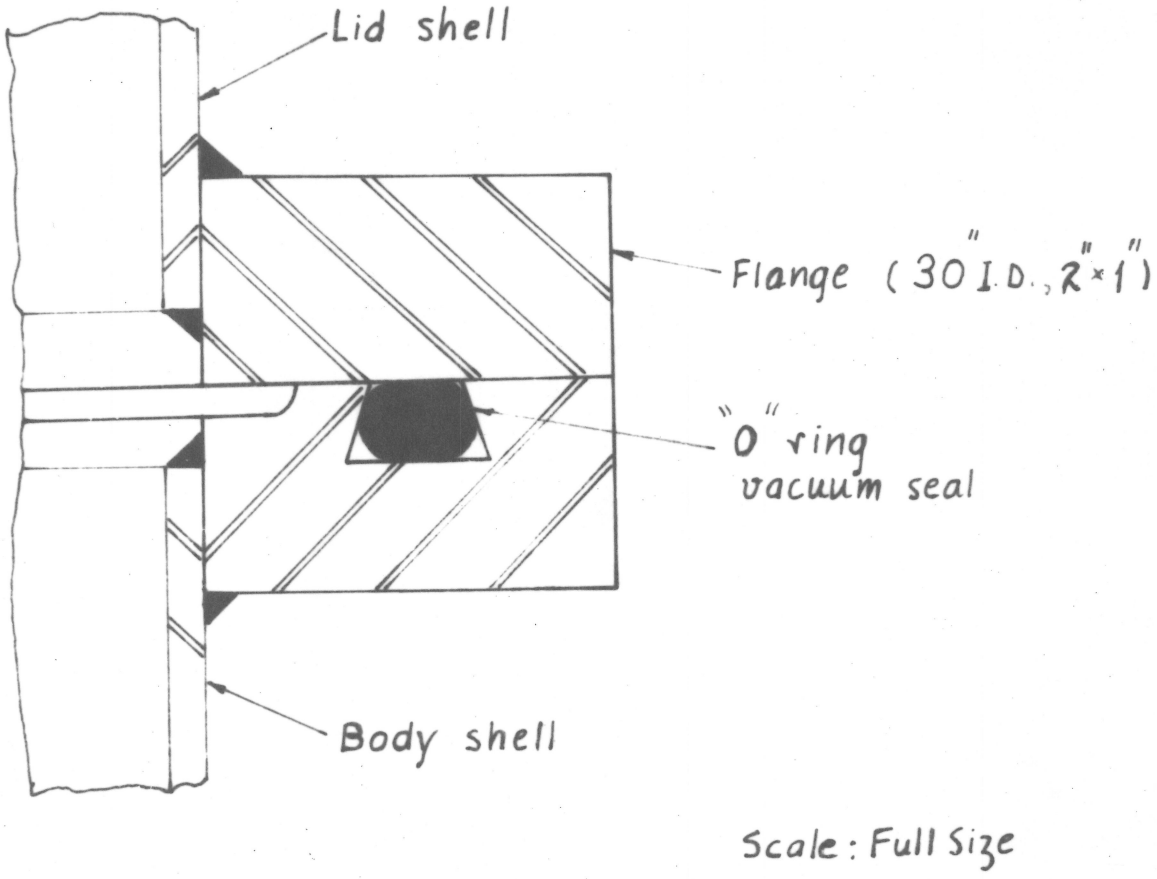


Fig. 2.6 Body and lid flanges.

After machining, the flange with its short length of shell (A) was welded to part B. There was no distortion on the flange resulting from the welding at the distance of three inches from the flange.

The section of the "O" ring groove and flanges is shown in Fig. 2.6.

(2) Sight hole flange. A piece of stainless steel $6\frac{1}{8}$ inches in diameter, $1\frac{1}{4}$ inches thick was welded on a ring of $3/16$ inch stainless steel sheet, $6\frac{1}{8}$ inches inside diameter and 10 inches outside diameter. The sight hole was machined and an "O" ring groove cut before the assembly was welded to the shell. The sight hole glass was made of armour plate glass, heat treated, by L.G. Abbott & Co.Ltd. of South Australia, and was clamped tight by three bolts onto the "O" ring seal.

A drawing of the sight hole is shown in Fig. 2.7.

(3) Electrical co-axial flange. The welding and machining was done in the same way as the sight hole. The drawing is shown in Fig. 2.8.

The lid was made in two operations as shown in Fig. 2.5. A large flange, 30 inches inside diameter, 1 inch thick and 2 inches wide, was welded on part M which was 4 inches long and the machining completed. Part M was then joined to

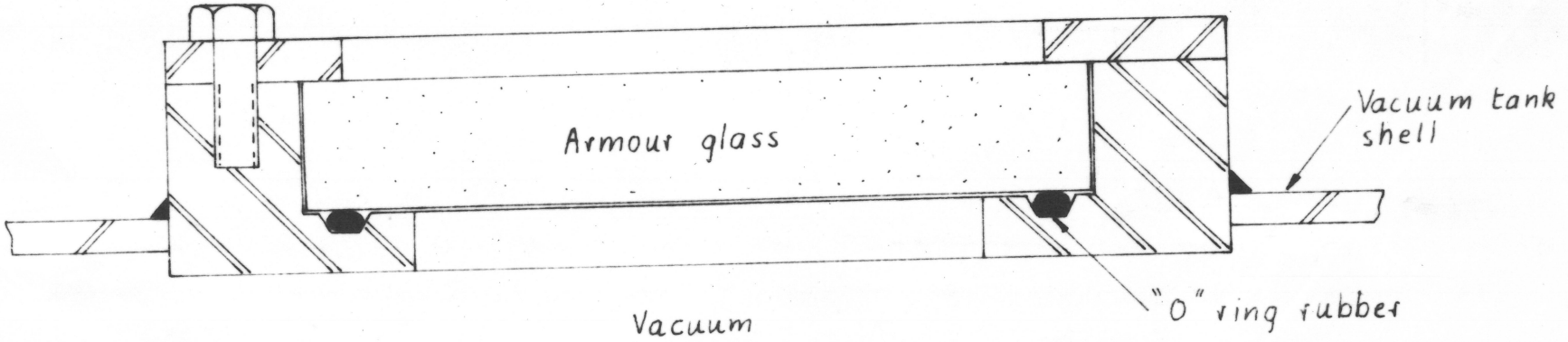


Fig. 2.7 Sight-hole

Scale : Full Size

part N by welding.

It may be mentioned that the flat flange was attached to the removable part, the lid. If there is any damage to it, and causes leakage, the lid may be taken off and remachined.

The lid was hung vertically on the body by two hinges. To support the lid from sagging when closed, a piece of steel, wedge shape, was welded on the support base to act as a ramp which guided the lid into its correct position during closure.

2.3.6 Accessories

When the lid is clamped on the body of the vacuum tank most of the equipment inside has to be operated manually from outside. This requires vacuum seal on all the apertures in the tank through which actuating rods and tubes must pass, namely:

(a) Co-axial lead, carrying heavy current and cooling water to the work-coil.

(b) Three rods for actuating alloy-addition buckets.

(c) One thermocouple sheath.

(d) One lid lifter.

(e) One bridge breaking rod.

2.3.7 Co-axial lead

The co-axial lead is an important part of the induction

INDEX OF FIG. 2.8

(Co-axial lead and flanges)

1	Inner copper tube
2	Fibre-glass epoxy resin laminate
3	Outer copper tube
4	Stainless steel supporting tube
5	U-cup neoprene packing
6	Brass ring
7	Babbit-metal bronze bearing
8	Screwed stainless steel cap
9	Stainless steel supporting tube flange
10	"O" ring
11	Flange attached to vacuum tank shell
12	Vacuum tank shell
13	Bolt
14 16	Water outlet from work-coil
15 17	Water inlet to work-coil
18	Greaser

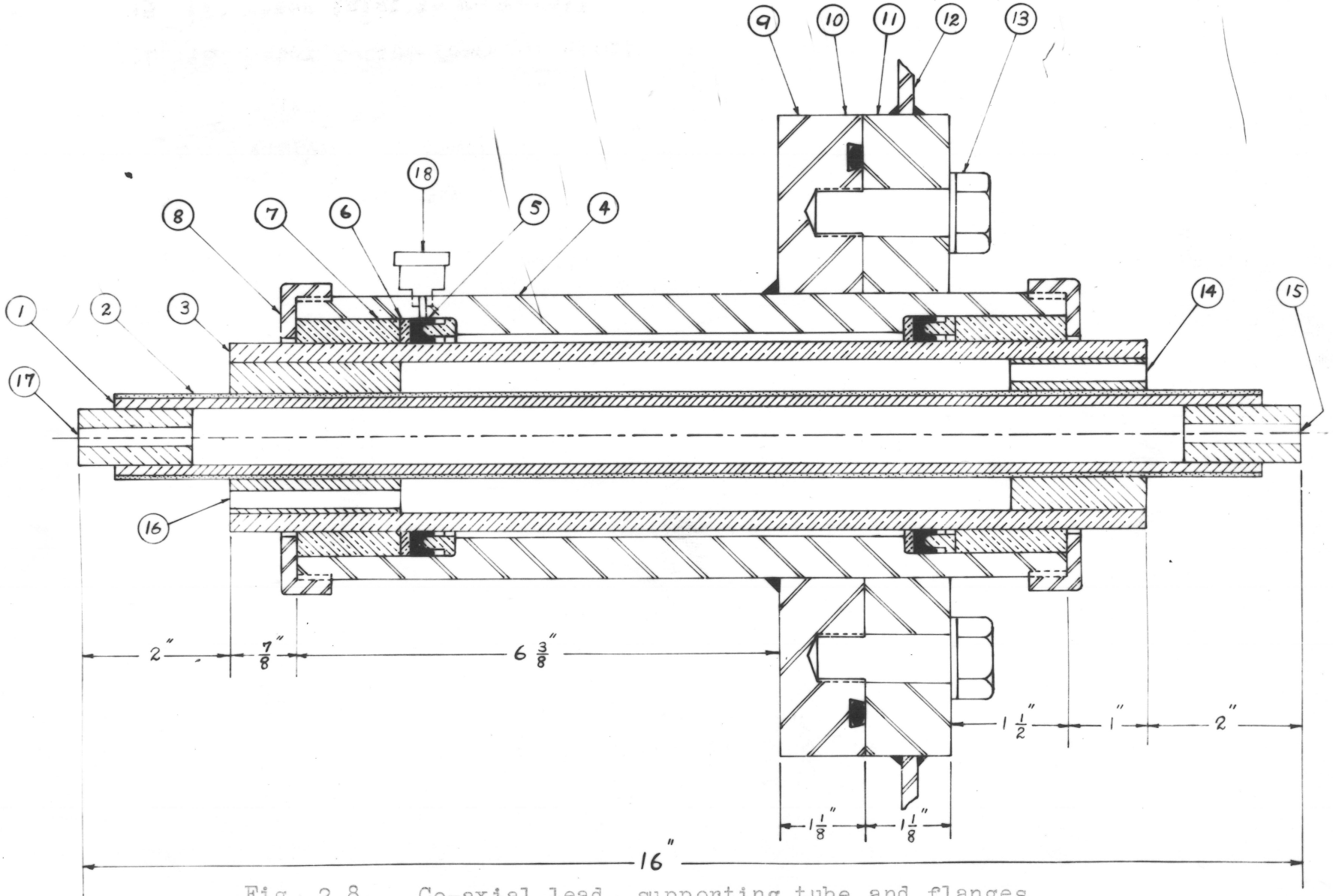


Fig. 2.8 Co-axial lead, supporting tube and flanges (excluding 6 studs on each end of No. 3)

heating circuit, since it carries heavy current and cooling water from outside the vacuum tank to the work-coil inside and back. There are two heavy weights hanging on its ends. On one end, inside the vacuum tank, the work-coil, crucible and insulating powder, charge and short piece of laminated core are suspended. These weigh 32 lbs. The transformer core, primary and secondary coil weighing 80 lbs. are on the outside end. When pouring the molten metal out of the crucible the co-axial lead and its hanging weights have to be rotated to about 135°.

The material required is two thick copper tubes for minimum heat loss under the heavy current flow. The tubes must be long enough so that the work-coil which is hanging on its inside end will be at about the middle of the vacuum tank.

The outer tube (No. 3, Fig. 2.8) is made of a 12 inch length of copper tubing, $2\frac{1}{2}$ inches outside diameter and $\frac{1}{4}$ inch wall thickness. Its ends are closed by cylindrical plugs, 2 inches outside diameter and $1\frac{3}{4}$ inches long and bored to $1\frac{1}{4}$ inches inside diameter, soft soldered into place. The whole tube was chromium plated to give a hard surface.

The inner tube was made of copper tubing 15 inches long, 1 inch outside diameter and $\frac{1}{8}$ inch wall thickness. Its ends were plugged with copper rods of $1\frac{1}{2}$ inches diameter.

A $\frac{1}{4}$ inch hole was drilled through these plugs for the passage of cooling water. The outside surface was covered with glass tape impregnated with epoxy resin, $3/16$ inch thick, then machined to $1\frac{1}{4}$ inches outside diameter. The inner tube was slid into the outer tube until each end projected 2 inches from the outer tube ends, then sealed in place with epoxy resin.

On each end of the outer tube 6 studs ($\frac{1}{4}$ inch x $1\frac{1}{4}$ inches) were attached for carrying the work-coil on one end and the transformer on the other.

The drawing of the co-axial lead is shown in Fig. 2.8.

The co-axial lead and its heavy loads are supported by a long stainless steel tube, $10\frac{1}{8}$ inches long and $3\frac{3}{4}$ inches outside diameter with a flange and "O" ring seal to attach it to the vacuum tank. The ends were accurately bored to $3\frac{1}{4} \pm .001$ inches to accommodate neoprene U-packings used for a vacuum seal between the co-axial lead and the stainless steel tube. The concave side of the U-packing was placed facing the atmosphere, and hence the atmospheric pressure will press the U-packing against the two tubes when the tank was under vacuum, this gives good vacuum seal as shown in Fig. 2.8.

Bronze bearing faced with babbit-metal support the co-axial lead inside the stainless steel housing.

2.3.8 Alloy Addition and Thermocouple Rod

Other sliding or rotating shafts enter the tank through "O" ring seals of the type shown in Fig. 2.9.

Although two "O" ring grooves were cut in each end plug, it was found that one "O" ring on each end would be sufficient for vacuum seal and supporting the rod.

2.3.9 Lid Lifter Rod

The vacuum seal between the lid lifter rod and its hole was similar to the alloy addition rods except that a tube plugged at both ends was used (instead of the solid rod) to let the hydrogen gas into the vacuum tank for deoxidation of the melt.

The lid lifter rod is on the opposite side to the sight hole window, so it is operated by a hand wheel with a chain drive, so as to permit its operation while looking at the melt through the sight hole.

2.3.10 Bridge Breaking Rod

The vacuum seal for this rod is different from the others, since it must have sufficient lateral movement to traverse the inside diameter of the crucible so that the cold surface formed over the melt may be broken off. Two "Fla-seal" rubber rings were used for sealing this rod, as shown in Fig. 2.10.

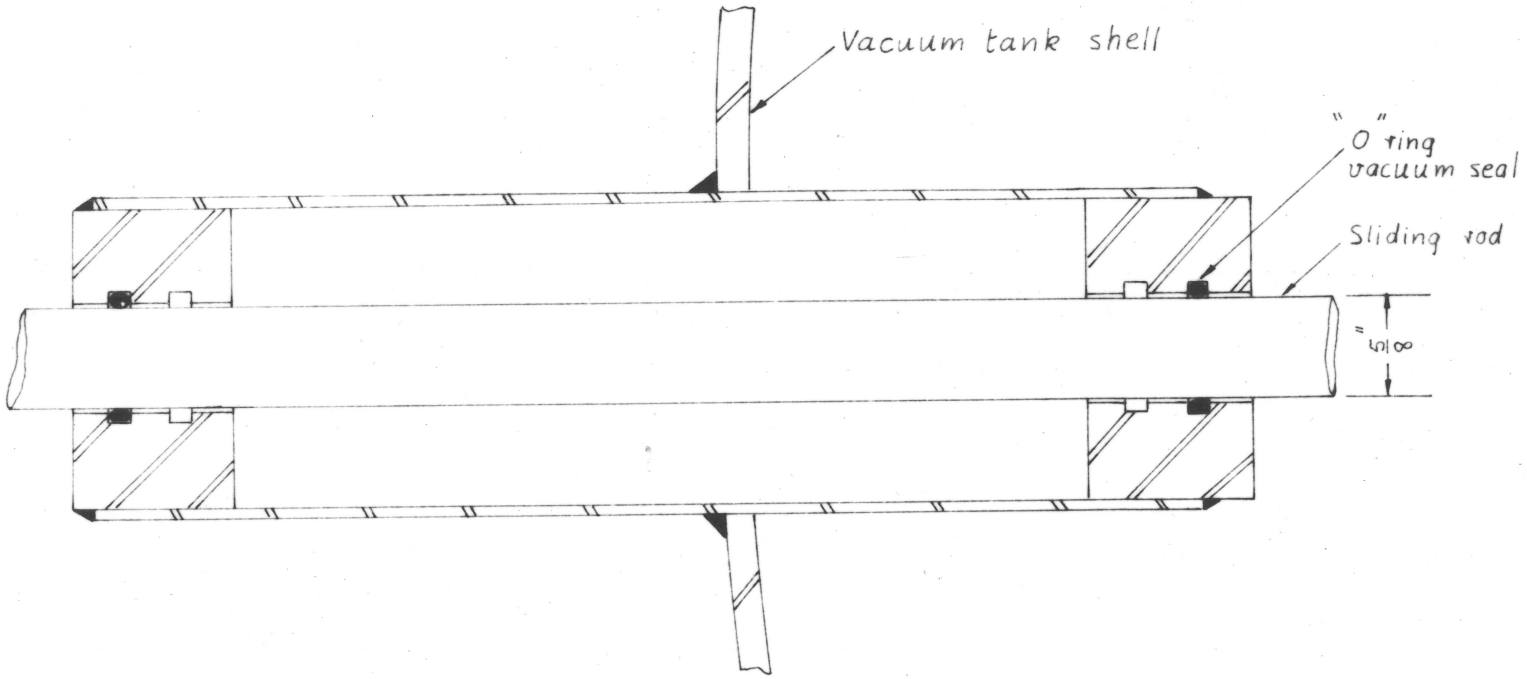


Fig. 2.9 Alloy addition rod

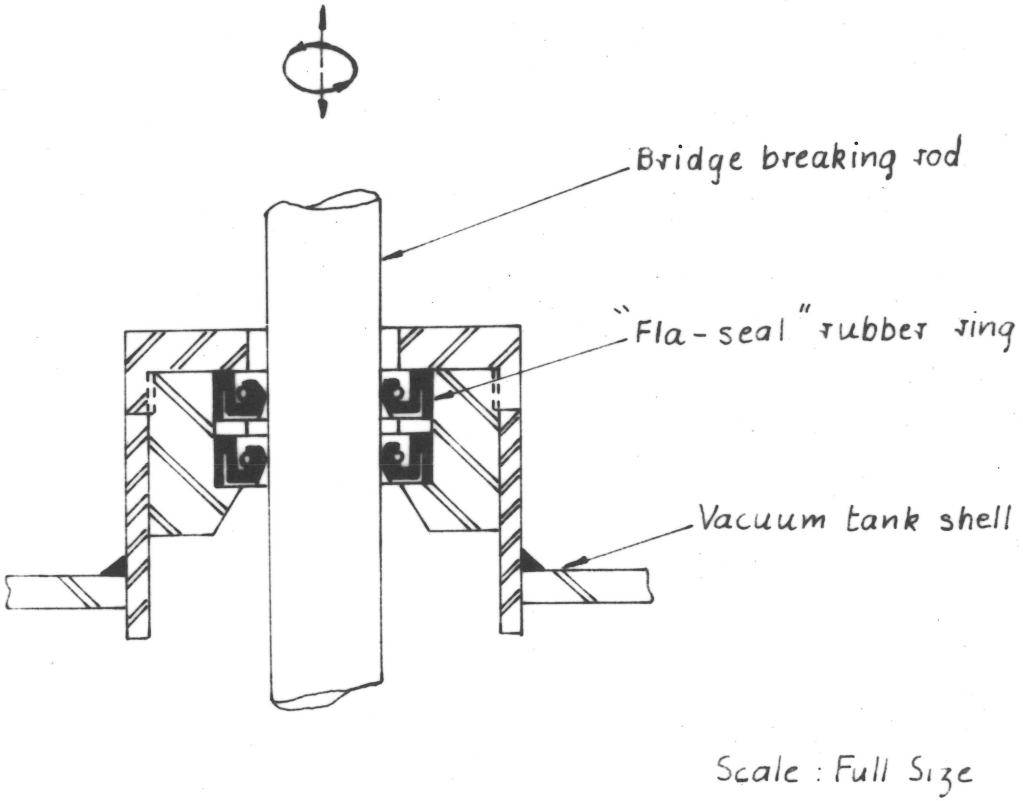


Fig. 2.10 Bridge breaking rod

2.4 VACUUM PUMPS

2.4.1 Selection of Vacuum Pump

The vacuum pumps were selected by considering the size of vacuum chamber, evacuating time, amount of gas to be handled and pressure of gas to be kept during the refining process.

The amount of gas evolved during refining process may come from

(a) molten iron

(b) gas absorbed in the refractory and at surface inside of the vacuum tank

(c) leakage into the tank.

The gas evolved from the molten iron may be calculated, but this is not very great because the volume of the charge is small and comparatively high purity material is used as a starting material.

The amount of gas absorbed and leakage of the tank are not certain. They may be kept to a minimum by avoiding opening the vacuum tank to the atmosphere for a long period and maintaining good vacuum seals. It may be assumed at this stage that they are small.

Thus the main factor governing the selection of the vacuum pumps is the operating pressure.

The low pressures used in the refining process are:

(a) during heating up the charge the pressure required is about 10^{-5} mm Hg. This is to reduce gases absorbed in the refractory as well as on the tank surface.

(b) decarburization, the pressure above the melt should be at 10^{-3} mm Hg. to promote the formation and evolution of CO from the melt.

The set of pumps to work under these conditions should consist of:

(a) A mechanical rotary pump capable of reducing the pressure of the vacuum tank from atmospheric pressure down to 10^{-1} mm Hg.

(b) An oil booster pump working at pressure $10^{-1} - 10^{-4}$ mm. Hg.

(c) An oil diffusion pump working at pressure $10^{-3} - 10^{-6}$ mm. Hg.

(d) A small mechanical pump working at pressure 10^{-1} mm. Hg. to back up the oil diffusion pump while it is idle.

Since the cost of the oil booster pump is high, and a suitable diffusion pump was readily available it was decided to delay purchase of the booster. The small backing pump was also omitted although this caused some operating inconvenience.

2.4.2 Size of Vacuum Pumps

There is no definite rule yet established for selecting

the size of vacuum pumps for vacuum induction melting furnaces. In the present case, use was made of empirical data. To melt a 12 lbs. ferrous metal charge the recommended pumps were a booster diffusion pump, 240 l/s, and a mechanical rotary pump, 14 l/s.[24] In view of the present intention to deal with comparatively high purity metals, the capacity of the pumps chosen was lower than that given in the data. They are as follows.

2.4.3 Oil Diffusion Pump

The oil diffusion pump is an Edwards "Speedivac" vapour diffusion pump, model 603, having pumping speed 600-650 litres per second without baffle valve and 300-350 litres per second with the baffle valve at 10^{-3} - 10^{-6} mm. Hg. The pump oil is silicone fluid No. 703, which has high molecular weight, low vapour pressure and exceptionally good resistance to oxidation at high temperatures.

The diagram of the pump is shown in Fig. 2.11. Its pumping speed with baffle valve is shown in Fig. 2.12.

In using the oil diffusion pump there is a risk of the pump oil contaminating the charge. The oil may go into the vacuum enclosure by evaporation from the upper part of the pump wall or by direct ejection from the jet. To avoid this an isolation baffle valve was put in between the oil diffusion pump and the vacuum enclosure.

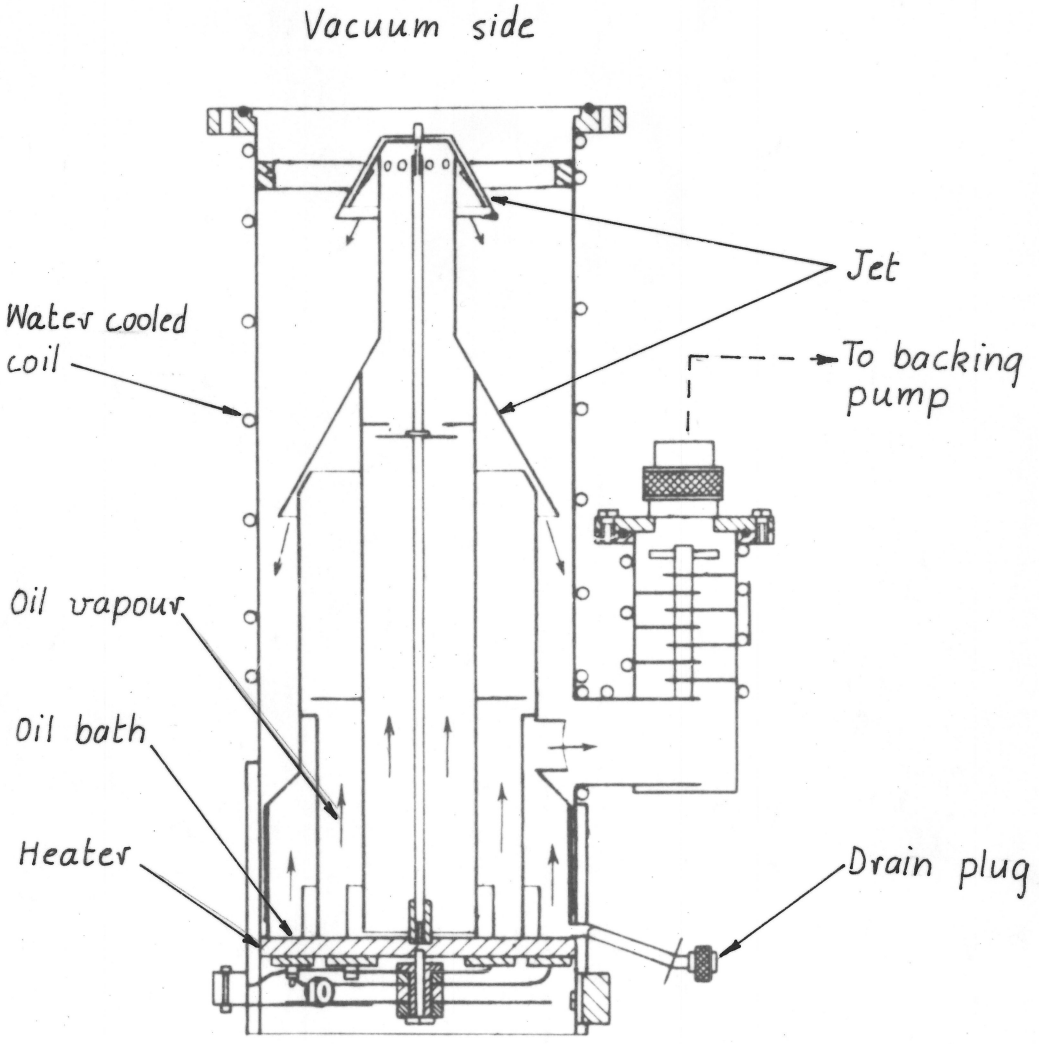


Fig. 2.11 Diagram of oil diffusion pump.25

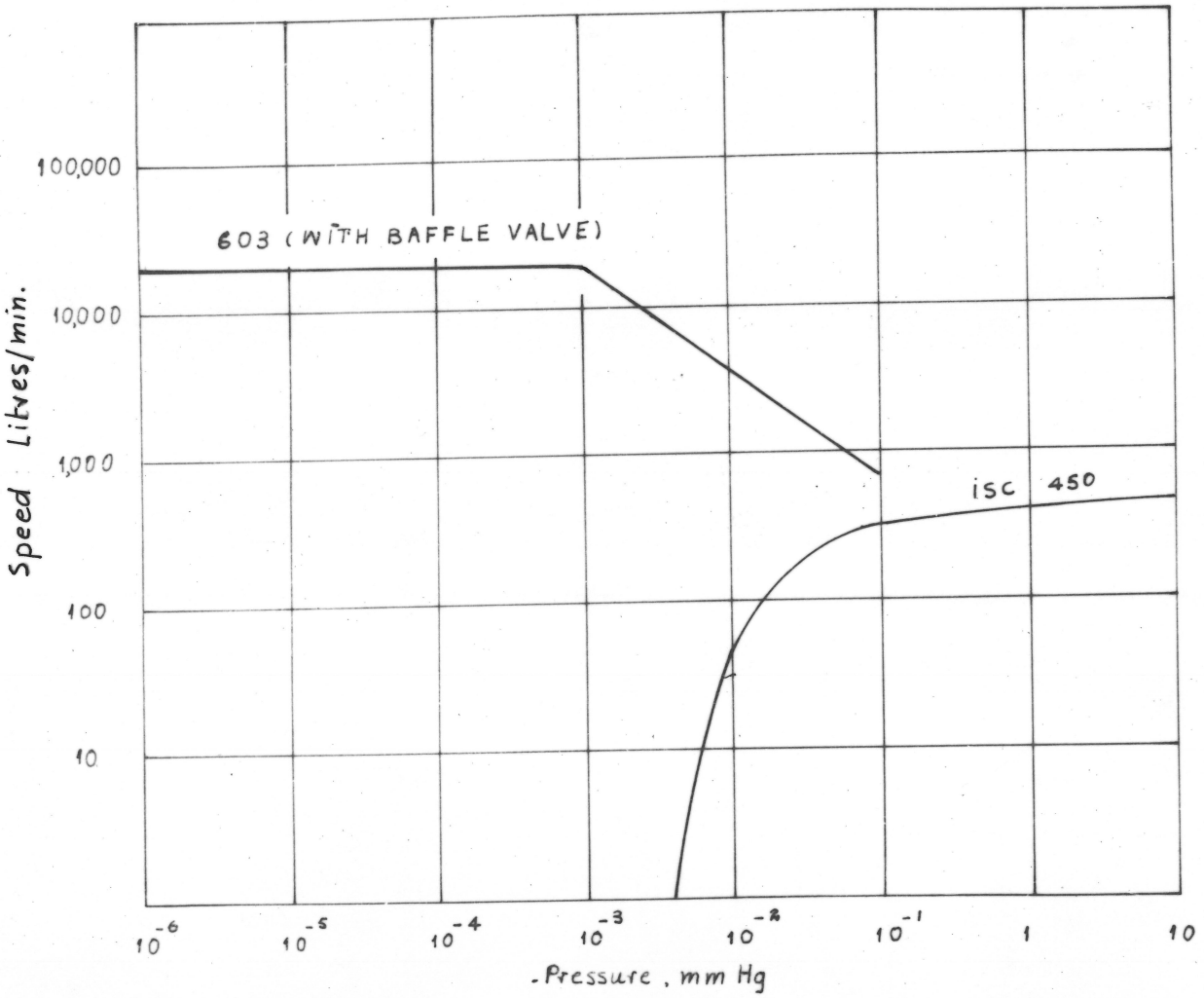


Fig. 2.12 Pumping speed of mechanical pump and oil diffusion pump.[25,26]

Since the pressure at the outlet of the oil diffusion pump is rather low (equal to the vapour pressure of the pump oil at the temperature of the pump boiler) the oil diffusion pump requires another pump to back it up.

According to the recommendation from the manufacturer, the backing pump for the diffusion pump model 603 should be the "Speedivac" rotary pump model 1 SC 450.

2.4.4 Mechanical Rotary Pump

The mechanical pump is used for two purposes:

(a) reduce the air pressure of the vacuum tank from atmospheric pressure to about 0.3 mm. Hg.

(b) backing the oil diffusion pump.

The "Speedivac" model 1 SC 450 has the volumetric speed of 450 litres per minute at atmospheric pressure. It is a rotary type with an air ballast as shown in Fig. 2.13. The use of the air ballast valve does not allow low ultimate pressure to be reached, but it has an advantage when dealing with the system which contains condensable vapour. When the air ballast is opened the compression ratio of the pump would be reduced from about 700:1 to 10:1.[22] In doing so the vapour pressure of the condensable vapour would be less than its saturation pressure and no condensation occurs. In practice when most of the condensable vapour is driven off the ballast valve is closed to get low ultimate pressure. The pumping speed

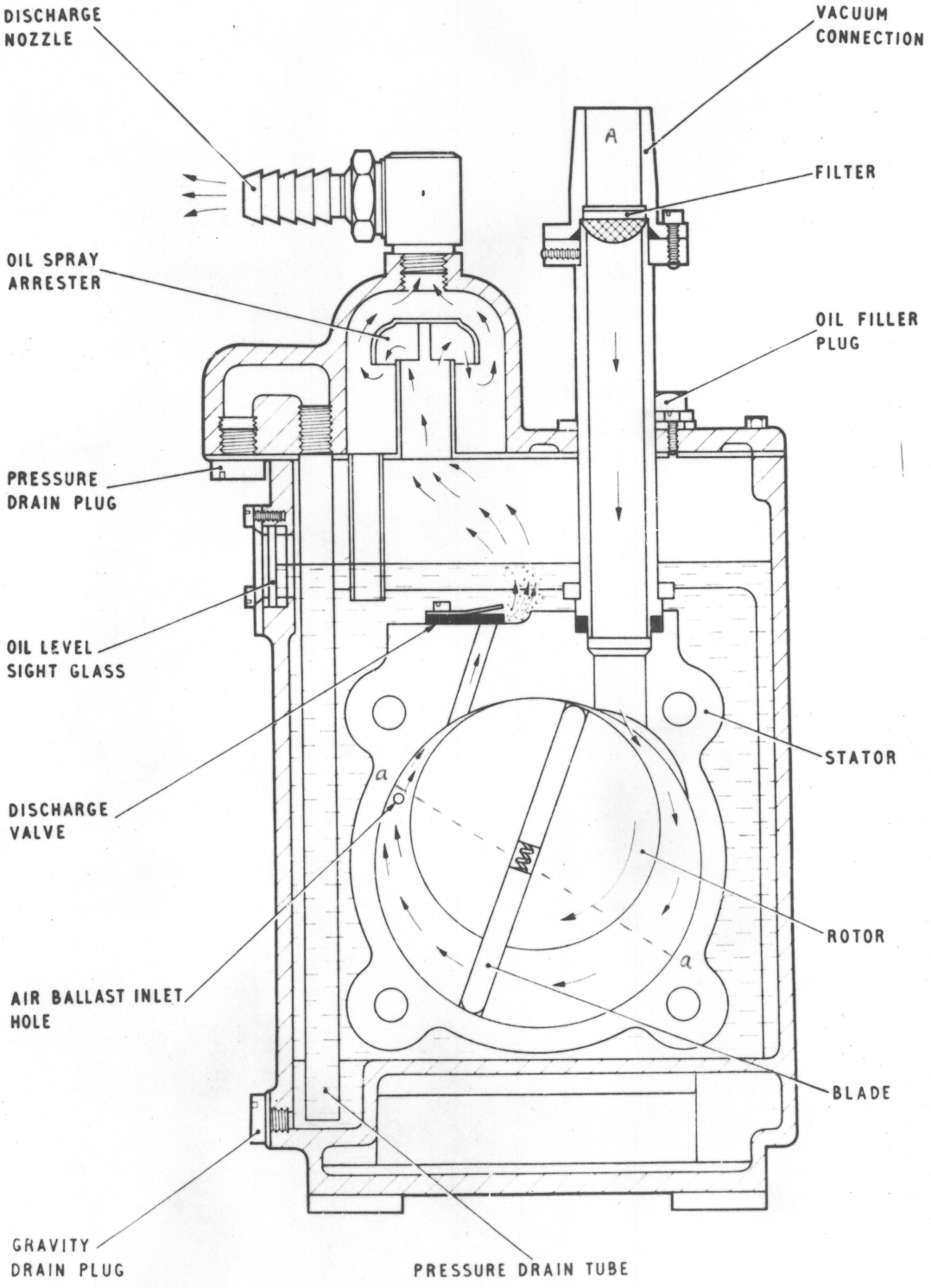


Fig. 2.13 Principle features of a typical "Speedivac" rotary high vacuum pump.26

curve is shown in Fig. 2.12.

In general the lowest possible pressure obtained by a mechanical pump depends on the vapour pressure of the pump oil, the vapour pressure of the contamination in the oil, and leakage of the pump joints.

2.5 Evacuation of Vacuum Tank

The evacuation of gas from the vacuum tank is done in two steps according to the capability of the vacuum pumps.

(a) Evacuation by the mechanical pump through 1.25 inch diameter pipe from one atmospheric pressure, 760×10^3 microns Hg. to 300 microns Hg.

(b) Evacuation by the oil diffusion pump through a 6 inch diameter pipe from 300 microns Hg. to 1 micron Hg.

Before proceeding to calculate the evacuation time the type of gas flow through the pipes and the corresponding pipe conductance would be considered first.

2.5.1 Type of Flow of Air

(a) For 1.25 inch pipe. From equations (2.11) and (2.12) when $P_a.d = 500$,

$$P_a = \frac{500}{1.25 \times 2.54}$$

$$= 157 \mu \text{ Hg}$$

when $P_a.d = 5$

$$P_a = 1.57 \mu \text{ Hg}$$

(b) For 6 inch pipe

when $P_a.d = 500$,

$$P_a = 33\,\mu \text{ Hg}$$

when $P_a.d = 5$,

$$P_a = .33\,\mu \text{ Hg}$$

Therefore the flow through 1.25 inch pipe was viscous at 157 μ Hg. and above. The flow through 6 inch pipe was viscous at 33 μ Hg. and above and molecular below .33 μ Hg.

2.5.2 Conductance of Pipes

At the beginning of evacuation the gas flow may be turbulent, but at high pressure the speed of the mechanical pump is high, and the reduction of pressure takes little time. It may be assumed for calculation that the flow through a 1.25 inch pipe is viscous from 760 mm Hg. to 300 μ Hg and the flow in 6 inch pipe is viscous from 300 μ Hg to .33 μ Hg and molecular below .33 μ Hg.

(a) Conductance of pipe of 1.25 inches diameter and 25 inches long.

For viscous flow at 300 μ Hg. from equation (2.15)

$$c = 0.182 \frac{d^4}{l} P_a \text{ litres/sec.}$$

$$d = 1.25 \times 2.54 \text{ cms.}$$

$$l = 25 \times 2.54 \text{ cms.}$$

$$P_a = 300\,\mu \text{ Hg.}$$

$$\therefore \quad C = 88.2 \text{ litres/sec}$$

(b) Conductance of 6 inch pipe under molecular flow.

From equation (2.17)

$$c = 12.1 \frac{d^3}{l} \text{ litres/sec.}$$

$d = 6 \times 2.54$ cms.

$l = 23 \times 2.54$ cms.

$\therefore C = 111 \times 10^2$ litres/sec.

The conductance of 1.25 inch and 6 inch pipe are so high that they may be neglected in considering the evacuating speed at the outlet of the vacuum tank.

2.5.3 Evacuating Time

(a) Reduce pressure from 760×10^3 micron Hg. to 300 micron Hg. by the mechanical pump.

The speed of the mechanical pump drops as the pressure is lowered as shown in Fig. 2.12. The total time may be obtained by calculating in steps.

When $P_1 = 760 \times 10^3 \mu$ Hg.

$P_2 = 10 \times 10^3 \mu$ Hg.

$S_p = 7.6$ l/s.

From equation (2.19)

$$t = 2.303 \frac{V}{S_t} \log \frac{P_1}{P_2}$$

$V = 310$ litres

$\therefore t = 176$ sec.

Similarly $P_1 = 10 \times 10^3 \mu$ Hg, $P_2 = 1 \times 10^3 \mu$ Hg.
$S_p = 6.6$ l/s, $t = 108$ sec.

$P_1 = 1 \times 10^3 \mu$ Hg, $P_2 = .3 \times 10^3 \mu$ Hg.
$S_p = 2$ l/s, $t = 186$ sec.

$\therefore$ Total time $\doteq$ 8 minutes.

(b) Reduce pressure from 300 micron Hg. to 10^{-3} micron Hg. by the oil diffusion pump.

The speed of the diffusion pump at various pressures was obtained from Fig. 2.12.

When $P_1 = .3 \times 10^3 \mu$ Hg, $P_2 = .1 \times 10^3 \mu$ Hg.
$S_p = 5$ l/s, $t = 68$ sec.

$P_1 = .1 \times 10^3 \mu$ Hg, $P_2 = .01 \times 10^3 \mu$ Hg.
$S_p = 15$ l/s, $t = 47.5$ sec.

$P_1 = .01 \times 10^3 \mu$ Hg, $P_2 = 1 \mu$ Hg.
$S_p = 100$ l/s, $t = 7.1$ sec.

$P_1 = 1 \mu$ Hg, $P_2 = 10^{-3} \mu$ Hg.
$S_p = 300$ l/s, $t =$ small.

$\therefore$ Total time = 2 minutes.

In a perfect vacuum system the time required to reduce the pressure of the vacuum tank from 760×10^3 micron Hg. to 1 micron Hg. by the pumps would be about 10 minutes.

But in practice there is always some leak associated with the vacuum system. The difficult period of evacuation would be in the region of 300-10 micron Hg. where the speed of both pumps is low. And at very low pressure, i.e. 10-1 micron Hg. where the small leak has large effects on the pressure. Working in the pressure region of 300-1 micron Hg. is done efficiently by an oil booster pump. But its high cost has prevented its use in the initial stages of the present work.

With a small leak taken into account it may be assumed that the evacuation time required would be about 30 minutes.

2.6 VACUUM GAUGES

The pressure range requiring measurement in the refining process is:

(a) at about 10^{-3} mm. Hg. during decarburization,

(b) at about 5-10 cm. Hg. when hydrogen is added to the vacuum tank to control spurting of molten iron during melting down and pouring.

The Pirani gauge and Bourdon gauge were chosen for (a) and (b) measurement respectively.

2.6.1 Pirani Gauge

The Pirani gauge works on the variation of the thermal conductivity of a gas with pressure.

The Pirani gauge used in the present work consisted of an Edwards Pirani gauge head, Model M6A, serial No. E-3836, and an electric circuit which supplied power to heat the long resistance wire in the gauge head and also measure the change of the wire resistance.

The gauge head consisted of a long resistance wire with high coefficient of resistance in a glass tube with one end opened for connecting to the vacuum system. The resistance measuring circuit is essentially a Wheatstone bridge having a long resistance wire of the gauge head as one of its arms. The simple circuit diagram is shown in Fig. 2.14.

When the gauge head is connected to a vacuum system at sufficiently low pressure, i.e. the mean free path of the gas molecule is in the order of the distance between the long resistance wire and the glass wall, the heat transfer from the long resistance wire will be a kinetic process. A gas molecule will collide with the hot wire, increase its kinetic energy, collide with the glass wall, lose part of its kinetic energy to the wall. In this process the temperature and resistance of the hot wire will drop. The change in resistance is measured by the Wheatstone bridge.

In this pressure region the ability of gas molecules to transfer heat (or the thermal conductivity of gas) is

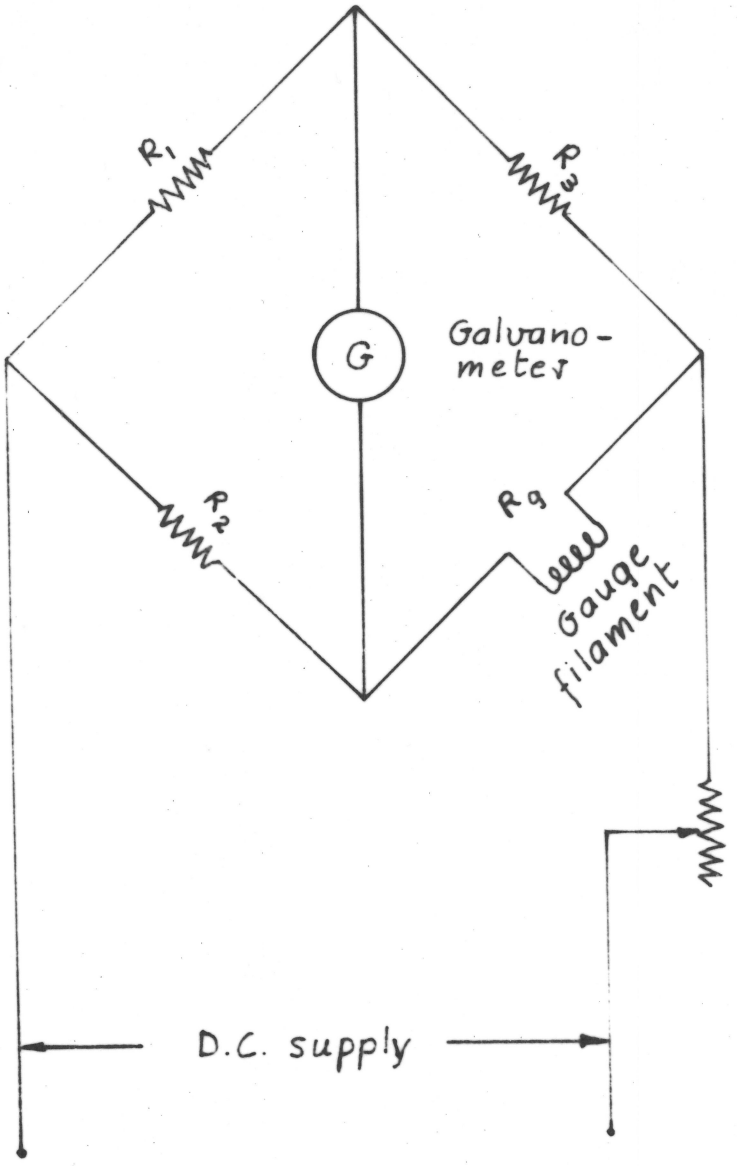


Fig. 2.14 Simple diagram of Pirani Wheatstone-bridge

approximately proportional to the gas pressure, and may be represented by an equation,

$$K = C \cdot P$$

K = gas thermal conductivity

C = a constant

P = gas pressure.

The thermal conductivity and the pressure of gas may be determined indirectly by measuring the change in resistance of the hot wire as mentioned above.

The working pressure range of the Pirani gauge is $10^{-1} - 10^{-4}$ mm. Hg. The upper pressure range is limited by the fact that the thermal conductivity of gas becomes independent of pressure at high pressure. At pressure lower than 10^{-4} mm. Hg. the conductivity of gas becomes very small and the gauge loses its sensitivity due to the rapid rise in temperature of the wire.

2.6.2 Bourdon Vacuum Gauge

The Bourdon vacuum gauge was of an ordinary type. It was used to measure the hydrogen pressure above the melt in the region of 10 cm. Hg. It indicates a rough pressure only as the accurate pressure measurement was not critical during melting down and pouring.

2.7 Leak Testing

There are a number of ways of detecting leaks in a

vacuum system. In the present work two methods of leak detection were used:

(a) Hydrogen jet and Pirani gauge detection.

(b) Shut-off and measure the pressure rise.

2.7.1 Hydrogen Jet and Pirani Gauge

This method was used to locate the positions of leak of the vacuum system, with no work-coil, crucible or charge in the vacuum tank. First the pressure of the vacuum tank was reduced to below 10^{-5} mm. Hg. An external galvanometer of high sensitivity of about 10 cm./micro-ampere was connected to the Pirani bridge circuit to increase its sensitivity. The hydrogen jet was passed over the vacuum tank shell and over the various vacuum seals. At a leak the hydrogen gas will diffuse rapidly into the vacuum tank and cause the pressure to rise. The thermal conductivity of the hydrogen is high so the diffused hydrogen will cause a change of the galvonometer reading and indicate the leak.

In the present instance there were no detectable leaks. It might be assumed that there was no large leak in the vacuum tank that would upset the refining process in vacuum.

2.7.2 Shut-off Method

This was to measure the pressure rise in the cold vacuum tank before proceeding to the vacuum refining. With the work-coil, crucible and charge inside the vacuum tank, the crucible was dried by induction heating the charge to

1000°C for half an hour. The tank was evacuated by the pumps and then shut off. The pressure rise was 80 μ Hg. per hour. The system was considered to be good for refining processes. In general the allowable cold leak is about 1 μ Hg. per minute.[27]

CHAPTER III

REFRACTORY

3.1 Introduction

There are two factors to be considered in the selection of refractories used in the production of high purity iron alloy by vacuum induction melting. Firstly the refractory should be chemically inactive with the molten iron to avoid contamination from the refractory. Secondly, melting by induction tends to produce high thermal stress in the container due to high temperature gradient being set up through the thickness of the container as well as on its length. To withstand the thermal stress the refractory should have high thermal shock resistance. The other requirement for physical properties are high softening point, low electrical conductivity and low thermal conductivity at high temperature.

For chemical inactivity with the molten iron the choice of refractory is confined to a few oxides, i.e. Al_2O_3, MgO, BeO and ZrO_2. Table 3.1 shows physical properties of some oxides.

Alumina has some advantage over the others, since it is available in high purity, has low reactivity, and good thermal shock resistance. It has been used by many workers to melt high purity iron with no significant contamination

Table 3.1 Physical Data on High Refractory Oxides[28]

Oxide	Melting Point °C.	Max. Service Temp., °C.	Softening Temp. at 2 kg/cm.^{2} pressure, °C.	Mean Expansion Coeff. at 20-1000°C x 10^{-6}	Thermal Conductivity at 1000°C K cal/mh°C	Thermal Shock Resistance cm.°C $sec^{-\frac{1}{2}}$
Alumina (Al_2O_3)	2050	1900	1800	8.6	4.3	10
Beryllia (BeO)	2570	2200	2000	8.9	12.9 (1200°C)	12
Magnesia (MgO)	2800	2300	2000	14.2	5.5	1.5
Thoria (ThO_2)	3000	2500	2000	9.3 (0-800°C)	-	2.5
Zirconia (ZrO_2)	2715	2300	2000	7.0	-	0

from the alumina crucible. For these reasons alumina was chosen to make the crucibles. The method of manufacture will be described later.

3.2 Zircon Lining[29]

3.2.1 Making of Zircon Lining

To test the behaviour of the induction melting of the motor generator set, work-coil, transformer and capacitor, the preliminary melting was carried out by melting a mild steel charge in a zircon lining.

There are large deposits of zircon sand in Australia. An example of its composition in 67.2 per cent ZrO_2, and 32.8 per cent SiO_2. It is usually associated with quartz, garnet and other minerals. The melting point of high purity zircon sand is 2550°C,[30] but it will dissociate at temperature 1650-1750°C,[31] depending on the impurities present.

Zircon ($ZrSiO_4$) has a good thermal shock resistance and high strength at elevated temperatures.

The zircon sand used consists of particle size as follows:

B.S.S.	Weight Per Cent
+72	0.3
-72 + 100	14.8
-100 + 150	68.6
-150 + 200	14.6
-200 + 300	0.3
-300	1.4

Under the microscope the grain shape appears semi-rounded as in Fig. 3.1. The semi-rounded grain when rammed to form a certain shape has low green strength and dry strength even with a binder, so that it is necessary to add zircon flour with the zircon sand. The zircon flour is finer and has an angular shape.

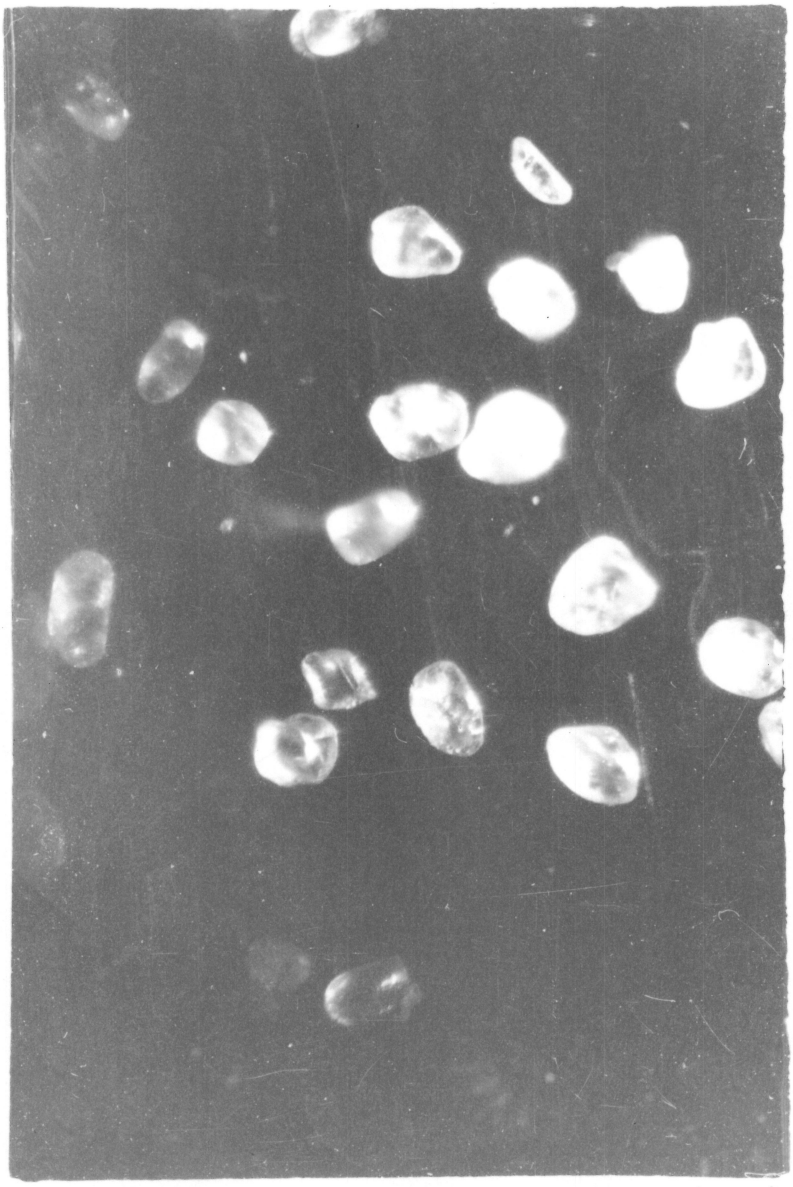
The same amount of zircon flour and zircon sand by weight was thoroughly mixed by rolling on a paper sheet.

The binder was ethyl silicate, prepared from the following reactants:

450 cc. "Silester 'O'" (Monsanto Chemical Co.)
100 cc. 0.5 per cent w/w hydrochloric acid
450 cc. alcohol (methylated spirit)

The reactants were mixed in a glass bottle and shaken vigorously for ten minutes. Silica and water dissolved in alcohol was hydrolysed with HCl acting as a catalyst. The hydrolysis was accompanied by heat evolved and its completion was noticed by the solution attained maximum temperature and given clear solution. The solution may be kept for two weeks in a refrigerator at temperature about $3^{o}C$. 250 cc. of solution was used for 2000 g. of zircon sand and zircon flour, with a small addition of magnesia.

The settling time of the lining mixture may be varied by the amount of magnesia powder added, with 0.5 per cent



(X80)

Fig. 3.1 Grain shape of zircon sand.

of magnesia the settling time was 10 minutes.

The lining mixture when thoroughly mixed was plastic and could be rammed in the space between the work-coil and steel core as in Fig. 3.2. During pouring the whole set up was shaken by an air vibrator placed on the wooden board. This helped to remove air bubbles in the filling mixture.

It has been found that by wrapping the steel core with a brown wrapping paper the core could be pulled out of the lining after it had set, otherwise the core had to be knocked hard when the lining started to set before it could be pulled out. This caused a severe cracking of the lining. The lining always had some cracks at the joint between its side and bottom, but after repairing with the lining mixture and firing it held molten iron well.

3.2.2 Firing Zircon Lining

First excess alcohol was burnt off, then a solid mild steel charge. 3 inches in diameter and $3\frac{3}{4}$ inches long was inserted and heated slowly by induction heating. The temperature was raised to 1000°C in one hour and kept there for $\frac{1}{2}$ hour. The lining was then ready for melting.

This lining has the advantage that a sintered ring forms at the inner surface only. The rest consists of tightly packed small particles bonded relatively loosely.

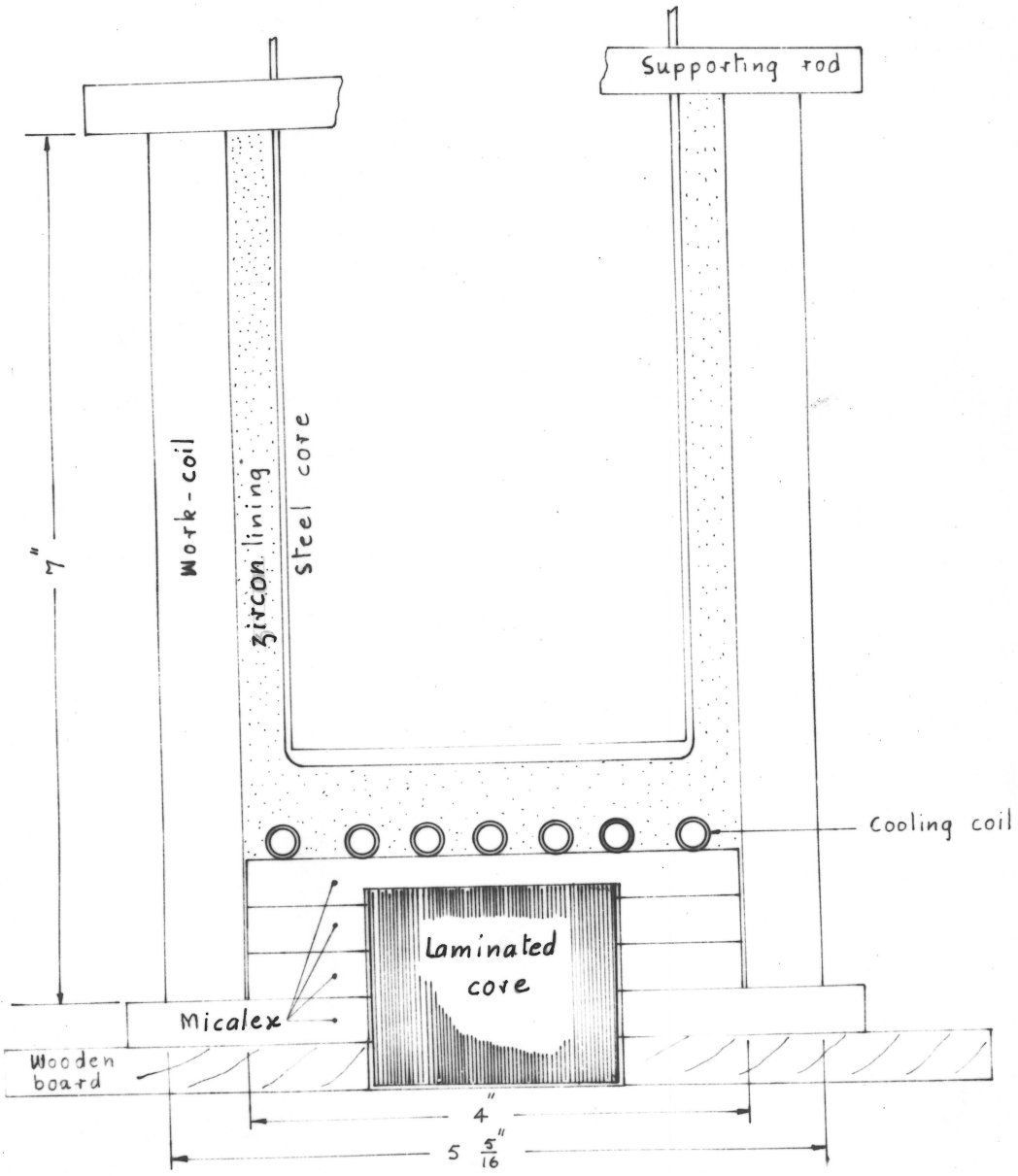


Fig. 3.2 Set-up for zircon lining

If there is any crack at the inner surface and the molten metal penetrates through the sintered ring, it will solidify before reaching the water cooled work-coil.

Experimental melting of low carbon steel showed that the zircon sand lining held molten iron quite well. It could be used for a number of heats if the lining was carefully checked and repaired before starting a new melt.

The number of heats per lining has not been investigated since only a few melts were made to test the melting capabilities of the equipment. The zircon lining will not be used for melting and refining high purity iron alloys because there is a strong tendency towards contamination by zirconium and silicon produced by dissociation of zircon.

3.3 Alumina Crucible

There are a number of ways to make alumina crucibles, e.g. hot pressing, extrusion, slip casting and tamping. In the present work the tamping method was chosen. It requires a simple crucible mould and cheap tamping tools, and the method of tamping is simple.

3.3.1 Tamping Mixture

Alumina of different grain sizes was obtained from Alan H. Reid, Pty. Ltd., Sydney, Australia. Example of

grain size distribution is as follows:

Grade 60 F

B.S.S.	Per Cent by Weight
+ 60	9.1
+ 72 - 60	14.6
+ 100 - 72	20.6
+ 150 - 100	19.5
+ 200 - 150	18.4
+ 300 - 200	10.3
- 300	8.5
Total	100.5

Grade 100 F

+ 150	22.2
+ 200 - 150	34.1
+ 300 - 200	23.8
- 300	20.7
Total	100.8

The chemical composition of the fused alumina is as follows:

Al_2O_3	99.5%
Na_2O	0.30%
Fe_2O_3	0.20%
SiO_2	0.05%
TiO_2	0.005%
V_2O_5	0.002%

In making a tamped alumina crucible, Stott[32] used

ramming mixture of two parts by weight of crushed fused alumina (passing through a sieve of 90 meshes per inch) and one part by weight of finely ground calcined alumina, moistened with water containing 4% ammonium alginate and ground in an edge runner mill for five hours.

In the present work an attempt has been made to prepare a ramming mixture containing no organic or inorganic binders. It has been found that using 80% of grade 60 F fused alumina and 20% of calcined defloculated alumina slip produces a crucible with enough green strength for handling, and with good thermal shock resistance after firing (due to the wide range of particle size).

3.3.2 Alumina Slip

The alumina slip used in the ramming mixture serves two purposes:

(a) as a pure alumina bonding material, it avoids contamination from impure binders,

(b) having fine slip particle it distributes evenly among the coarse alumina particles. This gives good green strength and a good sintering result. It had been suggested that the slip made from calcined alumina would give better sintering results than the fused alumina slip.[33]

The slip was prepared from a calcined alumina powder, Morganite Triangular R.R. No. 933, having the following

composition:

Al_2O_3	99.7%
SiO_2	0.02%
Fe_2O_3	0.1%
Alkalies	0.2%

The method of preparation was similar to that of Watt and Roberts[34]. The calcined alumina was mixed with equal weight of six normal hydrochloric acid. This acid will give approximately maximum hydrogen ion concentration. The mixture was allowed to stand for 48 hours with frequent stirring. Iron and some other impurities in the calcined alumina were dissolved into the solution. The liquid colour was light yellow.

After 48 hours the supernatant liquid was syphoned off and about the same amount of distilled water was added and the whole was stirred up over a day. The decantation and topping up with distilled water was repeated until the pH of supernatant liquid was about 2.5-3.0. At this pH the viscosity of the suspended alumina particle is nearly at minimum as in Fig. 3.3.

The minimum viscosity occurs when pH is between 3-4 but Watt and Roberts[34] found that the slip casting had better green strength when it was cast at pH 2.5-3.

In the present work the minimum viscosity was not critical because the crucible was prepared by tamping not

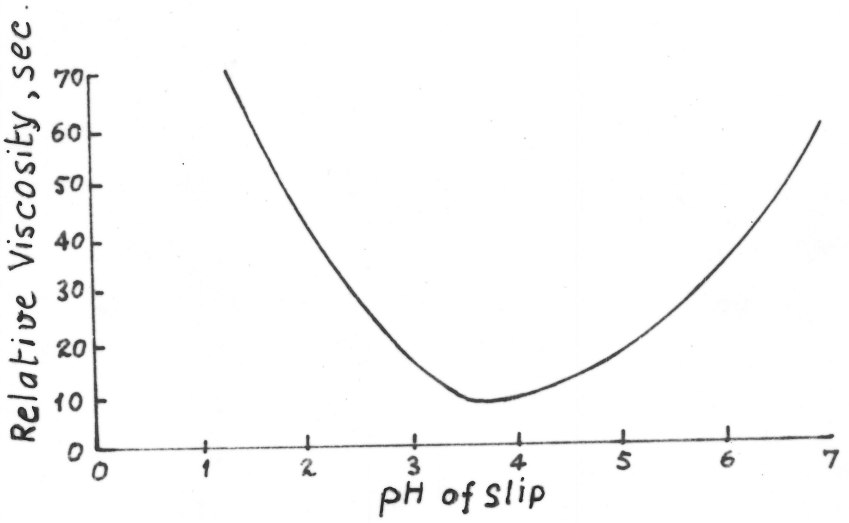


Fig. 3.3 Relation between relative viscosity and pH of alumina slip.[34]

slip casting. The pH chosen was 2.5-3. This would take less time to prepare than the slip of high pH.

The mechanism of formation of slip has been suggested,[34] namely that the hydrochloric acid attacks the surface of the alumina particles and forms a layer of $Al(OH)_3$. Hydrogen ion becomes adsorbed to the layer of $Al(OH)_3$, thus the alumina particles acquire a positive charge, so that they will repel each other or "deflocculate". Over the alumina surface there will be chlorine ion atmosphere which gives electrical neutrality.

When the slip was successfully made and settled, there were many alumina colloid particles in the liquid above the slip. This colloid was siphoned off. It was suspected that the colloid was one cause of cracking in the crucible.[33]

3.3.3 Mixing the Mixture

The firing furnace could accommodate two crucibles at a time, so the tamping mixture required was about 1800 grammes per one mixing. A suitable mill for grinding was not available, and it was decided to employ hand mixing. The alumina slip with 30% of very dilute hydrochloric acid was put in an earthenware mortar first and then fused alumina was added gradually and was coated by the slip. Mixing was then continued by hand. This method gave a

reasonable mixture but it contained too much moisture. It was found necessary to leave it overnight to let the water evaporate until the moisture was about 5%.

3.3.4 Crucible Mould

The crucible mould was similar to that of Stott.[32] It consisted of a bronze liner, a brass core and a bronze stand. Bronze was used because a large piece of wrought brass was not available.

The liner was split into three equal segments for ease of taking the liner off after tamping and to prevent cracking of the crucible. The liner segments were held together by two steel rings.

The core was made of 3 inch diameter brass tubing with its ends closed by $\frac{1}{4}$ inch brass plates. It was necessary to drill eight $^1/_{16}$ inch holes through both ends of the core. This was to allow the air to enter the space between the core and the inside bottom of the crucible while extracting the core. Otherwise vacuum would be created inside the crucible, causing it to crack. Before tamping these holes were covered by a thin sheet of brown paper to prevent the alumina particles from falling in and choking the holes. The setting of liner, core and base is shown in Fig. 3.4.

It was found that if a brown wrapping paper was wrapped

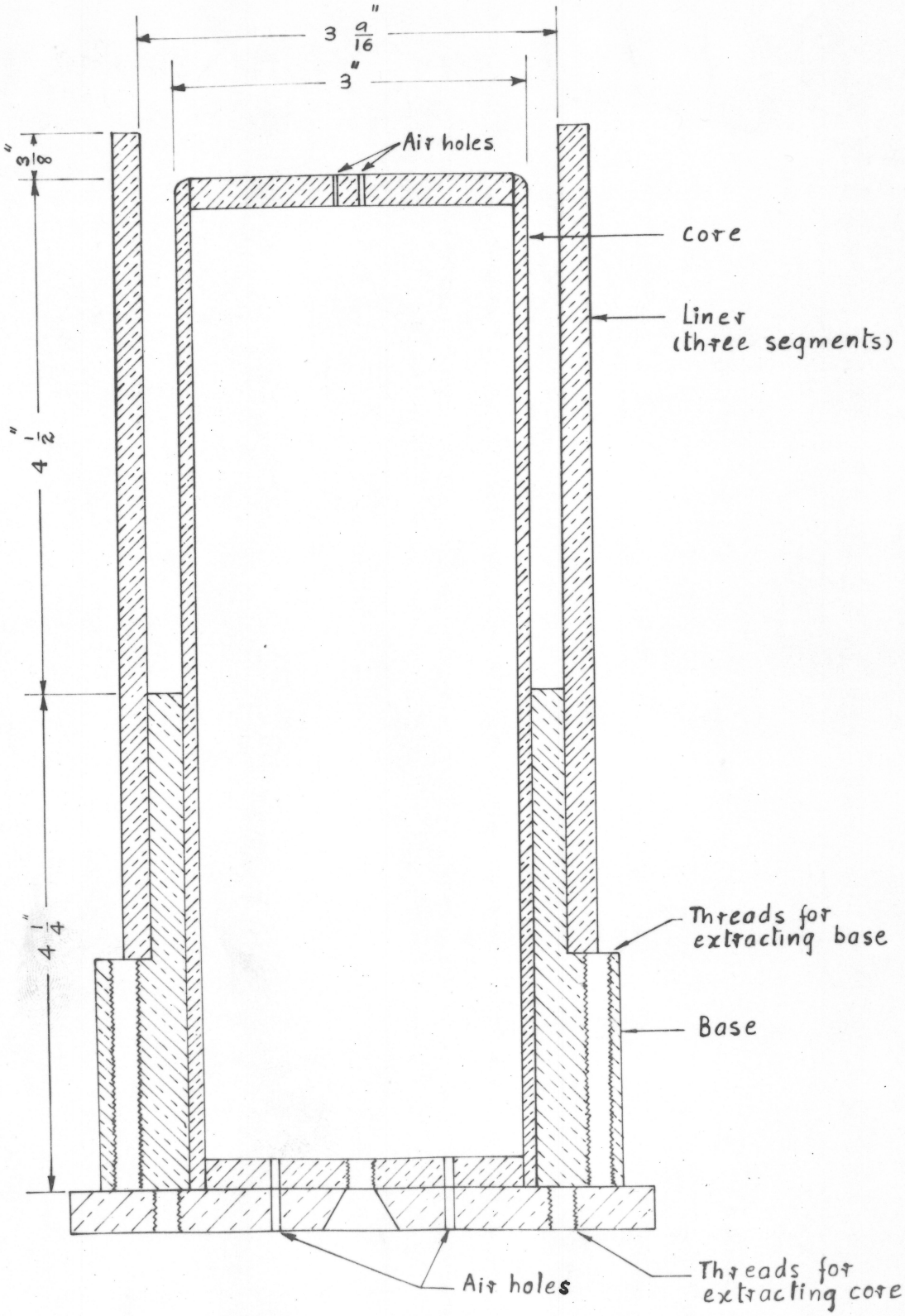


Fig. 3.4 Crucible Mould

around the inside surface of the liner it would prevent the moist ramming mixture from sticking to the liner surface. The liner could be taken off after ramming with ease. The brown wrapping paper also supported the crucible when it was moist and had little strength.

3.3.5 Tamping

The tamping tool had a stainless steel end. It had a blunt screw driver shape to give tight tamping. The tamping was carefully done to make the crucible with as uniform density as possible. After finishing tamping the mould was turned over and sat on a flat surface. The core was extracted by two long bolts, as shown in Fig. 3.4. The extraction of the core was done slowly to let air through the holes at the core end. If the core was extracted too fast it tended to cause cracking at the bottom of the crucible due to slight vacuum being created on the inside of the crucible bottom and atmospheric pressure acting on the outside. Then the liner and the crucible were placed on a 3/16 x 4 x 4 inch silica plate with fine alumina on the plate for cushion. The steel ring clamps were loosened and slipped out. The liner segments were then taken off carefully leaving the crucible (with the brown paper wrapped around it) inverted on the silica plate to simplify handling. This had an advantage that gripping the side of the crucible

and lifting it up which may cause cracking can be avoided. Now the crucible can be safely transferred to the firing furnace by lifting the silica plate.

3.3.6 Firing

The firing was done in two steps:

(a) Two crucibles were fired in an electric glow bar furnace to 1300°C in six hours and kept for 15 minutes, then cooled down in the furnace in 12 hours. After firing the crucible was quite strong and safe for handling.

(b) Firing for sintering. From the work of D. J. Ryschekewitsch, the firing temperature of alumina article should be at least 1800°C[33]. Sintering of alumina particles at 1800°C is a solid state reaction. Its mechanism is not fully explained. There are a number of possible reactions involved,[35] e.g. evaporation and condensation, surface diffusion, grain boundary diffusion. It seems that first the particles join together by evaporation from partswhich have big radius of curvature and condensation on the parts which have small radius of curvature then the mass transfer occurs by the other reactions mentioned above.

Physically after sintering there will be changes in grain size and shape, and a change in pore size and shape. The pores become smaller and more rounded, which gives rise to volumetric shrinkage which depends on the particle size,

sintering temperature and sintering time.

The sintering was carried out in a graphite susceptor heated by a radio frequency induction heater similar to that of McPherson,[29] shown in Fig.3.5. The heating coil (made of $\frac{3}{8}$ inch diameter copper tube) had nine turns, wound to $8\frac{1}{2}$ inches diameter and a length of 6 inches. Each turn was separated by soldering three brass screws on at 120° apart and attaching them to three ebonite bars. The ebonite posts and the heating coil were sat on a $\frac{3}{8}$ inch thick asbestos plate which was placed on two layers of insulating brick, 5 inches thick. This gave good insulation at the bottom.

The graphite susceptor (turned from a $5\frac{1}{4}$ inches diameter electrode butt) had an inside diameter of $4\frac{3}{8}$ inches, $7/_{16}$ inch wall thickness and was $6\frac{7}{8}$ inches long. The susceptor lid was made of the same graphite rod, and was fitted with two graphite chimneys, one is used for measuring the temperature inside the susceptor pot and admitting nitrogen gas and the other to let the gases out.

In firing alumina crucible it is necessary to have a neutral or oxidising atmosphere to prevent the alumina being reduced. Since an oxidizing atmosphere is not possible for the graphite pot heater, commercial nitrogen gas was used for making the neutral atmosphere. It was passed through molecular sieves to eliminate water before

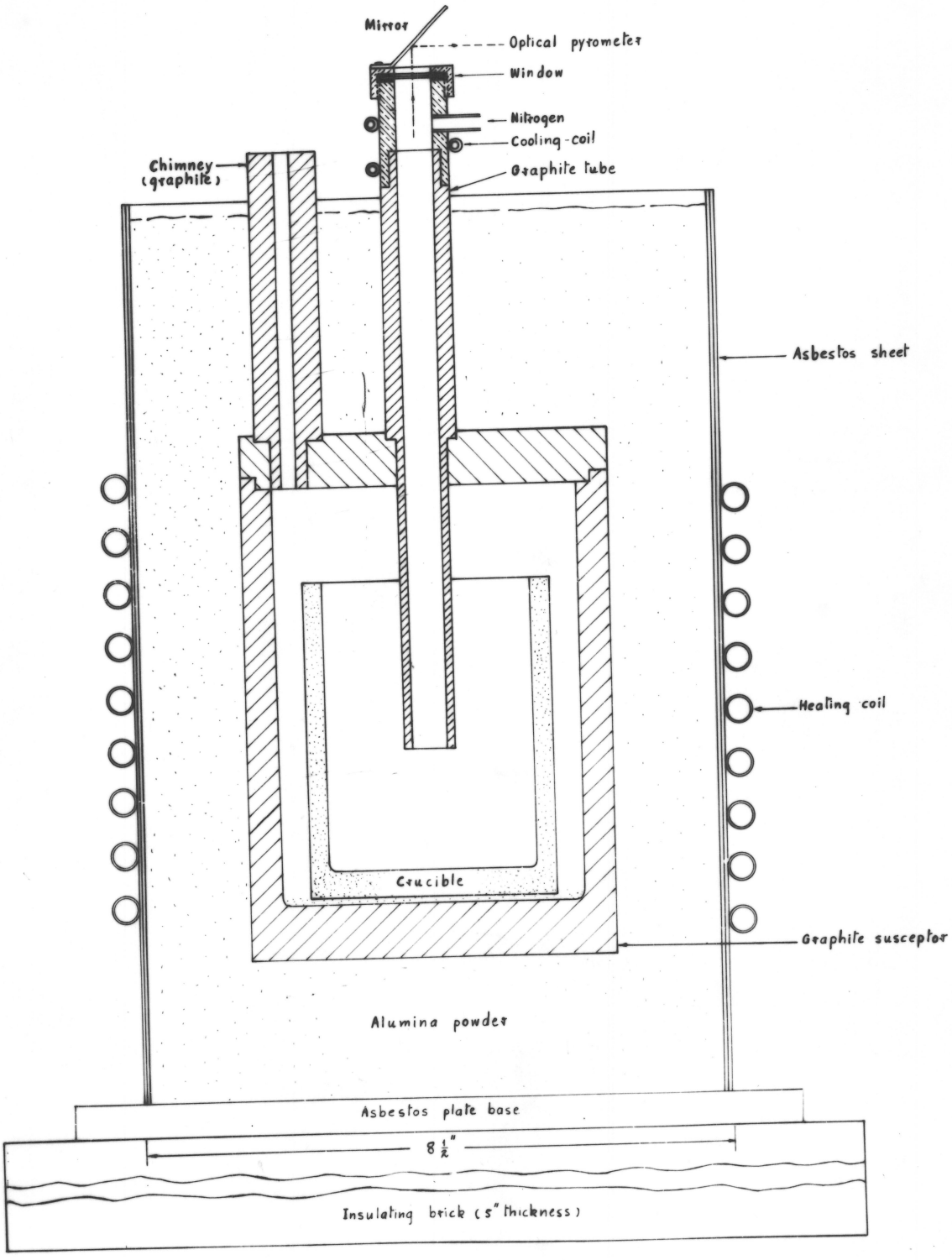


Fig. 3.5 Crucible firing furnace

letting into the graphite heater.

Alumina powder (settling tank fines) was packed between the graphite pot and the heating coil for insulation. This gave a large number of small pores throughout the packing. At high temperature the heat transfer from the graphite heater across the pore is mainly by radiation. The radiation across a pore is proportional to the diameter of the pore and proportional to the third power of mean temperature across the pore.[35] Hence the packing which gives small pores is a good insulator.

A sufficient clearance must be given to this insulation, otherwise heat loss through the surface of the graphite would be too high and high temperature around 1800°C could not be obtained.

In an early firing the diameter of the heating-coil was $6\frac{3}{4}$ inches, the outside diameter of the graphite heater was $5\frac{1}{4}$ inches, and the thickness of the packed alumina powder was $\frac{3}{4}$ inch. When fired with a 6 kW power source the maximum temperature attained was 1660°C. It could not be raised above this because the heat loss to surrounding was too high.

About 15% of pure graphite powder from the turning of the graphite pot was added to the insulating powder to prevent an excessive oxidation of the graphite pot.

The firing was as follows. The input power was 6 kW at the beginning of firing. When the temperature of the alumina crucible was about 1350°C (after 1½ hours) the input power was reduced to 5 kW. This was to decrease the shrinkage rate of alumina which was high, between 1350-1650°C.[36] After ½ hour the temperature reached 1650°C and the power was increased to 6 kW. When the temperature reached 1800°C it was kept there for 30 minutes. Then the power was turned off and the furnace was let to cool down.

The sintered alumina produced had a ringing sound when hit with a wooden pencil. It had a dirty grey colour, probably due to contamination from impurities[37] and from the graphite pot during firing[29]. When the crucible was reheated at 1000°C for ½ hour the dirty grey colour was lighter.

The photograph of sintered alumina crucible and crucible mould is shown in Fig. 3.6.

3.3.7 Temperature Measurement

The temperature inside the graphite heater was measured by an optical pyrometer, Cambridge Instrument Co., Lamp No. 4984, No. L 198298, focusing on the bottom of the crucible, via a polished stainless steel plate, through the sight hole glass window.

The sight hole was made of a graphite tube 1 inch outside diameter and 7 inches long, with a half inch bore.

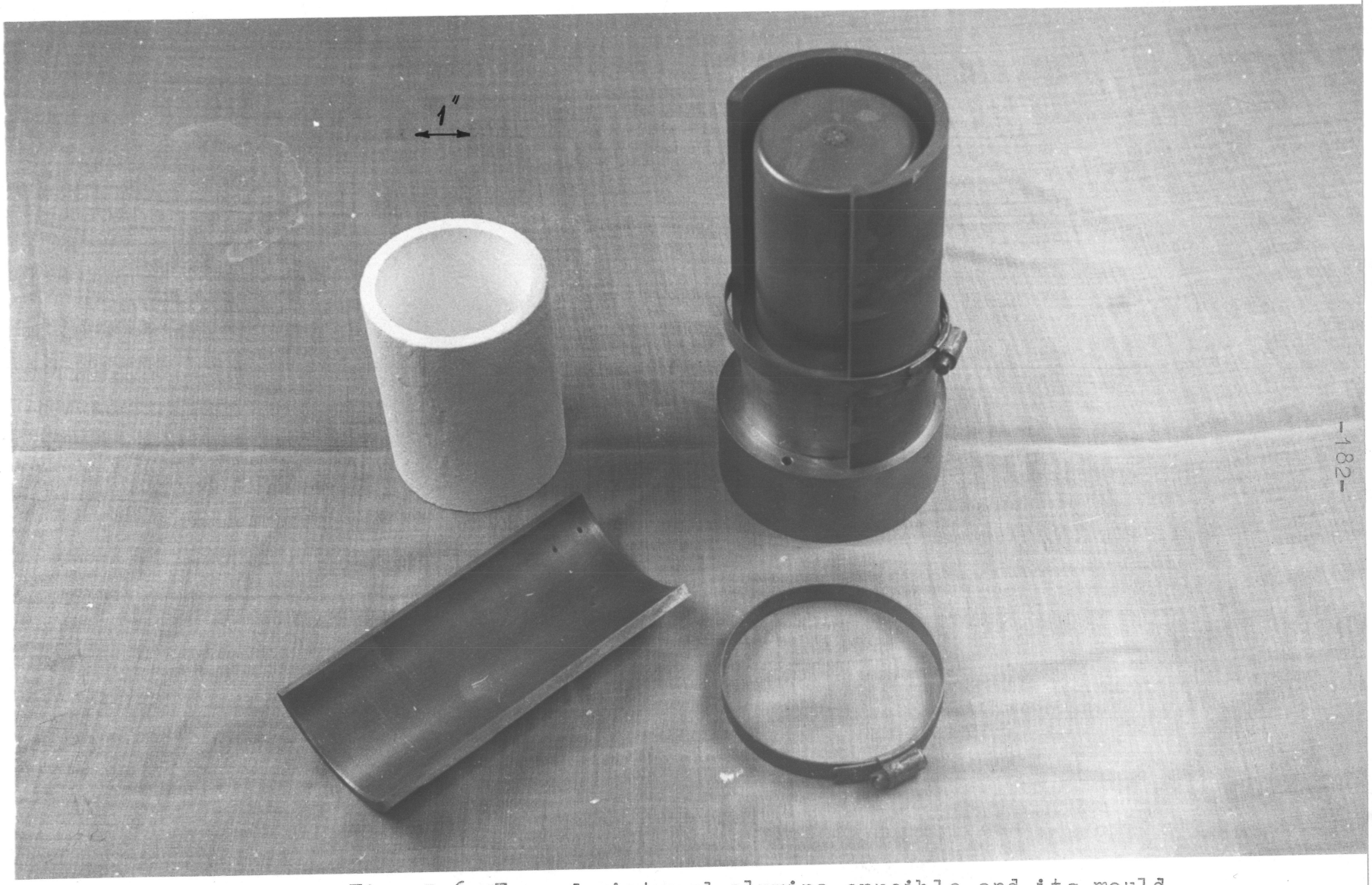


Fig. 3.6 Tamped sintered alumina crucible and its mould.

The temperature measured through this hole is approximately that of a block body, but part of the light is absorbed through the glass window and the reflectivity of the stainless steel mirror is less than one. The reflectivity of polished steel for red light (λ = about 0.65 μ) is 0.65.[38] This could be used for the polished stainless steel mirror.

The correction for the light absorbed at the glass window is + 16°C at 1600°C,[17] and the correction for the reflectivity of stainless steel mirror is + 100°C,[17] so if the temperature measured by the optical pyrometer is 1485°C the actual temperature should be about 1600°C.

During firing at temperature beyond 1600°C it was found that the chimney was choked by a deposited powder which may have consisted mainly of alumina and carbon. The choked chimney caused a smoky product inside the graphite pot, which gave low apparent temperature readings of the optical pyrometer, about 200°C below actual temperature. Hence before measuring temperature the chimney was cleared first.

CHAPTER IV

REFINING

4.1 Basic Principle of Refining Process

The program of refining of the Armco iron was carried out in two stages:

(a) Oxidation of impurities in Armco iron by melting in air.

(b) Reduction of carbon and oxygen content by melting under vacuum and under hydrogen atmosphere respectively.

The success of removal of impurities depends on the ability to control the factors which effect

(a) chemical equilibrium,

(b) reaction kinetics

of the chemical reaction of the impurity concerned.

The aim of this work was to shift the equilibrium in such a way that very small amounts of impurities were left in liquid iron after refining, e.g. removal of oxidation products from the reaction system.

The reaction kinetics of refining of impurities in liquid iron are not fully known, and involve many unknown factors. No special attempt was made to increase the reaction rate of reactants and products but the strong stirring of the melt by induction melting speeded up the

reaction kinetics considerably, e.g. increased the contact areas between reacting phases.

The following is a short account of the basic theory of energy and chemical reaction, chemical equilibrium and reaction kinetics, together with their applications to the reduction of the impurity content in liquid iron. The latter will be treated in detail.

4.1.1 Energy and Chemical Reaction[39,40]

The total energy of a substance may be divided into bound or thermal energy and free energy. The bound energy is associated with the motion of molecules or the potential energy of the molecules due to their relative position with respect to other molecules. It consists of a quantity factor, entropy (S), and a potential factor, temperature (T). The free energy is available for doing useful work such as carrying on a chemical reaction.

If H = total energy

G = free energy

S = entropy

T = absolute temperature

$$H = G + TS \quad \ldots\ldots \quad (4.1)$$

or $$\Delta G = \Delta H + T\Delta S \text{ at constant temperature} \quad \ldots\ldots \quad (4.2)$$

The free energy change, ΔG, is the maximum possible work which can be obtained from a chemical reaction. When ΔG is negative the reaction will occur spontaneously (if kinetic limitation allows it to occur).

In specifying the free energy change, ΔG, of a particular reaction the states of the reactants and products must be given, e.g. the condensed phases in pure state, gases at 1 atmosphere and 1% of solute in solutions are given as the standard states.

From equation (4.1) the free energy change for a system with the reactants and products at the standard states may be written as

$$\Delta G^{o} = \Delta H^{o} + T.\Delta S^{o} \quad \ldots\ldots (4.3)$$

which is the Gibb-Helmholtz equation. ΔH^{o} and ΔS^{o} are the heat of formation and entropy change at the standard states at the temperature T^{o} Kelvin respectively.

4.1.2 Chemical Equilibrium and Free Energy Change[39,40]

When a chemical reaction is at equilibrium, the rate of forward reaction of the active mass of the reactants is equal to the rate of reverse reaction of the active masses of the products, and the difference of free energy, ΔG, of the reactants and products is equal to zero. These are related by the equation

$$\Delta G^{o} = - RT \ln K \quad \ldots\ldots (4.4)$$

where ΔG^{o} = free energy change of the reaction at standard state

K = equilibrium constant of the reaction at temperature T^{o} Kelvin

R = gas constant

T = temperature of the reaction in degrees Kelvin.

From the law of mass action the equilibrium constant may be defined as

$$K = \frac{\prod a \text{ products}}{\prod a \text{ reactants}} \quad \ldots . \quad (4.5)$$

$\prod a_{\text{products}}$ = the product of product activities

$\prod a_{\text{reactants}}$ = the product of reactant activities

The value of K changes with temperature and from the van't Hoff equation,

$$\log K = -\frac{1}{T} \cdot \frac{\Delta H^{o}}{4.575} + \frac{\Delta S^{o}}{4.575} \quad \ldots . \quad (4.6)$$

ΔH^{o} and ΔS^{o} are the heat of formation and entropy change at the standard states respectively.

Equation (4.4), $\Delta G^{o} = -RT \ln K$, is very useful for calculation of the equilibrium constant, K, from the standard free energy change, ΔG^{o}.

The free energy changes under non-standard state conditions, ΔG, may be obtained from the standard free

energy change, ΔG°, by the van't Hoff Isotherm:

$$\Delta G = \Delta G^{\circ} + RT \ln \frac{(\prod a \text{ products})}{(\prod a \text{ reactants})} \quad \ldots (4.7)$$

$\prod a$ products = the product of product activities (at non-standard states)

$\prod a$ reactants = the product of the reactant activities (at non-standard states).

4.1.3 Relation between Equilibrium Constant and Standard Free Energy Change in Oxide Formation.[40,41]

The reaction between a metal and 1 gram mole of oxygen to form an oxide may be written as:

$$\frac{2x}{y} M + O_2 = \frac{2}{y} M_x O_y \quad \ldots (4.8)$$

Then the relation between the equilibrium constant and the standard free energy change is

$$\Delta G^{\circ} = - RT \ln K$$

$$\text{or } \Delta G^{\circ} = - RT \ln \frac{(a_{M_x O_y})^{\frac{2}{y}}}{(a_M)^{\frac{2x}{y}} P_{O_2}} \quad \ldots (4.9)$$

If the metal and oxide are at their standard states, and the oxygen pressure is P_{O_2}, then $a_{M_x O_y} = 1$ and $a_M = 1$, and

$$\Delta G^{\circ} = RT \ln P_{O_2}$$

The value of P_{O_2} is the equilibrium oxygen

dissociation pressure of the oxide concerned. When P_{O_2} is lower than the equilibrium value, the metal oxide will be unstable and decompose to metal and oxygen while oxygen pressure above that of equilibrium will lead to the disappearance of the metal phase.

The term RT log P_{O_2} is simply the negative work done in expanding 1 gram mole of oxygen at 1 atmosphere to pressure P_{O_2}, and it is generally called the chemical potential of oxygen, $\Delta\mu_{O_2}$, relative to oxygen at one atmosphere pressure as the zero potential.

4.1.4 Reaction Kinetics[42]

In refining molten iron in a crucible, the refining reactions occur at elevated temperature. Most of them are heterogeneous, taking place at the boundary between two phases, e.g. melt-slag, melt-crucible and melt-gas. The possible rate-limiting steps in the overall reactions include:

(a) transport of reactants to boundary

(b) chemical reaction at boundary

(c) transport of product away from the boundary

(d) nucleation of new phases and heat transfer.

In induction melting the melt is being strongly stirred by the force of attraction and repulsion between parallel current paths and causes circular motion in the molten metal. This will greatly aid (a) and (c), the

transport of reactants and products from and to the reaction site. It also speeds up heat transfer and the nucleation of new phases (d).

In addition, in the early stage of decarburization of the melt, the CO bubbles will form at the bottom of the crucible[43] and boil up. This further increases the rate of transport of reactants and products.

The reaction rate factor in (b) may be calculated from the theory of absolute reaction rates which postulates the formation of an activated complex from the reaction between the reactants. The activated complex is then decomposed into the products. When the chemical reaction occurs at high temperature the formation and decomposition of the activated complex are fast.

As a whole the reaction rate of the refining process in induction melting is comparatively fast, especially at the very early stage of refining when there are CO bubbles boiling. After boiling Machlin[44] postulated the theory that the layer of the melt adjacent to the gas-metal interface moves as a "rigid body". To bring about a further reduction of some impurities in the melt, e.g. carbon, the impurity must be discharged from the melt by diffusion through this layer. The diffusion process of reactants and products would be the reaction rate controlling factor in the final stage of refining. This process takes time.

4.2 Study of Oxidation of Impurities by Melting Iron in Air.

The oxidation of impurities in air starts with oxygen from the atmosphere dissolving in the liquid iron up to its saturation value when FeO will form. This is true because iron has the highest concentration. After this the impurities will combine with the oxygen in the melt or at a certain reaction site which favours deoxidation.

The impurities which can be removed successfully from the liquid iron may be determined from consideration of the standard free energy of formation of oxides from metals and 1 gram mole of oxygen as shown in Fig. 4.1. Any oxide which has a negative value of free energy of formation greater than that of iron oxide (FeO) at the oxidation temperature can be removed by oxidation in air. The extent of removal of impurities depends on the difference of the magnitude between the free energy of formation of impurity oxides and iron oxide (FeO), the slag formed, and the time allowed for the oxidation to reach equilibrium.

4.2.1 Oxygen Dissolved in Liquid Iron

The amount of oxygen dissolved in liquid iron will depend on the temperature of liquid iron and the oxygen pressure.

$$\tfrac{1}{2}\, O_{2\,(g)} = \underline{O} \qquad \ldots\ldots \quad (4.11)$$

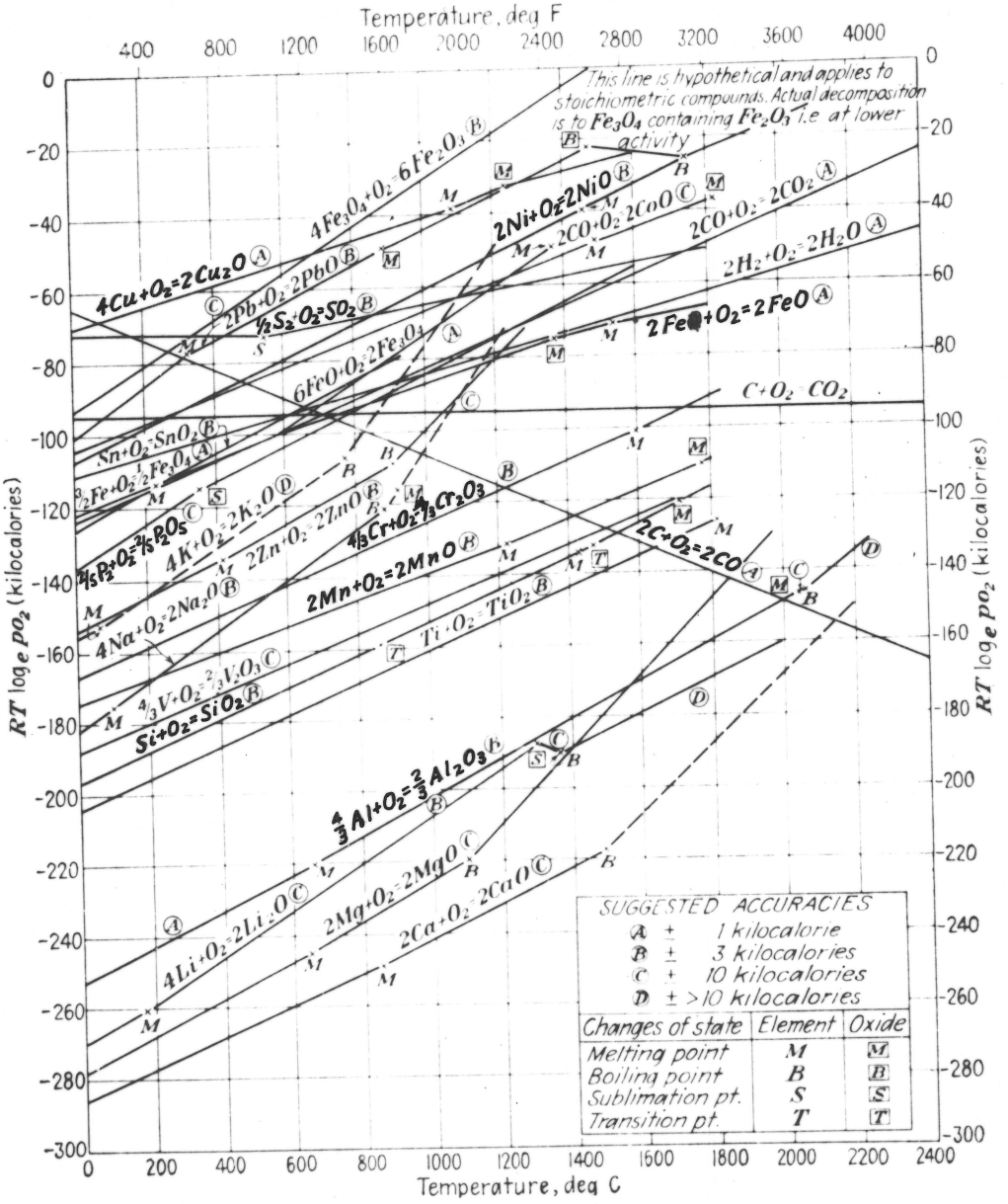


Fig. 4.1 Standard free energy of formation of metallurgically important oxides as a function of temperature.[45]

$$K_O = \frac{[a_o]}{P_{O_2}^{\frac{1}{2}}} \qquad \ldots . \quad (4.12)$$

$[a_o]$ = activity of oxygen in liquid iron

P_{O_2} = pressure of oxygen above the melt.

The maximum amount of oxygen dissolved in pure liquid iron may be calculated from,[46]

$$\log [\text{wt \% O}] = \frac{-6320}{T} + 2.734 \qquad \ldots . \quad (4.13)$$

[wt % O] = percentage by weight of oxygen in liquid iron

when T = 1873° Kelvin

[wt % O] = 0.226.

The oxygen pressure above liquid iron which is in equilibrium with 0.226% of oxygen at 1600°C (the oxidation temperature would be from 1550-1600°C) may be calculated from,[47]

$$\log P_{O_2} = \frac{-24.850}{T} + 5.22 \qquad \ldots . \quad (4.14)$$

$$P_{O_2} = 8.95 \times 10^{-9} \text{ atm.}$$

The oxygen content in air is about 21% by volume. For air at one atmosphere the oxygen partial pressure will be 0.21 atmosphere. This is far more than the equilibrium pressure of oxygen at 1600°C, therefore when

iron is melted in air the amount of oxygen dissolved in it will rapidly reach the saturation value and iron oxide will always form on the surface of molten iron.

The oxygen pressure of FeO and Fe_2O_3 at 1600°C are 10^{-8} and 10^{-3} - 10^{-2} atmosphere pressure respectively. Therefore most of the iron oxide will be FeO which constitutes 90-98%, the rest is Fe_2O_3.[48]

In theory if the iron is kept molten in air long enough all of it will become iron oxide. In practice we want maximum oxygen dissolved in liquid iron and only a small amount of iron oxide to be formed on the melt during oxidation in air. Therefore to reduce the iron loss the oxidation time should be as short as possible.

4.2.2 Oxidation of Copper, Nickel, Sulphur and Phosphorus

At 1600°C FeO is more stable than the oxides of copper, nickel, sulphur and phosphorus as shown in Fig. 4.1. This means that as soon as Cu_2O, NiO, SO_2 and P_2O_5 are formed by oxidation they will be deoxidised by iron and go back into the liquid iron.

$$Cu_2O + Fe_{(l)} = FeO + 2\,\underline{Cu} \quad \ldots \quad (4.15)$$

$$NiO + Fe_{(l)} = FeO + \underline{Ni} \quad \ldots \quad (4.16)$$

$$SO_{2(g)} + 2Fe_{(l)} = 2\,FeO + 2\,\underline{S} \quad \ldots \quad (4.17)$$

$$P_2O_{5(g)} + 5Fe_{(l)} = 5\,FeO + 2\,\underline{P} \quad \ldots \quad (4.18)$$

Cu represents copper dissolved in liquid iron.

Considering in terms of chemical equilibrium the above four reactions favour the formation of the product on the right hand side of the equations, so there will be only small amounts of Cu_2O, NiO, SO_2 and P_2O_5 present at equilibrium at 1600°C.

It is therefore not possible to remove copper, nickel, sulphur and phosphorus in a significant amount from liquid iron at temperature 1600°C by oxidation in air.

It may be mentioned that phosphorus and sulphur may be removed successfully by treating liquid iron with some slag, e.g. CaO, FeO, but this may introduce CaO contamination and require a big volume of slag. So an attempt to remove them would not be made at this stage.

4.2.3 Oxidation of Chromium, Manganese, Silicon and Carbon

At 1600°C oxides of manganese, silicon and carbon are more stable than iron oxide. It is possible to reduce these impurities in liquid iron by oxidation. The amounts of chromium, manganese, silicon and carbon left after deoxidation depend on the equilibrium condition at oxidation temperature, and also the removal of impurity oxides from the system during the oxidation process.

4.2.4 Oxidation of Chromium

It has been found that chromium and oxygen in liquid iron will form Cr_2O_3 when the percentage of chromium is more than 5.5% and Fe Cr_2O_4 is formed when the chromium content is less.[49] In the present study the chromium content was about 0.02%, therefore the reaction may be represented by

$$\underline{Fe} + 2\ \underline{Cr} + 4\ \underline{O} = Fe\ Cr_2O_{4(s)} \qquad \ldots (4.19)$$

At the oxidation temperature of 1600°C Fe Cr_2O_4 is solid and dissolves little in FeO. So the presence of FeO slag would not help much in the removal of chromium from liquid iron.

The equilibrium constant of the reaction in equation (4.19) may be written as

$$K_{Cr} = \frac{1}{[a_{Cr}]^2 [a_O]^2} \qquad \ldots (4.20)$$

$[a_{Cr}]$ = activity of chromium in liquid iron

$[a_O]$ = activity of oxygen in liquid iron.

Chen and Chipman[49] have found from their experiments of melting Cr-O-Fe alloys in chromite crucibles that $K_{Cr} = 4.1 \times 10^5$ at 1590°C.

4.2.5 Oxidation of Manganese

The solution of manganese has been shown to be an ideal, Fig. 4.2. Its activity is proportional to its mole fraction or weight percentage at low concentration of manganese.

The manganese content in the liquid iron varies with the mole fraction of MnO in the slag of FeO-MnO.[51]. This may be represented by

$$\underline{Mn} + FeO\ (\text{in slag}) = Fe_{(l)} + MnO\ (\text{in slag}) \quad \ldots \quad (4.21)$$

$$K_{Mn} = \frac{(x_{MnO})}{(x_{FeO_t})\,[\text{wt\% Mn}]} \quad \ldots \quad (4.22)$$

$$\therefore \quad [\text{wt \% Mn}] = \frac{1}{K_{Mn}} \frac{(x_{MnO})}{(x_{FeO_t})} \quad \ldots \quad (4.23)$$

(x_{MnO}) = mole fraction of manganese in slag.

(x_{FeO_t}) represents the figure obtained by calculating the total iron content of the slag as FeO.

K_{Mn} may be obtained from,[51]

$$\log K_{Mn} = \frac{6440}{T} - 2.95 \quad \ldots \quad (4.24)$$

when $T = 1600 + 273^{\circ}$ Kelvin

$K_{Mn} = 3.09$

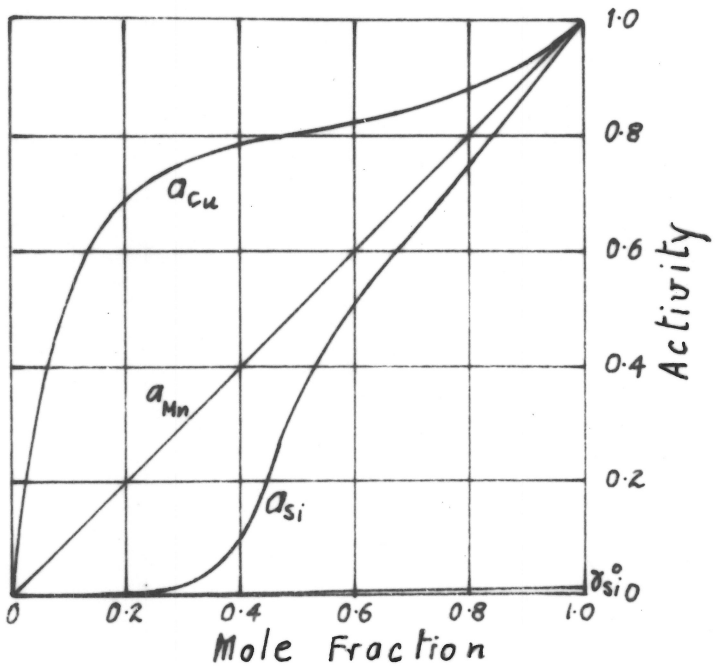


Fig. 4.2 The Raoultian activity of copper, manganese and silicon in solution in molten iron at 1600°C.[50]

Equation (4.23) shows that the amount of manganese in liquid iron may be decreased to a low value by decreasing the ratio of $\frac{(x_{MnO})}{(x_{FeO_t})}$. This may be done by prolonged oxidising of the molten iron, but the iron loss will be high. In the present work the oxidation in air was done for 30 minutes.

Fig. 4.3 shows that for the same ratio of $\frac{(x_{MnO})}{(x_{FeO_t})}$, oxidation at lower temperature will give a better result of manganese removal. This is due to the equilibrium constant, K_{Mn}, varying with the temperature.

4.2.6 Oxidation of Silicon

Silicon shows a very pronounced negative deviation from ideality in liquid iron, Fig. 4.2. Therefore its activity is less than its mole fraction, but at low percentage of silicon the difference is small. The chemical reaction between silicon and oxygen in liquid iron may be represented by

$$\underline{Si} + 2\,\underline{O} = Si\,O_{2\,(s)} \qquad \ldots \quad (4.25)$$

$$K_{Si} = \frac{(a_{Si\,O_2})}{[a_{Si}][a_O]^2} \qquad \ldots \quad (4.26)$$

$(a_{Si\,O_2})$ = activity of silica in slag

$[a_{Si}][a_O]$ = activity of silicon and oxygen in liquid iron respectively.

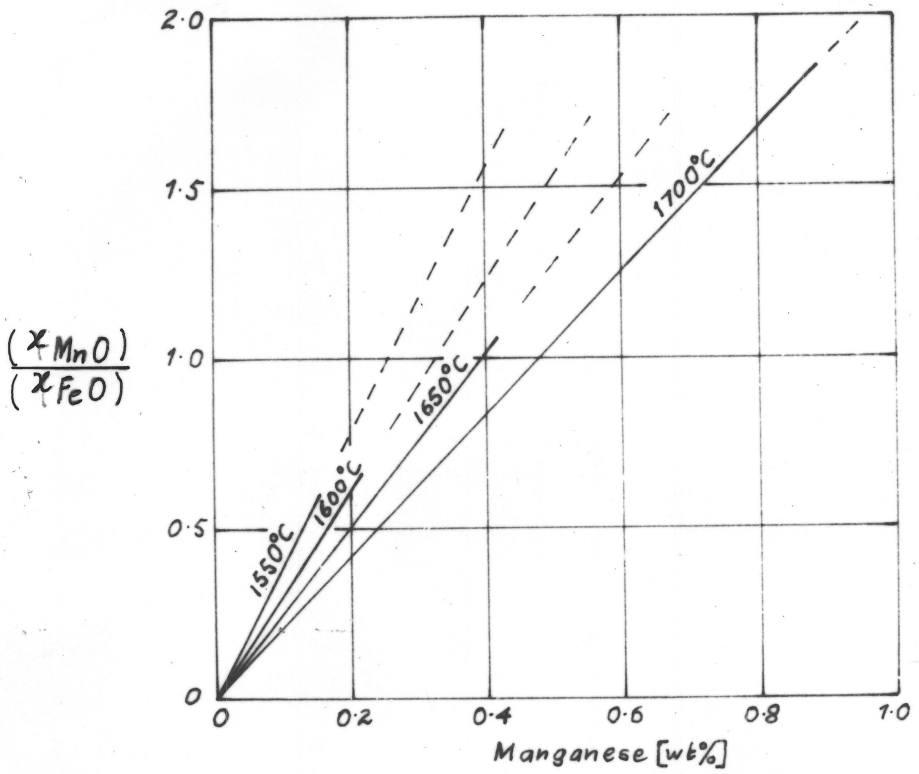


Fig. 4.3 Manganese-oxygen equilibrium under slags containing only MnO and FeO.[51]

Much work has been done to find the relationship between silicon and oxygen in liquid iron under a silica saturated slag.[52] This could not be applied directly to the present study because the slag was not saturated with silica; it consisted mostly of FeO. However the deoxidation product SiO_2 formed a compound with FeO, e.g.

$$2\ FeO + SiO_2 = 2\ FeO.SiO_2 \qquad \ldots \quad (4.27)$$

The dissociation of the compound, $FeO.SiO_2$ is small, so SiO_2 is removed from the right-hand side of equation (4.25). This promotes further removal of Si from liquid iron.

4.2.7 Oxidation of Carbon

Carbon and oxygen in the melt will combine and form CO. The reaction site of this combination, whether within the melt or at any interface, is not fully known, but in the early stage of melting they will combine at the bottom of the crucible in the capillary crevices in the refractory.[43,53]

The equilibrium reaction of carbon and oxygen in liquid iron may be considered as follows:[43]

$$\underline{C} + \underline{O} = CO_{(g)} \qquad \ldots \quad (4.28)$$

$$K_{CO} = \frac{P_{CO}}{[a_C][a_O]} \qquad \ldots \quad (4.29)$$

P_{CO} = pressure of CO above the melt.

$[a_C]$ and $[a_O]$ = activity of carbon and oxygen respectively in liquid iron.

and $$\log K_{CO} = \frac{1045}{T} + 2.131 \quad \ldots \quad (4.30)$$

when $T = 1600 + 273^{\circ}$ K

$K_{CO} = 488.$

The product of $[a_C][a_O]$ at 1580°C has been found to be,[43]

$$[a_C][a_O] = 0.00031 \quad \ldots \quad (4.31)$$

In general equation (4.31) may be expressed as

$$[a_C][a_O] = [\text{wt } \%C]\, f_C^C .\, f_C^O\, [\text{wt } \%O]\, f_O^O .\, f_O^C \quad \ldots \quad (4.32)$$

f_j^i = activity coefficient accounting for the influent of i on the element j in solution in molten iron.

From the work of Richardson and Dennis,[54]

$$\log f_C^C = 0.23\,[\text{wt } \%C] \quad \ldots \quad (4.33)$$

Bennett et al,[43]

$$\log f_O^C = -0.67\,[\text{wt } \%C] \quad \ldots \quad (4.34)$$

Florides and Chipman,[55]

$$\log f_O^O = -0.20\,[\text{wt } \%O] \quad \ldots \quad (4.35)$$

Turkdogan et al,[56]

$$\log f_C^O = -0.36\,[\text{wt } \%O] \quad \ldots \quad (4.36)$$

Assuming $[\text{wt }\%C] = .02$ and $[\text{wt }\%O] = .226$

$$f_C^C = 1.02, \quad f_O^C = 0.99$$

$$f_O^O = 0.9, \quad f_C^O = 0.83$$

$$f_C^C;\ f_O^C;\ f_O^O;\ f_C^O = 0.75$$

Therefore equation (4.29) may be written as

$$K_{CO} = \frac{P_{CO}}{0.75[\text{wt}\%C][\text{wt}\%O]} \qquad \ldots \quad (4.37)$$

This would be the case at the early stage of oxidising Armco iron in air.

Equations (4.29) and (4.32) show that the amount of carbon left in liquid iron depends on the percentage of oxygen, the pressure of CO, and the product of the activity coefficient concerned. The last factor increases as the percentage of carbon and oxygen decrease.

By oxidation in air, e.g. 1600°C, the saturation value of oxygen in the melt is about 0.226%, the carbon content will decrease gradually depending on the ease of formation of CO bubbles in the melt and CO partial pressure. To decrease the carbon content to a very low value the oxidation time must be prolonged. This causes many disadvantages.

The process adopted to shorten the time for carbon

reduction is to reduce the CO partial pressure above liquid iron by melting in vacuum. This method will be described later.

4.3 Study of Refining by Melting under Controlled Atmosphere

4.3.1 Further Removal of Carbon

From equation (4.29)

$$[\text{wt }\%C] = \frac{1}{K_{CO}} \cdot \frac{1}{F} \cdot \frac{P_{CO}}{[\text{wt}\%O]}$$

F = product of activity coefficients

These suggest that the lowering of CO pressure above the melt will encourage the combination of C and O in the melt, and hence the carbon content will be lowered, subject to some limitations[57] which may be considered as follows.

The formation of CO bubbles from the combination of carbon and oxygen in the melt may occur at three different reaction sites:

(a) at the surface of the molten iron

(b) at crucible-melt interface

(c) within the melt.

In general we may assume that a CO bubble is formed at a depth h within the melt. Under these conditions the pressure of the CO bubble will be equal to

$$P_{CO\ (bubble)} = p_1 + \rho h + \frac{2T}{r} \qquad \ldots (4.38)$$

p_1 = pressure above the melt

h = liquid iron head above the bubble

ρ = density of the melt

T = surface tension of liquid iron

r = radius of bubble.

The term, $\frac{2T}{r}$ in equation (4.38), is the surface tension forces which oppose the growth of the CO bubble. Samarin[57] calculated that when the diameter of CO molecule at 1600°C is about 3.28 A°, and assuming surface tension is equal to 1000 dynes cm^{-1}, the pressure of CO bubble in a homogeneous nucleation would be much greater than 10^{-3} atmosphere. This would require an impossible supersaturation of carbon and oxygen in the melt to satisfy equation (4.29), i.e.

$$P_{CO} = K_{CO} [a_C][a_O]$$

In practice the size of the CO bubble is much larger than 3.28 A° because the bubble formation is heterogeneous, e.g. occurs at the rough surface of the lining and the entrapped gas at the lining cavity serves as a nucleus from which the bubble can grow. Ward[58] showed that in the open hearth steel making, when the radius of the lining cavity was about 0.1 mm. the pressure of CO bubble was about 2 atmosphere pressures, (including one atmospheric pressure above the melt).

Therefore, under a favourable nucleation site, lowering the pressure above the melt will assist the formation of the CO bubble in equation (4.28) and decrease the carbon and oxygen content in liquid iron. This is true until

$$\rho h + \frac{2T}{r} \gg P_1$$

Further reduction of the pressure above the melt would have no significant value in lowering the carbon content because the pressure above the melt has a negligible effect on the CO bubble formation.

Samarin[57] found that the percentage of carbon and oxygen in iron when melted at 1590°C under the pressure of $1\text{-}5.10^{-2}$ mm. Hg. and $5\text{-}7.10^{-6}$ mm. Hg. were not much different.

Damara et al[59] mentioned that, in vacuum refining, reduced pressure below 3 mm. Hg. had no significant effect on lowering the carbon content. This needs experimental confirmation.

In the present work a pressure of about 10^{-3} mm. Hg. for 15 minutes has been employed for a further decrease in carbon content, and this will also promote the elimination of some impurities from liquid iron by evaporation.

4.3.2 Removal of Oxygen

After the removal of carbon in liquid iron by vacuum treatment, the percentage of oxygen was still high. Further decrease of oxygen content may be effected by

(a) melting iron under very low pressure

(b) addition of deoxidisers.

4.3.3 Melting under Low Pressure

Fig. 4.4 shows the oxygen content in pure iron at various oxygen pressures at 1600°C. To reduce the percentage of oxygen to 0.01 the oxygen pressure must be about 10^{-8} mm. Hg. This is not a practical method and besides the iron loss by vaporisation would be very high.

4.3.4 Addition of Deoxidisers

The common deoxidisers are carbon, silicon, manganese, aluminium and hydrogen. If carbon is used it should be added before decarburization by vacuum. Many workers have used carbon as a deoxidiser. The product of carbon deoxidation is CO which comes out of the liquid iron, but the amount of carbon added must be carefully determined otherwise the carbon content will be high. Other deoxidisers except hydrogen give solid oxides which cause inclusion in the iron.

Hydrogen was chosen as the deoxidiser in the present work. The hydrogen gas remaining in the liquid iron after deoxidation may be reduced by vacuum treatment.

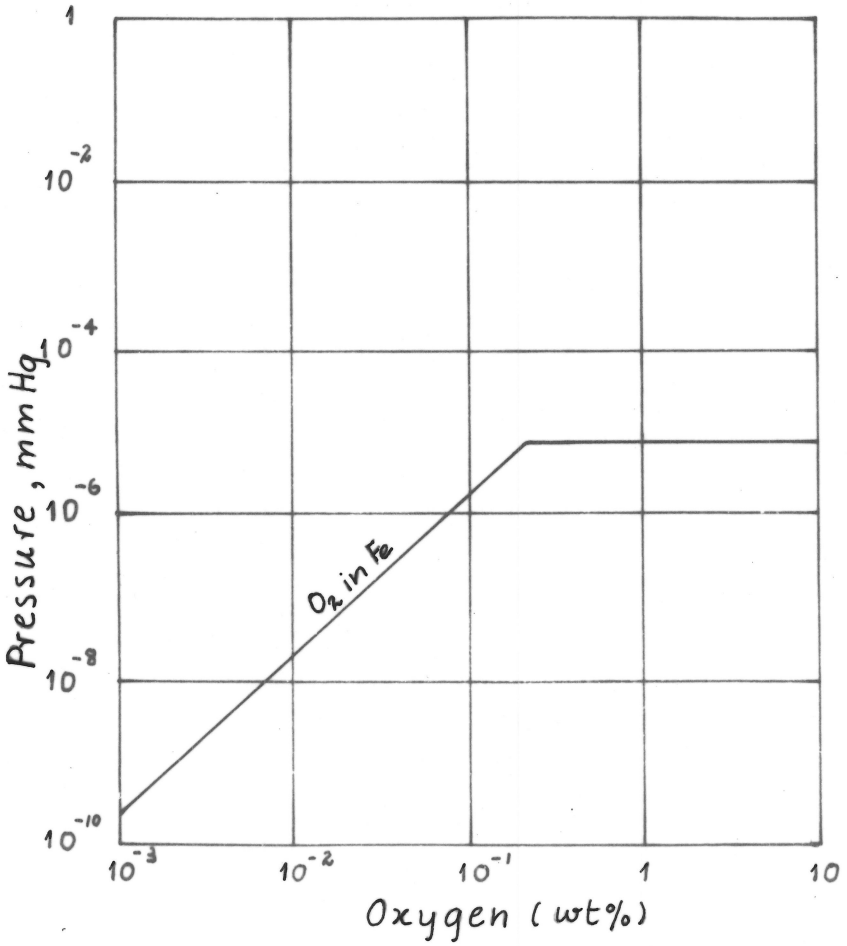


Fig. 4.4 Oxygen content in pure iron at 1600°C as a function of oxygen pressure.[28]

4.3.5 Deoxidation by Melting under Hydrogen Atmosphere

Deoxidation by hydrogen may be represented by equation,[55]

$$H_2 + \underline{O} = H_2O \qquad \ldots \quad (4.39)$$

$$K_{H_2O} = \frac{P_{H_2O}}{P_{H_2} \; f_O [\text{wt \%O}]} \qquad \ldots \quad (4.40)$$

$$\log K_{H_2O} = \frac{7050}{T} - 3.20 \qquad \ldots \quad (4.41)$$

$$\log f_O = - 0.20 [\text{wt \%O}] \qquad \ldots \quad (4.42)$$

It may be mentioned that the formation of H_2O bubbles in liquid iron would face the same problem as that of CO bubbles mentioned in section 4.3.1. Introducing hydrogen gas into the system by blowing it into the liquid iron would assist the formation of H_2O bubbles, but it was not attempted in this work at this stage.

The relationship of the ratio $\frac{P_{H_2O}}{P_{H_2}}$ to $[\text{wt \%O}]$ in equation (4.40) is shown in Fig. 4.5.

By decreasing the ratio $\frac{P_{H_2O}}{P_{H_2}}$ the oxygen content would be decreased. This can be done by removing H_2O and H_2 out of the system and readmit high purity H_2 in. There are two ways to do this:

(a) Circulation of hydrogen in a closed system connected to the vacuum tank;

(b) Let the hydrogen into the vacuum tank for

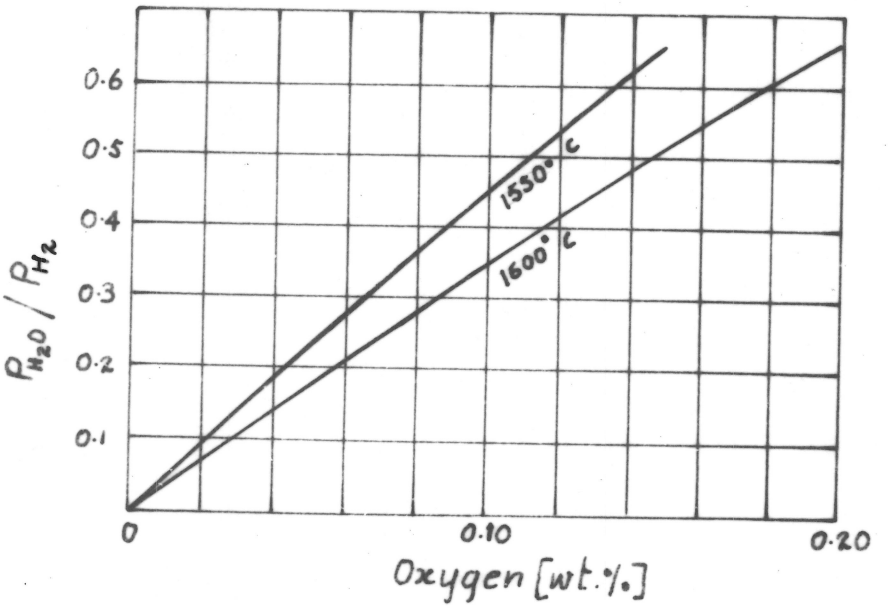


Fig. 4.5 Variation of oxygen content with the ratio $P_{H_2O}/_{H_2O}$ [55]

deoxidation, then remove through the vacuum pumps.

4.3.6 Closed system of Hydrogen Deoxidation

Hydrogen gas may be economically used by circulating it in a closed system. The deoxidation product, H_2O, may be removed by molecular sieves.

The hydrogen system, shown in Fig. 4.6, was similar to that of Hopkins et al[2]. The hot magnesium furnace for removal of nitrogen contains 500 g. of magnesium heated to 600°C. The hot gas from this furnace is cooled down by cold magnesium chips, then passed through the molecular sieves which absorb water. The molecular sieves may be regenerated by heating to 300°C.

Hadley and Bianchi[60] had studied the effect of flow rate and hydrogen pressure on the oxygen content in liquid iron during deoxidation. They found that variation in pressure and flow rate of hydrogen had no significant effect on the oxygen content in the range of their study as in Fig. 4.7. For hydrogen pressure of 20 mm. Hg. and the rate of flow 100 cu. ft. per hour the oxygen content was decreased to a low value within 15-20 minutes.

In the present work, as a safety precaution the pressure of hydrogen during the closed circuit deoxidation was above 1 atmosphere and the rate of flow 0.5 cu. ft. per minute. Any leak caused the hydrogen to flow outwards and prevented entry of air. Large leaks had been carefully prevented since diffusion of gasses may occur both ways.

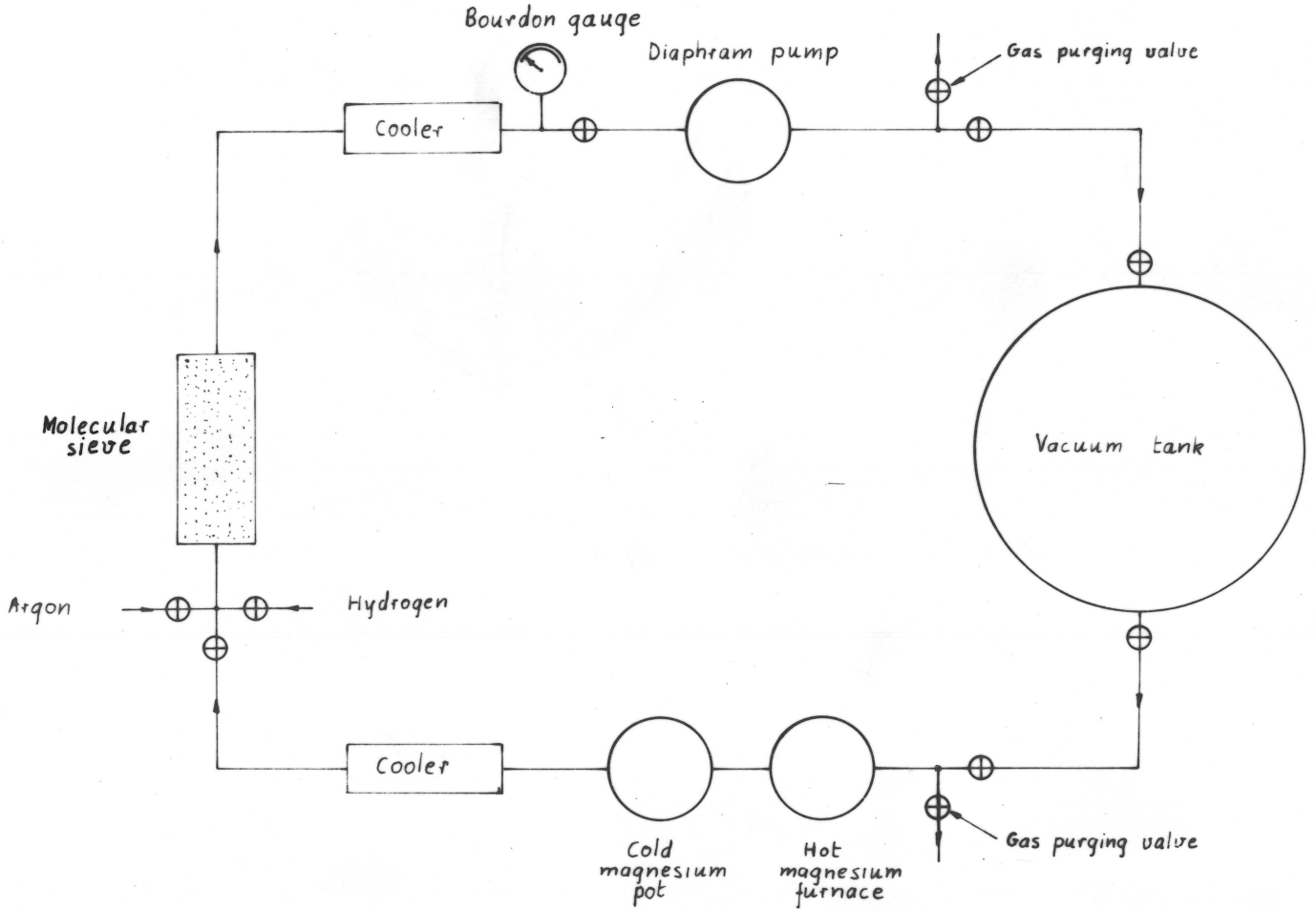


Fig. 4.6 Closed system of hydrogen deoxidation.

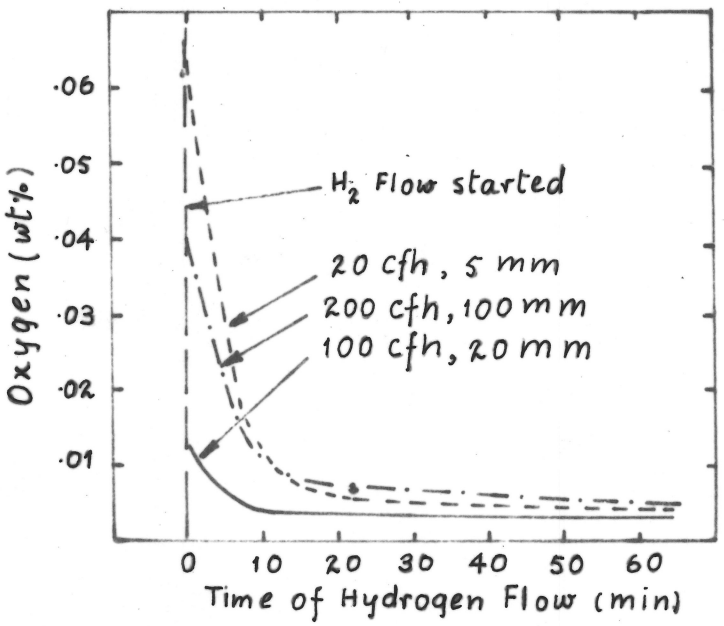


Fig. 4.7 Oxygen content of melt as a function of time for varying combinations of pressure and flow rate.[60]

4.3.7 Repeated Deoxidation by Hydrogen

This is an alternative method of deoxidation of molten iron by hydrogen. It does not require a closed system for hydrogen circulation.

The commercial hydrogen was passed through a "Deoxo" platinum catalyst, then through molecular sieves to eliminate its water content before letting into the vacuum tank.

Hiroshi Sawamura et al[61] carried out deoxidation by blowing hydrogen on to the surface of the molten bath and holding at a pressure of 30 mm. Hg. for 5 minutes before the gas was removed.

In the present work the method adopted was blowing hydrogen on the surface of the molten iron and holding at a pressure of 10 cm. Hg. for five minutes, then the hydrogen gas as well as the water vapour formed were removed by the vacuum pumps. This was repeated three times.

4.3.8 Limit of Minimum Oxygen Content

In theory the oxygen content after deoxidation can be decreased to the value determined by the ratio $\frac{P_{H_2O}}{P_{H_2}}$ in equation (4.40), but in practice the oxygen content could not be reduced lower than a certain minimum value. This is due to oxygen supplied to the liquid iron from

some sources such as the liquid iron-crucible reaction, or leakage of the system. When the rate of supply is equal to the rate of removal of oxygen by deoxidation the oxygen content tends to become constant.

The reaction between the liquid iron and crucible is an important factor in supplying the oxygen to the melt.[62,63]

For an alumina crucible such as used in this work, when carbon is present in the liquid iron it will react with aluminium oxide

$$Al_2O_3 + 3\,\underline{C} = 2\,Al + 3\,CO \qquad \ldots \quad (4.43)$$

$$3\,CO = 3\,\underline{C} + 3\,\underline{O} \qquad \ldots \quad (4.44)$$

This reaction will introduce oxygen as well as aluminium into the melt.

Fast et al[64] mentioned that even with no reaction between carbon and aluminium oxide the latter itself would dissociate into

$$Al_2O_3 = 2\,\underline{Al} + 3\,\underline{O} \qquad \ldots \quad (4.45)$$

$$K_{Al} = [\text{wt }\%Al]^2[\text{wt }\%O]^3 \qquad \ldots \quad (4.46)$$

$$= 10^{-13} \text{ (at } 1600^{\circ}C)$$

If the oxygen content of the molten metal is 0.001% the melt will take up about 0.01% Al from the crucible

according to equation (4.46). (In recent work,[65] the value of the equilibrium constant, K_{Al}, was found to be of the order of 10^{-14}).

However many workers have reported that the contamination from recrystalized alumina crucible was very small. Probably the equilibrium was not reached in practice.

In the present work a tamped sintered alumina crucible was used. This is not as good in some respects as the commercial slip cast sintered alumina crucibles, but it has superior thermal shock resistance, is much cheaper to produce and may be produced in a required shape and size to suit the work.

4.3.9 Removal of Hydrogen

After deoxidation of liquid iron by hydrogen the amount of this gas dissolved in iron depended on its pressure and temperature of deoxidation. At the deoxidation temperature hydrogen exists as diatomic molecules and the solubility of hydrogen in pure iron obeys Sieverts' law

$$H_2\ (g) = 2\ \underline{H} \qquad \ldots \quad (4.47)$$

$$K_H = \frac{[a_H]^2}{P_{H_2}} \qquad \ldots \quad (4.48)$$

At low concentration

$$a_H = [\text{wt \% H}]$$

$$\therefore \quad [\text{wt \% H}] = K_H \cdot \sqrt{P_{H_2}}$$

The equilibrium constant of hydrogen (K_H) at one atmosphere hydrogen pressure is given by[66]

$$\log K_H = -\frac{1670}{T} - 1.68 \qquad \ldots \quad (4.49)$$

At 1600°C $\qquad K_H = 0.0027$

Using equation (4.48) and equation (4.49) the amount of hydrogen dissolved may be calculated as shown in Fig. 4.8.

If the deoxidation pressure of hydrogen is 10 cm. Hg. and temperature of the melt is 1600°C

$$[\text{wt \% H}] = 0.0027\sqrt{\frac{10}{76}}$$

$$= 0.00097$$

To reduce the hydrogen dissolved the hydrogen pressure above the melt must be reduced. Hopkins et al[2] kept the deoxidised iron melted under 5 cm. Hg. pressure of hydrogen for $\frac{1}{2}$ hour before pouring. They found that this pressure prevented molten iron from spurting. The same pressure was used but the time was 15 minutes on account of a smaller charge. At 5 cm. Hg. hydrogen pressure

$$[\text{wt \% H}] = 0.00069$$

The elimination of hydrogen under vacuum may be described that the hydrogen atoms in the melt diffuse

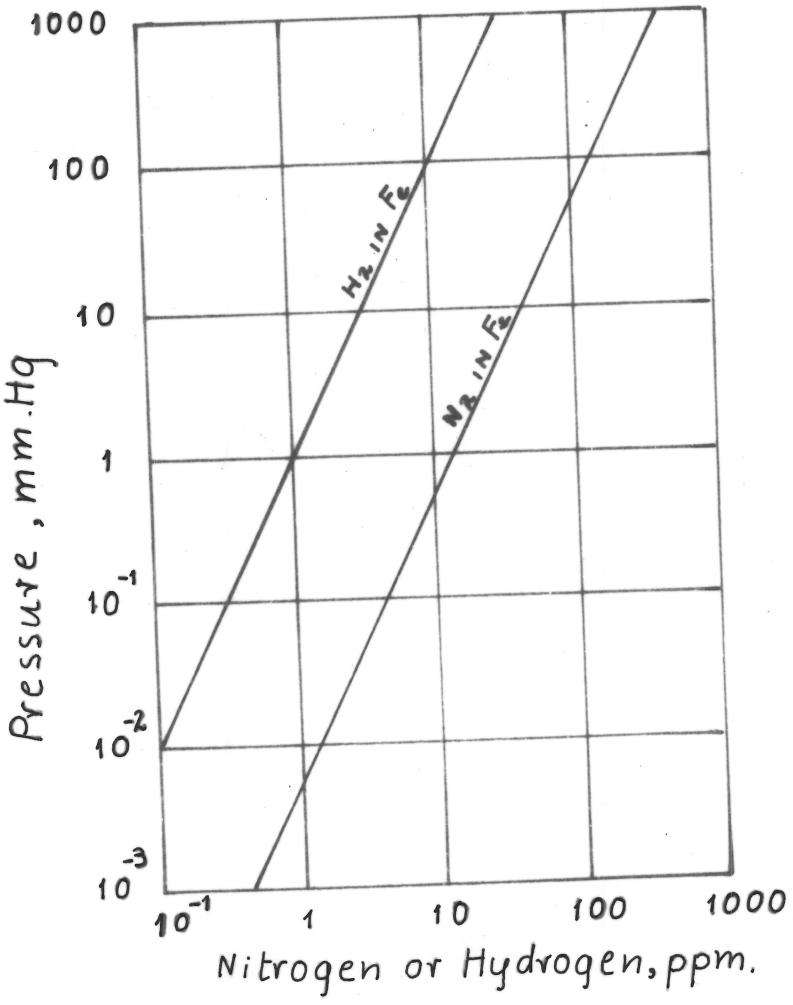


Fig. 4.8 Pressure-dependence of the nitrogen and hydrogen contents of liquid iron at 1600°C.[28]

to the surface through a stagnant layer, combine into molecules which escape into vacuum. With the stirring of the melt by induced current this process would increase considerably.

The elimination of nitrogen which will be described shortly would be the same.

4.3.10 Removal of Nitrogen

It has been observed that nitrogen absorption in liquid metals is negligible in the presence of oxidising gas, e.g. oxygen, due to the oxide film acting as a barrier to nitrogen transfer. But in the reducing atmosphere, e.g. nitrogen mixed with hydrogen or carbon monoxide, it is rapidly dissolved.[67]

Under the induction melting and oxidising of liquid iron in air, small amounts of nitrogen are dissolved directly from the atmosphere, but the stirring motion of the melt (Fig. 1.16, page 44) will trap some air, especially at the side of the crucible where the liquid current goes down, and may cause high nitrogen dissolved in the liquid iron.

The solution of nitrogen in liquid and solid iron may be considered as follows.

At the oxidation temperature gaseous nitrogen exists as diatomic molecules which dissociate on solution in liquid iron.

$$N_{2\,(g)} = 2\,\underline{N} \qquad \ldots \quad (4.50)$$

$$K_N = \frac{[a_N]^2}{P_{N_2}} \qquad \ldots \quad (4.51)$$

In a dilute solution

$$[a_N] = [\text{wt \% N}]$$

$$\therefore \quad [\text{wt \% N}] = K_N \; P_{N_2} \qquad \ldots \quad (4.52)$$

The equilibrium constant of nitrogen (K_N) in liquid iron may be calculated from,[68]

$$\log K_N = -\frac{188.1}{T} - 1.246 \qquad \ldots \quad (4.53)$$

At 1600°C $K_N = .045$

Therefore the amount of nitrogen dissolved in liquid iron at 1600°C is

$$[\text{wt \% N}] = 0.45\sqrt{P_{N_2}}$$

P_{N_2} = .79 atmosphere pressure for air at one atmosphere

$$\therefore [\text{wt \% N}] = .040$$

But when the liquid iron cooled and solidified in the mould nitrogen will come out as shown in Fig 4.9 for equilibrium cooling. In practice the cooling rate is far from equilibrium and the nitrogen content in liquid iron is more than that of equilibrium.

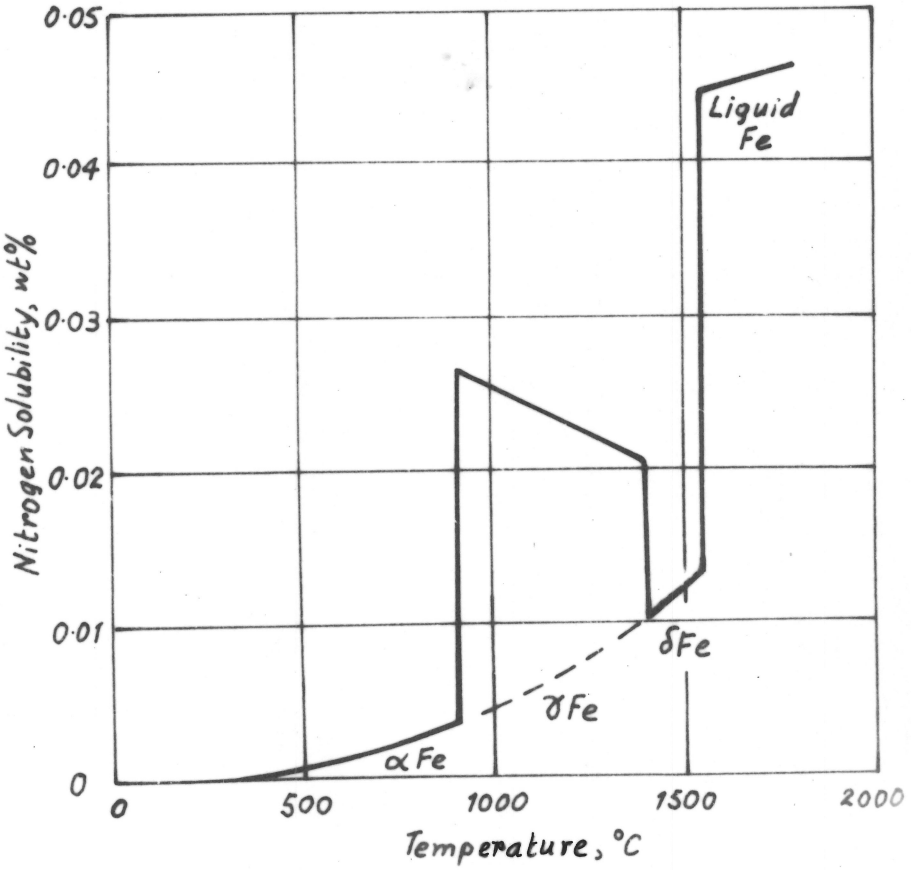


Fig. 4.9 Solubility of nitrogen in pure iron under a nitrogen partial pressure of one atmosphere.[67]

According to equation (4.52) nitrogen can be removed from iron by melting under low pressure. This has been done during carbon and hydrogen elimination under low pressure. Fig. 4.8 shows that at 10^{-3} mm. Hg. pressure of nitrogen the amount of nitrogen dissolved in liquid iron is about 0.7 part per million.

The presence of other elements in liquid iron effects the solubility of nitrogen in iron,[68] but in the present work the amount of impurities are small, and their effect may be neglected.

4.4 Preparation of Charge, Crucible and Mould

4.4.1 Charge

The Armco iron available was in the form of sheet $3/64$ inch thickness. The power source which has the frequency of 500 c/s cannot melt this thin sheet. The only way to melt it is as follows.

The Armco iron sheet was cut by die into round discs, $2\frac{3}{4}$ inches in diameter. The discs were stacked up to a height of $3\frac{3}{4}$ inches. They were clamped tightly in a vice and welded on the side by oxy-acetylene, using a neutral flame. This charge, shown in Fig. 4.10, would behave similarly to a solid charge under induction heating.

4.4.2 Crucible

The tamped sintered alumina crucible, 3 inches

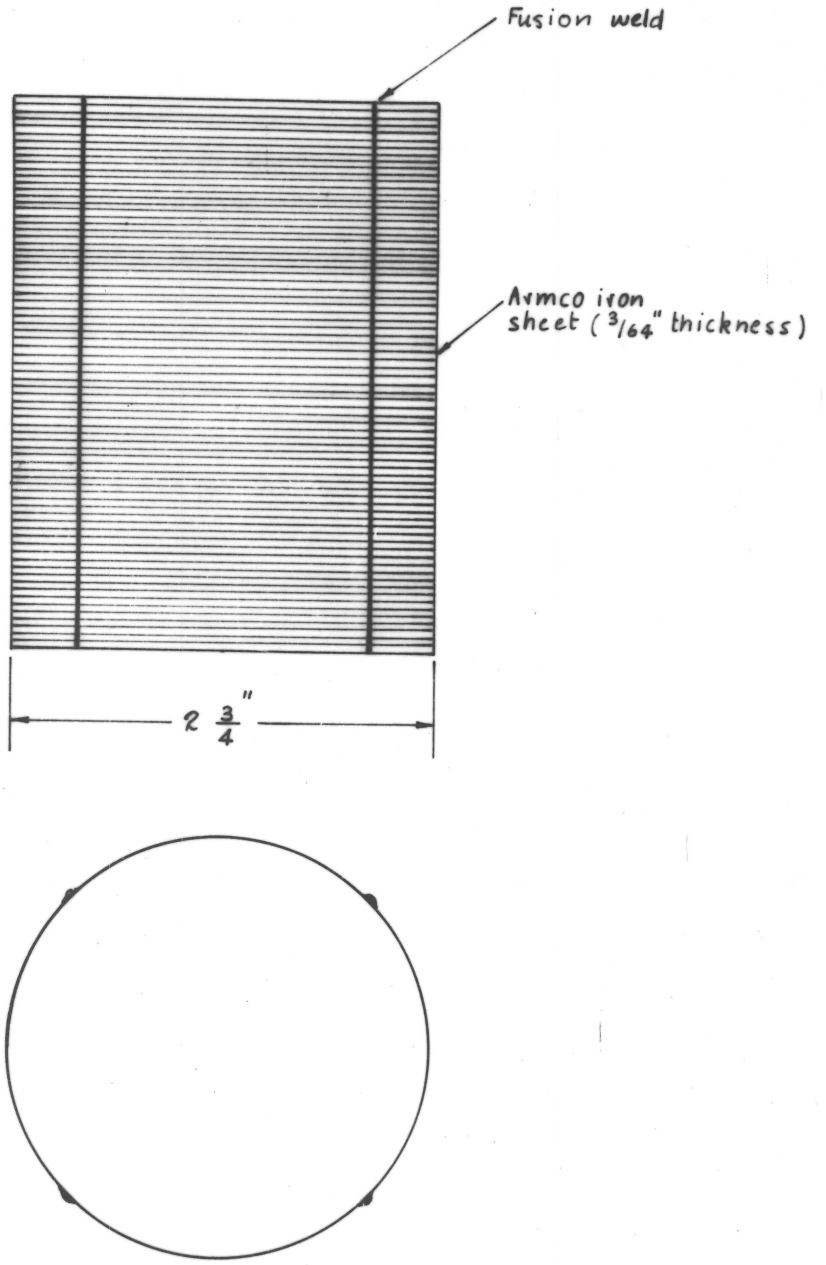


Fig. 4.10 Armco iron sheet charge

inside diameter, $5/16$ inch thick and $4\frac{7}{8}$ inches high was used. The method of manufacture was described in Chapter III.

The crucible pouring lip was made from the same mixture as the alumina crucible and fired in the same way. The lip has a neck of $\frac{3}{4}$ inch height.

The assembly of the crucible and its lip in the work-coil was as follows. The bottom of the work-coil was covered with fused alumina powder (settling tank fines) for a height of $\frac{3}{4}$ inch above the water cooling coil for the laminated core. The crucible was placed centrally on this powder for insulation as well as preventing the molten iron from breaking through at the bottom to the cooling coil. The lip neck was slid in the space between the crucible and the work-coil, then the space was filled with the alumina powder (settling tank fines) up to $\frac{1}{2}$ inch below the top of the coil. The mixture of the zircon sand, zircon flour and silester "O" solution was filled at the top. This was to hold the crucible and the lip to the work-coil. The excess alcohol of the silester "O" solution was burnt off. Fig. 4.11 shows the section of work-coil and crucible.

Pre-heating of the refractory was carried out with a stacked Armco iron charge placed in the crucible and heated by induction heating to 1000°C for 30 minutes to drive off

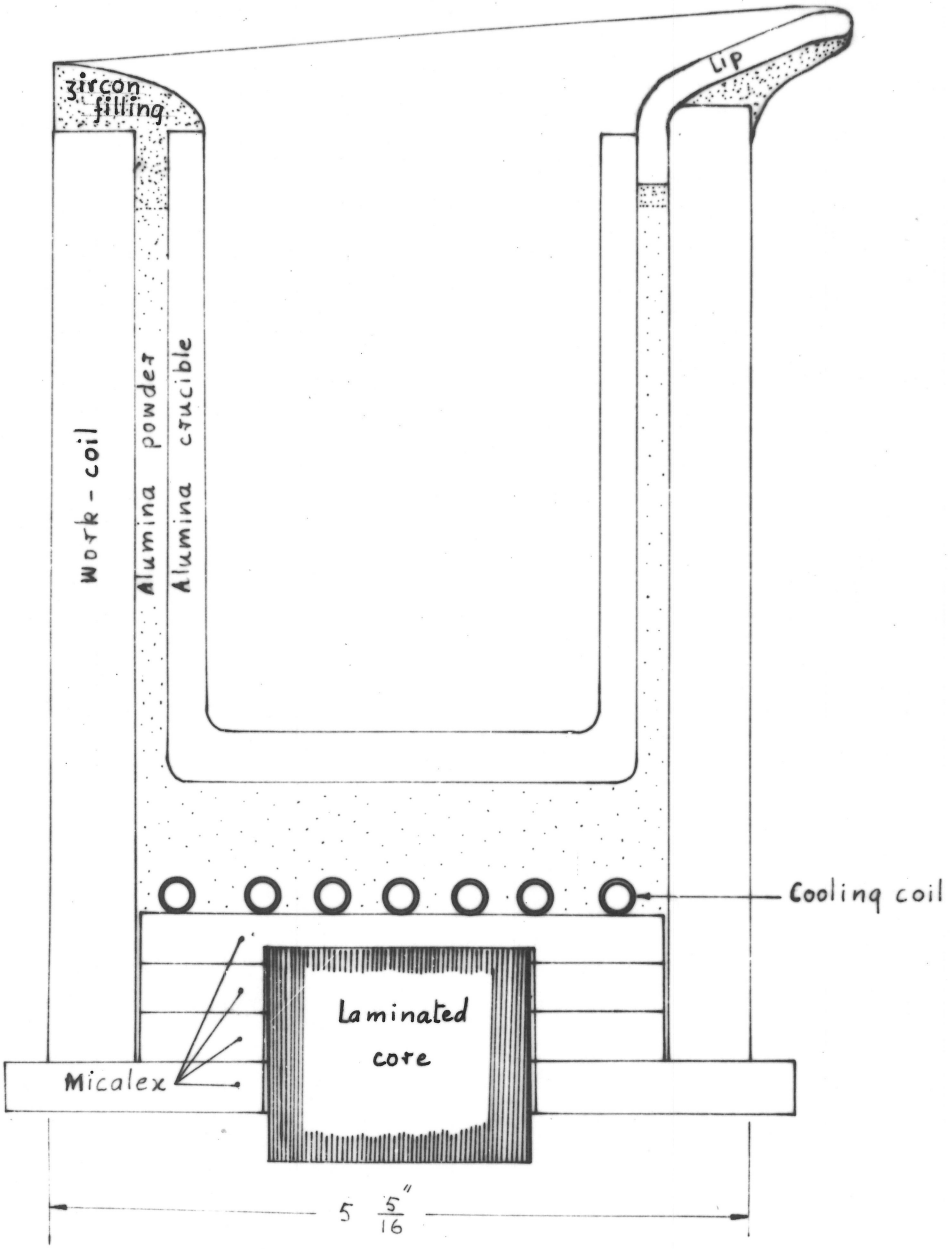


Fig. 4.11 Assembly of alumina crucible in work-coil.

moisture and gas absorbed in the refractory. During this heating the pressure inside the vacuum tank was reduced to 10^{-3} mm. Hg.

4.4.3 Mould

Two types of mould were used. The first, shown in Fig. 4.12(a), was made of a stainless steel tube $2\frac{3}{4}$ inches inside diameter, $3/16$ inches thick and $4\frac{1}{2}$ inches long. Copper was cast around the outside of this tube, the thickness of copper being 1 inch. The bottom of the mould was covered with a mild steel plate $\frac{1}{2}$ inch thick. A round piece of copper, $5\,3/16$ inches in diameter and $1\frac{1}{2}$ inches thick was placed under the mild steel cover. When the molten iron was poured into the mould the copper conducted the heat away from the stainless steel tube and prevented the iron from sticking to the mould. The total weight of copper was 45 lbs. The stainless steel and copper were used for the mould to reduce the energy loss from the work-coil and avoid heating of the mould, since it was placed near to the work-coil during melting. It had the advantage when used in vacuum that no water cooling was needed.

The first mould was used successfully when pouring in air. There was a possibility of chromium and nickel from the stainless steel tube contaminating the iron, but contamination would be a solid state diffusion process and

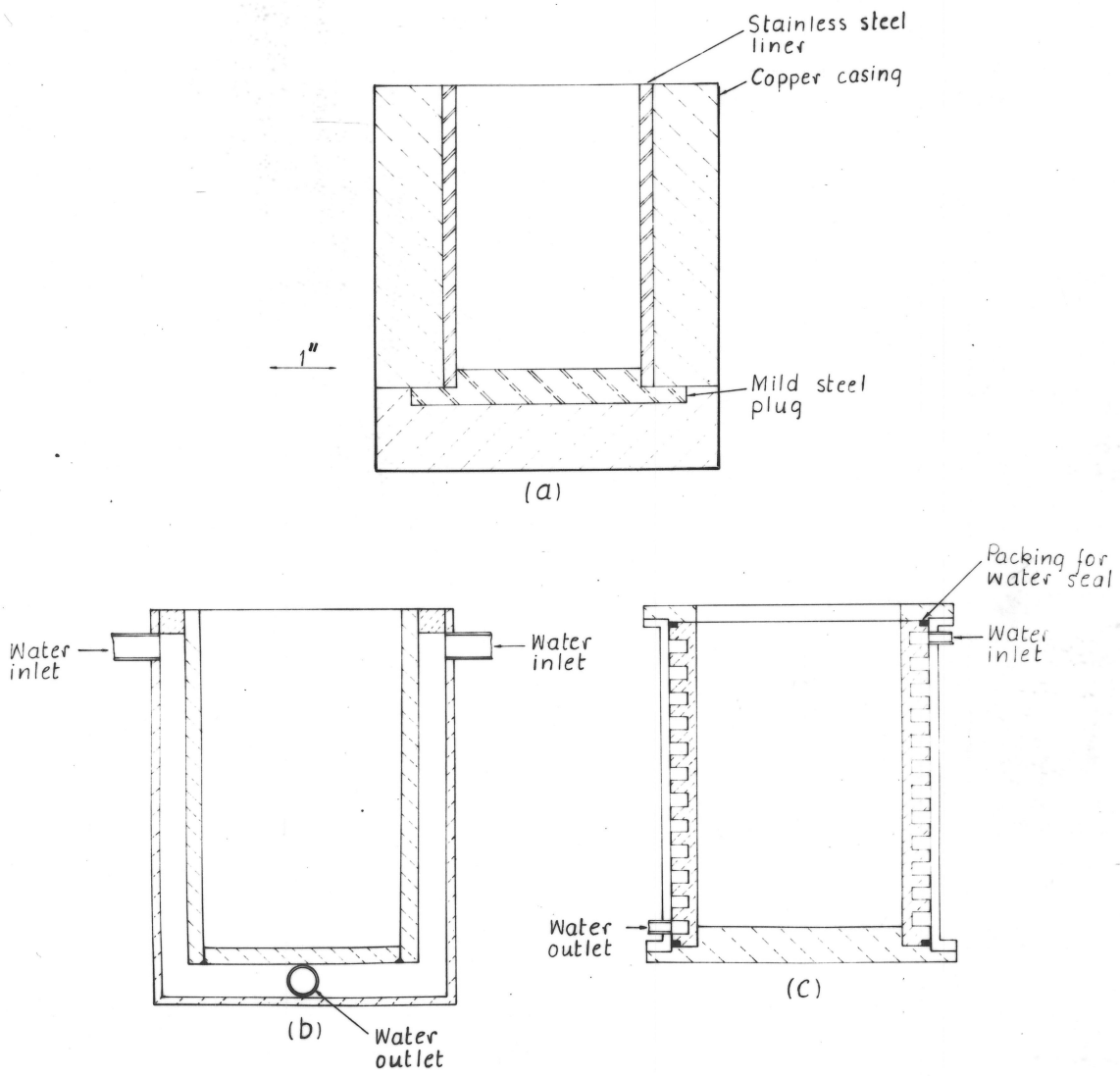


Fig. 4.12 Copper Moulds.

would require continued contact between solid iron and mould surface. It was found that the solidified iron shrank away from the stainless steel tube under slow pouring rate, so the contamination was negligible.

However during one pouring in vacuum the stream of molten iron impinged on the side of the stainless steel tube and stuck to it, and damaged the mould beyond repair.

The second mould, shown in Fig. 4.12(b) was a double walled water cooled copper mould. It was made of $\frac{1}{4}$ inch copper sheet formed into a square cup, 4 x 4 x $6\frac{1}{2}$ inches. The inner cup had a slight taper at the top for ease of removal of the solidified iron. The spacing between the outer and inner cup was $\frac{3}{8}$ inch at the side and $\frac{1}{2}$ inch at the bottom. The cooling water was let in at two opposite sides at the top and let out at the other two opposite sides at the bottom.

Before pouring molten iron, the mould was cleaned by dilute nitric acid and washed with water and dried. When poured the liquid iron in it was found that water leaked through the joint at the bottom of the mould. It was repaired. The second pouring was successful but the solidified iron stuck to a small spot at the bottom of the mould. It had to be pulled up by bolts and nuts. This suggested that a thoroughly cleaned mould was necessary.

It was difficult to clean the bottom of the deep mould. A better mould should have a separate base as in Fig. 4.12 (c).[69] Time was not available to make the third mould.

4.5 Preliminary Melting of Mild Steel in Air

Before refining the Armco iron in air an experimental melt using a piece of mild steel charge had been carried out in a zircon lining. This was to get familiar with the melting procedure and to investigate the behaviour of the electric circuit and equipment.

4.5.1 Melting of Mild Steel Charge

It was found that a piece of mild steel charge $2\frac{3}{4}$ inches in diameter and $3\frac{3}{4}$ inches long could be melted within 30 minutes. When the mild steel melted a shower of sparks came out due to CO gas evolved. It was prevented by adding a small amount of silicon to take up oxygen in the melt.

The zircon sand lining which was prepared by the method in Chapter III held the molten metal quite well. After pouring, it was checked and repaired when necessary before starting the next melt. After three melts the lining was chipped out. It showed little penetration of molten iron into the lining. This indicated that the zircon lining was a good lining for melting mild steel but was not used in the present work to produce high purity iron

alloys because it had a comparatively low temperature of dissociation, and would tend to contaminate the iron with zirconia and silica.

4.5.2 Change of Work-coil Effective Inductance during Heating up Charge

The effective inductance of the work-coil increased gradually when the charge was heated up from cold. When the temperature of the charge reached its Curie point the inductance decreased to a smaller value than when it was cold. This was due to, in the early stage of heating, the charge resistivity increasing gradually with temperature and causing a rise of work-coil effective inductance. Then when the temperature of the charge reached near to its Curie point, the permeability of the charge started to decrease and become unity at the Curie pcint which was several hundredths of its cold permeability. The work-coil effective inductance decreased with the permeability and reached its low value at the Curie point and above.

For these reasons the parallel capacitor of the electric circuit had to be decreased and increased during the heating up of the charge. This was done by decreasing the supply voltage to a minimum by reducing the generator field current then the parallel capacitor was decreased or increased as required.

4.5.3 Temperature of Auto-transformer Core

When the transformer was used at its full capacity for 30 minutes, it warmed up to 50°C. This suggested that an air cool by a blower was necessary for prolonged use of the auto-transformer at its full capacity.

4.5.4 Temperature of Work-coil Cooling Water

Using water from the main supply at 20°C, the temperature of the cooling water came out of the work-coil at 60°C when the mild steel charge was in molten state at about 1560°C. This temperature effects the power loss in induction heating in two ways -

(a) power loss through lining

(b) power loss, I^2R, in the work-coil.

The power loss in (a) will be low if the temperature of the cooling water is kept high, but the power loss in (b) will be high because of the increase of resistivity of copper with temperature. Using equation (1.65), page 52, the increase of heat loss through lining when the temperature of cooling water had risen 40°C is 0.205 kW, the increase in I^2R loss of the work-coil for the same temperature rise is 0.329 kW. The difference is not much, so no attempt was made to decrease the temperature of the cooling water by using a water pump.

The above consideration is for the present work only.

The heat loss in (a) may be greater than (b) if the contact area between the melt and the crucible is large and the lining thickness is small. Then the temperature of cooling water should be kept high.

4.6 Preliminary Refining of Armco Iron in Vacuum

The preliminary refining of the Armco iron in vacuum was carried out (in an alumina crucible produced in the laboratory) to investigate the capability of the crucible, the problem of gas evolution and evaporation of iron in vacuum.

The section of the vacuum tank with its lid closed shows the suspension of work-coil, crucible and charge and auto-transformer on the co-axial lead during melting as in Fig. 4.13.

A stack of Armco iron sheet $2\frac{3}{4}$ inches in diameter, $3\frac{3}{4}$ inches long was melted in the alumina crucible in the vacuum tank under 10 cm. Hg. argon pressure. Then the pressure was reduced to 10^{-3} mm. Hg. The melt was kept at this pressure for five minutes. During this period the iron vapour deposited on the glass window. When hydrogen at one atmosphere pressure was admitted, the surface of the molten iron started to solidify. It was necessary to reduce the hydrogen pressure to 5 cm. Hg. and poured.

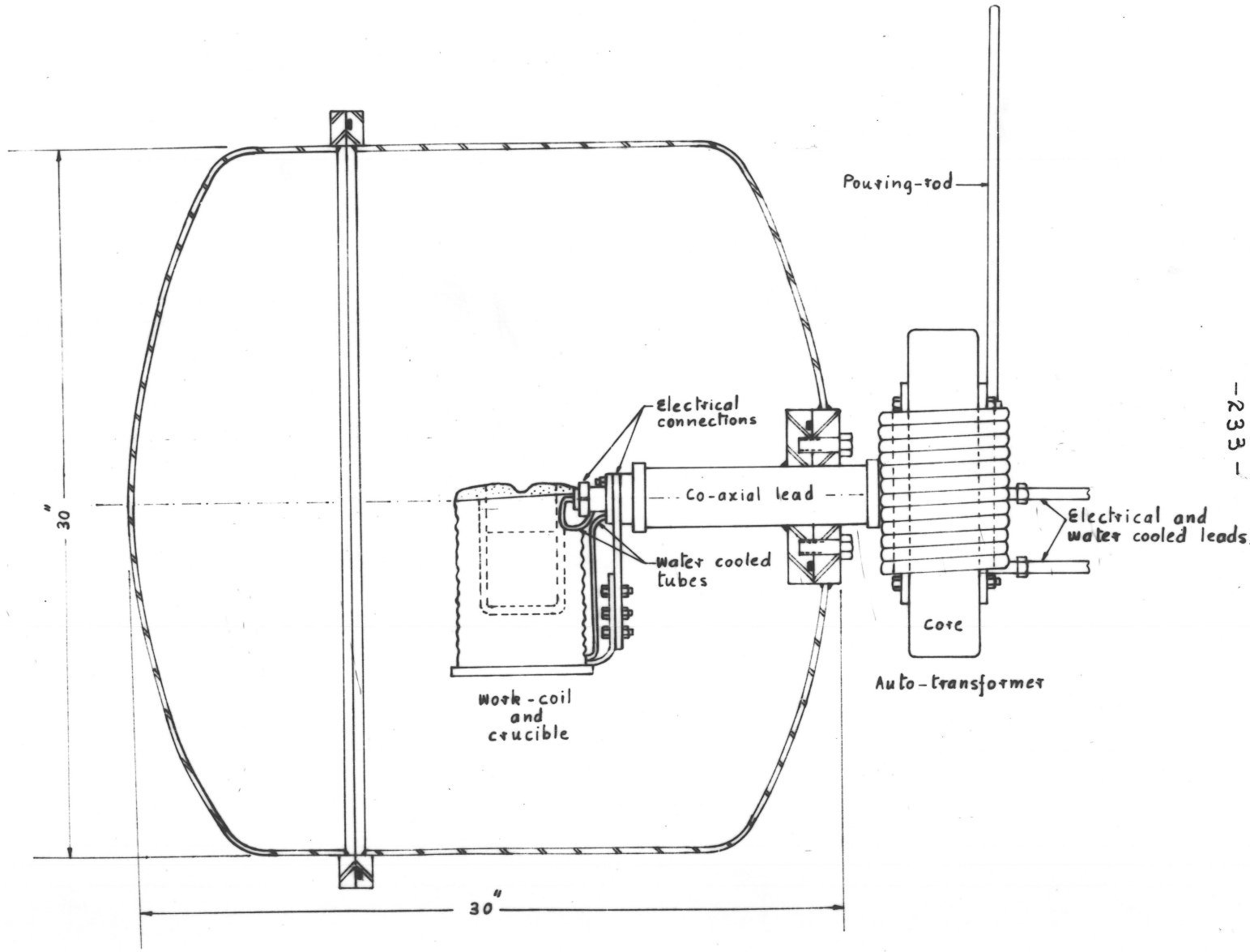


Fig. 4.13 Assembly of work-coil, co-axial lead and auto-transformer.

The details of the result are as follows:

(a) Alumina crucible

(b) Iron vapour

(c) Splashing

(d) Hydrogen

4.6.1 Alumina Crucible

The alumina crucible made in the laboratory held the molten Armco iron quite well. Under the pressure of argon at 10 cm. Hg. and the clearance between the charge and the crucible $\frac{1}{8}$ inch, the iron melted without forming the solidified surface or bridging. There was no need to use the bridge breaking rod.

4.6.2 Iron Vapour

At temperature 1600°C the vapour pressure of iron could be obtained from Fig. 4.14. With the vacuum pump working to remove the gas and vapour from the vacuum tank there is a constant evaporation of iron from the molten iron. This indicates high iron loss. However, the main problem here would be the iron vapour deposited on the furnace shell and sight hole glass which prevented the observation of the melt. It was necessary to put a cover plate on the sight hole, inside the vacuum tank, so the iron vapour would deposit on the cover plate and keep the sight hole glass clean. The cover plate was made of a mild steel sheet in the form of a fan with a

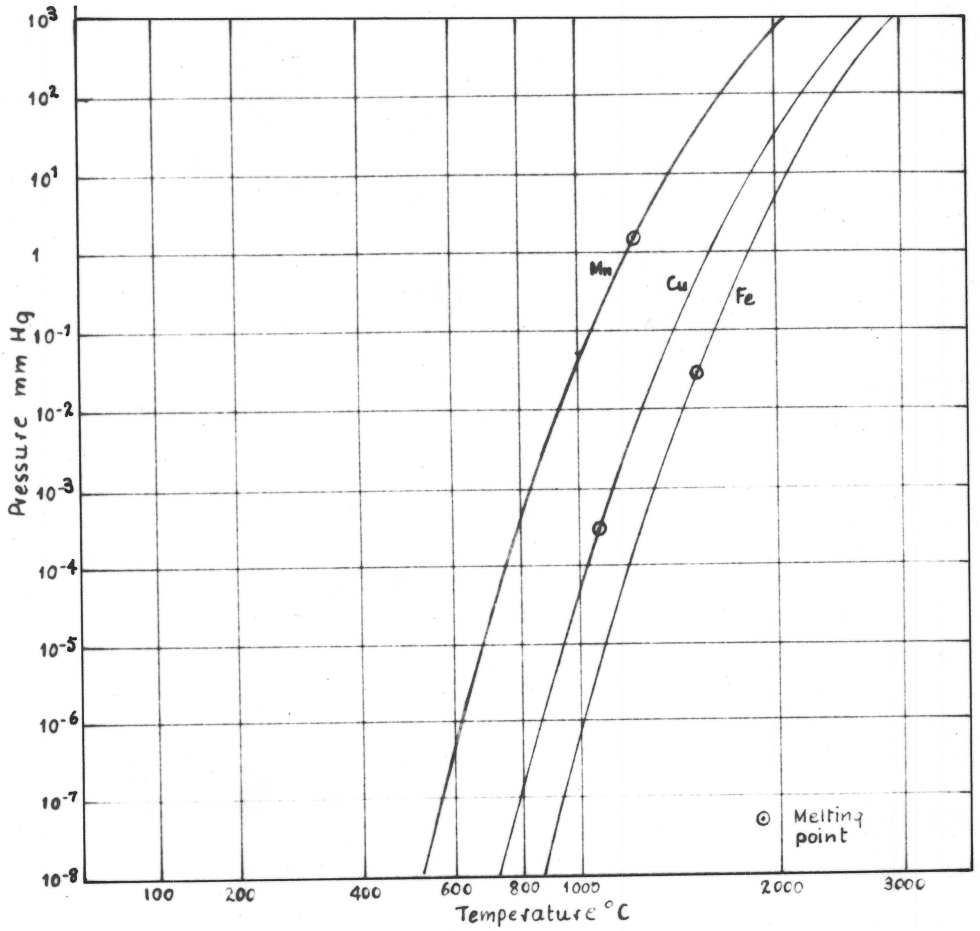


Fig. 4.14 Vapour pressure curves for solid and liquid iron, copper and manganese.[70]

long wide handle, rotated to uncover the sight hole glass by moving a piece of strong magnet outside the vacuum tank.

4.6.3 Splashing

In the early stages of carbon boiling under reduced pressure, CO bubbles carried iron droplets which deposited both on the crucible wall above the melt, and on the lid. The iron droplets solidified and caused the lid to stick on the crucible, so that it was difficult to open the lid afterwards. It was found necessary to lift the lid up a little before reducing pressure to 10^{-3} mm Hg. so the solidified droplets would not cause the lid to stick to the crucible.

4.6.4 Hydrogen Pressure for Deoxidation

When the hydrogen gas at one atmospheric pressure was circulated inside the vacuum tank to deoxidise the molten iron, it was found that the top of the charge started to solidify in the form of a ring. The ring began at the side of the crucible and grew to the middle of the melt. This was because the thermal conductivity of hydrogen was much higher than that of air. At 200°C the thermal conductivity of hydrogen is 63.4×10^{-5} cal./cm./sec./°C compared with 8.8×10^{-5} for dry air.[71] It took about 8 minutes for the surface to become solid with the power supply 12.5 kW. This prevented a further

deoxidation by hydrogen as well as overheating at the bottom of the crucible. It was impossible to deoxidise by this method with the limited power source available, so that repeated deoxidation by hydrogen at low pressure must be used.

4.7 Refining of Armco Iron

The Armco iron used as a starting material in the production of high purity iron alloys was sent to The Defence Standard Laboratory, South Australia, for chemical and spectrographic analysis as shown in Table 4.1.

Table 4.1 Chemical and Spectrographic Analysis of Armco Iron.

C* %	Mn+ %	Si+ %	Cu+ %	Cr+ %	Al+ %	Ti+ %
0.02	0.07	<0.001	0.04	0.02	0.01	trace

* chemical analysis by direct combustion method (± 0.005%)

\+ spectrographic analysis by direct comparison with H.S. Brand Electrolytic Iron Electrodes.

< less than

Usually there is about 0.025% sulphur present in Armco iron. It has not been analysed because sulphur could not be eliminated by the present method. To eliminate sulphur some treatment of liquid iron with special slag[72,73] is required, but it is beyond the scope of this work.

To reduce the amount of impurities in the Armco iron two steps were taken, namely:

(a) Melting the iron in air to oxidise carbon and other impurities and remove them in the form of gas or slag.

(b) Melting the oxidised iron under controlled atmosphere.

(1) Melting at low pressure for further reduction of carbon content.

(2) Melting under hydrogen atmosphere to reduce oxygen content.

(3) Melting under low pressure of hydrogen to reduce hydrogen content in the melt and pour.

From the above outline it is evident that to reduce the impurities to a minimum, the refining technique adopted would be

(a) Disturbing the chemical equilibrium by removing the products of the impurities from the reaction system. This will encourage the impurities to come out of the molten Armco iron.

(b) Allowing a reasonable time for the reaction to reach its state of equilibrium or near.

4.7.1 Oxidation of Impurities in Air

The melting was carried out in air, with the vacuum tank lid open. A typical melting time was as follows:

Time from start Mins.	Power at Transformer Primary
0	5 kW
7	10 kW
30	12.5 kW
40	12.5 kW, charge melted

After the charge melted, the power was reduced to 8.5 kW and the iron was kept molten for 30 minutes to oxidise impurities.

During melting slag, mainly FeO and some impurity oxide was formed on the surface of molten iron. Due to the stirring action of induction melting, the molten iron had a convex surface and the molten iron current flowed from the middle of the melt to the side of the crucible. Under these conditions the slag was driven to form a ring at the crucible side. It attached to the rough surface of the crucible. In this way some slag had been removed from the melt surface. This tended to promote a further reduction of impurity from the molten iron, and no special attempt was made to remove the slag from the melt.

After oxidising in air for 30 minutes some of the impurities, e.g. Mn, Si, C, would be removed from the molten iron. Before pouring the power was increased to 12.5 kW for five minutes (to raise the pouring temperature of the molten iron to about 1600°C) then the power was

reduced to 8 kW and the molten iron poured into the mould.

It was found that the iron shrank well away from the side of the mould.

4.7.2 Crucible Failure

After two meltings in air it was noticed that the top part of the crucible at the region of molten iron surface swelled out. The crucible was taken out and inspected. It was found that the molten iron had penetrated into the crucible about $\frac{1}{8}$ inch. This might be one cause of the damage to the crucible since the coefficient of thermal expansion of the iron is much more than that of alumina. Another possible cause would be that the part of the crucible contacting the molten iron was hotter than that above the surface of the melt. During heating and cooling their rate of change of volume were not the same.

At some parts of the crucible the molten iron had penetrated further than usual, but at that region the alumina powder filler had started to sinter and prevented the molten iron from leaking out and contacting the work-coil. This self-sealing behaviour of the alumina settling tank fines was useful in preventing short-circuiting of the work-coil.

The second crucible was used for three melts. The melting time of the third melt was longer than the other two, probably as a result of molten iron penetration

into the crucible in the earlier melts. The amount of heat loss through the side of the crucible would be more for the third melt than the previous two as the thermal conductivity of iron was much higher than alumina.

4.7.3 Refining in Vacuum

The oxidised iron was further refined in vacuum to reduce carbon, oxygen, nitrogen and hydrogen. The procedure was as follows.

4.7.4 Evacuating Vacuum Tank

The oxidised charge was cleaned to remove dirt, grease and foreign matter and was put in the dried crucible. The lid of the vacuum tank was closed. The tank was evacuated by the rotary mechanical pump, with its air ballast valve opened at first. When most of the moisture had been removed the ballast valve was closed. When the pressure inside the vacuum tank was reduced to about 0.3 mm. Hg. the oil diffusion pump was brought into operation, and the pressure further reduced to 10^{-5} mm. Hg. before the vacuum tank was shut off from the pump.

4.7.5 Melting Under Argon

The argon gas at pressure 10 cm. Hg. was used inside the vacuum tank during the melting down period instead of hydrogen. This was a safety precaution especially when the bridge breaking rod had to be used. There was some possibility of air leaking in through the

bridge breaking rod if it was not properly handled.

The rate of power supply to melt the charge was the same as that employed for melting in air. The charge was melted in 40 minutes.

4.7.6 Melting Under Low Pressure

This procedure was adopted to reduce carbon content. From equation (4.37)

$$[\text{wt } \%C] = \frac{1}{K_{CO}} \cdot \frac{1}{F} \frac{P_{CO}}{[\text{wt } \%O]}$$

F = product of activity coefficients.

When P_{CO} is reduced $[\text{wt } \%C]$ is reduced.

After the charge melted, the pressure inside the vacuum tank was reduced by the rotary pump and then diffusion pump to 10^{-3} mm. Hg. This lowering of pressure took about 25 minutes.

The iron was kept molten under 10^{-3} mm. Hg. for 15 minutes to eliminate its carbon content and also to evaporate copper, manganese and other high vapour pressure impurities.

4.7.7 Reduction of Oxygen Content

After reduction of carbon the deoxidation was carried on. The hydrogen gas was passed through a "Deoxo" catalyst, then through the molecular seives to eliminate oxygen and water respectively, and into the vacuum tank

at 10 cm. Hg. The melt was kept under this hydrogen pressure for five minutes after which the hydrogen and H_2O formed from the reaction of oxygen and hydrogen in the melt was removed through the pumps.

This treatment was repeated three times.

4.7.8 Pouring

After hydrogen treatment the pressure inside the vacuum tank was reduced to 5 mm. Hg. and kept for 15 minutes to remove hydrogen dissolved in the melt, then the temperature was raised to about 1600°C and the molten iron was poured slowly into the water-cooled copper mould.

Three pourings were made in vacuum. But the water leaked at the mould joint in the first and third pouring.

4.8 Chemical Analysis

There were five ingots poured from oxidised melts (marked Nos. 1 to 5 in Table 4.2). Samples were taken for chemical analysis for carbon by a direct combustion method, and the results are shown in the third column of Table 4.2. Ingots No. 1, 3 and 5 were remelted and refined in vacuum and marked 6, 7 and 8 respectively. The vacuum treated ingots were chemically analysed by the direct combustion method for carbon and spectrographically analysed for other impurities as shown in Table 4.2.

Table 4.2 Chemical and Spectrographic Analysis of Oxidised and Vacuum Treated Ingots

Process	Ingot No.	C_1 * %	C_2 ** %	Cu+ %	Mn+ %	Si+ %	Cr+ %	Al+ %
Oxidised in Air	1	<0.01	..	..	..	..	..	..
	2	<0.01	..	..	..	..	..	..
	3	<0.01	0.008	..	..	..	..	..
	4	<0.01	0.009	..	..	..	..	..
	5	<0.01	..	..	..	..	..	..
Vacuum treated	6	<0.01	0.012	0.01	<0.005	<0.003	0.005	0.0005
	7	<0.01	0.009	0.01	<0.005	<0.003	0.005	0.0005
	8	<0.01	..	0.01	<0.005	<0.003	0.005	0.0005

(Analyses by the Defence Standards Laboratory, South Australia).

* Chemical analysis by direct combustion method (± 0.005%)

** Chemical analysis by the method of H.G. Short[2] (± 0.002%)

\+ Spectrographic analysis by direct comparison with H.S. Brand Electrolytic Iron Electrodes.

Table 4.2 shows that the percentage of carbon in every refined ingot is less than 0.01%. Another method, i.e. the solution of iron in copper potassium chloride, has to be used to analyse more accurately for the small amount of carbon present. Ingots Nos. 3, 4, 6 and 7 were reanalysed and the results are shown in the fourth column, Table 4.2.

The amount of carbon in the vacuum treated ingot

No. 6 is higher than the oxidised ingots. This is probably due to some fault in vacuum treatment procedure or contamination of carbon during sample handling.

Other impurity contents except copper were decreased to low values.

CHAPTER V

DISCUSSION

The discussion will be presented as follows:

(a) Induction heating

(b) Vacuum system

(c) Refractory

(d) Refining

5.1 Induction Heating

5.1.1 Heat Loss Through Lining

With a small power source and rather low frequency, in the present case 10 kW continuous, 500 c/s, the heat loss through the lining is the governing factor in choosing the thickness of lining and the maximum size of charge which could be melted by induction melting.

From Chapter I, the heat loss through the lining is 4.23 kW for the lining thickness of $\frac{1}{2}$ inch and the molten charge size of $2\frac{3}{4}$ inches diameter and $3\frac{3}{4}$ inches height.

If the work-coil efficiency is 63% the power input required at the work-coil for this heat loss is 6.73 kW which is rather high compared to the continuous available power of 10 kW.

If the heat loss through lining is too high, e.g. 8 kW requiring 12.7 kW input at the work-coil the charge may be able to melt because the heat loss of the solid charge is not high, but once melted there would be some difficulty due to bridging on the top of the molten charge, as a result of excessive heat loss through the lining and radiation loss from the surface. When bridging occurs it is not possible to carry on the refining process.

It appears at first sight that a thick lining or small charge would give a better result in melting but this is limited by another factor, i.e. the coupled resistance. The coupled resistance is less when the lining is thick or the charge diameter is small, and there is a minimum size of charge below which the coupled resistance is too small and the charge can not be melted. This may be considered from equation (1.42), page 23

$$R_e = R_1 + R_c$$

and

$$I^2R_e = I^2R_1 + I^2R_c$$

I = current in work-coil

If R_c is too small and the power developed in the charge, I^2R_c is equal to the heat loss from the solid

charge, the charge will reach equilibrium temperature and remain solid.

5.1.2 Efficiency of Induction Melting

The efficiency of induction melting may be considered from the total loss in the system and the power input. There are two losses needed to be considered, heat loss through lining which is the highest for a thin lining and I^2R losses of the work-coil, transformer and leads. The overall efficiency may be improved by increasing the lining thickness, thereby reducing the heat loss through the lining. In doing so the coupled resistance is reduced and so is the power factor of the work-coil. This causes the rise of current in tank-circuit as well as secondary-circuit (Fig. 5.1) resulting in high I^2R loss in work-coil, transformer and leads.

Therefore the increase in lining thickness will cease to have any advantage when the heat loss through the lining is equal to the I^2R loss.

Economically the number of pounds of material produced per unit of overall cost is considered. This would lead to the use of maximum weight of material per melt, i.e. a large diameter charge and thin lining if adequate power were available.

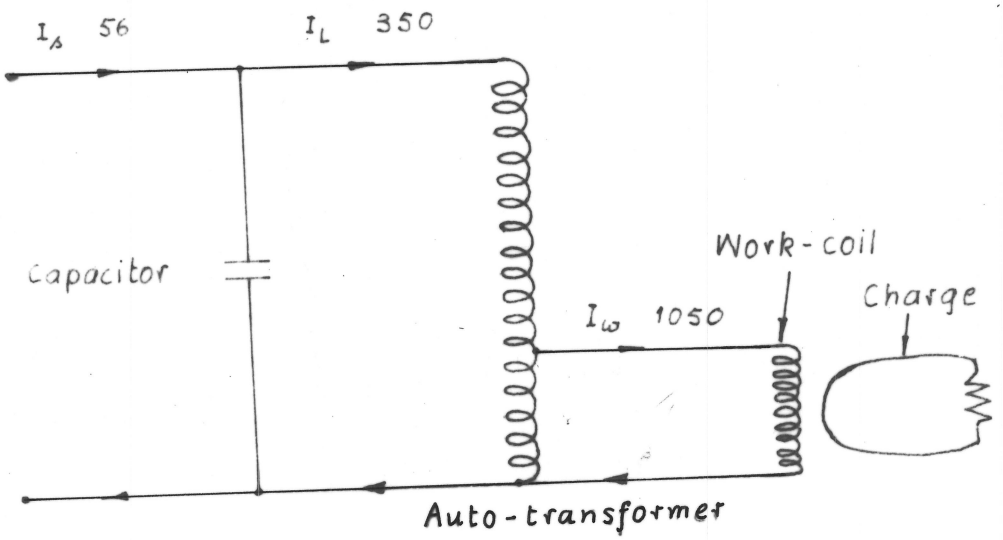


Fig. 5.1 Currents in Auto-transformer and in Work-Coil.

5.1.3 Number of Turns of Work-coil

If a set of factors concerning work-coil and charge is given, namely

(a) the inside and outside diameter of work-coil and charge, and

(b) the number of ampere-turns of work-coil,

the efficiency and power loss in the work-coil are independent of the number of work-coil turns or the amount of current flow in the work-coil, as long as the number of ampere-turns is kept constant (mentioned in Chapter I). In the present case the work-coil current is the secondary current of the auto-transformer causing I^2R loss in the other parts of secondary circuit as well as in the work-coil. To reduce the I^2R loss the work-coil current should be low and the number of work-coil turns should be as high as the size of its cooling coil permits. This, in effect, lowers the primary current and reduces the I^2R loss in the primary as well.

5.1.4 Performance of the Auto-transformer

The auto-transformer was used in the present work as an impedance matching device to increase the effective impedance of the heating circuit so that full power could be drawn from the power source. The performance of the transformer may be seen clearly by considering the amount of current required in the work-coil.

The power factor of the loaded work-coil is low (0.19), so that for 10 kW input and assuming a work-coil voltage of 50 volts, the current required is

$$I = \frac{10 \times 10^3}{50 \times 0.19}$$

$$= 1050 \text{ amperes}$$

When corrected to unity power factor, approximately 200 amperes must be delivered from the generator. This current could not be obtained directly from the power source because the rated current is only 56 amperes. By connecting the transformer between the work-coil and the power source and using parallel capacitors to correct the power factor of the heating circuit to unity the work-coil current can be stepped up from the rated supply current to the required amount (1050 amperes). The rated supply voltage (180 volts) of course is brought down to about 50 volts measured at the work-coil. The increasing of current may be considered as follows.

First the current in the supply line (I_s) is increased by the magnification factor Q, of the tank circuit, i.e.

$$I_L = Q . I_s,$$

where $Q = \frac{X_L}{R_L}$, and I_L is the current flowing in the primary.

Assuming a perfect transformer the current in the work-coil (I_w) or in the secondary circuit is

$$I_w = \frac{T_1}{T_2} . I_L$$

T_1, T_2 = no. of turns of primary and secondary respectively.

$$\therefore \quad I_w = \frac{T_1}{T_2} \cdot Q \cdot I_s$$

$$= \frac{T_1}{T_2} \cdot \frac{X_L}{R_L} \cdot I_s \qquad \ldots\ldots (5.1)$$

Equation (5.1) may be represented by a given set of measurements,

where $I_s = 56$, $I_L = 350$

$$\therefore \quad Q = \frac{350}{56}$$

$$= 6.25.$$

With the transformation ratio of 3:1 the current in the secondary would be 1050 amperes.

The currents flowing in each part of the circuit are shown in Fig. 5.1.

The above consideration shows that the auto-transformer acted as a power transferring device which is its normal function, with the aid of tank circuit current, the high current required in the work-coil may be obtained.

By using the transformer the reactance of the secondary circuit measured at the primary is increased by the square of ratio of primary to secondary turns.

$$X_{01} = X_1 + X_2\left(\frac{T_1}{T_2}\right)^2 \quad \ldots\ldots \quad (5.2)$$

X_{01} = equivalent reactance at primary

X_1 = reactance of primary

X_2 = reactance of secondary circuit.

When the reactance at the primary is increased the amount of parallel capacitor required for unity power factor correction will be less, i.e.

$$\frac{1}{2\pi f\, c} = 2\pi f L$$

$$c = \frac{1}{(2\pi f)^2 L}$$

c = parallel capacitor, farads

L = inductance at primary, henries

It appears at first consideration that once the transformer is manufactured and used as an impedance matching device, the ratio of primary to secondary should be as high as possible to reduce the amount of capacitor used for unity power factor correction to minimum. But this is limited by the value of maximum impedance of the circuit which is in turn depends on the rated voltage and rated current of the power source. In the present case the rated voltage is 180 volts and the rated current is 56 amperes, hence the limited impedance is

$$Z = \frac{180}{56}$$

$$= 3.22 \text{ ohms.}$$

From equation (1.58), page 37, the total impedance of the parallel resonance circuit is

$$Z_p = \frac{X_L^2}{R_L}$$

where $X_L = X_{01}$ in equation (5.2)

$$= X_1 + X_2\left(\frac{T_1}{T_2}\right)^2$$

It is clear that Z_p is increased when the ratio $\frac{T_1}{T_2}$ is increased and this ratio should not be increased beyond $Z_p = 3.22$ ohms, otherwise the full power of the source can not be utilized.

The one disadvantage of using an auto-transformer as the impedance matching device is that the transformer must transfer the full KVA of the tank circuit. Thus, in systems such as that employed here the efficiency of the transformer must be very high to avoid excessive losses. In the present case, Table 1.12 shows that although the tank circuit efficiency of the transformer is 96%, its efficiency with respect to power transfer is only 80%. Much heavier conductors for the primary winding must be used to improve this.

5.1.5 Laminated Iron Core

The advantage of using a laminated iron core to reduce the reluctance of the magnetic circuit of the work-coil may be considered from the fundamental principle

of magnetic circuit as follows.

The total magnetic flux produced by a long coil of n turns, l cms. in length, A sq.cm. cross-sectional area, with current I amperes flowing, is

$$\phi = \frac{0.4\pi n I}{\mathcal{R}} \text{ maxwell} \qquad \ldots . \quad (5.3)$$

$\mathcal{R}$ = reluctance

$$\mathcal{R} = \frac{l}{\mu A} \qquad \ldots . \quad (5.4)$$

$$\therefore \quad \phi = \frac{0.4\pi n I}{\frac{l}{\mu A}} \text{ maxwell} \qquad \ldots . \quad (5.5)$$

μ = relative permeability of medium inside the coil.

In heating the iron charge above its Curie point the permeability of the charge is unity. If two pieces of laminated iron core are put inside the coil, one at the top and the other at the bottom, Fig. 5.2, the reluctance of the magnetic path will be less than when the spaces were filled with air. Thereby the magnetic flux produced by the work-coil is increased, and hence the power developed in the charge is increased.

The ability of the laminated core to reduce the reluctance depends on its length inside the coil and its cross-sectional area. It has been mentioned that the reluctance of the magnetic path outside the coil is zero because the flux outside the coil travels in infinite space which means the area in equation (5.4) is infinity, but this is not the case at outside space near to the ends of the coil because the magnetic flux density around this region is still high. So using the laminated core

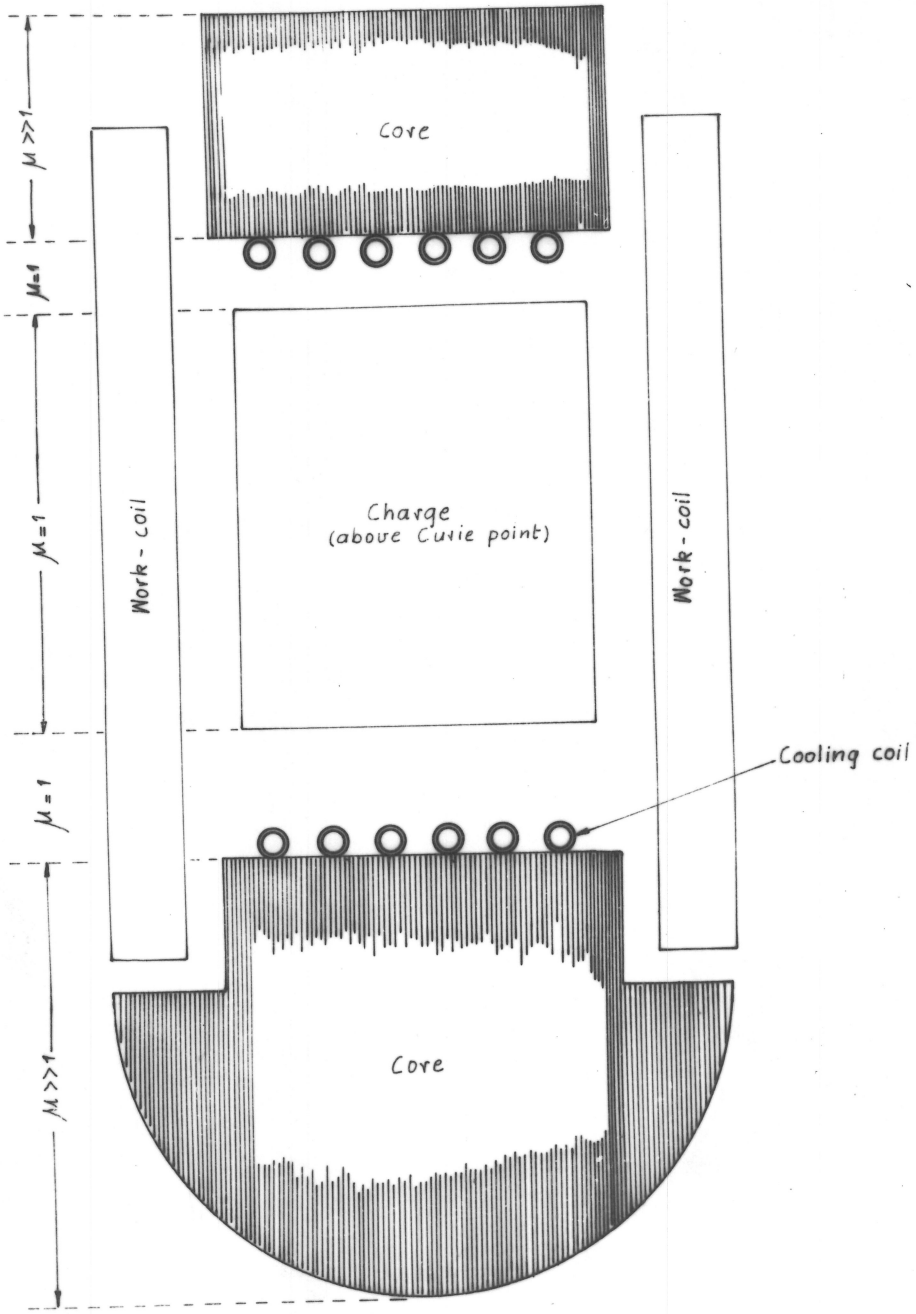


Fig. 5.2 Laminated core of Work-coil. (The bottom core is a suggested mushroom shape).

projected to a short distance outside the coild would give a better result. Also if the end of the laminated core has a mushroom shape, Fig. 5.2, it will increase the area of the core before the magnetic flux enters into space to complete its magnetic circuit. This will result in a further reduction of reluctance.

The main disadvantage of inserting the laminated core is that it required a water cooled coil on its surface and a considerable amount of heat was lost from the molten charge. Its advantage will stop when the power increase in the charge from the presence of the laminated core is equal to the power loss from the charge through the cooling water.

The other disadvantages are:

(1) it introduces more gas absorption surface inside the vacuum tank owing to the laminated nature of the core (but it can be covered by a material with smaller gas absorption);

(2) its cost; and

(3) the problem of fixing.

5.2 Vacuum System

5.2.1 Atmosphere Leak

One aim of vacuum refining is to prevent the molten metal from being contaminated from gases in the atmosphere, i.e. oxygen and nitrogen.

When there is a large atmosphere leak into the vacuum tank, the pressure of the tank is not a true indication of

the gas contamination of the melt especially when large vacuum pumps are used, e.g. a pressure of 1 μ-Hg. may be kept in the tank when the atmosphere leak may be of the order of 100 μ-Hg. per minute or more.[27] This indicates that there will be some contamination of gases to the melt more than that shown by the vacuum gauge.

High atmosphere leak rate causes inferior properties of the metal produced, e.g. the rupture life (25,000 psi at 871°C) of nickel-base age hardening alloys was 170 hours when the leak rate was 10 μ-Hg. per minute compared to 70 hours when the leak rate was 300 μ-Hg. per minute.[27]

In the present work before starting refining in vacuum the inside surface of the vacuum tank was cleaned and the crucible dried, then the cold leak rate was measured by the shut-off method. It was 80 μ-Hg. per hour or below 2 μ per minute which is normal in practice.

5.3 Refractory

The tamped alumina crucibles produced in the laboratory have been used throughout. Their service in melting and refining may be considered in relation to

(1) Crucible life

(2) Molten-iron crucible reaction.

5.3.1 Crucible Life

The crucible life may be considered in terms of the number of heats for which it can be used. Two alumina crucibles were used for oxidising in air and another two for refining in vacuum. They were never used until

destruction. The maximum number of heats attempted for one crucible was three for melting in air. This crucible, when taken off and cracked, showed that some of the liquid iron had penetrated $\frac{1}{8}$ inch into the crucible. This indicates that the crucible contained a large number of small pores. The causes of porosity may be as follows:

(a) Particle size. The crucible did not contain enough small particle size to fill the voids among large particles.

(b) Firing temperature. Neither the sintering temperature was high enough nor the holding time at 1800°C for 30 minutes was long enough to allow the sintering process to close the pores.

The crucible may be improved by careful selection of the grain size distribution of the fused alumina particles and using more slip in the tamping mixture. The sintering temperature should be raised to 1900°C and the holding time prolonged. This requires an accurate measurement of temperature and controlling the sintering atmosphere. The progress of sintering may be checked by density measurement. Time did not permit this work to be carried out.

5.3.2 Melt-crucible Reaction

During melting and refining the molten iron is in

contact with the crucible all the time, the chemical reaction between them will introduce impurities into the molten iron. This depends on the chemical composition of the fused alumina and slip and also the degree of the chemical inactivity of the crucible after sintering. The chemical composition of the fused alumina and slip are shown in Chapter III; they contain small amounts of metallic oxides and are considered to be good for experimental work.

The chemical stability of sintered alumina crucible may be considered from the presence of aluminium in the iron produced. From Table 4.2, Chapter IV, the aluminium in the vacuum treated iron ingot was less than 0.001 per cent. Comparing this to Al 0.001-0.002 per cent in vacuum treated iron ingots of Hiroshi Sawamura et al[61] and Al 0.001 per cent or less in the ingot produced by Hopkins et al,[2] the alumina crucibles are satisfactory from the point of view of aluminium contamination.

Oxygen in liquid iron has been mentioned as a troublesome contaminant to reduce to a low value. The oxygen will reach its equilibrium value when the difference between the rate of removal of oxygen by a deoxidiser and the rate of supply of oxygen to the liquid iron by the chemical reaction of refractory oxide is constant.[43, 62,63] It is a kinetic process.

In the present work only one ingot was successfully poured in vacuum, therefore gaseous analysis for oxygen was not done because the result was not enough to indicate the amount of oxygen present after deoxidation.

5.4 Refining

5.4.1 Problem in Deoxidation by Hydrogen

During the closed circuit circulation of hydrogen at one atmosphere to deoxidise the molten iron there was some difficulty due to too much heat being conducted away from the melt by the hydrogen gas. Bridging occurred on the melt surface even when the power source of 12.5 kW was supplied to the heating circuit. This made refining impossible and caused overheating of the crucible.

The repeated deoxidation by hydrogen at 10 cm. Hg. was workable but required more attention in letting hydrogen in and removing out through the vacuum pumps. With the minimum number of pumps used, i.e. one diffusion pump and one mechanical pump and the operating pressure was 10 cm.-10^{-3} mm Hg. the heater in the boiler of the diffusion pump had to be turned off when the mechanical pump was used to reduce the pressure from 10 cm. Hg. and turned on when the diffusion pump was used to reduce the pressure further. This caused some delay during operation.

The closed circuit deoxidation seems to be better but the pressure of the circulating hydrogen must be of the order of 10 cm. Hg. to prevent bridging. This required leak-proof closed circuit system to avoid any air leak into the system which may cause explosion. The alternative method may be pre-heating the hydrogen to a temperature of 1500°C or so before letting into the vacuum. This had been done by Chipman et al[47] on a number of their experiments. The power from the main may be used to pre-heat hydrogen.

The use of hydrogen as deoxidiser tends to introduce hydrogen contamination in the iron. It has been found that no advantages result from the presence of hydrogen in iron or steel; but causes numerous harmful effects, e.g. flaking or hairline cracking, blistering, brittle delayed failure, discontinuous crack propagation and stress corrosion cracking.[74] It is true that hydrogen may be removed after deoxidation by vacuum but there is always some hydrogen left in the iron. It is not known yet how much hydrogen is permitted to remain in iron without causing a harmful effect. Further, melting under high vacuum will cause high iron loss and excessive splashing.

The better deoxidiser would be carbon, but its addition must be carefully controlled to prevent contamination from carbon.[28,75]

5.4.2 Results of Refining

The discussion of the results of refining may be started by comparing the average chemical composition of Armco iron and refined iron alloys as shown in Table 5.1.

Table 5.1. Average Values of Chemical and Spectrographic Analysis of Armco Iron and Refined Iron Alloys

Iron	C* %	Cu+ %	Mn+ %	Si+ %	Cr+ %	Al+ %
Armco	0.02	0.04	0.07	<0.001	0.02	0.01
Oxidised	0.009	..	..	..	..	..
Vacuum treated	0.009	0.01	<0.005	<0.003	0.005	0.0005

* Chemical analysis (± 0.002%)

\+ Spectrographic analysis

< Less than

The amount of impurities removed may be considered as follows.

5.4.3 Removal of Carbon

Carbon was removed from liquid iron in two steps; by oxidation in air and melting under vacuum.

After oxidation in air the carbon content was decreased to 0.009% which is quite low. One factor which assisted the carbon removal was the stirring of the melt by the induced current.

After remelting the oxidised iron under 1 μ Hg. for 15 minutes the carbon content was practically the same as that of the oxidised iron. Theoretically the carbon content in vacuum treated iron should be lower, but the results may be within the error of chemical analysis ($\pm$ 0.002%). These indicate that a prolonged time is needed for a further removal of carbon content in a significant amount from liquid iron under vacuum.

However refining under vacuum of 1 μ Hg. during carbon elimination assisted in evaporating other impurities, e.g. copper and manganese.

5.4.4 Removal of Copper

From the standard free energy of formation of oxides in Chapter IV, FeO is more stable than Cu_2O at the molten iron temperature. Therefore copper in liquid iron cannot be removed by oxidation, but under vacuum treatment the solute copper evaporated out. From the collected data of Gill et al,[76] the vapour pressures of some elements of interest are shown in Table 5.2.

The activity of copper in liquid iron has a positive deviation from Raoult's law, therefore its vapour pressure is comparatively high. Hence some copper was removed by evaporation in vacuum, but the amount of copper left

after refining (0.01%) is still high. It may be decreased further by prolonged vacuum treatment. From the work of Gill et al,[76] after refining in vacuum at 1 μ Hg. at 1600°C for 90 minutes the amount of copper was decreased from its initial value of 0.92% to 0.002%.

Table 5.2. Vapour pressure of elements under consideration[76]

Element	Approx. vapour pressure at 1600°C (pure element) mm.Hg.	Approx. vapour pressure in 1% solution in iron at 1600°C mm. Hg.	
		Assuming ideality	Using known activities
Al	16.7	0.035	0.0015
Si	0.98	0.0035	0.00006
Cr	1.55	0.0017	0.0017
Mn	25	0.25	0.25
Fe	0.10	-	-
Ni	0.099	0.00094	0.00094
Cu	1.03	0.0091	0.11

5.4.5 Removal of Manganese

Manganese is removed by oxidation as well as evaporation. Its vapour pressure in Table 5.2 is about double that of copper, and from Fig. 4.14, page 235, the vapour pressure of manganese at 1600°C is much higher than those of copper and iron. So after vacuum treatment the percentage of manganese was decreased to $<0.005\%$.

5.4.6 Removal of Silicon

The silicon content should be decreased from liquid iron by oxidation, but there is not much difference between silicon in the raw material and product. Probably there was some silicon contamination from the loosened pieces of zircon lining at the top of the alumina crucible falling into the liquid iron during refining, since zircon may dissociate into silica and zirconia.

To prevent contamination from the loosened pieces of zircon lining a crucible of about $\frac{5}{8}$ inch longer than that shown in Fig. (page) must be used with the zircon filling so placed that no particle of it can fall into the melt.

5.4.7 Removal of Chromium

Chromium was decreased to 0.005 per cent. It was also shown that there was little chromium contamination from the stainless steel lined copper mould mentioned in Chapter IV, because the solidified iron shrank away from the mould surface.

5.4.8 Removal of Aluminium

The aluminium content was decreased to a low value in the refined ingots. This is expected because Al_2O_3 has high negative free energy of formation at the standard state compared to FeO. The amount of aluminium present in equilibrium with liquid iron saturated with oxygen from

air may be calculated from equation (4.52) page

$$K = [\text{wt\% Al}]^2[\text{wt\% O}]^3$$

at 1600°C

$$K = 10^{-14}$$

when $[\text{wt\% O}] = 0.226$

$[\text{wt\% Al}] = .93 \times 10^{-6}$

But the result obtained in practice would be more than equilibrium value.

The small amount of aluminium left also indicates that there was little contamination from the alumina crucible.

5.4.9 Removal of gases

The gas analysis was not done because only one ingot was successfully poured in vacuum. There was water leakage from the water-cooled copper mould when the other ingots were poured and this caused hydrogen and oxygen contamination in them. In theory oxygen should be eliminated by deoxidation with hydrogen. Nitrogen and hydrogen should be removed by vacuum treatment. In general the amount of gases left in the refined ingot depends on the method of refining, the time allowed for the reaction to proceed and the leak rate of the system.

RECOMMENDATION FOR FUTURE WORK

The following additional work is recommended:-

(a) The I^2R loss of auto-transformer may be decreased by using heavy copper conductors capable of carrying 600 amperes or more for the primary winding.

(b) Arrangement should be made for completely surrounding the work-coil with a laminated iron core to increase the efficiency of induction heating.

(c) A series of small sampling moulds should be installed for intermittent pouring in vacuum so that the reaction kinetics of refining may be studied.

(d) The tamped sintered alumina crucible may be improved by selecting a suitable grain size of fused alumina and using the proper amount of alumina slip for binding. A gas fired furnace to sinter the alumina crucibles should be constructed, so that they can be fired efficiently and economically.

(e) An oil booster pump should be fitted in the vacuum system for efficient operation in the pressure region of 10^{-4} - 0.5 mm. Hg. Such a pump has now been purchased for the equipment.

(f) Deoxidation by carbon as well as hydrogen should be carried out to study the oxidation process and to investigate the amount of carbon and hydrogen left in

iron after deoxidation under a given set of conditions.

(g) Removal of sulphur in Armco iron should be tried by melting in a crucible coated with slaked lime.[72]

(h) The liquid iron should be kept molten under 10^{-3} mm. Hg. for a prolonged time to evaporate copper.

(i) If the power output and frequency of the power source could be increased, e.g. 30 kW, 3000 c/s, the melting and refining operations will be greatly improved.

(j) A staff of at least two is required to operate the equipment during melting, refining and pouring operations. Equipment for analysis of small percentage of impurities and gases in iron should be installed; this would required trained operators so that the results of the refining processes could be followed at each stage.

REFERENCES

1. Rengstorff, G.W.P. and Goodwin, H.B., "Preparation and arc melting of high-purity iron", Trans. AIME, 1955, 203, 467-471.
2. Hopkins, B.E., Jenkins, G.C.M. and Stone, H.E.N., "Production of high-purity iron and iron alloys on a 25 lb. scale", JISI, 1951 168, 377-383.
3. Adcock, F., "The preparation of high-purity iron on a large laboratory scale", Journal of the Society of Chemical Industry, 1940, 19, 28-31.
4. Cottrell, A.H., "Theoretical Structural Metallurgy", Edward Arnold, 1959, 77-84.
5. Stansel, R.N., "Induction Heating", McGraw-Hill, 1949.
6. Simpson, P.G., "Induction Heating", McGraw-Hill, 1960.
7. McLachlan, N.W., "Bessel Function for Engineer", Oxford Press, 1961, 153-175.
8. Wall, T.F., "The high frequency induction furnace", The Engineer, 1942, 172, 209-211.
9. May, E., "Industrial High Frequency Electric Power", John Wiley & Sons, 1950.
10. Burge, C.R. and Davies, N.R., "An Introduction to the Theory of Eddy Current Heating", Ernest Benn, 1928.

11. Yensen, T.D., "Magnetic and other properties of electrolytic iron melted in vacuo", The Electricians, 1915, 75, 119-122.

12. Cotton, H., "Applied Electricity", Cleaver-Hume, 1960, 254-259.

13. Dawes, C.L., "Electrical Engineer, Vol. II", McGraw-Hill, 1944, 244-289.

14. Private communication, Denholm, W.T., Forte, W.G. and Burden, F., South Australian Institute of Technology.

15. Private communication, Denholm, W.T. and Forte, W.G., South Australian Institute of Technology.

16. "Metal Handbook", ASM, 1949, p. 29.

17. "Technical Paper No. 170", U.S. Bureau of Standards, 1921, p. 114.

18. Baker, R.M., "Heating of non-magnetic induction longitudinal flux", Trans. AIEE, 1944, 63, 273-278.

19. Dawes, C.L., "Electrical Engineer, Vol. I", McGraw-Hill, 1944, 228-236.

20. Scott, W.T., "The Physics of Electricity and Magnetism", John Wiley & Sons, 1959, p. 294.

21. Guthrie, A. and Walkering, R.K., "Vacuum Equipment and Technique", McGraw-Hill, 1949.

22. Yarwood, J., "High Vacuum Technique", Chapman and Hall, 1956.

23. Dushman, S., "Scientific Foundation of Vacuum Technique", John Wiley & Sons, 1962, p. 81.

24. Steinherz, H.A., "Vacuum Pumping System", Chapter in "Vacuum Metallurgy", Bunshal, R.F. (edited), Reinhold, 1958, 3-20.

25. "Working Instructions" for Oil Diffusion Pump, Edward High Vacuum Ltd., England.

26. "Working Instructions" for Mechanical Rotary Pump, Edward High Vacuum Ltd., England.

27. Jones, W.E., "Vacuum induction melting - process considerations", Metal Progress, 1957, 72, 133-138.

28. Winkler, O., "The theory and practice of vacuum melting", Metallurgical Review, 1960, 5, 1-117.

29. McPherson, R., M.Sc. Thesis, "Laboratory Application of High Frequency Induction Heating", University of Melbourne, 1954.

30. Seybolt, A.U. and Burke, J.E., "Experimental Metallurgy", John Wiley & Sons, 1953.

31. Chesters, J.H., "Steelplant Refractories", United Steel Companies, Sheffield, 1957.

32. Stott, V.H., "Laboratory production of cylindrical alumina crucible of 5½ litres capacity", JISI, 1957, 185, 82-85.

33. "Technical Service to Industry Report No. E.16", Commonwealth of Australia.

34. Watt, W. and Roberts, J.P., "The preparation of alumina bodies by the slip-casting method", Metallurgia, 1951, 43, 307-308.

35. Kingery, W.D., "Introduction to Ceramics", John Wiley & Sons, 1960.

36. Carruthers, T.G., "The production of sintered alumina ware", Metallurgia, 1951, 44, 103-107.

37. Bosworth, T.J., "Vacuum melting: influence of hydrogen pre-treatment of crucibles on oxygen content of iron charges", Trans AIME, 1958, 214, 489-493.

38. "American Institute of Physics Handbook", Gray, D.E. (Co-editor), McGraw-Hill, 1957, 6-109.

39. Chipman, J., "Physical chemistry of high-temperature reactions", Chapter in "Basic Open Hearth Steelmaking", A.I.M.E., New York, 1951, 531-591.

40. Ward, R.G., "An Introduction to the Physical Chemistry of Iron and Steel Making", Edward Arnold, 1962, 56-65.

41. Richardson, F.D. and Jeffes, J.H., "The thermodynamics of substances of interest in iron and steel making from 0°C to 2400°C", JISI, 1948, 160, 261-270.

42. King, T.B., "Thermodynamics and kinetics in vacuum metallurgy", Chapter in "Vacuum Metallurgy", Bunsha, R.F. (edited), 1958, 35-38.

43. Bennett, G.H.J., Protheroc, H.T. and Ward, R.G., "The role of carbon as a deoxidising agent in the production of vacuum melted steel", JISI, 1960, 195, 174-180.

44. Machlin, E.S., "Kinetics of vacuum induction refining theory", Trans. AIME, 1960, 314-326.

45. Darken, L.S. and Gurry, R.W., "Physical Chemistry of Metals", McGraw-Hill, 1953, p. 349.

46. Taylor, C.R. and Chipman, J., "Equilibrium of liquid iron and simple basic and acid slags in a rotating induction furnace", Trans. AIME, 1943, 154, 228-245.

47. Dastur, M.N. and Chipman, J., "Equilibrium in the reaction of hydrogen with oxygen in liquid iron", Metals Transactions, 1949, 185, 441-445.

48. Chipman, J., "Physical Chemistry of liquid steel", Chapter in "Basic Open Hearth Steelmaking", A.I.M.E., 1951, 621-690.

49. Chen, H.M. and Chipman, J., "The Chromium-oxygen equilibrium in liquid iron", Trans. ASM, 1947, 38, 70-113.

50. Ward, R.G., "An Introduction to the Physical Chemistry of Iron and Steel Making", Edward Arnold, 1962, p. 25.

51. Chipman, J., Gero, J.B. and Winkler, T.B., "The manganese equilibrium under simple oxide slags", Trans. AIME, 188, 341-345, (1950).

52. Gokcen, N.A. and Chipman, J., "Silicon-oxygen equilibrium in liquid iron", Trans. AIME, 1952, 194, 171-181.

53. Larsen, B.M., "Rates of open-hearth reactions", Chapter in "Basic Open Hearth Steelmaking", A.I.M.E., 1951, 867-903.

54. Richardson, F.D. and Dennis, W.E., "Thermodynamic study of dilute solution of carbon in molten iron", Trans. Faraday Society, 1953, 49, 171-179.

55. Floridis, T.P. and Chipman, J., "Activity of oxygen in liquid iron alloys", Trans. AIME, 1958, 212, 549-553.

56. Turkdogan, E.T., Leake, L.E. and Nasson, C.R., "Thermodynamics of iron-carbon melts", Acta Metallurgica, 1956, 4, 396-406.

57. Samarin, A.M., "Deoxidation of steel in vacuum", Chapter in "Vacuum Metallurgy", Bunsha, R.F. (edited), Reinhold, 1958, 255-265.

58. Reference 40, page 81-98.

59. Damara, F.N., Huntington, J.S. and Machlin, E.S., "Vacuum induction melting", JISI, 1959, 191, 266-275.

60. Hadley, R.L. and Bianchi, L.M., "Hydrogen deoxidation of vacuum-melted high-temperature alloys", Vacuum Metallurgy Symposium, 1954, Electrochem. Soc., 106-121.

61. Hiroshi Sawamura, Toshisada Mori, Masao Yakushi ji and Hiromasa Inone, "Fundamental study of vacuum melting of pure iron and stainless steel. I. On the crucibles, ingotism and the recovery of alloy additions", Memoirs, Faculty of Engineering, Kyoto University, 1960, 22, 236-248.

62. Turillon, P.P. and Machlin, E.S., "Deoxidation of pure iron by vacuum induction melting", Trans. Vacuum Metallurgy Conference, 1959, Bunsha, R.F. (edited), New York, 1960, 81-92.

63. Moor, J.H., "Some aspects of vacuum melted metals", Metal Progress, 1953, 63, 103-105.

64. Fast, J.D., Lutelin, A.I. and Overgosch, E., "Preparation and casting of metals and alloys under high vacuum", Philips Tech. Rev., 1953, 15, 115-121.

65. d'Entremont, J.C., Guernsey, D.L. and Chipman, J., "Aluminium-oxygen interaction in liquid iron", Trans. AIME, 1963, 227, 14-17.

66. Eptstein, H., Chipman, J. and Grant, N.J., "Hydrogen in steel making practice", Trans. AIME, 1957, 209, 597-608.

67. Reference 40, page 175-183.

68. Pehlke, R.D. and Elliott, J.F., "Solubility of nitrogen in liquid iron alloys. I. Thermodynamics", Trans. AIME, 1960, 218, 1088-1101.

69. Rohn, W.J.P., "The reduction of shrinkage cavities and vacuum melting", JISI, 1929, 42, 203-214.

70. Elliott, J.F. and Gleiser, M., "Thermochemistry for Steelmaking, Vol. 1", Addison-Wesley, 1960, p. 269.

71. "Handbook of Physics", Condon, E.U. and Odishaw, H. (edited), McGraw-Hill, 1958, 6-64.

72. Ward, R.G. and Hall, R., "Desulphurization of molten steel by solid lime during vacuum melting", JISI, 1960, 195, 75-78.

73. Florides, T.P., "Vacuum desulphurization of liquid iron alloys", Trans. AIME, 1959, 215, p. 870.

74. Troiano, A.R., "The influence of hydrogen on the mechanical behaviour of steel", Papers and Discussions, Harrogate Conference, Oct. 1961, The Iron and Steel Institute, p. 1-6.

75. Strawley, J.E., "Vacuum induction melting, oxygen and carbon in iron", U.S. Naval Research Lab., Report No. 5516, Sept. 21, 1960.

76. Gill, G.M., Ineson, E. and Wesley, G., "The behaviour of various elements in vacuum steelmaking", JISI, 1959, 191, 172-175.